

# Simulation of Time-Dependent Viscoelastic Fluid Flows by Spectral Elements

THÈSE N° 4955 (2011)

PRÉSENTÉE LE 25 MARS 2011

À LA FACULTÉ SCIENCES ET TECHNIQUES DE L'INGÉNIEUR  
LABORATOIRE D'INGÉNIERIE NUMÉRIQUE  
PROGRAMME DOCTORAL EN MÉCANIQUE

ÉCOLE POLYTECHNIQUE FÉDÉRALE DE LAUSANNE

POUR L'OBTENTION DU GRADE DE DOCTEUR ÈS SCIENCES

PAR

**Azadeh JAFARI**

acceptée sur proposition du jury:

Dr M. Farhat, président du jury  
Prof. M. Deville, Prof. D. Favrat, directeurs de thèse  
Prof. F. Gallaire, rapporteur  
Prof. G. Mompean, rapporteur  
Prof. T. N. Phillips, rapporteur



ÉCOLE POLYTECHNIQUE  
FÉDÉRALE DE LAUSANNE

Suisse  
2011



To my parents

تقدیم بہ مادر و پدر عزیزم مہری و علی





# Abstract

---

The research work reported in this dissertation is aimed to develop efficient and stable numerical schemes in order to obtain accurate numerical solution for viscoelastic fluid flows within the spectral element context. The present research consists in the transformation of a large class of differential constitutive models into an equation where the main variable is the logarithm of the conformation tensor or a quantity related to it in a simple way. Particular cases cover the Oldroyd-B fluid and the FENE-P model. Applying matrix logarithm formulation in the framework of the spectral element method is a new type of approach that according to our knowledge no one has implemented before.

The reformulation of the classical constitutive equation using a new variable namely the logarithmic formulation, enforces the eigenvalues of the conformation tensor to remain positive for all steps of the simulation. However, satisfying the symmetric positive definiteness of the conformation tensor during the simulation is the necessary condition for stability; but definitely, it is not the sufficient condition to reach meaningful results. The main effort of this research is devoted to introduce a new algorithm in order to overcome the drawback of direct reformulating the classical constitutive equation to the logarithmic one.

To evaluate the capability of the extended matrix logarithm formulation, comprehensive studies have been done based on the linear stability analysis to show the influence of this method on the resulting eigenvalue spectra and explain its success to tackle high Weissenberg numbers. With this new method one can treat high Weissenberg number flows at values of practical interest.

One of the worst obstacle for numerical simulation of viscoelastic fluids is the presence of spurious modes during the simulation. At high Weissenberg number, many schemes suffer from instabilities and numerical convergence may not be attainable. This is often attributed to the presence of solution singularities due to the geometry, the dominant non-linear terms in the constitutive equations, or the change of type of the underlying mixed-form differential system. Refining the mesh proved to be not very helpful. In this

study, to understand more deeply the mechanism of instability generation a comprehensive study about the growth of spurious modes with time evolution, mesh refinement, boundary conditions and Weissenberg number or any other affected parameters has been performed. Then to get rid of these spurious modes the filter based stabilization of spectral element methods proposed by Boyd was applied with success.

**Keywords:** viscoelastic fluid flows, High Weissenberg number problem, Matrix logarithm conformation tensor, spectral element method, filter based stabilization method, linear stability analysis.

# Résumé

---

Le travail de recherche décrit dans cette dissertation a pour but de développer des méthodes numériques efficaces et stables afin d'obtenir des solutions précises des écoulements de fluides viscoélastiques dans le cadre des éléments spectraux. Cette recherche consiste en la transformation d'une grande classe de modèles constitutifs différentiels en une équation dont la variable principale est le logarithme du tenseur de conformation ou d'une quantité qui lui soit reliée de manière simple. Les cas particuliers couvrent les modèles d'Oldroyd-B et FENE-P. L'application de la formulation du logarithme matriciel dans le cadre de la méthode des éléments spectraux est une nouvelle approche qui à notre connaissance n'a pas été implantée auparavant.

La reformulation de l'équation de comportement classique au moyen d'une nouvelle variable, c.-à-d. la formulation logarithmique, exige que les valeurs propres du tenseur de conformation demeurent positives pendant toute la simulation. Cependant, satisfaire la propriété de symétrie définie positive du tenseur de conformation durant la simulation est une condition nécessaire pour la stabilité; mais elle n'est de loin pas la condition suffisante pour atteindre des résultats significatifs. L'effort principal de cette recherche est consacré à l'introduction d'un nouvel algorithme afin de surmonter l'inconvénient de la réécriture de l'équation constitutive classique en la formulation logarithmique.

Afin d'évaluer la capacité de la formulation du logarithme matriciel étendu, des études très complètes ont été réalisées sur la base de l'analyse de la stabilité linéaire pour montrer l'influence de cette méthode sur les spectres de valeurs propres qui en résultent et pour expliquer son succès à traiter des nombres de Weissenberg élevés. Avec cette nouvelle méthode, on peut traiter des écoulements à hauts nombres de Weissenberg pour des valeurs d'intérêt pratique.

Un obstacle majeur dans la simulation numérique des fluides visco-élastiques provient de la présence de modes parasites durant la simulation. A nombre de Weissenberg élevé, beaucoup de schémas souffrent d'instabilités et la convergence numérique n'est pas at-

teinte. Cette déficience est souvent attribuée à la présence dans la solution de singularités dues à la géométrie, aux termes non linéaires dominants dans l'équation de comportement, ou encore le changement de type du système différentiel mixte sous-jacent. Le raffinement de maillage ne permet pas de surmonter cette difficulté. Dans cette étude, afin de comprendre plus profondément le mécanisme de génération de l'instabilité, une étude complète de la croissance des modes parasites avec l'évolution temporelle, le raffinement de maillage, les conditions aux limites, le nombre de Weissenberg ou de tout autre paramètre impliqué a été entreprise. Afin de se débarrasser de ces modes parasites, une stabilisation de la méthode des éléments spectraux par un filtre proposé par Boyd a été appliquée avec succès.

**Mots-clés:** écoulements de fluides viscoélastiques, problème du nombre de Weissenberg élevé, tenseur de conformation en formulation matricielle logarithmique, éléments spectraux, stabilisation par filtrage, analyse de stabilité linéaire.

# Acknowledgements

---

I take this opportunity to offer my regards and blessings to all who have directly or indirectly helped This project.

First, I owe my deepest gratitude to Prof. Michel O. Deville who has supervised this work and guided me in different matters regarding the topic. I am extremely grateful of his encouragement, guidance and support from the initial to the final level enabled me to complete my thesis effectively and moreover on time. I would also like to tank Professor Daniel Favrat, my thesis co-supervisor, for his kind and supportive consideration.

I would aslo like to express my special appreciation to Dr Nicolas Fiétier, First Assistant of the Laboratory of Computational Engineering for his invaluable inputs and immense guidance throughout the duration of my project.

I am thankful to Dr Roland Bouffannais, former PhD student in the laboratory of computational engineering, for illuminating discussion about filtering and his immediate response for dozens of my questions.

I am grateful of everyone at the Laboratory of Computational Engineering (LIN) and Industrial Energy System (LENI). I am indebted to many of my colleagues and friends. It is my pleasure to thank Mrs Heidi Francelet, Mrs Marie-Madeleine Gruaz and Suzanne Zahnd for a very precious assistance in all non-scientific matters; Mr. Ali Tolou for his permanent assistance related to the cluster management; my dear firens Farzaneh, Leila, Samira, Behnaz, Mina, Fereshteh, Ameneh and absolutely a non-exhaustive list of them for giving cooperation.

I am very grateful to Prof. Tim Phillips, Prof. Gilmar Mompean and Prof. Francois Gallaire for their participation in the thesis committee and for taking the time to read through the manuscript and attend the private defense. Their comments and suggestions have been greatly appreciated. I would also like to thank Dr Mohamed Farhat, for pre-

siding over the committee.

I would like to acknowledge the Swiss National Science Foundation Grant (No. 200020-112085) for its financial support.

Last and definitely not least, I reserve my respects and love to my parents, my sister, Arezou my brother, Sadegh and my brother in law , Mohammad for their love, moral support and encouragement.

# Contents

---

<b>Abstract</b>	<b>i</b>
<b>Résumé</b>	<b>iii</b>
<b>Acknowledgements</b>	<b>v</b>
<b>Contents</b>	<b>vii</b>
<b>1 Introduction</b>	<b>1</b>
1.1 The state-of-the-art of numerical simulation for viscoelastic flows . . . . .	2
1.2 The state-of-the-art of the matrix logarithmic conformation tensor . . . . .	3
1.3 Physical phenomena in viscoelastic fluids . . . . .	4
1.3.1 Viscoelasticity . . . . .	4
1.3.2 Shear rheology of non-Newtonian fluids . . . . .	5
1.4 Organization of the dissertation . . . . .	7
1.4.1 Description . . . . .	7
<b>2 Constitutive models for viscoelastic flows</b>	<b>9</b>
2.1 Introduction . . . . .	9
2.2 Differential constitutive models . . . . .	10
2.2.1 Dumbbell models . . . . .	11
2.2.2 Linear elastic dumbbell models . . . . .	12
2.2.3 Nonlinear elastic dumbbell model . . . . .	15
2.2.4 Retarded motion expansions . . . . .	17

2.2.5	Generalized Newtonian and quasi-Newtonian models . . . . .	17
2.3	Integral constitutive models . . . . .	20
2.3.1	Doi-Edwards model . . . . .	20
2.3.2	K-BKZ . . . . .	21
2.4	Selecting a constitutive equation . . . . .	22
<b>3</b>	<b>Numerical methods for simulating viscoelastic flows</b>	<b>25</b>
3.1	Introduction . . . . .	25
3.2	Space discretization methods . . . . .	25
3.2.1	Finite difference methods . . . . .	26
3.2.2	Finite volume methods . . . . .	26
3.2.3	Finite element methods . . . . .	27
3.2.4	Lattice Boltzmann method . . . . .	28
3.2.5	Spectral methods . . . . .	29
3.2.6	Spectral element methods . . . . .	29
3.3	Legendre spectral element method . . . . .	30
3.3.1	Governing equations . . . . .	31
3.3.2	Boundary conditions . . . . .	32
3.3.3	Weak formulation of the problem . . . . .	32
3.3.4	Galerkin approximation . . . . .	33
3.3.5	Semi-discrete formulation . . . . .	37
3.4	Time discretization . . . . .	39
3.5	System solving techniques . . . . .	40
3.6	Stabilization technique . . . . .	43
3.7	Summary . . . . .	43
<b>4</b>	<b>Mathematical improvement of constitutive equation to treat high Weissenberg number pr</b>	



---

4.1	Introduction . . . . .	46
4.2	Classical matrix logarithm formulation (CMLF) . . . . .	49
4.3	The extended matrix logarithm formulation (EMLF) . . . . .	52
4.4	The hyperbolic tangent conformation tensor . . . . .	54
4.5	Problem description . . . . .	57
4.6	Results and discussion . . . . .	60
4.6.1	Classical Matrix logarithm conformation (CMLF) . . . . .	60
4.6.2	Extended matrix logarithm formulation (EMLF) . . . . .	70
4.7	Conclusion . . . . .	73
<b>5</b>	<b>Simulation of abrupt contraction flow</b>	<b>75</b>
5.1	Introduction . . . . .	75
5.2	Test problems . . . . .	80
5.3	Results and discussion . . . . .	83
5.3.1	2-D 4:1 planar contraction flow . . . . .	83
5.3.2	2-D 4:1 planar contraction-expansion flow . . . . .	92
5.4	Conclusion . . . . .	98
<b>6</b>	<b>Linear Stability analysis</b>	<b>99</b>
6.1	Introduction . . . . .	99
6.2	Linear stability analysis . . . . .	103
6.3	Problem description . . . . .	105
6.4	Results and discussion . . . . .	105
6.4.1	Influence of Weissenberg number . . . . .	106
6.4.2	Influence of mesh refinement . . . . .	108
6.4.3	Influence of finite extensibility . . . . .	110
6.5	Influence of outflow boundary condition . . . . .	110

---

6.6	Conclusion . . . . .	112
<b>7</b>	<b>Filter-based stabilization technique</b>	<b>115</b>
7.1	Introduction . . . . .	115
7.2	Filter-based stabilization technique . . . . .	119
7.2.1	Description of the filter . . . . .	120
7.2.2	Transfer function . . . . .	121
7.2.3	Problem description . . . . .	122
7.3	Results and discussion . . . . .	125
7.4	Results without filtering . . . . .	126
7.4.1	Influence of Weissenberg number . . . . .	126
7.4.2	Influence of mesh refining . . . . .	128
7.4.3	Influence of finite extensibility parameter . . . . .	129
7.4.4	Influence of outflow boundary condition . . . . .	130
7.5	Results with filtering . . . . .	131
7.5.1	Influence of filter-based stabilization of spectral element method . . . . .	131
7.5.2	Influence of mesh-transfer technique . . . . .	132
7.5.3	Influence of time step . . . . .	151
7.6	Conclusion . . . . .	155
<b>8</b>	<b>Summary and conclusion</b>	<b>159</b>
8.1	General summary . . . . .	159
8.2	Outlook and perspectives . . . . .	163
<b>A</b>	<b>Appendix A</b>	<b>165</b>
	<b>Bibliography</b>	<b>167</b>

Curriculum vitae

189



# Chapter 1

---

## Introduction

The challenge for computational rheologists is to develop efficient and stable numerical schemes in order to obtain accurate numerical solutions for the governing equations at values of practical interest of the Weissenberg number,  $We$ , i.e. within the range [0-150]. The Weissenberg number is the ratio of the material relaxation time of viscoelastic fluids to the inertial time of the flow.

In the past three decades, considerable efforts have been devoted to the development of robust and stable numerical methods for simulating non-trivial flows of complex fluids. Without any exception, the standard viscoelastic models like Oldroyd-B, Maxwell, Phan-Thien-Tanner, FENE-P, etc. have failed in the simulation of high Weissenberg number flows in any available numerical techniques such as: finite differences, finite volumes, finite elements, spectral elements, etc. Nowadays one has come to the conclusion that selection of an appropriate constitutive equation constitutes a very crucial step to simulate viscoelastic fluid flows, although implementing a suitable numerical technique is still important for successful discrete modelling of non-Newtonian flows [129].

The present dissertation is devoted to a new type of approach published in the recent past [69, 70, 102, 51, 120] within the framework of spectral element method [60]. It consists in the transformation of a large class of differential constitutive models into an equation where the main variable is the logarithm of the conformation tensor or a quantity related to it in a simple way. Particular cases cover the Oldroyd-B fluid and the FENE-P model. Applying matrix logarithm formulation in the framework of spectral element method is a new type of approach that according to our knowledge no one has implemented before. Therefore, on the one hand, this dissertation is devoted to this new type of approach, transforming differential constitutive models into an equation where the main variable is the logarithm of the conformation tensor. The research may have important consequences

for the simulation of fluid behavior in modern industrial processes like plastics, polymers, paints, foods, oils, etc., in blood flow simulation and many other situations where complex fluids are present. The C++ toolbox SPECULOOS [66] has been used and adapted to handle this simulation and analysis.

## 1.1 The state-of-the-art of numerical simulation for viscoelastic flows

Let us bias this state-of-the-art review toward high order methods. Finite element and finite volume methods are extensively described and covered in the monograph of Owens and Phillips [173]. The leading practitioners of spectral element methods for viscoelastic fluids are quite identified: Mark Gerritsma, George Karniadakis, Vincent Legat, Robert Owens, Tim Phillips, and their co-author(s). A non exhaustive list of references is given in the bibliography [100, 41, 136, 170, 218, 219, 221, 220, 227, 226]. Most of these numericists have faced the same problem, i.e. the loss of convergence of the numerical simulations for high  $We$  number values. However, there has been indeed an obvious trend of building up more robust and more efficient algorithms and solvers over the last five years. One can expect that, with a reasonable choice of a proper rheological constitutive equation, the solution of all other particular problems is a subject of computational art. However, this conclusion is invalid because, in this case, two principal problems arise, and these problems are beyond the scope of the continuum dynamics but are directly related to rheology: the problem of stability and the problem of boundary conditions [143]. As was shown in [122], the solutions to various forms of numerous rheological constitutive equations appear to be mathematically unstable; therefore, the use of numerical methods does not always yield reliable results. This formal but crucial aspect of the choice and formulation of the rheological constitutive equation requires strict limitations on possible various approaches to solving applied problems. As far as stability analysis is concerned, most of the published studies deal with physical instabilities observed experimentally e.g. [148, 195, 124, 149] or intrinsic instabilities of a given constitutive equation at the continuous level [186, 190, 198, 215, 236]. In this project, we would rather concentrate our research efforts towards the nature of the mathematical models and the associated sources of instabilities generated by those models [74, 73]. Understanding the origin of the spurious instabilities related to the numerical method and of intrinsic instabilities of constitutive models is a necessary

step before being able to simulate steady viscoelastic flows at high Weissenberg numbers and unsteady flows where physical instabilities observed experimentally would occur.

## **1.2 The state-of-the-art of the matrix logarithmic conformation tensor**

Since the high Weissenberg number problem (HWNP) is due to the inadequacy of polynomial interpolation in finite difference, finite volume, finite element, etc. to approximate exponential profiles, two possible remedies come to mind: either to use an exponential basis function for the stress variables, or to make a change of variables into new variables that scale logarithmically with the stress. In either case, this requires the stress field, to remain strictly positive, which can not be guaranteed. A physical quantity, directly related to the stress that preserves positivity is the conformation tensor which is symmetric positive definite (SPD) by definition. As such the conformation tensor has a well defined matrix logarithm.

In this context, Fattal and Kupferman [69] suggested to resort to a variable transformation in such a way that the new variable is the matrix logarithm of the conformation tensor. This transformation removes part of the stiffness associated with the hyperbolic nature of the constitutive equations. Fattal and Kupferman [70] tackled the lid-driven cavity with a *MAC* type algorithm. The reported computations were obtained till  $We = 5$ . They claim they have elucidated the high Weissenberg instability. Nonetheless, in the conclusions of their paper, they write "this change of variables does not guarantee that accurate computations can be performed at arbitrarily high  $We$ ".

In [102], Hulsen, Fattal and Kupferman have implemented a finite element method (FEM) with the *DEVSS/DG* formulation. The viscoelastic flow past a cylinder is investigated with the log-conformation approach for the Oldroyd-B and Giesekus models. They reach the value of  $We = 100$  for the Giesekus case while for the Oldroyd-B fluid, the computations do not show converged results for the stress in the wake beyond  $We = O(1)$ . In their conclusions, the use of high order methods to obtain convergence in localized regions is evoked.

Similarly, Kwon [120] and Coronado et al. [51] have used successfully the log-conformation formulation in slightly different forms to simulate efficiently the flow of viscoelastic fluids. Within the same type of approach, Vaithianathan et al. [213, 214] have suggested the use of different change of variables in the constitutive equation to enforce boundedness of the trace of the conformation tensor and remove numerical instabilities occurring during the simulations of viscoelastic fluids with a finite difference method.

### 1.3 Physical phenomena in viscoelastic fluids

Some phenomena in viscoelastic materials are: (i) if the stress is held constant, the strain increases with time (creep); (ii) if the strain is held constant, the stress decreases with time (relaxation); (iii) the effective stiffness depends on the rate of application of the load; (iv) if cyclic loading is applied, hysteresis (a phase lag) occurs, leading to a dissipation of mechanical energy; (v) acoustic waves experience attenuation; (vi) rebound of an object following an impact is less than 100%; (vii) during rolling, frictional resistance occurs [151]. In this section principal viscoelastic features of fluids of interest are presented. Fuller description of non-Newtonian phenomena are given by Bird et al. [26, 29] and Bird and Wiest [25] and Tanner [207, 206]. We select here the items of greatest concern for the understanding of visco-elastic effects.

#### 1.3.1 Viscoelasticity

Viscoelasticity is the property of materials that exhibit both viscous and elastic characteristics when undergoing deformation. Viscous materials, like honey, resist shear flow and strain linearly with time when a stress is applied. Elastic materials strain instantaneously when stretched and just as quickly return to their original state once the stress is removed. Viscoelastic materials have elements of both of these properties and, as such, exhibit time dependent strain. Whereas elasticity is usually the result of bond stretching along crystallographic planes in an ordered solid, viscosity is the result of the diffusion of atoms or molecules inside an amorphous material [152, 151].

All materials exhibit some viscoelastic response. In common metals such as steel or aluminum, as well as in quartz, at room temperature and at small strain, the behavior does



not deviate much from linear elasticity. Synthetic polymers, wood, and human tissue as well as metals at high temperature display significant viscoelastic effects. In some applications, even a small viscoelastic response can be significant. To be complete, an analysis or design involving such materials must incorporate their viscoelastic behavior. Knowledge of the viscoelastic response of a material is based on measurement. Some examples of viscoelastic materials include amorphous polymers, semicrystalline polymers, biopolymers, metals at very high temperatures, and bitumen materials.

Unlike purely elastic substances, a viscoelastic substance has an elastic component and a viscous component. The viscosity of a viscoelastic substance gives the substance a strain rate dependent on time. Purely elastic materials do not dissipate energy (heat) when a load is applied, then removed. However, a viscoelastic substance loses energy when a load is applied, then removed. Hysteresis is observed in the stress-strain curve, with the area of the loop being equal to the energy lost during the loading cycle. Since viscosity is the resistance to thermally activated plastic deformation, a viscous material will lose energy through a loading cycle. Plastic deformation results in lost energy, which is uncharacteristic of a purely elastic material's reaction to a loading cycle. Specifically, viscoelasticity is a molecular rearrangement. When a stress is applied to a viscoelastic material such as a polymer, parts of the long polymer chain change position. This movement or rearrangement is called creep. Polymers remain a solid material even when these parts of their chains are rearranging in order to accompany the stress, and as this occurs, it creates a back stress in the material. When the back stress is the same magnitude as the applied stress, the material no longer creeps. When the original stress is taken away, the accumulated back stresses will cause the polymer to return to its original form. The material creeps, which gives the prefix visco-, and the material fully recovers, which gives the suffix -elasticity.

### **1.3.2 Shear rheology of non-Newtonian fluids**

Probably the single most important characteristic of polymeric liquids is the fact that they have "shear-rate dependent" or "non-Newtonian" viscosity. In a non-Newtonian fluid, the relation between the shear stress and the strain rate is non-linear, and can even be time-dependent. Therefore a constant coefficient of viscosity cannot be defined. Depending on the change of strain rate versus stress inside a material (Fig. 1.1) the viscosity can be

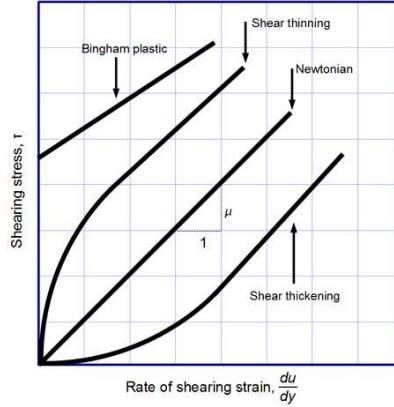


Fig. 1.1: Different types of responses (stress) to a change in strain rate  $\dot{\gamma}$

categorized as having a linear, non-linear, or plastic response. When a material exhibits a linear response it is categorized as a Newtonian material [1]. In this case the stress is linearly proportional to the strain rate. If the material exhibits a non-linear response to the strain rate, it is categorized as Non-Newtonian fluid. There is also an interesting case where the viscosity decreases as the shear/strain rate remains constant. A material which exhibits this type of behavior is known as thixotropic [151]. In addition, when the stress is independent of this strain rate, the material exhibits plastic deformation [151]. Many viscoelastic materials exhibit rubber like behavior explained by the thermodynamic theory of polymer elasticity. In reality all materials deviate from Hooke's law in various ways, for example by exhibiting viscous-like as well as elastic characteristics. Viscoelastic materials are those for which the relationship between stress and strain depends on time. In steady simple shear, having a velocity vector  $\mathbf{u} = (\dot{\gamma}y, 0, 0)$ , it may be shown that any incompressible simple fluid will have a stress tensor with, in general, four nonzero components:

$$\begin{bmatrix} \sigma_{22} + N_1 & \sigma_{12} & 0 \\ \sigma_{12} & \sigma_{22} & 0 \\ 0 & 0 & \sigma_{22} - N_2 \end{bmatrix} \quad (1.1)$$

As a result of the incompressibility, the stress is undetermined to within addition of an isotropic pressure term. For a Newtonian fluid,  $N_1 = N_2 = 0$  and  $\sigma_{12}/\dot{\gamma} = \mu$ . In a viscoelastic fluid, however, these three quantities may vary with  $\dot{\gamma}$ .

Other important characteristics of viscoelastic fluids are normal stress effects, secondary flows, elastic effects such as extrudate or die swell, tubeless siphon, contraction flow, elastic recoil, cavity flows. Many other examples with comprehensive explanations could be found in Ref. [26, 29, 25]

## 1.4 Organization of the dissertation

### 1.4.1 Description

The present dissertation is organized into eight different chapters including the present introduction which is the first chapter.

Chapter 2 reports a brief overview of the constitutive models for viscoelastic fluids including differential and integral constitutive models and justify the reason for selecting FENE family model for this project.

Chapter 3 is devoted to high-order numerical methods. Finite element, finite difference and finite volume methods are extensively described and covered in the monograph of Owens and Phillips [173]. Necessary details associated with the Legendre spectral element method are recalled.

Chapter 4 comprises three different sections. The first part corresponds to the classical matrix logarithm formulation (CMLF). In this part, we show that although the use of log conformation tensor can be helpful to preserve symmetric positive definiteness of the conformation tensor, it is also mandatory for FENE family to satisfy the boundness of the conformation tensor. Thus, we show that applying classical matrix logarithm formulation for the FENE family is not enough to enforce stability. The second part of this discussion deals with a new extension matrix logarithm formulation (EMLF) algorithm developed by us in order to remove instabilities in computational viscoelastic flows. This work has been reported in a published paper [104]. In the last part of this chapter a possible mathematical formulation that enforces stability as much as possible is discussed. This formulation is an enhanced format of hyperbolic tangent of the conformation tensor.

Chapter 5 is devoted to apply this new extended matrix logarithm formulation for complex geometries such as: 4:1 contraction and contraction-expansion flow. This work is submitted to the journal of non-Newtonian fluid mechanics in November 2010.

Chapter 6 deals with the concept of linear instability analysis to determine the sensitivity of the flow to the infinitesimal perturbations. The result of which are submitted to the Computers and Fluids in August 2010.

Chapter 7 focuses on applying filter-based stabilization method originally proposed by Boyd [32]. It also presents a novel methodology to implement the so-called mesh transfer technique.

Finally chapter 8 summarizes the conclusions of the different aspects of the work reported in the dissertation. Outlook and perspectives are finally proposed.

# Chapter 2

---

## Constitutive models for viscoelastic flows

The usefulness of a constitutive equation lies in its ability to predict viscoelastic flows accurately in a wide range of deformation histories for as many polymer systems with as few adjustable parameters as possible. To simulate viscoelastic flows processing realistically, this equation must be able to describe material behavior from the linear to the nonlinear regime. Further, since the nonlinear behavior of melts in shear and in the extensional deformations-uniaxial, biaxial and planar, can strongly differ from each other, it is particularly important that the constitutive equation be capable of simultaneous description of these types of deformations.

### 2.1 Introduction

In order to simulate the flow of incompressible viscous Newtonian fluids, the Navier-Stokes equations are solved. More information is needed to deal with the flows of non-Newtonian fluids for which the expression for the extra-stress tensor cannot be reduced to a simple linear relationship with the rate-of-deformation tensor. Constitutive models consist of a set of hypotheses and simplifications about the sources of stress like the molecular or structural forces and motions. Constitutive equations are the mathematical expression of the theoretical models.

A fluid dynamicist analyzing the flow of a non-Newtonian fluid is faced with a formidable task. Before the numerical analysis can begin, a constitutive equation must be selected to describe the properties of the fluid. Constitutive equations fall into two general categories: (i) integral constitutive equations and (ii) differential constitutive equations. Integral constitutive equations involve time integrals over the kinematic history of fluid elements, and they have the associated disadvantage that their use requires tracking the trajectories of those fluid elements. Nonetheless, they are capable of describing many material proper-

ties. Differential constitutive equations do not, in general, require the tracking of fluid elements, so that they are easier to solve numerically. However, many modes of a differential constitutive equation are usually required to describe material properties accurately (i.e., the stress is given as a sum of tensors, each of which is governed by a replicate of the differential constitutive equation with different values for the parameters, and each replicate is called a "mode" [233, 147]). This compounds the difficulty of the numerical analysis of a flow by dramatically increasing the number of unknowns.

Like Newtonian fluids, the flow of complex fluids is governed by the conservation of mass and momentum equations. The momentum equation is modified with respect to the Newtonian case in order to account for the additional contribution due to the non-Newtonian stress tensor. The Cauchy stress is split in a Newtonian and a polymeric part. The Cauchy stress tensor is given by the following equation:

$$\boldsymbol{\sigma} = \boldsymbol{\tau} - p\mathbf{I} + 2R_\mu\mathbf{D} \quad (2.1)$$

The symbols  $\boldsymbol{\sigma}$ ,  $\mathbf{I}$  and  $\mathbf{D}$  are respectively the Cauchy stress, identity and rate of deformation tensors.  $\boldsymbol{\tau}$  is the non-Newtonian stress and  $-p\mathbf{I} + 2R_\mu\mathbf{D}$  is the Newtonian stress. The rate of deformation tensor is defined by:

$$\mathbf{D} = \frac{1}{2}(\nabla\mathbf{u} + (\nabla\mathbf{u})^T) \quad (2.2)$$

$\mathbf{u}$  is the velocity field with the superscript  $T$  indicating the transpose. The parameters  $R_\mu$  is the ratio of Newtonian solvent viscosity,  $\mu_N$ , to the total viscosity,  $R_\mu = \mu_N/\mu_t$ , where  $\mu_t = \mu_N + \mu_p$ . The symbol  $\mu_p$  represents the polymeric viscosity.

## 2.2 Differential constitutive models

Ideally, one wants a simple differential constitutive equation that can describe a large number of material properties with a small number of modes. If that constitutive equation can be derived from some type of molecular theory, then the situation is even better because it may be possible to assign some physical significance to the parameters that appear in the equation. In this section the most commonly used differential constitutive equations, namely, the dumbbell models are presented.

### 2.2.1 Dumbbell models

The most simple kinetic theory model for a dilute solution of linear flexible polymers consists of a Hookean dumbbell, that is two beads connected by a Hookean spring, (Fig. 2.1) suspended in an incompressible Newtonian fluid [26]. The beads represent molecular segments of several monomers and the spring describe the entropic effects to which the end-to-end vector,  $\mathbf{R}$ , of the polymer is subject. The linear (Hookean) spring force is realistic only for small deformations from the equilibrium (Gaussian distribution) and puts no limit to the extent to which the dumbbell can be stretched. An approach which corrects this unphysical behaviour and seems to play an important role in non-linear rheological phenomena is the idea of finite extensibility [26]. Dumbbell models with finitely extensible non-linear elastic (FENE) spring forces are now widely used in numerical flow calculations, both in the classical approach via a closed constitutive equation, and in a new approach in which the polymeric stress tensor is computed via Brownian dynamics (BD) simulations [126, 25].

Dumbbell models are very crude representations of polymer molecules. Too crude to be of much interest to a polymer chemist, since it, in no way, accounts for the details of the molecular architecture. It certainly does not have enough internal degrees of freedom to describe the very rapid motions that contribute, for example, to the complex viscosity at high frequencies. On the other hand, the elastic dumbbell is orientable and stretchable, and these two properties are essential for the qualitative description of steady-state rheological properties and those involving slow changes with time. For dumbbell models one can go through the entire program of endeavor from molecular model to fluid dynamics for illustrative purposes, in order to point the way towards the task that has ultimately to be performed for more realistic models. Dumbbell models must, to some extent then, be regarded as mechanical playthings, somewhat disconnected from the real world of polymers. When used intelligently, however, they can be useful pedagogically and very helpful in developing a qualitative understanding of rheological phenomena [119]. Dumbbell models, on the other hand, are relatively straightforward for application to the numerical solution of flow problems, and have the virtue of being the simplest molecularly inspired model that retains the generic viscoelastic features of flow-induced anisotropy through re-orientation and stretch, coupled with a diffusion-based relaxation to an isotropic equilibrium state [160].

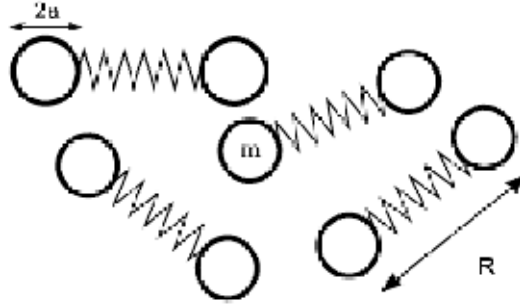


Fig. 2.1: The polymers are modelled by dumbbells connected by spring

## 2.2.2 Linear elastic dumbbell models

In this section two practical linear elastic dumbbell models, Oldroyd-B and Upper Convected Maxwell model will be introduced. Even though these two models can predict qualitatively some features of a class of dilute polymer solution called Boger fluids characterized by an almost constant shear viscosity, they present drawback such as the prediction of an infinite value of the elongational viscosity at a finite value of the extension rate. Another shortcoming in describing correctly the behavior of more general dilute solutions is the inability to produce shear thinning effects. Several mechanisms not embedded in the linear dumbbell model are responsible for shear thinning: finite extensibility, hydrodynamic interaction, configuration dependent friction coefficient, excluded volume effects and internal viscosity.

### 2.2.2.1 Oldroyd-B model

The simplest constitutive equations suitable for modeling the behavior of dilute polymeric solution under general flow conditions are those of the Oldroyd type. In particular, the Oldroyd-B model, derived by Oldroyd [163] in 1950, is an empirical expression generalizing the linear viscoelastic equation by writing the stress/strain relation in tensorial form and satisfying certain admissibility criteria [163, 162, 55, 25, 26]. The Oldroyd-B model is also derivable from a molecular model consisting of a suspension of Hooken dumbbells in a Newtonian solvent, and this is the approach we choose to present the model in this section. The Oldroyd-B model [163] may be derived by considering a suspension of



Hookean dumbbells, in which the spring force  $\mathbf{F}$  is directly proportional to the extension of the spring:

$$\mathbf{F} = G\mathbf{R} \quad (2.3)$$

The beads, which define the dumbbell ends, move under the action of: a Stokes drag from the solvent, Brownian motion and the spring force. Because of the stochastic nature of Brownian motion, the macroscopic properties of the fluid are derived from ensemble averages (denoted by  $\langle \dots \rangle$ ). The polymeric stress is given by:

$$\boldsymbol{\tau}^p = \langle \mathbf{R}\mathbf{F} \rangle = G \langle \mathbf{R}\mathbf{R} \rangle \equiv G\mathbf{C} \quad (2.4)$$

where  $\mathbf{C}$  is called the conformation tensor. Instead of solving an equation for extra stress tensor we solve for the conformation tensor and afterwards from the value of which we obtain the viscoelastic stress. Its evolution is governed by the equation:

$$\mathbf{C} + \lambda \overset{\nabla}{\mathbf{C}} = \mathbf{I} \quad (2.5)$$

with a relaxation time defined as  $\lambda = \zeta/G$ , where  $\zeta$  is the drag coefficient ( $6\pi\mu_N a$ ) acting on an isolated bead, the diameter of bead is  $2a$  (see Fig. 2.1). The cases  $\lambda = 0$  ( $\mathbf{C} = \mathbf{I}$ ) and  $G = 0$  ( $\boldsymbol{\tau}^p = 0$ ) correspond to a Newtonian fluid, and the case  $\eta_s = 0$  ( $\lambda = 0$ ) is the Upper-Convected Maxwell model (section 2.2.2.2). The time derivative in Eq. (2.5) is the upper-convected derivative, defined as:

$$\overset{\nabla}{\mathbf{C}} = \frac{\partial}{\partial t} \mathbf{C} + \mathbf{u} \cdot \nabla \mathbf{C} - \nabla \mathbf{u} \cdot \mathbf{C} - \mathbf{C} \cdot (\nabla \mathbf{u})^T \quad (2.6)$$

It is the failure of the molecules to deform with fluid elements that generates elastic stress in the fluid. The Oldroyd-B model is, in shear flows, a quantitatively good model for Boger fluids. Nevertheless, its simplicity means that in general it cannot capture the full nature of a polymeric fluid. For example, it has only one relaxation time (whereas real fluids have a relaxation spectrum), and does not contain shear-thinning effects. More seriously, in extensional flows it can produce an unbounded extensional viscosity because of the linear spring behaviour of the dumbbells. In a real fluid, the molecules become fully extended and the viscosity saturates.

### 2.2.2.2 Upper-Convected Maxwell model

The Upper-Convected Maxwell fluid (UCM) [168, 125, 26] is the high-concentration limit of an Oldroyd-B fluid. As such, it is used as a model for polymer melts. It is given by:

$$\boldsymbol{\tau} = -p\mathbf{I} + \boldsymbol{\tau}^p \quad (2.7)$$

$$\boldsymbol{\tau}^p + \lambda \overset{\nabla}{\boldsymbol{\tau}}^p = \mathbf{I} \quad (2.8)$$

The relation between  $\boldsymbol{\tau}^p$  and  $\mathbf{C}$  is given by Eq. (2.4). It has all the disadvantages of the Oldroyd-B fluid: unbounded extensional viscosity, single relaxation time, zero  $N_2$  (Eq. (1.1)) and constant shear viscosity. However, because it has one less parameter, it is mathematically even more simpler than the Oldroyd-B fluid.

### 2.2.2.3 Other modification of the Oldroyd-B model

Several other modifications of the Oldroyd-B model have been proposed. We add an extra term to (Eq. 2.5) to produce any or all of shear-thinning, or a bounded extensional viscosity. The Oldroyd-B model may be expressed as:

$$\boldsymbol{\tau}^p + \lambda \overset{\nabla}{\boldsymbol{\tau}}^p = 2(1 - R_\mu)\mathbf{D} \quad (2.9)$$

Without violating any of fluid assumptions we may add an extra term:

$$\boldsymbol{\tau}^p + \lambda \overset{\nabla}{\boldsymbol{\tau}}^p + \mathbf{f}(\boldsymbol{\tau}^p, \mathbf{D}) = 2(1 - R_\mu)\mathbf{D} \quad (2.10)$$

Some of the popular choices for  $\mathbf{f}$  are:

#### Johnson-Segalman [106, 114]

$$\mathbf{f}(\boldsymbol{\tau}^p, \mathbf{D}) = \alpha\lambda(\mathbf{D} \cdot \boldsymbol{\tau}^p + \boldsymbol{\tau}^p \cdot \mathbf{D}) \quad (2.11)$$

$\alpha$  is an adjustable parameter. When  $\alpha$  is set to zero the Johnson-Segalman model reverts to the upper-Convected Maxwell model (UCM). As  $\alpha$  increases, stresses decrease from the UCM predictions. We define that strain softening occurs whenever stress levels fall below the UCM predicted values.

**Phan-Thien Tanner [178, 153]**

Phan-Thien Tanner (PTT) model is derived from the evolution equation of the configuration distribution function. The stress tensor is related to the second moment of this function. For the PTT model the destruction probability depends on the instantaneous stress. This leads to the following equation:

$$\mathbf{f}(\boldsymbol{\tau}^p, \mathbf{D}) = \xi \lambda (\mathbf{D} \cdot \boldsymbol{\tau}^p + \boldsymbol{\tau}^p \cdot \mathbf{D}) + [\epsilon (\text{tr}(\boldsymbol{\tau}^p)) - 1] \boldsymbol{\tau}^p \quad (2.12)$$

where  $\xi$  and  $\epsilon$  are adjustable parameters for Phan-Thien Tanner model.

**Giesekus [87, 86]**

Giesekus has introduced a slight modification to the Oldroyd-B equation by adding a quadratic term in stress in order to allow for the extensional viscosity to grow with the extension rate while remaining finite. This is a generalisation of the UCM fluid (using an anisotropic drag force), so we set  $\eta_s = 0$  and use:

$$\mathbf{f}(\boldsymbol{\tau}^p, \mathbf{D}) = \alpha \lambda \boldsymbol{\tau}^p \cdot \boldsymbol{\tau}^p \quad (2.13)$$

where  $0 \leq \alpha \leq 1$  The detailed expressions are given in [125].

**2.2.3 Nonlinear elastic dumbbell model**

For strong deformations of the macromolecule the pure Hookean law of Eq. (2.3) for the internal force is no longer valid. In order to introduce a finite extensibility of the dumbbell the FENE (finitely extendable nonlinear elastic) model [26] has been developed. The problem of infinite extensional viscosity for finite extension rate in the Oldroyd-B fluid is caused by unbounded extension of the dumbbells. Thus, a sensible modification of the model is to use a nonlinear force law and limit the maximum extension of the springs. The original empirical FENE spring force is given by:

$$\mathbf{F} = \frac{H}{1 - \frac{R^2}{b^2}} \mathbf{R} \quad (2.14)$$

and was first proposed for dumbbells by Warner [228]. In Eq. (2.14)  $H$  is the spring constant,  $\mathbf{R}$  is the three-dimensional connector vector of the beads,  $R^2 = \mathbf{R} \cdot \mathbf{R}$  and  $b$  is the maximum possible spring length. It exhibits, for small extensions the expected linear

behaviour and a finite length  $b$  in the limit of an infinite force. The price to pay for the non-linearity of the spring force is that no closed constitutive equation for the polymeric stress tensor exists and no simple analytical solutions are possible [26]. Because of the nonlinearity in  $\mathbf{F}$ , a closed evolution equation for  $\langle \mathbf{R}\mathbf{R} \rangle$  (and hence for the stresses) is not available; a closure approximation is needed.

### 2.2.3.1 FENE-P model

If the average length of all dumbbells is taken to define  $R$ , the force law  $f(R)$  is replaced by  $f(\langle R \rangle)$ , giving a pre-averaging approximation:

$$\mathbf{F} = H\mathbf{R}f(\langle R \rangle) \quad (2.15)$$

which leads (Peterlin [177]) to the FENE-P model:

$$\tau^p = \langle \mathbf{R}\mathbf{F} \rangle = H \langle \mathbf{R}\mathbf{R} \rangle f(\langle R \rangle) \quad (2.16)$$

and therefore:

$$\tau = -p\mathbf{I} + 2\eta_s\mathbf{D} + Hf(R)\mathbf{C} \quad (2.17)$$

$$\mathbf{C} + \frac{\lambda}{f(R)}\overset{\nabla}{\mathbf{C}} = \frac{\lambda}{f(R)}\mathbf{I} \quad (2.18)$$

where, in this case:

$$R^2 = tr(\mathbf{C}) \quad (2.19)$$

$$f(R) = \frac{1}{1 - \frac{R^2}{b^2}} \quad (2.20)$$

The FENE-P model improves the behaviour of the model in extension, and gives a shear-thinning viscosity. It is therefore worse at describing shear flows of Boger fluids.

### 2.2.3.2 FENE-CR

In this model, the extension behaviour remains of FENE type, but the evolution of the quantity  $\mathbf{C}$  is altered from the FENE-P equation 2.18 to give a constant shear viscosity. It becomes (Chilcott and Rallison[46]):

$$\mathbf{C} + \frac{\lambda}{f(R)}\overset{\nabla}{\mathbf{C}} = \mathbf{I} \quad (2.21)$$

where  $f(R)$  is given by Eq. (2.20).

### 2.2.4 Retarded motion expansions

If the motion is weak and slow enough (or, correspondingly, the longest relaxation time is relatively short), any simple fluid may be expanded as a perturbation to the Newtonian limit (Rivlin and Ericksen [187]). The dimensionless parameter for viscoelastic fluids is the Weissenberg number, which is the ratio of the material relaxation time,  $\lambda$ , of viscoelastic fluids to the inertial time,  $L/U$ ,

$$We = \frac{\lambda U}{L} \quad (2.22)$$

If these characteristic times are both small, then the retarded motion expansion will be valid, and the form of the result is independent of the specific constitutive equation used. These equations are known as  $n$ th-order fluids according to how many powers of the small quantity are retained. In particular, the second-order fluid is given in Section 2.2.5.4.

### 2.2.5 Generalized Newtonian and quasi-Newtonian models

Two very important features of polymer solutions are that the steady shear viscosity decreases with increasing shear rate, shear-thinning, and that the elongational viscosity grows with the strain rate, shear-thickening. A Generalized Newtonian fluid is an idealized fluid for which the shear stress,  $\boldsymbol{\tau}$ , is a function of shear rate,  $\dot{\gamma}$ , at the particular time, but not dependent upon the history of deformation

$$\boldsymbol{\tau} = f(\dot{\gamma}) \quad (2.23)$$

The class of Generalized Newtonian fluids to be considered is characterized by the constitutive relation:

$$\eta = \eta(\dot{\gamma}) \quad (2.24)$$

and the requirement that the viscosity,  $\eta$ , and the derivative of  $\eta(\dot{\gamma})$  are uniformly bounded from above and below [48]:

$$0 < m_0 \leq \eta(\dot{\gamma}) \leq M_0 < \infty \quad (2.25)$$

$$0 < m_1 \leq (\eta(\dot{\gamma}))' \dot{\gamma} \leq M_1 < \infty \quad (2.26)$$

Typically, the viscosity is also a decreasing function. Generalized Newtonian fluids do not exhibit memory-effects. So this type of fluids are not viscoelastic. The most commonly used types of Generalized Newtonian fluids are:

### 2.2.5.1 Carreau-Yasuda

Carreau-Yasuda [26] fluid is a type of Generalized Newtonian fluid where the viscosity,  $\eta$ , depends upon the shear rate,  $\dot{\gamma}$ , by the following equation:

$$\frac{\eta - \eta_\infty}{\eta_0 - \eta_\infty} = [1 + (\lambda\dot{\gamma})^a]^{\frac{n-1}{n}} \quad (2.27)$$

where  $\lambda$  is a time constant and  $n$  the power law exponent. The parameter  $a$  is dimensionless and describes the transition between the constant viscosity region and the shear thinning one. This model describes pseudoplastic flow with asymptotic viscosities at zero ( $\eta_0$ ) and infinite  $\eta_\infty$  shear rates, and with no yield stress. The case  $n = 1$  corresponds to the Newtonian fluid.

### 2.2.5.2 Power Law

A Power law [26, 97] fluid is a type of Generalized Newtonian fluid for which the viscosity is given by:

$$\eta = m\dot{\gamma}^{n-1} \quad (2.28)$$

where  $m$  and  $n$  are two parameters. This mathematical relationship is useful because of its simplicity, but only approximately describes the behaviour of a real non-Newtonian fluid. For example, if  $n$  were less than one, the power law predicts that the effective viscosity would decrease with increasing shear rate indefinitely, requiring a fluid with infinite viscosity at rest and zero viscosity as the shear rate approaches infinity, but a real fluid has both a minimum and a maximum effective viscosity that depend on the chemistry at the molecular level. Therefore, the power law is only a good description of fluid behaviour across the range of shear rates to which the coefficients were fitted. Power-law fluids can be subdivided into three different types of fluids based on the value of their flow behaviour index:

If  $n < 1$ , the fluid is shear-thinning or pseudo-plastic. If  $n = 1$  and  $m = \mu$ , the fluid is Newtonian. If  $n > 1$  the fluid is shear-thickening or dilatant.

Pseudoplastic, or shear-thinning fluids have a lower apparent viscosity at higher shear rates, and are usually solutions of large, polymeric molecules in a solvent with smaller molecules. It is generally supposed that the large molecular chains tumble at random and affect large volumes of fluid under low shear, but that they gradually align themselves in

the direction of increasing shear and produce less resistance. A common household example of a strongly shear-thinning fluid is styling gel, which primarily composed of water and a fixative such as a vinyl acetate/vinylpyrrolidone copolymer (PVP/PA).

A Newtonian fluid is a power-law fluid with a behaviour index of 1, where the shear stress is directly proportional to the shear rate:

$$\boldsymbol{\tau} = \mu \dot{\boldsymbol{\gamma}} \quad (2.29)$$

These fluids have a constant viscosity,  $\mu$ , across all shear rates and include many of the most common fluids, such as water, most aqueous solutions, oils, corn syrup, glycerine, air and other gases.

Dilatant, or shear-thickening fluids increase in apparent viscosity at higher shear rates. They are rarely encountered, but one common example is an uncooked paste of cornstarch and water. Under high shear the water is squeezed out from between the starch molecules, which are able to interact more strongly. While not strictly a dilatant fluid, Silly Putty is an example of a material that shares these viscosity characteristics.

### 2.2.5.3 Cross fluid

A Cross fluid [56] is a type of Generalized Newtonian fluid whose viscosity depends upon shear rate according to the following equation:

$$\frac{\eta - \eta_\infty}{\eta_0 - \eta_\infty} = \frac{1}{1 + (\lambda \dot{\boldsymbol{\gamma}})^{1-n}} \quad (2.30)$$

At low shear rate (  $\lambda \dot{\boldsymbol{\gamma}} \ll 1$  ), Cross fluids behave as Newtonian fluids and at high shear rate (  $\lambda \dot{\boldsymbol{\gamma}} \gg 1$  ) as power law fluids.

### 2.2.5.4 Second-order fluid

The second-order fluid (Coleman and Noll [50]) is given by:

$$\boldsymbol{\tau} = -p\mathbf{I} + 2\eta\mathbf{D} + 4\Psi_2\mathbf{D} \cdot \mathbf{D} - \Psi_1\overset{\nabla}{\mathbf{D}} \quad (2.31)$$

If all three material properties  $\eta$ ,  $\Psi_1$  and  $\Psi_2$  are allowed to be functions of  $\dot{\boldsymbol{\gamma}}$  this becomes the CEF equation (Criminale, Ericksen and Filbey [54, 56]). This is the simplest model

to allow exact correspondence with all the observed viscometric functions.

The second-order fluid is a second-order asymptotic approximation about the state of the rest of a viscoelastic fluid. Hence, the applicability of the second-order fluid is restricted to slow and slowly varying flow fields. In other flow situations the second-order fluid fails completely. There are even some situations in which the "second-order fluid" indicates its inapplicability [26, 108, 6, 34, 88].

## 2.3 Integral constitutive models

### 2.3.1 Doi-Edwards model

Understanding of the rheological behavior of entangled polymers is based on the theory of Doi and Edwards [61, 62, 63, 64, 65] which is now widely accepted as fundamental. Successes of the theory include the prediction of the plateau modulus of linear viscoelasticity, and the so-called 'damping function' for the nonlinear response to a step strain. Another positive aspect of the theory is the 'natural' occurrence of a nonzero second normal stress difference in shear. For a long time, a negative feature of the basic theory has been the prediction of excessive shear thinning. In fact the theory predicts an intrinsic instability for moderately fast shear flows, which is not in agreement with the observed obedience of the Cox-Merz rule, and which has long prevented use of the Doi-Edwards constitutive equation in numerical simulation of complex flows. That feature, however, has recently been improved upon by accounting for the fact that flow sweeps chains one past the other, thus effectively removing topological constraints (Marrucci [146]).

The Doi-Edwards model is a specific example of a K-BKZ fluid (Kaye [111], Bernstein et al. [24]), for which:

$$\boldsymbol{\tau} = \int_{-\infty}^t \left[ \frac{\partial}{\partial I_1} X(I_1, I_2, t-t') \mathbf{C}^{-1}(t, t') - \frac{\partial}{\partial I_2} X(I_1, I_2, t-t') \mathbf{C}(t, t') \right] dt' \quad (2.32)$$

$\mathbf{C}(t, t')$  is the strain tensor accumulated between past time  $t'$  and current time  $t$ , and  $I_1$  and  $I_2$  are its two invariants:  $I_1 \equiv \text{tr}(\mathbf{C})$  and  $I_2 \equiv \text{tr}(\mathbf{C}^{-1})$ .  $X$ ; is a general damping function, which defines a specific model within the class. The Doi-Edwards model describes melts



in which individual molecules move by reptating along their length. This is given by:

$$X(I_1, I_2, s) = \chi(I_1, I_2)m(s) \quad (2.33)$$

$$m(s) = G \sum_{p \text{ odd}}^{\infty} \frac{8}{\pi^2} \frac{1}{p^2} \frac{1}{\lambda_p} \exp(-s/\lambda_p) \quad \lambda_p = \lambda_1/p^2 \quad (2.34)$$

and an approximate form for  $\chi$  (Currie [57]) by:

$$\chi = \frac{5}{2} \ln(J - 1) - 4.87, \quad J = I_1 + 2(I_2 + \frac{13}{4})^{1/2} \quad (2.35)$$

This model predicts a very high level of shear-thinning, even higher than that observed in real polymer melts.

### 2.3.2 K-BKZ

Another class of equations derived from continuum mechanics considerations is the so-called K-BKZ (after Kaye [111], Bernstein, Kearsley and Zapas [24]) family for polymer melts and concentrated solutions. It has been obtained from concepts of rubber elasticity theory [125]:

$$\boldsymbol{\tau} = \int_{-\infty}^t [2 \frac{\partial w}{\partial I_1} \mathbf{C}^{-1}(t, t') - 2 \frac{\partial w}{\partial I_2} \mathbf{C}(t, t')] dt' \quad (2.36)$$

where  $I_1 = \text{tr}(\mathbf{C}^{-1})$  and  $I_2 = \frac{1}{2}[(\text{tr}(\mathbf{C}^{-1}))^2 - \text{tr}(\mathbf{C}^{-2})]$  are the first and second invariants of  $\mathbf{C}^{-1}$ . A particular constitutive equation is obtained by selecting a given expression for  $w(I_1, I_2, t - t')$  with a few nonlinear parameters. The kernel  $w$  comes from the hypothesis that the elastic free energy  $W_e$ , which is a function of the elastic strain imposed on the fluid, is a history integral over a function of  $I_1$  and  $I_2$  and  $t - t'$ :  $W_e = \int_{-\infty}^t w(I_1, I_2, t - t') dt'$ . A simpler version called the separable or factorized K-BKZ equation is obtained when  $\boldsymbol{\tau}$  is expressed in the form:

$$\boldsymbol{\tau}^e = \int_{-\infty}^t m(t - t') [2 \frac{\partial W(I_1, I_2)}{\partial I_1} \mathbf{C}^{-1}(t, t') - 2 \frac{\partial W(I_1, I_2)}{\partial I_2} \mathbf{C}] dt' \quad (2.37)$$

The coefficients of the two tensors  $\mathbf{C}^{-1}$  and  $\mathbf{C}$  in the previous integrals are functions of time and invariants of  $\mathbf{C}^{-1}$  are determined from a series of step-strain experiments. This type of equation enables effects like stress growth and relaxation to be reproduced qualitatively but is inaccurate for processes involving reversing double-step strains and elastic recovery.

Deriving more complex constitutive equations enables more understanding of the fluid behavior to be obtained. But, such equations may be tedious to implement and time-consuming for the numerical simulation of complex viscoelastic flows. It is sometimes preferable to resort to simpler models in differential or integral form adapted to the rheological data available for a given fluid by incorporating additional empirical parameters. For other integral differential equations such as Rivlin Sawyer, Wagner's equation, readers are referred to Ref. [173, 58].

## 2.4 Selecting a constitutive equation

In this chapter a brief overview of the constitutive models for viscoelastic fluids including differential and integral constitutive models is reported. The most commonly used models for numerical simulation of non-Newtonian fluids are presented here and a non exhaustive list of references is given in the bibliography [26, 29, 125, 108, 65, 58] The selection of a constitutive equation must be carried out according to four main criteria: the type of flow (mostly shearing or extensional or combination of both, steady or transient, with strain reversal), the type of material (dilute or concentrated solution or melt, linear or branched polymers) and the numerical method to be used which may impose constraints on the equation form (differential or integral) or require that no singularities or that double values of stress or deformation are present for convergence. The number of relaxation modes that can be handled is also of importance in the choice of the equation since it has a direct impact on computer requirements. The last criterion concerns the type of phenomenon that one is expecting to describe and the quantitative aspect of the prediction. It is not easy to estimate a priori what should be the equation of choice for a complex flow like e.g. the flow through an abrupt contraction, but one may determine what essential features observed in simple flows should be present in the chosen model.

From numerical point of view for calculation of complex fluids, differential constitutive equations for the stress tensor are generally preferred over those of the integral type. Among differential constitutive models FENE-P due to its features is chosen for this study. FENE-P is one of few polymer models that can be used in fluid dynamics simulations since it removes the need of statistical averaging at each grid point at any instant in time. It is demonstrated to be able to capture some of the most important polymeric flow behaviors

such as polymer turbulence drag reduction and shear thinning. It is the most commonly used polymer model that can be used in a turbulence simulation since turbulence DNS is already extremely expensive. Disadvantage of this model is due to its simplifications, FENE-P is not able to show the hysteresis effects that polymers have, which to the contrast the FENE model is capable of. Moreover, Oldroyd-B is also considered as a particular case of the FENE-P model when  $b \rightarrow \infty$ .



# Chapter 3

---

## Numerical methods for simulating viscoelastic flows

The numerical solution to a system of partial differential equations involves two stages. In the first stage the governing equations are discretized in a consistent fashion on some mesh using a convergent discrete representation of the solution, i.e. the discrete approximation converges to the exact solution of the problem as the mesh is refined. Note that, for the system of equations governing the flow of viscoelastic materials, it is not known a priori whether this property is satisfied by a given discretization. In the second stage the discrete problem, which may be nonlinear, needs to be solved accurately and efficiently [173].

### 3.1 Introduction

In order to obtain a solution of the typical set of partial differential equations presented in Chapter 2, they must be discretized in space and in time. In this chapter we present first a brief review of some of the methods that have been used in the field of computational viscoelastic fluid dynamics for the discretization in space. Relevant references are the books by Crochet, Davies and Walters [55], Owens and Phillips [173] and Chapter 7 of Ref. [101]. Special emphasis will be made on the spectral element method that has been used to carry out all the simulations that are reported in the following chapters.

### 3.2 Space discretization methods

The objective of this section is to provide the reader with a rapid overview of the main groups of discretization methods at hand to simulate the viscoelastic flows of interest in this dissertation. This overview aims at highlighting the advantages and drawbacks

associated with each group of methods, in order to justify a priori the choice of a spectral element method in relation with the physical problems to be investigated.

### 3.2.1 Finite difference methods

The finite difference method (FDM) was among the first numerical methods applied to the numerical solution of differential equations. It was first utilized by Euler, probably in 1768. It is also the easiest method to use for simple geometries. The FDM is directly applied to the differential form of the governing equations. The principle is to employ a Taylor series expansion for the discretization of the derivatives of the flow variables. Local expansions with truncated Taylor series are used to transform the original set of PDEs into a set of algebraic equations. Discretization by FDM leads to systems with banded matrices that are usually solved by iterative techniques. Important advantage of the FDM is its simplicity but, because the method requires a structured grid, the range of application is clearly restricted. Another disadvantage of the FDM is that the conservation is not enforced unless special care is taken. Moreover most of FDM converge as second order method on structured mesh.

FDM has been used for viscoelastic flow simulations by some authors like Olsson [167, 166], Woods [238], Webster [232], Sun et al. [201], Zhao et al. [245]. Demir et al. [59], Asvadurov [18], Saegner et al. [191], Kristek et al. [118], Tomé et al. [210], Ariel [17] and Habetle et al. [95]. Other examples are given in the books of Crochet, Davies and Walters [55, 173] and Owens and Phillips [173].

### 3.2.2 Finite volume methods

The finite volume method (FVM) directly utilizes of the conservation laws-the integral formulation of the mass/momentum and constitutive equations. As pointed out by Hirsch [99] finite volume schemes were introduced by Godunov in 1959 [92]. The FVM discretizes the governing equations by first dividing the physical space into a number of arbitrary polyhedral control volumes. The surface integral appearing in the integral formulation of the conservation equations is then approximated by the sum of the fluxes crossing the individual faces of the control volume. The accuracy of the spatial discretization depends on the particular scheme with which the fluxes are evaluated: cell-centered scheme, cell-

vertex scheme, etc. The main advantages of the FVM are that the spatial discretization is carried out directly in the physical space and that it can be implemented on unstructured grids. This latter property renders the FVM particularly suitable for the treatment of flows in complex geometries. Because of its attractive properties, the FVM is very popular amongst CFD practitioners and in wide use.

In the domain of viscoelastic flows, it has been extensively used during the past decade. Most of them resort to either a pseudo-transient formulation to obtain the steady-state solution as an asymptotic one while an artificial compressibility condition is introduced to satisfy the continuity equation (Chorin-type of FVMs) or are based on the SIMPLER algorithm devised by Patankar [174] or some variants. FVMs are related on the idea of conservative discretization [101]. Up to now, it is probably the method that has enabled the most difficult problems to be tackled, specially if time-dependent phenomena are to be observed. The most recent ones have been carried out by numerous research groups e.g. Mompean et al. [155, 156], Xue et al. [241], Oliveria et al. [164], Fu et al. [80], Sahin et al. [193, 192], Muniz et al. [158], Aguayo et al. [5], Webster et al. [231], Aboubacar et al. [2, 3], Chandio et al. [38], Edussuriya et al. [67], Wachs et al. [225, 224], Al Moatassime et al. [8, 9] and Alves et al. [13].

### 3.2.3 Finite element methods

The finite element method (FEM) is more popular than FVM. It was originally employed for structural analysis only. It was first introduced by Turner et al. in 1956 [212]. About ten years later, researchers started to use the FEM also for the numerical simulation of field equations in continuous media. However, only in the early eighties, did the FEM gain popularity in the solution of the Navier-Stokes equations. The domain is broken into a set of discrete volumes or finite elements that are generally unstructured; in 3D tetrahedral or hexahedral are most often used. Finite elements are such a choice of considerable practical importance, because they enable the implementation of Galerkin approximation with great programming and computational efficiency. The distinguishing feature of FEM is that equations are formulated in a weak form by multiplying a test function before they are integrated over the entire domain. The solution is approximated on each element by a piecewise varying function (usually polynomial) on each element and the result is a set of nonlinear algebraic equations. An important advantage of the FEM is the ability to deal

with arbitrary geometries. The grids are easily refined; each element is simply subdivided. The principal drawback of the FEM, which is shared by any method relying on unstructured grids, is that the matrices of the linearized equations are not as well structured as those for methods based on regular grids, making it more difficult to find efficient solution methods.

FEM is also the most widely used discretization method in the context of viscoelastic flows [55], [22], [144]. Unlike FVMs, they are not restricted to relatively simple geometries and are able to deal with more complex (e.g. no traction or natural) boundary conditions than those of the Dirichlet and Neumann types. FEMs have been mostly applied to two-dimensional (steady and unsteady) problems. Only a few attempts to solve three-dimensional problems have been reported in the literature [157]. Both low-order [133, 115] and high-order [226] approximation polynomials have been used in the literature. Like the two previous methods, low-order FEMs induce numerical dissipation and dispersion that might be detrimental to the observation of physical phenomena. A non exhausted list of references is given in the bibliography. The most recent ones are Baaijens [22], Marchal et al. [144], Chen et al. [44], Mu et al. [157], Choi et al. [47], Carneiro et al. [37], Zang et al. [244], Hao et al. [98], Ganvir et al. [82], Nadau et al. [159], Sandri [194], Lee et al. [127] Machmoum et al. [137], Lu et al. [135], Sun et al. [202].

There are two important issues that need to be addressed in the finite element approximation of viscoelastic flow problems. The first is concerned with the choice of approximation spaces for velocity, pressure and extra-stress. The second issue is concerned with the treatment of the convection term,  $\mathbf{u} \cdot \nabla \boldsymbol{\tau}$ , particularly for large values of the Weissenberg number. Readers can find very interesting discussion about these topics in the fifth chapter of the monograph of Owens and Phillips [173].

### 3.2.4 Lattice Boltzmann method

Nowadays the lattice Boltzmann method (LBM) has established itself as a powerful tool for the simulation of a wide range of physical phenomena. One of its main applications is the field of computational fluid dynamics where it has proved successful to solve the weakly compressible Navier-Stokes equations (see Wolf-Gladrow [237], Succi [200]). This method is not solving directly the macroscopic conservation equations, but rather models



the statistics of collision of particles and offers more modelling freedom. Therefore the LBM is a very good alternative to classical solvers like finite differences, finite volumes, finite elements, or spectral element methods (see respectively Smith [197], Versteeg and Malalasekera [223], Zienkiewicz et al. [246], Deville et al. [60] for example).

One of the great advantages of this method is that it is unconditionally stable. However, it suffers from the statistical noise due to the discreteness of the particles. This method is used by a few authors like Frank et al. [79], Onishi et al. [169], Li et al. [132], Lallemand et al. [123], Ispolatov et al. [103], Malevanets et al. [142], Giraud et al. [89], Malaspina et al. [140, 141]. The readers are referred to the thesis of Malaspina [141] for a comprehensive study of the lattice Boltzmann method for the simulation of viscoelastic fluid flows.

### 3.2.5 Spectral methods

Spectral methods which are based on high-order approximations (usually Chebyshev) polynomials is usually restricted to the study of problems with simple geometries [23, 20]. Their use for complex geometries is not an easy task unless decomposition techniques are introduced, often leading to an arduous implementation of the complete numerical method.

Very few studies of viscoelastic simulation using the spectral method are reported in the literature. We can mention to the works of Pilitsis et al. [182, 181] and Sureshkumar et al. [203]. Sureshkumar and Beris [203] stabilized their spectral method by introducing a stress diffusion term into the constitutive equation. However, in doing so the constitutive equation was effectively modified.

### 3.2.6 Spectral element methods

Spectral element methods combine the ability to treat complicated geometries like the classical (low-order) finite element methods with the accuracy of high-order approximation polynomials encountered in spectral methods. For smooth problems, exponential convergence to the exact solution with mesh refinement is observed. Their relatively difficult implementation is balanced by the appealing ability to resolve correctly high gradient regions. They have been used in the context of viscoelastic flow only recently

[216, 172, 40]. Much effort is presently dedicated in the spectral element community to the critical issue of stabilizing these methods for viscoelastic flows. Successful techniques have been reported very recently for steady-state computations [171, 39]. Stabilizing time-dependent simulations without introducing side effects is still a major source of concern, specially if the constitutive model is embodied in a partial differential equation. The leading practitioners of spectral element methods for viscoelastic fluids are quite identified: Mark Gerritsma, George Karniadakis, Vincent Legat, Robert Owens, Tim Phillips, and their co-author(s). A non exhaustive list of references is given in the bibliography [100, 218, 41, 136, 219, 221, 220, 227, 226, 94, 83, 150, 72, 134, 217].

Spectral element methods are presented in more detail in the following section since it is the method that has been employed for the simulations reported in this thesis.

### 3.3 Legendre spectral element method

In this section, the spectral element method (SEM) based on the Galerkin formulation is presented. It was first proposed by Patera in 1984 [175] in the Chebyshev framework. The SEM is a high-order method which has a very low numerical dissipation and dispersion. As high-order finite element techniques, they can deal with arbitrary geometrical complexity, and are capable of local mesh adaption by either increasing the number of elements (h-refinement) or increasing the polynomial order within elements (p-refinement). For smooth solution spaces, the method provides asymptotically exponential rates of spatial convergence with p-refinement, although in the present work it is the low numerical diffusion and dispersion exhibited by the discretization that is potentially more significant.

After having reviewed the main groups of space discretization methods in Sec. 3.2, we are now in a position to rationalize the choice of the Legendre spectral element method to elucidate the physics associated with the flows studied in the following chapters. Our main requirement is to ensure low numerical dissipation and dispersion which excludes low-order methods such as the FVM and low-order FEM. The complexity introduced by the presence of a free surface and the treatment of the stress-free boundary condition on it, is the second most important choice criterion. In the high-order subgroup of methods, spectral methods are automatically ruled out because of their severe limitations in terms

of capabilities to handle complex geometries. Hence, one is left with spectral element methods or high-order FEM which are both capable of treating the stress-free boundary condition on the free surface as a natural boundary condition embodied into the weak formulation of the problem. In this study we chose spectral element method.

### 3.3.1 Governing equations

In this section we summarize the equations that govern the flow of a uniform dilute polymer solution. The corresponding viscoelastic stress time evolution is described by the FENE-P model. Like Newtonian fluids, the flow of complex fluids is governed by the conservation of mass and momentum equations. The momentum equation is modified with respect to the Newtonian case in order to account for the additional contribution due to the viscoelastic stress tensor. The dimensionless equations are given by the following equations:

$$\nabla \cdot \mathbf{u} = 0 \quad (3.1)$$

$$\frac{\partial \mathbf{u}}{\partial t} + Re(\mathbf{u} \cdot \nabla)\mathbf{u} = \nabla \cdot \boldsymbol{\sigma} \quad (3.2)$$

with:

$$\boldsymbol{\sigma} = \boldsymbol{\tau} - p\mathbf{I} + 2R_\mu\mathbf{D} \quad (3.3)$$

The symbols  $\boldsymbol{\sigma}$ ,  $\mathbf{I}$  and  $\mathbf{D}$  are respectively the Cauchy stress, identity and rate of deformation tensors.  $\boldsymbol{\tau}$  is the viscoelastic stress,  $\mathbf{u}$  is the velocity field and  $p$  is the pressure. The rate of deformation tensor is defined by Eq. (2.2)

The parameter  $Re$  is the Reynolds number ( $Re = \rho UL/\mu_t$ ), where  $\mu_t = \mu_N + \mu_p$ ,  $U$  and  $L$  are the reference velocity and length, respectively. The polymer stress for FENE-P model is defined as:

$$\boldsymbol{\tau} = \frac{1 - R_\mu}{We} \frac{1}{1 - (tr(\mathbf{C})/b^2)} \left( \mathbf{C} - \frac{(1 - \frac{tr(\mathbf{C})}{b^2})}{K} \mathbf{I} \right) \quad (3.4)$$

where  $\mathbf{C}$  is the conformation tensor, which satisfies the following differential equation:

$$We \left( 1 - \frac{tr(\mathbf{C})}{b^2} \right) \left( \frac{D\mathbf{C}}{Dt} - \mathbf{C} \cdot (\nabla \mathbf{u})^T - \nabla \mathbf{u} \cdot \mathbf{C} \right) + \mathbf{C} = \frac{(1 - \frac{tr(\mathbf{C})}{b^2})}{K} \mathbf{I} \quad (3.5)$$

and  $K$  is defined as:

$$K = 1 - \frac{3}{b^2} \quad (3.6)$$

The symbol  $tr$  denotes the trace. The parameter  $b$  measures the extensibility of the dumbbells. When  $b \rightarrow \infty$  the FENE-P model is equivalent to the Oldroyd-B model. Finite extensibility of the polymer implies that [213]:

$$tr(\mathbf{C}) < b^2 \quad (3.7)$$

### 3.3.2 Boundary conditions

So far we have met two types of homogeneous boundary conditions: Dirichlet conditions for velocity, specifying values of the velocity function, and natural or free conditions, specifying velocity and viscoelastic stress tensor are not imposed on the outflow boundary. There is no explicit boundary condition for pressure while no pressure grid point lies on the boundary of computational domain.

### 3.3.3 Weak formulation of the problem

The problem consisting of solving the continuity, momentum and constitutive equations Eqs. (3.1),(3.2) and (3.5) if a FENE-P fluid is considered, on a flow domain  $\Omega \subset \mathbb{R}^d$ , where  $d$  is the problem dimension, in order to determine the three variables (pressure, velocity and conformation tensor) can be expressed with a general weak (Galerkin) formulation, which is also used in the finite element context.

With this aim, it is necessary to define first a set of functional spaces  $X_p$ ,  $X_u$  and  $X_C$  to which the functions representing respectively the pressure,  $p$ , velocity,  $\mathbf{u}$  and conformation tensor,  $\mathbf{C}$ , will belong. These spaces are respectively subspaces of  $L^2(\Omega)$ ,  $H^1(\Omega)^d$  and  $L^2(\Omega)^{d \times d}$ , where  $L^2(\Omega)$  and  $H^1(\Omega)$  represent the space of measurable functions that are square-integrable on  $\Omega$  and the space of differentiable functions of which first-order partial derivatives are measurable and square-integrable on  $\Omega$ . Their definition includes the specification of boundary conditions.

Second, multilinear forms  $A$ ,  $B$  and  $C$  involving the three variables can be defined based on integral inner products with test functions belonging to the functional spaces. The initial problem is then expressed in the weak formulation as: Find  $(p, \mathbf{u}, \mathbf{C}) \in X_p \times X_u \times X_C$  such that:

$$A(\mathbf{u}, \Psi_p) = \int_{\Omega} (\nabla \cdot \mathbf{u}) \Psi_p \, d\Omega = 0, \quad \forall \Psi_p \in X_p \subset L^2(\Omega) \quad (3.8)$$

$$\begin{aligned}
B(p, \mathbf{u}, \mathbf{C}, \Psi_u) &= \int_{\Omega} \frac{\partial \mathbf{u}}{\partial t} \cdot \Psi_u \, d\Omega + \int_{\Omega} -p(\mathbf{I} : \nabla \Psi_u) \, d\Omega \\
&\quad + R_{\mu} \int_{\Omega} (\nabla \mathbf{u}) : \nabla \Psi_u \, d\Omega + Re \int_{\Omega} [(\mathbf{u} \cdot \nabla) \mathbf{u}] \cdot \Psi_u \, d\Omega \\
&\quad + \int_{\Omega} \boldsymbol{\tau} \cdot \nabla \Psi_u \, d\Omega - \int_{\partial\Omega} (\boldsymbol{\sigma} \cdot \mathbf{n}) \cdot \Psi_u \, d\Gamma \\
&= 0, \quad \forall \Psi_u \in X_u \subset H^1(\Omega)^d
\end{aligned} \tag{3.9}$$

The FENE-P constitutive equation in weak form reads:

$$\begin{aligned}
C(\mathbf{u}, \mathbf{C}, \Psi_C) &= We \int_{\Omega} \frac{\partial \mathbf{C}}{\partial t} : \Psi_C \, d\Omega + \int_{\Omega} \frac{1}{(1 - \frac{tr(\mathbf{C})}{b^2})} \mathbf{C} : \Psi_C \, d\Omega \\
&\quad - We \left\{ \int_{\Omega} [\nabla \mathbf{u} \cdot \mathbf{C}] : \Psi_C \, d\Omega + \int_{\Omega} [\mathbf{C} \cdot (\nabla \mathbf{u})^T] : \Psi_C \, d\Omega \right\} \\
&\quad - \frac{1}{K} \int_{\Omega} \mathbf{I} : \Psi_C \, d\Omega + We \int_{\Omega} [(\mathbf{u} \cdot \nabla) \mathbf{C}] : \Psi_C \, d\Omega \\
&= 0, \quad \forall \Psi_C \in X_C \subset L^2(\Omega)^{d \times d}
\end{aligned} \tag{3.10}$$

### 3.3.4 Galerkin approximation

Instead of solving the previous continuous problem, an approximate projected solution is sought in a finite dimensional subspace  $X_p^{N_p} \times X_u^{N_u} \times X_C^{N_C}$  of  $X_p \times X_u \times X_C$ , where  $X_p^{N_p}$ ,  $X_u^{N_u}$  and  $X_C^{N_C}$  are respectively included in the spaces spanned by polynomials of order less than or equal to  $N_p$ ,  $N_u$  and  $N_C$  in each spatial direction. In practice, some restrictions occur as far as the selection of the polynomial degrees is concerned. In particular, the inf-sup condition imposes restrictions on the pressure subspace once the velocity subspace is prescribed, to prevent locking and spurious oscillation phenomena. In the spectral element context, the inf-sup condition is satisfied if  $N_p = N_u - 2$  as emphasized by Maday and Patera [139]. No such condition has been clearly defined for the viscoelastic stress subspace although some relevant investigations have been carried out. A studies carried out by Van Kemenade and Deville [216] has shown that selecting the polynomial degrees for the velocity and viscoelastic stress approximations should be such that  $N_u \leq N_C \leq N_u + 2$  for optimal results in the case of a viscoelastic flow through a corrugated tube. Gerritsma and Phillips [85] considered the mixed formulation of the Stokes problem in terms of the velocity, pressure and extra-stress variables under a constrained minimization of the viscous stress tensor. They found that the problem is well-posed as long as the stress approximation space contains polynomials of at least the same degree as the velocity. In most computations relative to viscoelastic flows with spectral element methods, the velocity and

viscoelastic stress grids are taken to be the same. Furthermore, it has been recommended by the last two authors to use a discontinuous extra-stress approximation space (between elements) in order to satisfy a compatibility condition between the discrete velocity and stress spaces [84]. This idea can be extended to the viscoelastic stress when a viscoelastic problem is considered.

To summarize, in order to avoid spurious pressure and satisfy a compatibility condition between velocity and viscoelastic stress, if the velocity is represented by polynomials in  $\mathbf{P}_N$  then the pressure and viscoelastic stress may be represented in  $\mathbf{P}_{N-2}$  and  $\mathbf{P}_N$  respectively.

The system of equations (3.8)-(3.10) is discretized using the spectral element formulation [139]. The domain is decomposed into a number of elements  $\Omega_k$  on which each integral is computed. The evaluation of the integrals on each element is made easier by the use of a mapping of the physical system e.g of coordinates  $(x_1, x_2)$  in two dimensions into a local  $(r_1, r_2)$ -system. Physical elements are mapped onto parent elements defined on  $[-1, 1]^d$ . Thus, the derivatives appearing in the integrals can be expressed in terms of the local coordinates by the following Jacobian transformation:

$$\frac{\partial}{\partial x_i} = J_{i\alpha}^{-1} \frac{\partial}{\partial r_\alpha} \quad (3.11)$$

The Jacobian matrix  $J$  is given by:

$$J_{i\alpha} = \frac{\partial x_\alpha}{\partial r_i} \quad (3.12)$$

Its inverse  $J^{-1}$  can be written in two dimensions as:

$$J^{-1} = \frac{1}{|J|} \begin{bmatrix} \frac{\partial x_2}{\partial r_2} & -\frac{\partial x_2}{\partial r_1} \\ -\frac{\partial x_1}{\partial r_2} & \frac{\partial x_1}{\partial r_1} \end{bmatrix} \quad (3.13)$$

where  $|J|$  is the determinant of the Jacobian matrix:

$$|J| = \frac{\partial x_1}{\partial r_1} \frac{\partial x_2}{\partial r_2} - \frac{\partial x_1}{\partial r_2} \frac{\partial x_2}{\partial r_1} \quad (3.14)$$

Therefore, the integral of an arbitrary integrable function  $u(x_1, x_2)$  over the domain  $\Omega_k$

can be written:

$$\int_{\Omega_k} u(x_1, x_2) dx_1 dx_2 = \int_{-1}^1 \int_{-1}^1 u^k(r_1, r_2) \left| J^k(r_1, r_2) \right| dr_1 dr_2 \quad (3.15)$$

In the previous set of equations derived from the weak formulation (3.8)-(3.10), the integrals involving the pressure in the momentum equation or present in the continuity equation are approximated with the Gauss-Legendre integration rule e.g. in two dimensions:

$$\int_{\Omega_k} g dx_1 dx_2 \simeq \sum_{m=0}^{N-2} \sum_{n=0}^{N-2} \tilde{\gamma}_m \tilde{\gamma}_n |J^k(\tilde{\xi}_m, \tilde{\xi}_n)| g^k(\tilde{\xi}_m, \tilde{\xi}_n) \quad (3.16)$$

where  $g$  is a function continuous over  $\Omega_k$ ,  $g^k$  is its counterpart on  $[-1, 1] \times [-1, 1]$ ,  $(\tilde{\xi}_m, \tilde{\xi}_n)$  are the coordinates of the collocation points in the reference domain  $[-1, 1] \times [-1, 1]$  and  $|J^k|$  is the Jacobian of the mapping transformation from  $\Omega_k$  to  $[-1, 1] \times [-1, 1]$ . The quantities  $\tilde{\gamma}_i$  are weights corresponding to the Gauss-Legendre quadrature. They are given by:

$$\tilde{\gamma}_j = \frac{2}{(1 - \tilde{\xi}_j^2)} \frac{1}{\left[ \frac{dL_{N-2}}{dz}(\tilde{\xi}_j) \right]^2}, \quad j = 0, \dots, N-2 \quad (3.17)$$

where the quantities  $\tilde{\xi}_j$  ( $j = 0 \dots N-2$ ) are the local Gauss-Legendre collocation points in the interval  $[-1, 1]$ , which are the roots of the Legendre polynomial of degree  $N-1$ . In the previous equation,  $L_{N-2}$  is the Legendre polynomial of degree  $N-2$ .

The pressure is approximated using the Lagrangian interpolants  $\tilde{h}(z)$  in the following tensor-product form:

$$p^k(r_1, r_2) = \sum_{m=0}^{N-2} \sum_{n=0}^{N-2} \tilde{p}_{mn}^k \tilde{h}_m(r_1) \tilde{h}_n(r_2) \quad (3.18)$$

The corresponding Lagrangian interpolants can be written as:

$$\tilde{h}_p(z) = -\frac{L_{N-1}(z)}{\frac{dL_{N-1}}{dz}(\tilde{\xi}_p)(z - \tilde{\xi}_p)}, \quad p = 0, \dots, N-2 \quad (3.19)$$

In particular, the following relation holds:

$$\tilde{h}_p(\tilde{\xi}_m) = \delta_{mp} \quad (3.20)$$

where  $\delta_{mp}$  is the usual Kronecker symbol.

All the other integrals in the weak formulation are approximated with the Gauss-Lobatto-Legendre integration rule e.g. in two dimensions:

$$\int_{\Omega_k} f^k dx_1 dx_2 \simeq \sum_{m=0}^N \sum_{n=0}^N \gamma_m \gamma_n |J(\xi_m, \xi_n)| f^k(\xi_m, \xi_n) \quad (3.21)$$

where  $f$  is a function continuous over  $\Omega_k$ ,  $f^k$  is its counterpart on  $[-1, 1] \times [-1, 1]$ ,  $(\xi_m, \xi_n)$  are the coordinates of the collocation points in the reference domain  $[-1, 1] \times [-1, 1]$ ,  $|J^k|$  is the Jacobian of the mapping transformation from  $\Omega_k$  to  $[-1, 1] \times [-1, 1]$ . The quantities  $\gamma_j$  are weights corresponding to the Gauss-Lobatto-Legendre quadrature. They are given by:

$$\gamma_j = \frac{2}{N(N+1)} \frac{1}{L_N(\xi_j)^2}, \quad j = 0, \dots, N \quad (3.22)$$

where the quantities  $\xi_j$  ( $j = 0 \dots N$ ) are the local Gauss-Lobatto-Legendre collocation points in the interval  $[-1, 1]$  given by:

$$\xi_0 = -1; \quad \frac{dL_N}{dz}(\xi_j) = 0, \quad 1 \leq j \leq N-1; \quad \xi_N = 1 \quad (3.23)$$

where  $L_N$  is the Legendre polynomial of degree  $N$ .

The variable components like  $u_i$  or  $C_{ij}$  are approximated using the Lagrangian interpolants  $h(z)$  in the following tensor-product form:

$$u^k(r_1, r_2) = \sum_{m=0}^N \sum_{n=0}^N u^k_{mn} h_m(r_1) h_n(r_2) \quad (3.24)$$

The corresponding Lagrangian interpolants can be written as:

$$h_p(z) = -\frac{(1-z^2) \frac{dL_N}{dz}(z)}{N(N+1)L_N(\xi_p)(z-\xi_p)}, \quad p = 0, \dots, N \quad (3.25)$$

with the cardinality condition:

$$h_p(\xi_m) = \delta_{mp} \quad (3.26)$$

The introduction of the quadratures to compute the various integrals results in a discretization of the original set of equations. It is only necessary to determine the values of the pressure, velocity and viscoelastic stress at the collocation points to know the values anywhere in the computational domain.



Terms involving partial derivatives of the two types of Lagrangian interpolants are present in the integrals displayed in the set of flow equations. Therefore, nodal interpolant derivative operators  $D_{ij} = \frac{dh_j(\xi_i)}{dz}$  appear in the corresponding discretized equations.

For instance, the convective term in the momentum equation over the element  $\Omega_k$  can be approximated by:

$$\begin{aligned} \int_{\Omega_k} [(\mathbf{u} \cdot \nabla) \mathbf{u}] \cdot \Psi_u d\Omega = & \\ \sum_{m=0}^N \sum_{n=0}^N \sum_{j=1}^2 \sum_{i=1}^2 \gamma_m \gamma_n |J(\xi_m, \xi_n)| (\Psi_u)_i^k(\xi_m, \xi_n) \mathbf{u}_j(\xi_m, \xi_n) \frac{\partial \mathbf{u}_i}{\partial x_j}(\xi_m, \xi_n) = & \quad (3.27) \\ \sum_{m=0}^N \sum_{n=0}^N \sum_{j=1}^2 \sum_{i=1}^2 \gamma_m \gamma_n |J|_{mn}^k ((\Psi_u)_i)_mn^k (\mathbf{u}_j)_{mn} (G_j)_{mnpq}^k (\mathbf{u}_i)_{pq} & \end{aligned}$$

where:

$$(G_j)_{mnpq}^k = (J_{j1}^{-1})_{mn}^k D_{mp} \delta_{nq} + (J_{j2}^{-1})_{mn}^k \delta_{mp} D_{nq} \quad (3.28)$$

The test functions are chosen so that they vanish at all but one collocation point. Therefore, the convective term in the momentum equation is approximated by ( $N_{el}$  being the total number of elements):

$$\int_{\Omega} [(\mathbf{u} \cdot \nabla) \mathbf{u}] \cdot \Psi_u d\Omega = \sum_{k=1}^{N_{el}} \sum_{i=1}^2 \sum_{p=0}^N \sum_{q=0}^N (\Psi_{u_i})_{pq}^k (C_i)_{pq}^k \quad (3.29)$$

where:

$$(C_i)_{pq}^k = \sum_{j=1}^2 \sum_{r=0}^N \sum_{s=0}^N \gamma_p \gamma_q |J|_{pq}^k (\mathbf{u}_j)_{pq} (G_j)_{pqrs}^k (\mathbf{u}_i)_{rs} \quad (3.30)$$

The symbol  $\sum'$  indicates that direct stiffness is operated on the nodes located on the element boundaries.

All terms can be expressed in a form similar to the one in the previous equation.

### 3.3.5 Semi-discrete formulation

The discretization process leads to a set of equations, which can be cast in matrix form. Adopting the notation of Deville, Fischer and Mund [60]:

$$- D_k \underline{V}_k = 0, \quad k = 1, \dots, d \quad (3.31)$$

$$M \frac{d\underline{V}_i}{dt} = - Re C(\underline{V}) \underline{V}_i + D_i^T \underline{P} - R_\mu K_{ij} \underline{V}_j - VE_j \underline{T}_{ij} + (M_b)_{ij} \underline{S}_{b_j} \quad (3.32)$$

The symbols  $\underline{P}$ ,  $\underline{V}_i$  and  $\underline{T}_{ij}$  correspond to the vectors relative to the degrees of freedom for the pressure, velocity and viscoelastic stress components ( $1 \leq i \leq d$ ,  $1 \leq j \leq d$ ). The matrices  $M$  and  $K_{ij}$  are respectively diagonal mass and stiffness matrices. The discrete divergence operator is given by  $D_i$  and its transpose  $D_i^T$  yields the discrete gradient operator. The convection term is given by  $C(\underline{V}) \underline{V}_i$  where the nonlinear operator  $C(\underline{V})$  depends on the velocity field.

The last two matrix operators are derived from the following integrals:

$$\int_{\Omega} \boldsymbol{\tau} \cdot \nabla \boldsymbol{\Psi}_u \, d\Omega \implies VE_j \underline{T}_{ij}, \quad \int_{\partial\Omega} (\boldsymbol{\sigma} \cdot \mathbf{n}) \cdot \boldsymbol{\Psi}_u \, d\Gamma \implies (M_b)_{ij} \underline{S}_{b_j}$$

The constitutive equation in semi-discrete form reads:

$$WeM \frac{d\underline{C}_{ij}}{dt} = NL_{ij}(\underline{C}_{mn}, \underline{V}_l) \quad (3.33)$$

where:

$$NL_{ij}(\underline{C}_{mn}, \underline{V}_l) = We[-LC_{ij}(\underline{V}_l) + GC_{ij}(\underline{V}_l, \underline{C}_{mn}) + (GC)_{ij}^T(\underline{V}_l, \underline{C}_{mn})] \quad (3.34)$$

$$QC_{ij}(\underline{C}_{mn}) + \frac{1}{K} IC_{ij}(\underline{C}_{mn})$$

Again, these operators written in matrix form are derived from the following integrals:

$$\int_{\Omega} \frac{\partial \mathbf{C}}{\partial t} : \boldsymbol{\Psi}_C \, d\Omega \implies M \frac{d\underline{C}_{ij}}{dt}, \quad (3.35)$$

$$\int_{\Omega} [(\mathbf{v} \cdot \nabla) \mathbf{C}] : \boldsymbol{\Psi}_C \, d\Omega \implies LC_{ij}(\underline{V}_l), \quad \int_{\Omega} [\nabla \mathbf{v} \cdot \mathbf{C}] : \boldsymbol{\Psi}_C \, d\Omega \implies GC_{ij}(\underline{V}_l, \underline{C}_{mn})$$

$$\int_{\Omega} \mathbf{I} : \boldsymbol{\Psi}_C \, d\Omega \implies IC_{ij}(\underline{C}_{mn}) \quad \int_{\Omega} \left( \frac{1}{1 - \frac{tr(\mathbf{C})}{b^2}} \right) \mathbf{C} : \boldsymbol{\Psi}_C \, d\Omega \implies QC_{ij}(\underline{C}_{mn})$$

When Gauss-Legendre quadrature is selected, the pressure grid (of which nodes are the quadrature collocation points) is staggered with respect to the velocity grid (of which nodes are the Gauss-Lobatto-Legendre collocation points), which is usually the same as the viscoelastic stress and conformation tensor grid.

### 3.4 Time discretization

Once the original set of continuous equations (3.1), (3.2) and (3.5) is discretized in space, the resulting semi-discrete set of nonlinear ordinary equations must still be approximated in time in order to generate the time marching scheme. As high-order spatial discretization techniques are needed in order to obtain either accurate results or to decrease the number of grid points, high temporal accuracy is also required for the time-dependent problems that we want to tackle.

The stability of the temporal schemes can be investigated by computing the roots of a characteristic polynomial derived from some simple test equation

$$\frac{dy}{dt} = \sum_{i=1}^n \lambda_i y \quad (3.36)$$

where  $\lambda_i$  is the  $i$ th eigenvalues [35] [52]. Absolute stability is obtained if all the moduli of the roots are smaller than one. This enables to select a suitable scheme for a given problem. Other factors coming into play before making a decision are also the accuracy, storage requirements and amount of implementation work. The accuracy of the time scheme can be obtained from a truncation error analysis.

The computational cost of high-order methods does not increase drastically with respect to first-order methods while the same level of temporal accuracy can be obtained with larger time steps i.e. faster. Among the standard high order methods, multi-step methods like the backward differentiation formula scheme (BDF), the Adams-Bashforth method (including forward Euler), the predictor-corrector schemes combining usually the actions of two multi-step methods are widely used. A popular alternative is to use Runge-Kutta methods well-known for their high stability characteristics.

We have used in particular a backward differentiation formula for linear Stokes problem and the extrapolation scheme (EX) for the nonlinear terms [110] to discretize in time Eqs. (3.31)-(3.33). In order to simplify the notation with respect to Eqs. (3.31)-(3.33), we introduce a shorthand notation where  $\underline{V}$  and  $\underline{C}$  represent the full vectors of all velocity and viscoelastic stress unknowns. The block diagonal matrices  $\mathbf{M}$  and  $\mathbf{K}$  are respectively composed with  $d$  block matrices  $M$  and  $K$ . The matrix  $\mathbf{D}$  corresponds to the full divergence operator and  $\mathbf{D}^T$  to the full gradient operator. The following system of equations

results:

$$-\mathbf{D}\underline{V}^{n+1} = 0 \quad (3.37)$$

$$\begin{aligned} & \left(\frac{\beta_{s_i}}{\Delta t}\right) \mathbf{M}\underline{V}^{n+1} - \mathbf{D}^T \underline{P}^{n+1} + R_\mu \mathbf{K} \underline{V}^{n+1} = \\ & \frac{1}{\Delta t} \sum_{q=1}^{s_i} \beta_{s_i-q} \mathbf{M}\underline{V}^{n+1-q} - \sum_{r=0}^{s_e-1} \alpha_r Re \mathbf{C}(\underline{V}^{n-r}) \end{aligned} \quad (3.38)$$

$$\begin{aligned} & -\mathbf{V}\mathbf{E} \underline{T}^{n+1} + \mathbf{M}_b \underline{S}_b^{n+1} \\ \frac{We}{\Delta t} \beta_{s_i} \mathbf{M}\underline{C}^{n+1} &= \frac{We}{\Delta t} \sum_{q=1}^{s_i} \beta_{s_i-q} \mathbf{M}\underline{C}^{n+1-q} + \sum_{r=0}^{s_e-1} \alpha_r \mathbf{NL}(\underline{C}^{n-r}, \underline{V}^{n-r}) \end{aligned} \quad (3.39)$$

where an extrapolation method of order  $s_e$  has been used to determine the value of the nonlinear term at time step  $n+1$ . The associated BDF scheme is of order  $s_i$ . The coefficients  $\alpha_i$  and  $\beta_j$  are dependent on the orders of each method, e.g. for a BDF2/EX2 ( $s_i = 2$ ,  $s_e = 2$ ) scheme:  $\alpha_0 = 2$ ,  $\alpha_1 = -1$ ,  $\beta_0 = -\frac{1}{2}$ ,  $\beta_1 = 2$ ,  $\beta_2 = \frac{3}{2}$ .

Following the study of Couzy [52], one can easily show that the BDF2/EX2 scheme provides global second-order accuracy. This decoupling BDF2/EX2 has also been used in the past by Fiétier and Deville [74] for the simulation of visco-elastic flows and by Bodard [27] for fluid-structure interaction problems. All the simulations presented in this dissertation use in particular BDF2/EX2.

### 3.5 System solving techniques

Once the set of equations (3.1), (3.2) and (3.5) is fully discretized in space and time, a system of nonlinear equations with respect to the values of the unknown variables (velocity, pressure and viscoelastic stress) at the grid points must be solved. Two main types of approach can be used to this effect.

The decoupled approach consists of solving separately the mass-momentum and constitutive equations. More precisely, the constitutive equation is integrated at time step  $n+1$  for the extra-stress tensor while using velocity gradient terms obtained at the previous time step  $n$ . The extra-stress tensor is then plugged as a source term into the momentum equation. The mass-momentum system of equations is then solved for the velocity and pressure at the new time step  $n+1$  using a classical technique for solving Stokes-like problems. Such iterative techniques are cheap in terms of CPU time, but they suffer from poor

convergence properties. Depending on the way the stress and velocity fields are updated at each iteration, such schemes approximate the solution of time-dependent problems in a more or less loose manner, which may be a source of strong numerical instabilities.

In the coupled approach, the three partial differential equations are solved altogether from time step  $n$  to time step  $n+1$ . Generally, coupled methods are more stable than decoupled ones but the required computer resources (memory and CPU time) are more stringent. The full nonlinear coupled problem is generally solved by a succession of Newton iterations applied to a discretization of the entire set of equations. The computer storage to set up and invert the Jacobian matrix for the Newton iteration is very demanding. Newton schemes provide quadratic convergence and therefore, few iterations are needed to reach a solution provided the initial guess is good enough. There is no explicit treatment of some operators in these schemes, which makes them a priori less sensitive to time-dependent numerical instabilities and avoids limitations due to CFL-type criteria on the time step. Because three dimensional numerical simulations with a fully-coupled treatment are still out of reach even on the most powerful supercomputers, in this dissertation we only deal with the decoupled approach. The efficiency of this decoupled method depends critically on the availability of an efficient and robust solver for the underlying Stokes problem at each time step. Our approach consists of solving the mass-momentum set of Eqs. (3.37)-(3.38) with an efficient solver as designed by Couzy [52] for Newtonian flows, which can be easily extended to viscoelastic flows by simply adding the divergence term corresponding to the viscoelastic stress tensor as a source term in the momentum equation. The mass-momentum set of equations is treated via a generalized block LU decomposition with pressure correction [176], which can be summarized by the following steps:

Step 1: Solve for the conformation tensor:

$$\mathbf{R} \underline{C}^{n+1} = \underline{L} \quad (3.40)$$

$$\mathbf{R} = \left( \frac{\beta_{s_i}}{\Delta t} \right) \mathbf{M} \quad (3.41)$$

$$\underline{L} = \frac{We}{\Delta t} \sum_{q=1}^{s_i} \beta_{s_i-q} \mathbf{M} \underline{C}^{n+1-q} + \sum_{r=0}^{s_e-1} \alpha_r \mathbf{NL}(\underline{C}^{n-r}, \underline{V}^{n-r}) \quad (3.42)$$

Step 2: Compute the viscoelastic stress

$$\underline{T}^{n+1} = \frac{1 - R_\mu}{We} \frac{1}{1 - (\text{tr}(\underline{C}^{n+1})/b^2)} \left( \underline{C}^{n+1} - \frac{(1 - \frac{\text{tr}(\underline{C}^{n+1})}{b^2})}{K} \underline{I} \right) \quad (3.43)$$

Step 3: Compute the tentative velocity vector  $\underline{V}^*$  by solving the equation:

$$\mathbf{H} \underline{V}^* = \underline{F} + \mathbf{D}^T \underline{P}^n \quad (3.44)$$

which is a short-hand notation for Eq. (3.38) where the pressure term has been shifted to the right-hand side. The Helmholtz operator matrix  $\mathbf{H}$  comprises both mass and Laplacian contributions while all other terms including the convective one are in the right-hand side vector  $\underline{F}$ :

$$\mathbf{H} = \left( \frac{\beta_{s_i}}{\Delta t} \right) \mathbf{M} + R_\mu \mathbf{K} \quad (3.45)$$

$$\begin{aligned} \underline{F} = & \frac{1}{\Delta t} \sum_{q=1}^{s_i} \beta_{s_i-q} \mathbf{M} \underline{V}^{n+1-q} - \sum_{r=0}^{s_e-1} \alpha_r \text{Re} \mathbf{C}(\underline{V}^{n-r}) \\ & - \mathbf{V} \mathbf{E} \underline{T}^{n+1} + \mathbf{M}_b \underline{T}_b^{n+1} \end{aligned} \quad (3.46)$$

Step 4: Solve for the pressure:

$$- \mathbf{D} \mathbf{Q} \mathbf{D}^T \underline{\Delta P}^{n+1} = \frac{\beta_{s_i}}{\Delta t} \mathbf{D} \underline{V}^* \quad (3.47)$$

$$\underline{P}^{n+1} = \underline{P}^n + \underline{\Delta P}^{n+1} - R_\mu \mathbf{D} \underline{V}^* \quad (3.48)$$

The last term in Eq. (3.48) has been introduced to obtain an overall consistent scheme as suggested by Timmermans et al. [209]. The symbol  $\underline{\Delta P}^{n+1}$  represents some intermediate pressure correction term.

Step 5: Compute the final velocity at step n+1 after a pressure correction:

$$\underline{V}^{n+1} = \underline{V}^* + \frac{\Delta t}{\beta_{s_i}} \mathbf{Q} \mathbf{D}^T \underline{\Delta P}^{n+1} \quad (3.49)$$

The choice of the matrix  $\mathbf{Q}$  is critical. If one sets :

$$\mathbf{Q} = \mathbf{H}^{-1} \quad (3.50)$$

one obtains the Uzawa algorithm [138] or if one writes an approximation of  $\mathbf{H}^{-1}$  e.g. for

a BDF2/EX2 scheme:

$$\begin{aligned} \mathbf{Q} = & \frac{\Delta t}{\beta_2} \mathbf{M}^{-1} - R_\mu \left( \frac{\Delta t}{\beta_2} \right)^2 (\mathbf{M}^{-1} \mathbf{K}) \mathbf{M}^{-1} \\ & + (R_\mu)^2 \left( \frac{\Delta t}{\beta_2} \right)^3 (\mathbf{M}^{-1} \mathbf{K})^2 \mathbf{M}^{-1} \end{aligned} \quad (3.51)$$

As proposed by Couzy and Deville [53] one obtains a fourth-order approximation in time. If accuracy in time is limited to second order, only the first term in the previous expansion need be retained. Efficient preconditioners for the iterative solver of the pressure step Eq. (3.47), which is by far the most expensive one in terms of CPU time, have been prescribed by Couzy and Deville [53] and Couzy [52]. Simple diagonal preconditioners are used for the two velocity steps.

Since the nonsymmetric (nonlinear) terms in Eqs. (3.37)-(3.39) are located in the right-hand sides, cheap preconditioned conjugate gradient solvers can be used to solve the resulting system for the unknowns at the grid points. Eq. (3.39) is readily solved since there are no implicit terms with non-trivial matrix operators.

### 3.6 Stabilization technique

As mentioned by Fischer and Mullen [75], despite the numerous advantages of the SEM, stability problems have been encountered in the past, which required very fine space and time resolutions for applications at moderate Reynolds number ( $10^3$ ). Stabilization can easily be obtained with the Legendre-SEM by using a nodal filtering technique introduced by Fischer and Mullen [75] or modal filtering introduced by Boyd [32]. The filter is applied at the end of each step of the Navier-Stokes and constitutive time integration of the problem governed by Eqs. (3.37)-(3.39) and aims at removing nascent instabilities induced by the treatment of the nonlinear convective term. This specific technique is mainly used in the applications presented in Chapter 6.

### 3.7 Summary

In this section, we have tried to provide an overview of the main computational methods to solve flow problems of viscoelastic fluids the behavior of which may be modelled with a

partial differential equation. It is clearly non exhaustive but is an attempt to justify the choice of the computational method that we have employed among the numerous possibilities. A spectral element method with a second-order time discretization scheme has been selected since time-dependent accurate solutions are expected. In addition, non-dissipative and non-dispersive properties are required if one expects to observe transient or periodic phenomena like physical instabilities.

The semi-discretized problem based on the SEM is decoupled into an unsteady Stokes problem treated implicitly and the nonlinear advective term into its convective form, treated explicitly. The constitutive equation which acts as a source term in momentum equation is treated explicitly. The time-integration schemes used to treat the previous two subproblems is BDF2/EX2 respectively. No time-splitting error is induced by this choice which leads to a global second-order time accuracy for the method. The details of the velocity-pressure decoupling using a generalized block LU decomposition with pressure correction have been discussed. Finally, the iterative solution of the discretized problem using the preconditioned conjugate gradient method has been briefly introduced.



## Chapter 4

---

# Mathematical improvement of constitutive equation to treat high Weissenberg number problem

This chapter comprises three different sections. The first part corresponds to the classical matrix logarithm formulation (CMLF). In this part, we show that although the use of log conformation tensor can be helpful to preserve symmetric positive definiteness of the conformation tensor, it is also mandatory for FENE family to satisfy the boundness of the conformation tensor. We then show that applying classical matrix logarithm formulation for the FENE family is not enough to enforce stability.

The second part of this discussion presents an extended matrix logarithm formulation (EMLF) in order to remove instabilities observed in the simulation of unsteady viscoelastic fluid flows in the framework of the spectral element method. In this study, we consider a particular model of the finite extensible nonlinear elastic family, FENE-P, but the method could be applied to other differential constitutive equations. Two distinct constraints for the FENE-P equation are imposed: (i) the square of the corresponding finite extensibility parameter of the polymer must be an upper limit for the trace of the conformation tensor and (ii) the eigenvalues of the conformation tensor should remain positive at all steps of the simulation. Negative eigenvalues cause the unbounded growth of instabilities in the flow. The proposed transformation is an extension of the matrix logarithm formulation originally presented by Fattal and Kupferman [69, 70]. With this new method one can tackle high Weissenberg number flow at values of practical interest. A neat improvement of the computational algorithm with stable convergence has been demonstrated in this study. This work has been reported in the international literature [104].

In the last part of this chapter a possible mathematical formulation that enforces stability as much as possible is discussed. This formulation is an enhanced format of hyperbolic tangent of the conformation tensor.

## 4.1 Introduction

The challenge for computational rheologists is to develop efficient and stable numerical schemes in order to obtain accurate numerical solutions for the governing equations at values of practical interest of the Weissenberg number,  $We$ , within the range [0-150]. The Weissenberg number is the ratio of the relaxation time of viscoelastic fluids to the inertial time.

In the past two decades, considerable efforts have been devoted to the development of robust and stable numerical methods for simulating non-trivial flows of complex fluids. Without any exception, the standard viscoelastic models like Oldroyd-B, Maxwell, Phan-Thien-Tanner, FENE-P, etc. have failed in the simulation of high Weissenberg number flows in any available numerical techniques such as: finite difference, finite volume, finite elements, spectral elements etc. Nowadays one has come to the conclusion that selection of an appropriate constitutive equation constitutes a very crucial step although implementing a suitable numerical technique is still important for successful discrete modeling of non-Newtonian flows [129].

Recently a logarithm representation of the conformation tensor was proposed by Fattal and Kupferman [69, 70]. The essential idea is based on the fact that the high Weissenberg number problem (HWNP) may be caused by the failure of polynomial-based approximations to properly represent exponential profiles developed by the conformation tensor. Under this transformation, the extensional components of the deformation field act additively, rather than multiplicatively. This representation grants the positive definiteness of the conformation tensor, which is a compulsory condition to obtain positive eigenvalues which represent the local strain and orientation of the micro constituents.

Hulsen et al. [102] first implemented the log conformation in a finite element context, using the DEVSS/DG formulation for the flow around a cylinder for Oldroyd-B and Giesekus

models. With the log conformation representation, they obtained solutions beyond a value of Weissenberg number,  $We = 100$ . However, even though in large parts of the flow the solution converges, they have not been able to obtain convergence near the cylinder of the flow for Oldroyd-B model.

Kwon [120] presented an alternative procedure to derive the tensor logarithmic representation of the differential constitutive equation and provided a numerical example with the Leonov model in 4:1 planar contraction flow using SUPG and SU stabilization techniques. Dramatic improvement of the computational algorithm with the stable convergence has been demonstrated. The author could achieve  $De = 132$  with a coarse mesh and  $De = 193$  for a refined mesh. This new formulation works only for a few differential constitutive equations proven Hadamard stable. Hadamard stability means well-posedness of constitutive equations under low and high frequency wave disturbance [130].

A simple alternate form of the log conformation formulation is presented by Coronado et al. [51]. The flows of Oldroyd-B and Larson-type fluids are tested in the benchmark problems of flow past a cylinder in a channel with the DEVSSS-TG/SUPG methods. For the Oldroyd-B fluids, the maximum Weissenberg number was extended to 1.05 as compared to 0.75 obtained with the original DEVS-TG/SUPG method. For the Larson-1 model the maximum Weissenberg number was extended from 4.49 to 12.3 and for the Larson-2 model from 1.13 to 1.41.

In the context of spectral methods, Chauvière and Owens [41], and Van Kemenade and Deville [216] applied the Legendre spectral element method with success to simulate steady viscoelastic flows. They combined the versatility of the classical (low-order) finite element methods with the accuracy of high-order approximation polynomials encountered in spectral method in order to investigate the potential of spectral element method in the field of viscoelastic flows.

Van Os and Phillips [221] applied spectral element methods for solving steady and transient flows of viscoelastic fluids for a plane Poiseuille flow. The fluids are modeled using the upper-convected Maxwell and Oldroyd-B constitutive relationships. They found that any type of refinement in streamwise direction decreases the maximum attainable Weissenberg number whereas this number is insensitive to refinement in the cross channel direction.

Fiétier and Deville [74] presented a method based on the spectral element formulation for the simulation of time dependent flows of viscoelastic fluids for various type of constitutive equations. They tested simple steady and unsteady Poiseuille flows as well as a more complex flow in an abrupt contraction as opposed to simulation of Poiseuille flows with models of the FENE type with low values of the extensibility parameter, which have been found stable for various discretizations. The stability of the results obtained with the Oldroyd-B model has been shown to be strongly dependent on the computational grid.

The aim of this part is to introduce and study the capability of a new extended algorithm for the matrix logarithm formulation. First, we investigate the ability of time dependent simulation originally proposed by Fattal and Kupferman [69] without considering the extended algorithm on a simple unsteady FENE-P Poiseuille flow in the spectral element framework. We study the effect of each differential term in the constitutive equation for both classical and log representation. Moreover, the influence of the boundary conditions on attainable Weissenberg number and accuracy of the results is considered. We have observed that applying the log formulation for at least FENE-P fluids is not sufficient for curing the instability problem observed in the numerical simulation. Then, according to the observation in the previous simulations we introduce a new extended algorithm for the log matrix conformation. The study of this new algorithm is performed based on the linear stability analysis as developed in Ref. [73, 204] which will be presented in the next chapter. The aim of the last part of this chapter is to introduce a mathematical model to preserve both SPD of the conformation tensor and also bound magnitude of the eigenvalues. A possible remedy in this context is to use an enhanced format of hyperbolic tangent of the conformation tensor. Because this new formulation of equations involves with some complexity, we did not find time to completely test the capability of this new formulation for numerical simulation, but we expect that this variable transformation within the spectral element method will bring some breakthrough(s) in the high Weissenberg number problem as it removes some of the stiffness related to the usual model forms.

## 4.2 Classical matrix logarithm formulation (CMLF)

Since the HWNP may be related to the inadequacy of polynomial interpolation to approximate exponential profiles, one possible remedy that was proposed by Fattal and Kupferman [69] is to reformulate the constitutive equations using new variables that scale logarithmically. This transformation enforces the eigenvalues of the conformation tensor to remain positive for all steps of the simulation. They transform the classical constitutive equation based on the conformation tensor,  $\mathbf{C}$ , to a new one based on the tensor  $\mathbf{H}$  defined as:

$$\mathbf{H} = \ln(\mathbf{C}) \quad (4.1)$$

In this study attention is drawn to the approach followed by Kwon [120] for deriving the evolution equations. In the case of 2D planar flow, adopting the notations of Kwon, the eigenvalue problem for the  $\mathbf{H}$  conformation tensor in the continuous domain yields the eigenvalues:

$$h_1 = \frac{1}{2}[h_{11} + h_{22} + \sqrt{(h_{11} - h_{22})^2 + 4h_{12}^2}] \quad (4.2)$$

$$h_2 = \frac{1}{2}[h_{11} + h_{22} - \sqrt{(h_{11} - h_{22})^2 + 4h_{12}^2}] \quad (4.3)$$

The eigenvectors of the matrix are defined as:

$$\mathbf{n}_1 = \begin{bmatrix} n_1 \\ n_2 \end{bmatrix} \quad \text{and} \quad \mathbf{n}_2 = \begin{bmatrix} -n_2 \\ n_1 \end{bmatrix} \quad (4.4)$$

with  $n_1^2 + n_2^2 = 1$ . The components of the eigenvectors can be determined by:

$$n_1^2 = \frac{h_{12}^2}{(h_1 - h_{11})^2 + h_{12}^2} \quad (4.5)$$

$$n_2^2 = \frac{(h_1 - h_{11})^2}{(h_1 - h_{11})^2 + h_{12}^2} \quad (4.6)$$

$$n_1 n_2 = \frac{h_{12}(h_1 - h_{11})}{(h_1 - h_{11})^2 + h_{12}^2} \quad (4.7)$$

The characteristic relation for  $\mathbf{C}$  is written as:

$$\mathbf{C} \cdot \mathbf{n}_i = c_i \mathbf{n}_i \quad (4.8)$$

Differentiation of the above equation with respect to time yields:

$$\dot{\mathbf{C}} \cdot \mathbf{n}_i + \mathbf{C} \cdot \dot{\mathbf{n}}_i = \dot{c}_i \mathbf{n}_i + c_i \dot{\mathbf{n}}_i \quad (4.9)$$

Then scalar product with another eigenvector yields the following result:

$$\begin{aligned} \mathbf{n}_j \cdot \dot{\mathbf{C}} \cdot \mathbf{n}_i &= \mathbf{n}_j (\dot{c}_i \mathbf{n}_i) + \mathbf{n}_j (c_i \dot{\mathbf{n}}_i) - \mathbf{n}_j \cdot (\mathbf{C} \cdot \dot{\mathbf{n}}_i) \\ &= \dot{c}_i \delta_{ij} + (c_i - c_j) \dot{\mathbf{n}}_i \cdot \mathbf{n}_j \end{aligned} \quad (4.10)$$

In the other form:

$$\left\{ \begin{array}{l} i) \quad \dot{c}_i = \mathbf{n}_i \cdot \dot{\mathbf{C}} \cdot \mathbf{n}_i \quad \text{when } i = j \\ ii) \quad \dot{\mathbf{n}}_i \cdot \mathbf{n}_j = \frac{1}{c_i - c_j} \mathbf{n}_j \cdot \dot{\mathbf{C}} \cdot \mathbf{n}_i \quad \text{when } i \neq j \end{array} \right\} \quad (4.11)$$

Due to the isotropic function relation,  $\mathbf{C}$  and  $\mathbf{H}$  have the same set of eigenvectors. For the  $\mathbf{H}$ -tensor, an equivalent relation is readily obtained as:

$$\mathbf{n}_j \cdot \dot{\mathbf{H}} \cdot \mathbf{n}_i = \dot{h}_i \delta_{ij} + (h_i - h_j) \dot{\mathbf{n}}_i \cdot \mathbf{n}_j \quad (4.12)$$

by introducing  $c_i = e^{h_i}$  and thus  $\dot{h}_i = \frac{\dot{c}_i}{c_i}$ , Combining Eqs. (4.11) and (4.12), one obtains:

$$\left\{ \begin{array}{l} i) \quad \mathbf{n}_i \cdot \dot{\mathbf{H}} \cdot \mathbf{n}_i = \frac{\dot{c}_i}{c_i} = \frac{1}{c_i} \mathbf{n}_i \cdot \dot{\mathbf{C}} \cdot \mathbf{n}_i \quad \text{when } i = j \\ ii) \quad \mathbf{n}_i \cdot \dot{\mathbf{H}} \cdot \mathbf{n}_j = (h_j - h_i) \dot{\mathbf{n}}_j \cdot \mathbf{n}_i = \frac{h_i - h_j}{c_i - c_j} \mathbf{n}_i \cdot \dot{\mathbf{C}} \cdot \mathbf{n}_j \quad \text{when } i \neq j \end{array} \right\} \quad (4.13)$$

In the 2D case Eq. (4.13) yields:

$$A \begin{pmatrix} \dot{H}_{11} \\ \dot{H}_{12} \\ \dot{H}_{22} \end{pmatrix} = B \quad (4.14)$$

where A is defined as:

$$A = \begin{pmatrix} n_1^2 & 2n_1n_2 & n_2^2 \\ n_2^2 & -2n_1n_2 & n_1^2 \\ -n_1n_2 & (n_1^2 - n_2^2) & n_1n_2 \end{pmatrix} \quad (4.15)$$

and B:

$$B = \begin{pmatrix} \frac{1}{c_1}(n_1^2\dot{C}_{11} + 2n_1n_2\dot{C}_{12} + n_2^2\dot{C}_{22}) \\ \frac{1}{c_2}(n_2^2\dot{C}_{11} - 2n_1n_2\dot{C}_{12} + n_1^2\dot{C}_{22}) \\ \frac{h_1-h_2}{c_1-c_2}(-n_1n_2\dot{C}_{11} + (n_1^2 - n_2^2)\dot{C}_{12} + n_1n_2\dot{C}_{22}) \end{pmatrix} \quad (4.16)$$

By multiplying both sides of the Eq. (4.14) by  $A^{-1}$  one obtains the evolution of the components  $\mathbf{H}$  tensor as:

$$\begin{aligned} \dot{H}_{11} = & (n_1^4e^{-h_1} + n_2^4e^{-h_2} + 2n_1^2n_2^2\frac{h_1-h_2}{e^{h_1}-e^{h_2}})\dot{C}_{11} + \\ & (2n_1^3n_2e^{-h_1} - 2n_1n_2^3e^{-h_2} - 2n_1n_2(n_1^2 - n_2^2)\frac{h_1-h_2}{e^{h_1}-e^{h_2}})\dot{C}_{12} + \\ & (n_1^2n_2^2e^{-h_1} + n_1^2n_2^2e^{-h_2} - 2n_1^2n_2^2\frac{h_1-h_2}{e^{h_1}-e^{h_2}})\dot{C}_{22} = G_{11}\dot{C}_{11} + G_{12}\dot{C}_{12} + G_{13}\dot{C}_{22} \end{aligned} \quad (4.17)$$

$$\begin{aligned} \dot{H}_{12} = & (n_1^3n_2e^{-h_1} - n_1n_2^3e^{-h_2} - n_1n_2(n_1^2 - n_2^2)\frac{h_1-h_2}{e^{h_1}-e^{h_2}})\dot{C}_{11} + \\ & (2n_1^2n_2^2e^{-h_1} + 2n_1^2n_2^2e^{-h_2} + (n_1^2 - n_2^2)^2\frac{h_1-h_2}{e^{h_1}-e^{h_2}})\dot{C}_{12} + \\ & (n_1n_2^3e^{-h_1} - n_1^3n_2e^{-h_2} + n_1n_2(n_1^2 - n_2^2)\frac{h_1-h_2}{e^{h_1}-e^{h_2}})\dot{C}_{22} = G_{21}\dot{C}_{11} + G_{22}\dot{C}_{12} + G_{23}\dot{C}_{22} \end{aligned} \quad (4.18)$$

$$\begin{aligned} \dot{H}_{22} = & (n_1^2n_2^2e^{-h_1} + n_1^2n_2^2e^{-h_2} - 2n_1^2n_2^2\frac{h_1-h_2}{e^{h_1}-e^{h_2}})\dot{C}_{11} + \\ & (2n_1n_2^3e^{-h_1} - 2n_1^3n_2e^{-h_2} + 2n_1n_2(n_1^2 - n_2^2)\frac{h_1-h_2}{e^{h_1}-e^{h_2}})\dot{C}_{12} + \\ & (n_2^4e^{-h_1} + n_1^4e^{-h_2} + 2n_1^2n_2^2\frac{h_1-h_2}{e^{h_1}-e^{h_2}})\dot{C}_{22} = G_{31}\dot{C}_{11} + G_{32}\dot{C}_{12} + G_{33}\dot{C}_{22} \end{aligned} \quad (4.19)$$

where  $\dot{H}_{ij}$  and  $\dot{C}_{ij}$  are the components of the material time derivative of the corresponding matrices which can be expressed by:

$$\dot{\mathbf{H}} = \frac{\partial \mathbf{H}}{\partial t} + (\mathbf{u} \cdot \nabla) \mathbf{H} \quad (4.20)$$

$$\dot{\mathbf{C}} = \frac{\partial \mathbf{C}}{\partial t} + (\mathbf{u} \cdot \nabla) \mathbf{C} \quad (4.21)$$

The approach to derive  $\dot{\mathbf{C}}$  as a function of  $\dot{\mathbf{H}}$  is explained in appendix A. The above system of equations (4.17)-(4.19) can be summarized as:

$$\begin{pmatrix} \dot{H}_{11} \\ \dot{H}_{12} \\ \dot{H}_{22} \end{pmatrix} = \begin{pmatrix} G_{11} & G_{12} & G_{13} \\ G_{21} & G_{22} & G_{23} \\ G_{31} & G_{32} & G_{33} \end{pmatrix} \begin{pmatrix} \dot{C}_{11} \\ \dot{C}_{12} \\ \dot{C}_{22} \end{pmatrix} \quad (4.22)$$

If we substitute Eq. (4.20) and (4.21) in Eq. (4.22), we get the following equation:

$$\frac{\partial \mathbf{H}}{\partial t} + (\mathbf{u} \cdot \nabla) \mathbf{H} = \begin{pmatrix} G_{11} & G_{12} & G_{13} \\ G_{21} & G_{22} & G_{23} \\ G_{31} & G_{32} & G_{33} \end{pmatrix} \left( \frac{\partial \mathbf{C}}{\partial t} + (\mathbf{u} \cdot \nabla) \mathbf{C} \right) \quad (4.23)$$

i.e.  $\dot{\mathbf{H}} = \mathbf{G}\dot{\mathbf{C}}$

### 4.3 The extended matrix logarithm formulation (EMLF)

The proposed transformation by Fattal and Kupferman enforces the eigenvalues of the conformation tensor to remain positive for all steps of the simulation. However, satisfying the symmetric positive definiteness (SPD) of the conformation tensor during the simulation is the necessary condition to achieve stability, but, for the FENE family, one has to consider that the square of the corresponding finite extensibility parameter of the polymer should be an upper limit for the trace of the conformation tensor which can be also written as  $\sum_i c_i < b^2$  where  $c_i$  is the  $i$ th eigenvalue of the conformation tensor. To mathematically satisfy these two conditions, we introduce a new method based on the transformation of the classical constitutive equation. In the first stage, we transform the classical constitutive equation based on the conformation tensor,  $\mathbf{C}$ , to a new one based on the tensor  $\mathbf{J}$  defined hereafter, which satisfies the condition of Eq. (3.7) at each time step

$$\mathbf{J} = \frac{K}{1 - \frac{tr(\mathbf{C})}{b^2}} \mathbf{C} \quad (4.24)$$



where  $K$  is a constant.

In the second stage, we transform the tensor  $\mathbf{J}$  to a so-called matrix logarithm conformation tensor  $\mathbf{H}$ , following the lead of Fattal and Kupferman in order to obtain positive eigenvalues for the  $\mathbf{J}$  and  $\mathbf{C}$  conformation tensors.

$$\mathbf{H} = \ln(\mathbf{J}) \quad (4.25)$$

Substituting Eq. (4.24) into Eq. (3.5) leads to the following evolution equation for the  $\mathbf{J}$  conformation tensor:

$$\begin{aligned} \frac{\partial \mathbf{J}}{\partial t} + (\mathbf{u} \cdot \nabla) \mathbf{J} = & \mathbf{J} \cdot (\nabla \mathbf{u})^T + \nabla \mathbf{u} \cdot \mathbf{J} - f(\mathbf{J}) \left[ \frac{\mathbf{J} - \mathbf{I}}{KWe} \right] + \\ & \mathbf{J} \left[ \frac{\text{tr}(\mathbf{J} \cdot (\nabla \mathbf{u})^T + \nabla \mathbf{u} \cdot \mathbf{J})}{Kb^2} - \frac{f(\mathbf{J}) (\text{tr}(\mathbf{J}) - \text{tr}(\mathbf{I}))}{Kb^2 KWe} \right] \end{aligned} \quad (4.26)$$

where  $f(\mathbf{J})$  is a transformation function between  $\mathbf{C}$  and  $\mathbf{J}$  conformation tensors, defined as:

$$f(\mathbf{J}) = \frac{Kb^2 + \text{tr}(\mathbf{J})}{b^2} \quad (4.27)$$

Note that in Eq. (4.26),  $\text{tr}(\mathbf{I}) = d$  for a  $d$ -dimensional problem. To finalize our transformation we need an evolution equation for  $\mathbf{H} = \ln(\mathbf{J})$ . The eigenvalues and eigenvectors of the  $\mathbf{H}$  conformation tensor are exactly those ones reported in Eq. (4.2)-(4.4)

Evolution of the components of the  $\mathbf{H}$  tensor is:

$$\begin{aligned} \dot{H}_{11} = & (n_1^4 e^{-h_1} + n_2^4 e^{-h_2} + 2n_1^2 n_2^2 \frac{h_1 - h_2}{e^{h_1} - e^{h_2}}) \dot{J}_{11} + \\ & (2n_1^3 n_2 e^{-h_1} - 2n_1 n_2^3 e^{-h_2} - 2n_1 n_2 (n_1^2 - n_2^2) \frac{h_1 - h_2}{e^{h_1} - e^{h_2}}) \dot{J}_{12} + \\ & (n_1^2 n_2^2 e^{-h_1} + n_1^2 n_2^2 e^{-h_2} - 2n_1^2 n_2^2 \frac{h_1 - h_2}{e^{h_1} - e^{h_2}}) \dot{J}_{22} = G_{11} \dot{J}_{11} + G_{12} \dot{J}_{12} + G_{13} \dot{J}_{22} \end{aligned} \quad (4.28)$$

$$\begin{aligned} \dot{H}_{12} = & (n_1^3 n_2 e^{-h_1} - n_1 n_2^3 e^{-h_2} - n_1 n_2 (n_1^2 - n_2^2) \frac{h_1 - h_2}{e^{h_1} - e^{h_2}}) \dot{J}_{11} + \\ & (2n_1^2 n_2^2 e^{-h_1} + 2n_1^2 n_2^2 e^{-h_2} + (n_1^2 - n_2^2)^2 \frac{h_1 - h_2}{e^{h_1} - e^{h_2}}) \dot{J}_{12} + \\ & (n_1 n_2^3 e^{-h_1} - n_1^3 n_2 e^{-h_2} + n_1 n_2 (n_1^2 - n_2^2) \frac{h_1 - h_2}{e^{h_1} - e^{h_2}}) \dot{J}_{22} = G_{21} \dot{J}_{11} + G_{22} \dot{J}_{12} + G_{23} \dot{J}_{22} \end{aligned} \quad (4.29)$$

$$\begin{aligned}
\dot{H}_{22} = & (n_1^2 n_2^2 e^{-h_1} + n_1^2 n_2^2 e^{-h_2} - 2n_1^2 n_2^2 \frac{h_1 - h_2}{e^{h_1} - e^{h_2}}) \dot{J}_{11} + \\
& (2n_1 n_2^3 e^{-h_1} - 2n_1^3 n_2 e^{-h_2} + 2n_1 n_2 (n_1^2 - n_2^2) \frac{h_1 - h_2}{e^{h_1} - e^{h_2}}) \dot{J}_{12} + \\
& (n_2^4 e^{-h_1} + n_1^4 e^{-h_2} + 2n_1^2 n_2^2 \frac{h_1 - h_2}{e^{h_1} - e^{h_2}}) \dot{J}_{22} = G_{31} \dot{J}_{11} + G_{32} \dot{J}_{12} + G_{33} \dot{J}_{22}
\end{aligned} \tag{4.30}$$

where  $\dot{H}_{ij}$  and  $\dot{J}_{ij}$  are the components of the material time derivative of the corresponding matrices which can be expressed by:

$$\dot{\mathbf{H}} = \frac{\partial \mathbf{H}}{\partial t} + (\mathbf{u} \cdot \nabla) \mathbf{H} \tag{4.31}$$

$$\dot{\mathbf{J}} = \frac{\partial \mathbf{J}}{\partial t} + (\mathbf{u} \cdot \nabla) \mathbf{J} \tag{4.32}$$

The above system of equations (4.28)-(4.30) can be summarized as:

$$\begin{pmatrix} \dot{H}_{11} \\ \dot{H}_{12} \\ \dot{H}_{22} \end{pmatrix} = \begin{pmatrix} G_{11} & G_{12} & G_{13} \\ G_{21} & G_{22} & G_{23} \\ G_{31} & G_{32} & G_{33} \end{pmatrix} \begin{pmatrix} \dot{J}_{11} \\ \dot{J}_{12} \\ \dot{J}_{22} \end{pmatrix} \tag{4.33}$$

If we substitute Eq. (4.31) and (4.32) in Eq. (4.33), we get the following equation:

$$\frac{\partial \mathbf{H}}{\partial t} + (\mathbf{u} \cdot \nabla) \mathbf{H} = \begin{pmatrix} G_{11} & G_{12} & G_{13} \\ G_{21} & G_{22} & G_{23} \\ G_{31} & G_{32} & G_{33} \end{pmatrix} \left( \frac{\partial \mathbf{J}}{\partial t} + (\mathbf{u} \cdot \nabla) \mathbf{J} \right) \tag{4.34}$$

Along the centerline in the fully developed Poiseuille flow  $h_1$  tends to  $h_2$ . Therefore the quantity  $\frac{(h_1 - h_2)}{e^{h_1} - e^{h_2}}$  in Eqs. (4.28)-(4.30) is undetermined. To alleviate this problem, the limit,  $e^{-h_1}$  value has been used instead of the above equations in the centerline.

#### 4.4 The hyperbolic tangent conformation tensor

As we explained in section (4.2), Fattal and Kupferman [69] proposed to reformulate the classical constitutive equation using a new variable namely logarithmic formulation. This transformation enforces the eigenvalues of the conformation tensor to remain positive for all steps of the simulation. However, satisfying the symmetric positive definiteness (SPD)

of the conformation tensor during the simulation is the necessary condition for stability, but definitely, it is not the sufficient condition to reach meaningful results. Actually, solving the constitutive equation in the new formulation, logarithmically, lets the eigenvalues of the new conformation tensor,  $\mathbf{H}$ , change from infinite positive to infinite negative,  $[-\infty, +\infty]$ , which enforces the eigenvalues of the classical conformation tensor,  $\mathbf{C}$ , change from zero to infinite positive,  $[0, +\infty]$ , (Fig. 4.1a). Reconstructing the classical conformation and

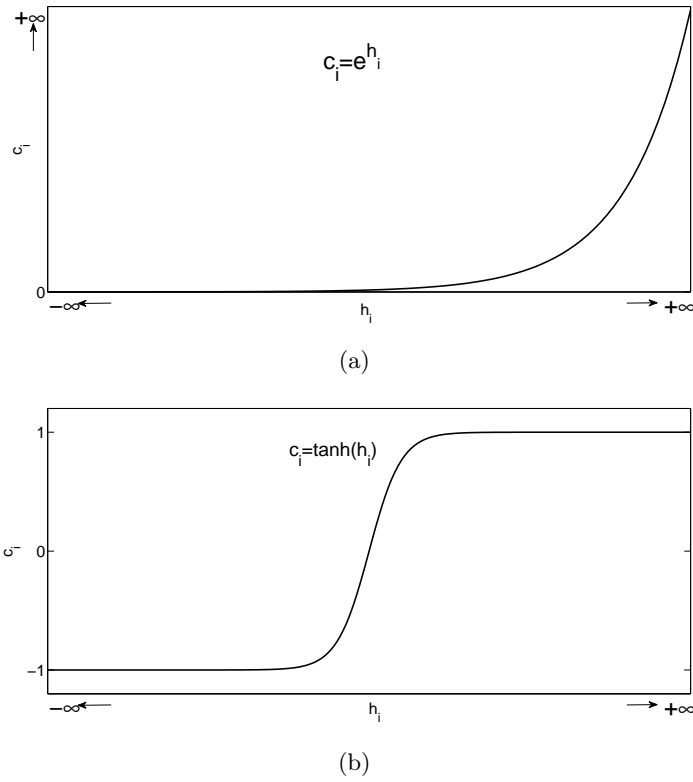


Fig. 4.1: Typical variation of  $c_i$  versus  $h_i$  for a) logarithm formulation, b) hyperbolic tangent formulation.

viscoelastic stress tensor from infinite positive eigenvalues does not have any physical meaning. A possible remedy to bound magnitude of the eigenvalues of  $\mathbf{C}$  tensor is to use the hyperbolic tangent of the  $\mathbf{H}$  conformation tensor (Fig. 4.1b). As it is obvious in this figure, however the variation of eigenvalues of  $\mathbf{H}$  tensor is in the interval  $[-\infty, +\infty]$ , the eigenvalues of  $\mathbf{C}$  conformation is totally bounded and contained in the interval  $[-1, +1]$ . To preserve the symmetric positive definiteness of the conformation tensor, it is mandatory to avoid the negative eigenvalues of  $\mathbf{C}$  conformation tensor. To do so, we use the enhanced

format of hyperbolic tangent of the conformation tensor. We transform the classical constitutive equation based on the conformation tensor,  $\mathbf{C}$ , to a new one based on the tensor  $\mathbf{H}$  defined as:

$$\mathbf{C} = \frac{b^2}{4} \tanh(\mathbf{H}) + \frac{b^2}{4} \mathbf{I} \quad (4.35)$$

or:

$$\mathbf{C} = \frac{b^2}{4} \frac{e^{\mathbf{H}}}{e^{\mathbf{H}} + e^{-\mathbf{H}}} \quad (4.36)$$

This new formulation preserves both SPD of the conformation tensor and also bounds the magnitude of the eigenvalues of  $\mathbf{C}$  formulation.

Again the eigenvalues and eigenvectors of the  $\mathbf{H}$  conformation tensor are exactly those ones reported in Eq. (4.2)-(4.3) and (4.5)-(4.7) Evolution of the components of the  $\mathbf{H}$  tensor is:

$$\begin{aligned} \dot{H}_{11} = & \left( \frac{b^2}{2c_1(b^2 - c_1)} n_1^4 + \frac{b^2}{2c_2(b^2 - c_2)} n_2^4 + 2n_1^2 n_2^2 \frac{h_1 - h_2}{c_1 - c_2} \right) \dot{C}_{11} + \\ & \left( \frac{b^2}{2c_1(b^2 - c_1)} 2n_1^3 n_2 - \frac{b^2}{2c_2(b^2 - c_2)} 2n_1 n_2^3 - 2n_1 n_2 (n_1^2 - n_2^2) \frac{h_1 - h_2}{c_1 - c_2} \right) \dot{C}_{12} + \\ & \left( \frac{b^2}{2c_1(b^2 - c_1)} n_1^2 n_2^2 + \frac{b^2}{2c_2(b^2 - c_2)} n_1^2 n_2^2 - 2n_1^2 n_2^2 \frac{h_1 - h_2}{c_1 - c_2} \right) \dot{C}_{22} = G_{11} \dot{C}_{11} + G_{12} \dot{C}_{12} + G_{13} \dot{C}_{22} \end{aligned} \quad (4.37)$$

$$\begin{aligned} \dot{H}_{12} = & \left( \frac{b^2}{2c_1(b^2 - c_1)} n_1^3 n_2 - \frac{b^2}{2c_2(b^2 - c_2)} n_1 n_2^3 - n_1 n_2 (n_1^2 - n_2^2) \frac{h_1 - h_2}{c_1 - c_2} \right) \dot{C}_{11} + \\ & \left( \frac{b^2}{2c_1(b^2 - c_1)} 2n_1^2 n_2^2 + \frac{b^2}{2c_2(b^2 - c_2)} 2n_1^2 n_2^2 + (n_1^2 - n_2^2)^2 \frac{h_1 - h_2}{c_1 - c_2} \right) \dot{C}_{12} + \\ & \left( \frac{b^2}{2c_1(b^2 - c_1)} n_1 n_2^3 - \frac{b^2}{2c_2(b^2 - c_2)} n_1^3 n_2 + n_1 n_2 (n_1^2 - n_2^2) \frac{h_1 - h_2}{c_1 - c_2} \right) \dot{C}_{22} \\ = & G_{21} \dot{C}_{11} + G_{22} \dot{C}_{12} + G_{23} \dot{C}_{22} \end{aligned} \quad (4.38)$$

$$\begin{aligned}
\dot{H}_{22} = & \left( \frac{b^2}{2c_1(b^2 - c_1)} n_1^2 n_2^2 + \frac{b^2}{2c_2(b^2 - c_2)} n_1^2 n_2^2 - 2n_1^2 n_2^2 \frac{h_1 - h_2}{c_1 - c_2} \right) \dot{C}_{11} + \\
& \left( \frac{b^2}{2c_1(b^2 - c_1)} 2n_1 n_2^3 - \frac{b^2}{2c_2(b^2 - c_2)} 2n_1^3 n_2 + 2n_1 n_2 (n_1^2 - n_2^2) \frac{h_1 - h_2}{c_1 - c_2} \right) \dot{C}_{12} + \\
& \left( \frac{b^2}{2c_1(b^2 - c_1)} n_2^4 + \frac{b^2}{2c_2(b^2 - c_2)} n_1^4 + 2n_1^2 n_2^2 \frac{h_1 - h_2}{c_1 - c_2} \right) \dot{C}_{22} = G_{31} \dot{C}_{11} + G_{32} \dot{C}_{12} + G_{33} \dot{C}_{22}
\end{aligned} \tag{4.39}$$

where  $c_1$  and  $c_2$  are the eigenvalues of the conformation tensor  $\mathbf{C}$ .

$$c_i = \frac{b^2}{2} \frac{e^{h_i}}{e^{h_i} + e^{-h_i}} \tag{4.40}$$

and  $h_i$  is the eigenvalues of the conformation tensor  $\mathbf{H}$  which obtains according to Eq. (4.2) and (4.3).  $\dot{H}_{ij}$  and  $\dot{C}_{ij}$  are the components of the material time derivative of the corresponding matrices which can be expressed by Eqs (4.20) and (4.21).

The above system of equations (4.37)-(4.39) can be summarized as:

$$\begin{pmatrix} \dot{H}_{11} \\ \dot{H}_{12} \\ \dot{H}_{22} \end{pmatrix} = \begin{pmatrix} G_{11} & G_{12} & G_{13} \\ G_{21} & G_{22} & G_{23} \\ G_{31} & G_{32} & G_{33} \end{pmatrix} \begin{pmatrix} \dot{C}_{11} \\ \dot{C}_{12} \\ \dot{C}_{22} \end{pmatrix} \tag{4.41}$$

If we substitute Eq. (4.20) and (4.21) in Eq. (4.41), we get the following equation:

$$\frac{\partial \mathbf{H}}{\partial t} + (\mathbf{u} \cdot \nabla) \mathbf{H} = \begin{pmatrix} G_{11} & G_{12} & G_{13} \\ G_{21} & G_{22} & G_{23} \\ G_{31} & G_{32} & G_{33} \end{pmatrix} \left( \frac{\partial \mathbf{C}}{\partial t} + (\mathbf{u} \cdot \nabla) \mathbf{C} \right) \tag{4.42}$$

This topic is an open door for future works in the area of viscoelastic fluids and because of the lack of time, we only focus on introducing the mathematical formulation for this promising method and the numerical simulation will be postponed for the future works.

## 4.5 Problem description

Here, we first investigate the ability of time dependent simulation originally proposed by Fattal and Kupferman [69] without considering the extended algorithm on a simple unsteady FENE-P Poiseuille flow in the spectral element framework. Then we study the

effect of each differential terms in the constitutive equation for both classical formulation (CF) and log representation (CMLF). Moreover, the influence of boundary condition on attainable Weissenberg number and accuracy of the results has been considered. We will observe that applying the log formulation for at least FENE-P fluids is not sufficient for curing the instability problem observed in numerical simulation in the spectral element context as opposed to what is observed in the context of low-order finite elements for Oldroyd-B, Giesekus [102] and Leonov models [130]. Then in the second part the ability of extended matrix logarithm formulation is compared with CF and CMLF.

The 2-D dependent Poiseuille flow shown in figure 4.2 has been considered in this approach. The computational domain consists of two parallel fixed walls. A constant nonzero pressure gradient is imposed on the flow. The magnitude of the applied pressure gradient is selected such that the channel flow rate is equal to one. All data plots shown correspond to  $\Delta t = 0.002$ ,  $Re = 1$ ,  $H = 1$ , (channel height),  $L = 4$ , (channel length),  $R_\mu = 1/9$ ,  $b = \sqrt{6}$ . Dirichlet boundary conditions for velocity and viscoelastic stress, imposed at the inflow boundary, are obtained by computing a steady Poiseuille flow. At the outflow, natural and velocity Dirichlet boundary conditions are applied. Free or natural boundary condition means here that velocity and viscoelastic stress tensor are not imposed on the outflow boundary. Only and only to compare the effect of outflow boundary on the results in term of convergence, Dirichlet condition for velocity and viscoelastic stress is also considered. No explicit boundary condition is imposed on the pressure since no pressure grid point lies on the boundary of the computational domain.

The full analytical prescription of the steady flow has been chosen as the initial condition. For fluids of the FENE family in spite of the fact no simple expression for  $\mathbf{H}$  conformation can be derived analytically, the constitutive equation becomes a set of nonlinear algebraic equations where for fully developed Poiseuille flow the transverse component of the velocity is equal to zero and all quantities except the pressure are dependent on  $y$  only. The

set of Eqs. (4.28)-(4.30) become:

$$\begin{aligned}
0 = & (n_1^4 e^{-h_1} + n_2^4 e^{-h_2} + 2n_1^2 n_2^2 \frac{h_1 - h_2}{e^{h_1} - e^{h_2}}) \times \\
& (2n_1 n_2 (e^{h_1} - e^{h_2}) (1 + (n_1^2 e^{h_1} + n_2^2 e^{h_2}))) \frac{1}{R_\mu} \left( \frac{\partial p}{\partial x_1} \left( x_2 - \frac{H}{2} \right) - \tau_{12} \right) - \frac{1}{W_e} \psi_{11}) + \\
& (2n_1^3 n_2 e^{-h_1} - 2n_1 n_2^3 e^{-h_2} - 2n_1 n_2 (n_1^2 - n_2^2) \frac{h_1 - h_2}{e^{h_1} - e^{h_2}}) \times \\
& ((n_2^2 e^{h_1} + n_1^2 e^{h_2} + 2[n_1 n_2 (e^{h_1} - e^{h_2})]^2) \frac{1}{R_\mu} \left( \frac{\partial p}{\partial x_1} \left( x_2 - \frac{H}{2} \right) - \tau_{12} \right) - \frac{1}{W_e} \psi_{12}) + \\
& (n_1^2 n_2^2 e^{-h_1} + n_1^2 n_2^2 e^{h_2} - 2n_1^2 n_2^2 \frac{h_1 - h_2}{e^{h_1} - e^{h_2}}) \times \\
& (2n_1 n_2 (e^{h_1} - e^{h_2}) (n_2^2 e^{h_1} + n_1^2 e^{h_2}) - \frac{1}{W_e} \psi_{22})
\end{aligned} \tag{4.43}$$

$$\begin{aligned}
0 = & (n_1^3 n_2 e^{-h_1} - n_1 n_2^3 e^{-h_2} - n_1 n_2 (n_1^2 - n_2^2) \frac{h_1 - h_2}{e^{h_1} - e^{h_2}}) \times \\
& (2n_1 n_2 (e^{h_1} - e^{h_2}) (1 + (n_1^2 e^{h_1} + n_2^2 e^{h_2}))) \frac{1}{R_\mu} \left( \frac{\partial p}{\partial x_1} \left( x_2 - \frac{H}{2} \right) - \tau_{12} \right) - \frac{1}{W_e} \psi_{11}) + \\
& (2n_1^2 n_2^2 e^{-h_1} + 2n_1^2 n_2^2 e^{-h_2} + (n_1^2 - n_2^2)^2 \frac{h_1 - h_2}{e^{h_1} - e^{h_2}}) \times \\
& ((n_2^2 e^{h_1} + n_1^2 e^{h_2} + 2[n_1 n_2 (e^{h_1} - e^{h_2})]^2) \frac{1}{R_\mu} \left( \frac{\partial p}{\partial x_1} \left( x_2 - \frac{H}{2} \right) - \tau_{12} \right) - \frac{1}{W_e} \psi_{12}) + \\
& (n_1 n_2^3 e^{-h_1} - n_1^3 n_2 e^{-h_2} + n_1 n_2 (n_1^2 - n_2^2) \frac{h_1 - h_2}{e^{h_1} - e^{h_2}}) \times \\
& (2n_1 n_2 (e^{h_1} - e^{h_2}) (n_2^2 e^{h_1} + n_1^2 e^{h_2}) - \frac{1}{W_e} \psi_{22})
\end{aligned} \tag{4.44}$$

$$\begin{aligned}
0 = & (n_1^2 n_2^2 e^{-h_1} + n_1^2 n_2^2 e^{-h_2} - 2n_1^2 n_2^2 \frac{h_1 - h_2}{e^{h_1} - e^{h_2}}) \times \\
& (2n_1 n_2 (e^{h_1} - e^{h_2}) (1 + (n_1^2 e^{h_1} + n_2^2 e^{h_2}))) \frac{1}{R_\mu} \left( \frac{\partial p}{\partial x_1} \left( x_2 - \frac{H}{2} \right) - \tau_{12} \right) - \frac{1}{W_e} \psi_{11}) + \\
& (2n_1 n_2^3 e^{-h_1} - 2n_1^3 n_2 e^{-h_2} + 2n_1 n_2 (n_1^2 - n_2^2) \frac{h_1 - h_2}{e^{h_1} - e^{h_2}}) \times \\
& ((n_2^2 e^{h_1} + n_1^2 e^{h_2} + 2[n_1 n_2 (e^{h_1} - e^{h_2})]^2) \frac{1}{R_\mu} \left( \frac{\partial p}{\partial x_1} \left( x_2 - \frac{H}{2} \right) - \tau_{12} \right) - \frac{1}{W_e} \psi_{12}) + \\
& (n_2^4 e^{-h_1} + n_1^4 e^{-h_2} + 2n_1^2 n_2^2 \frac{h_1 - h_2}{e^{h_1} - e^{h_2}}) \times \\
& (2n_1 n_2 (e^{h_1} - e^{h_2}) (n_2^2 e^{h_1} + n_1^2 e^{h_2}) - \frac{1}{W_e} \psi_{22})
\end{aligned} \tag{4.45}$$

where  $\psi$  is a symmetric tensor defined as:

$$\psi = -f(\mathbf{J}) \frac{(\mathbf{J} - \mathbf{I})}{K} - \frac{f(\mathbf{J})}{K b^2} \frac{\text{tr}(\mathbf{J}) - \text{tr}(\mathbf{I})}{K} \mathbf{J} \tag{4.46}$$

and  $f(\mathbf{J})$  is given by Eq. (4.27).

The solution of this nonlinear system of equations is obtained numerically by the Levenberg-Marquardt or Powell's Dog Leg method with  $10^{-4}$  initial guess for the  $\mathbf{H}$  conformation tensor [131, 145, 7]. Readers are referred to Chapter 3 for comprehensive explanation of numerical methods.

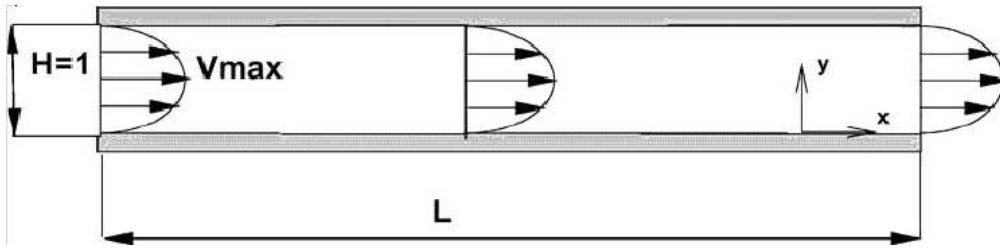


Fig. 4.2: Poiseuille flow in a planar channel.

## 4.6 Results and discussion

Results and figures shown in this section are presented in two parts. The first part corresponds to the classical matrix logarithm configuration for a time dependent Poiseuille FENE-P fluid simulation without considering the proposed extended algorithm. In this part, we show that although the use of log conformation tensor can be helpful to preserve symmetric positive definiteness of the conformation tensor, it is also mandatory for FENE family to satisfy the boundness of the conformation tensor. We show that applying the classical matrix logarithm formulation for the FENE family is not enough to enforce stability. The second part of this discussion deals with the new extension matrix logarithm conformation algorithm for a time dependent Poiseuille FENE-P fluid. The influence of this method on the resulting eigenvalue spectra can also be observed.

### 4.6.1 Classical Matrix logarithm conformation (CMLF)

To check the ability of the classical matrix logarithm formulation to describe correctly transient flow such as the generation (constant non zero pressure gradient) and decay of Poiseuille flow (zero pressure gradient starting from steady Poiseuille flows) at low Weis-



senberg number,  $We = 0.5$ ,  $4 \times 2$  equally sized elements discretization and  $4 \times 5$  polynomial degrees in the stream-wise and cross-stream directions have been considered respectively. Only Dirichlet boundary condition for velocity is imposed at outflow and no boundary for viscoelastic stress are employed at outlet. The global variations of the nonzero velocity and viscoelastic components with zero initial condition for all flow variables are shown in Figure 4.3. Since the difference between the log and classical conformation is indistinguishable only the result of log conformation is represented. The validity of the classical conformation algorithm to simulate the transient flows has been shown by Fiétier and Deville [74]. The numerical solution of the classical and log conformation formulation coincide to 6 significant figures so this guarantees the validity of this algorithm to simulate the transient flow of viscoelastic fluids.

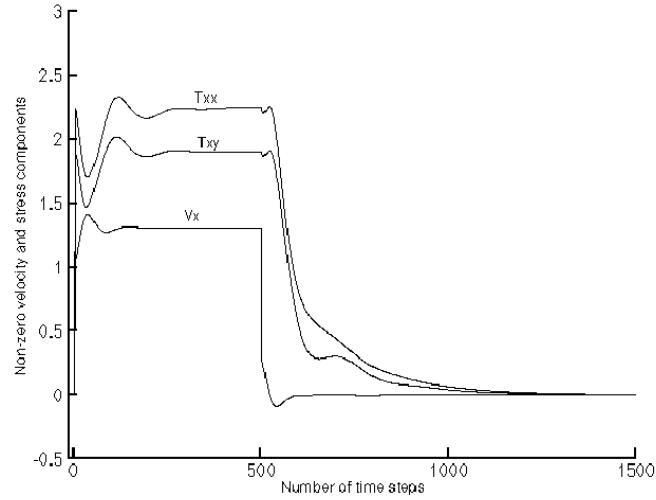


Fig. 4.3: Generation and decay of planar Poiseuille flow of a FENE-P fluids at  $We = 0.5$

#### 4.6.1.1 Influence of differential terms in the constitutive equation

Most differential constitutive models can be written in the following general form:

$$\frac{\partial \mathbf{C}}{\partial t} + (\mathbf{u} \cdot \nabla) \mathbf{C} - \mathbf{C} \cdot (\nabla \mathbf{U})^T - \nabla \mathbf{u} \cdot \mathbf{C} + \frac{1}{We} \Psi = 0 \quad (4.47)$$

which  $\Psi$  for the FENE fluids is defined as:

$$\Psi = \frac{\mathbf{C}}{1 - \frac{\text{tr}(\mathbf{C})}{b^2}} - \frac{\mathbf{I}}{K} \quad (4.48)$$

The corresponding results in this section are due to the parameters given in section 4.5. Equation (4.47) corresponds to the classical formulation. The relative error of the velocity field is based on the Euclidian norm computed after 14,000 timesteps. This number of time steps is large enough to satisfy the steady state situation at the end and also to ensure us that the blow up of the code is not due to the time marching scheme. The infinity symbol indicates that the computation breaks down during the simulation. In the first row of Table 4.1 the maximum Weissenberg number one can reach by direct computation is  $We_{max} = 56$ . According to the fully developed Poiseuille flow assumption the convection term in the momentum equation,  $\mathbf{u} \cdot \nabla \mathbf{u}$ , and the constitutive equation,  $(\mathbf{u} \cdot \nabla) \mathbf{C}$  should be equal to zero. By imposing directly these two conditions in the momentum and constitutive equations, no improvement was observed.

To check the origin of the instability in the viscoelastic fluids, two simple test cases have been done. As explained in the numerical algorithm, the constitutive equation is integrated at time step  $n+1$  for the configuration tensor using velocity obtained at previous time step. Then this viscoelastic stress tensor acts as a source term into the momentum equation. The first test case was using the analytical values for the velocity field. This means that instead of solving a system of equations, including the mass-momentum and constitutive equations, only the constitutive equation with prescribed fully developed values of velocity has been computed. Even though, stable simulation can be carried out well above the previous critical value,  $We = 56$ , magnitude of the relative error for viscoelastic stress is large for high Weissenberg numbers,  $O(10^{-2})$ . At this situation one can reach  $We = 105$  with very high relative errors for computed variables. In the second test case a fully developed expression of the viscoelastic stress tensor is prescribed in the mass-momentum equations which are only solved. As it is obvious in the fifth row of Table 4.1 the computed variables are obtained with very high accuracy,  $O(10^{-12})$ . In other words, considering both the conformation tensor and viscoelastic stress as prescribed fields leads to a stable computation. These two easy test cases reveal that the instability generation is definitely due to the constitutive equation and the coupling between momentum and constitutive equations.

By considering the deformation term,  $\mathbf{C} \cdot (\nabla \mathbf{u})^T + \nabla \mathbf{u} \cdot \mathbf{C}$ , partially or fully as an an-

alytical term, the computation can pass the critical value of the Weissenberg number,  $We = 56$ , while the convection term has no effect on the instability. As explained in Ref. [69] the manifestation of the HWNP may be caused by the failure of polynomial based approximation to properly represent exponential profiles of the deformation rate developed by the conformation tensor.

The last row of Table 4.1 corresponds to adding an extra diffusion term,  $\epsilon\Delta\mathbf{C}$ , to the constitutive equation. Different values of epsilon varying from 0.01 to 0.0005 have been considered for this test case. The effect of this extra diffusion term is only on increasing the number of iterations before breaking down but it has no effect on improving the critical Weissenberg number. In Table 4.2 the same analysis restricted to the deformation

Different cases	relative errors	$We_{critical}$
$\frac{\partial\mathbf{C}}{\partial t} + (\mathbf{u} \cdot \nabla)\mathbf{C} - \mathbf{C} \cdot (\nabla\mathbf{u})^T - \nabla\mathbf{u} \cdot \mathbf{C} + \frac{1}{We}\Psi = 0$	$\infty$	56
$\mathbf{u} \cdot \nabla\mathbf{u} = 0$	$\infty$	56
$\mathbf{u} \cdot \nabla\mathbf{C} = 0$	$\infty$	56
$\mathbf{u}_{analytical}$	$\frac{\ \boldsymbol{\tau} - \boldsymbol{\tau}_{analytical}\ }{\ \boldsymbol{\tau}_{analytical}\ } = O(10^{-2})$	105
$\boldsymbol{\tau}_{analytical}$ and $\mathbf{C}_{analytical}$	$\frac{\ \mathbf{u} - \mathbf{u}_{analytical}\ }{\ \mathbf{u}_{analytical}\ } = O(10^{-12})$ $\frac{\ p - p_{analytical}\ }{\ p_{analytical}\ } = O(10^{-12})$	150
$\frac{\partial\mathbf{C}}{\partial t} + [(\mathbf{u} \cdot \nabla)\mathbf{C} - \mathbf{C} \cdot (\nabla\mathbf{u})^T - \nabla\mathbf{u} \cdot \mathbf{C}]_{analytical} + \frac{1}{We}\Psi = 0$	$\frac{\ \mathbf{u} - \mathbf{u}_{analytical}\ }{\ \mathbf{u}_{analytical}\ } = O(10^{-2})$ $\frac{\ p - p_{analytical}\ }{\ p_{analytical}\ } = O(10^{-2})$ $\frac{\ \boldsymbol{\tau} - \boldsymbol{\tau}_{analytical}\ }{\ \boldsymbol{\tau}_{analytical}\ } = O(10^{-2})$	110
$\frac{\partial\mathbf{C}}{\partial t} + [(\mathbf{u} \cdot \nabla)\mathbf{C}]_{analytical} - \mathbf{C} \cdot (\nabla\mathbf{u})^T - \nabla\mathbf{u} \cdot \mathbf{C} + \frac{1}{We}\Psi = 0$	$\infty$	56
$\frac{\partial\mathbf{C}}{\partial t} + (\mathbf{u} \cdot \nabla)\mathbf{C} + [-\mathbf{C} \cdot (\nabla\mathbf{u})^T - \nabla\mathbf{u} \cdot \mathbf{C}]_{analytical} + \frac{1}{We}\Psi = 0$	$\infty$	75
$\frac{\partial\mathbf{C}}{\partial t} + (\mathbf{u} \cdot \nabla)\mathbf{C} - [\mathbf{C} \cdot (\nabla\mathbf{u})^T]_{analytical} - \nabla\mathbf{u} \cdot \mathbf{C} + \frac{1}{We}\Psi = 0$	$\infty$	75
$\frac{\partial\mathbf{C}}{\partial t} + (\mathbf{u} \cdot \nabla)\mathbf{C} - \mathbf{C} \cdot (\nabla\mathbf{u})^T - [\nabla\mathbf{u} \cdot \mathbf{C}]_{analytical} + \frac{1}{We}\Psi = 0$	$\infty$	75
Adding diffusion term, $\epsilon\Delta\mathbf{C}$ , to the constitutive equation	$\infty$	56

Table 4.1: Analyzing the differential terms in the classical constitutive equations.

term in the classical constitutive equation has been represented. The gist point is that the velocity gradient has been decomposed according to Ref. [69] in extension,  $\boldsymbol{\Omega}\mathbf{C} - \mathbf{C}\boldsymbol{\Omega}$ , and rotation,  $2\mathbf{B}\mathbf{C}$ , components, where  $\boldsymbol{\Omega}$  is an anti-symmetric matrix and  $\mathbf{B}$  is a symmetric

matrix. The first test case corresponds to solving the constitutive equation with the new decomposition. The critical Weissenberg number at this situation is the same as before i.e. equal to 56. In the first and second test cases reported in Table 4.2, the prescribed extension and deformation terms are directly introduced to the constitutive equation. The results indicate that there is no enhancement to achieve a higher Weissenberg number. In the fourth test case we considered the deformation term, consisting of extension and rotation, as an analytical parameter. For this test case, a stable numerical simulation can be carried out above the critical Weissenberg number, in spite of the fact the relative error for variables at this critical Weissenberg number is very high.

These analyses reveal that the source of instability is simultaneously inside both the extensional and rotational terms. The striking point of the log conformation is that the rotational component operates on  $\log(\mathbf{C})$  in the same way as it operates on  $\mathbf{C}$ . The extensional component operates on  $\log(\mathbf{C})$  additively. The transformation of the advection and the source terms is relatively straightforward [69].

Let us focus on the same analysis for the log conformation tensor after transformation

Different cases	relative errors	$We_{critical}$
$\frac{\partial \mathbf{C}}{\partial t} + (\mathbf{u} \cdot \nabla) \mathbf{C} - (\boldsymbol{\Omega} \mathbf{C} - \mathbf{C} \boldsymbol{\Omega}) - 2\mathbf{B}\mathbf{C} + \frac{1}{We} \boldsymbol{\Psi} = 0$	$\infty$	56
$\frac{\partial \mathbf{C}}{\partial t} + (\mathbf{u} \cdot \nabla) \mathbf{C} - [(\boldsymbol{\Omega} \mathbf{C} - \mathbf{C} \boldsymbol{\Omega})]_{analytical} - 2\mathbf{B}\mathbf{C} + \frac{1}{We} \boldsymbol{\Psi} = 0$	$\infty$	56
$\frac{\partial \mathbf{C}}{\partial t} + (\mathbf{u} \cdot \nabla) \mathbf{C} - (\boldsymbol{\Omega} \mathbf{C} - \mathbf{C} \boldsymbol{\Omega}) - [2\mathbf{B}\mathbf{C}]_{analytical} + \frac{1}{We} \boldsymbol{\Psi} = 0$	$\infty$	56
$\frac{\partial \mathbf{C}}{\partial t} + (\mathbf{u} \cdot \nabla) \mathbf{C} - [(\boldsymbol{\Omega} \mathbf{C} - \mathbf{C} \boldsymbol{\Omega}) - 2\mathbf{B}\mathbf{C}]_{analytical} + \frac{1}{We} \boldsymbol{\Psi} = 0$	$\frac{\ \mathbf{u} - \mathbf{u}_{analytical}\ }{\ \mathbf{u}_{analytical}\ } = O(10^{-2})$ $\frac{\ p - p_{analytical}\ }{\ p_{analytical}\ } = O(10^{-2})$ $\frac{\ \boldsymbol{\tau} - \boldsymbol{\tau}_{analytical}\ }{\ \boldsymbol{\tau}_{analytical}\ } = O(10^{-2})$	110

Table 4.2: Analyzing the deformation term of the classical FENE-P constitutive equations.

from classical constitutive equation  $\mathbf{C}$  in Table 4.3. The general form of the classical Matrix logarithm formulation can represent as:

$$\frac{\partial \mathbf{H}}{\partial t} + (\mathbf{u} \cdot \nabla) \mathbf{H} = \mathbf{f}_{nonlinear} \quad (4.49)$$

where  $\mathbf{f}_{nonlinear}$  depends on the rheological model and for FENE-P model is similar to the right hand side of the equation (4.23). As for the classical representation, the convection terms in both momentum and constitutive equations have no effect on the instability. The

validity of this statement has been demonstrated by imposing directly a zero convection term in the relevant equations. The computation collapses in both cases at  $We = 56$  for the same discretization as in the classical formulation.

By prescribed fully developed values for the velocity and only solving the constitutive equation, stable simulation could be obtained with Weissenberg numbers around 100 with low accuracy for the viscoelastic stress. In contrast by solving only the momentum equation and imposing directly the fully developed values for viscoelastic stress and conformation tensor, no restriction to simulate flows at high Weissenberg number was observed. Similarly to the classical formulation, the instabilities originate from the constitutive equation.

The other interesting test cases is the investigation of the effect of each nonlinear terms,  $\mathbf{u} \cdot \nabla \mathbf{H}$  and  $\mathbf{f}_{analytical}$ , in the constitutive equation. If one replaces each term separately with the corresponding analytical fully-developed term, the computation collapses at  $We = 56$ . In contrast, considering an analytical prescription for the nonlinear term enables one to reach a Weissenberg number equal to 150. Further analysis shows that the manifestation of the instabilities is related to the rheological model,  $\mathbf{f}_{analytical}$ , and the convection term,  $\mathbf{u} \cdot \nabla \mathbf{H}$  as opposed to the classical formulation for which the convection term does not act on the instability generation.

Different cases	relative errors	$We_{critical}$
$\frac{\partial H}{\partial t} + u \cdot \nabla H = f$	$\infty$	56
$u \cdot \nabla u = 0$	$\infty$	56
$u \cdot \nabla H = 0$	$\infty$	56
$u_{analytical}$	$\frac{\ \tau - \tau_{analytical}\ }{\ \tau_{analytical}\ } = O(10^{-3})$	100
$\tau_{analytical}$ and $H_{analytical}$	$\frac{\ u - u_{analytical}\ }{\ u_{analytical}\ } = O(10^{-6})$	150
	$\frac{\ p - p_{analytical}\ }{\ p_{analytical}\ } = O(10^{-6})$	
$\frac{\partial H}{\partial t} + u \cdot \nabla H = f_{analytical}$	$\infty$	56
$\frac{\partial H}{\partial t} + (u \cdot \nabla H)_{analytical} = f$	$\infty$	56
$\frac{\partial H}{\partial t} + (u \cdot \nabla H)_{analytical} = f_{analytical}$	$\frac{\ u - u_{analytical}\ }{\ u_{analytical}\ } = O(10^{-3})$	150
	$\frac{\ p - p_{analytical}\ }{\ p_{analytical}\ } = O(10^{-3})$	
	$\frac{\ \tau - \tau_{analytical}\ }{\ \tau_{analytical}\ } = O(10^{-3})$	

Table 4.3: Analyzing the log matrix FENE-P constitutive equations.

#### 4.6.1.2 Influence of outflow boundary condition

Here, the specification of suitable boundary conditions at outflow is considered. Several kinds of outflow boundary conditions, including natural boundary condition (NBC), velocity Dirichlet and free viscoelastic stress boundary condition (VDFVSBC) (no viscoelastic stress is imposed at outflow in this case) and full (velocity and viscoelastic stress) Dirichlet boundary condition (FDBC) for both velocity and viscoelastic stress are evaluated for 2D-Poiseuille flow with  $4 \times 2$  equal spectral elements in the stream and cross-stream directions respectively. The streamwise velocity field visible in Figures (4.4)-(4.6) is exactly shown one step before the numerical simulation breaks down at critical Weissenberg number.

Figure 4.4 corresponds to natural boundary condition (NBC) at outflow for critical Weissenberg number equal to 19. In both log, top, and classical representation, bottom, the perturbation is generated at the channel exit indicating that some mismatch occurs at outflow.

Imposing a Dirichlet boundary condition for velocity (VDFVSBC) at outflow instead of a natural one (NBC) implies that the perturbation is generated at the end of the domain. However, the configuration of the perturbation is completely different from the one obtained with outflow natural boundary condition as this can be observed by comparing Figures 4.4 and 4.5. It must then be emphasized, that a perturbation is generated at the end of the domain for either outflow natural or velocity Dirichlet boundary condition. Imposing Dirichlet boundary condition solely postpones the instability. On the other hand, no instability is observed at  $We = 19$  for outflow velocity Dirichlet boundary condition.

Figure 4.6 shows the stream wise velocity field where both outflow velocity and viscoelastic stress Dirichlet boundary condition are imposed at critical Weissenberg number,  $We = 56$ . Imposing this condition allows to obtain the Poiseuille field at the expense of higher relative errors for other flow variables. However no enhancement is achieved concerning the attainable maximum Weissenberg number. One can conclude that the instability might be due to an unsuitable boundary condition at outflow.

One may therefore wonder what is the correct outflow boundary condition when the system of equations is solved in a finite domain delimiting an internal flow.

The constitutive equation is inherently of the hyperbolic type [173], so the time evolution of the system is governed not only by the state in the interior of the region, but also by the information brought by incoming characteristics which enter the region. Thus boundary conditions which describe the incoming waves are required to completely specify the behavior of the system. The outgoing waves are described by characteristic equations, the incoming waves may often be specified by a non-reflecting boundary condition [208], so imposing a Dirichlet boundary condition on the viscoelastic stress at outflow is inappropriate, even though doing so was found slightly better in terms of convergence. A critical value of  $We = 56$  is observed when imposing full Dirichlet boundary condition for both velocity and viscoelastic stress.

Last but not least, a striking point for this part is that for all three boundary conditions, (NBC), (VDFVSBBC), (FDBC), the accuracy of all variables decreases as the Weissenberg number increases. For full Dirichlet boundary condition this statement is even much stronger.

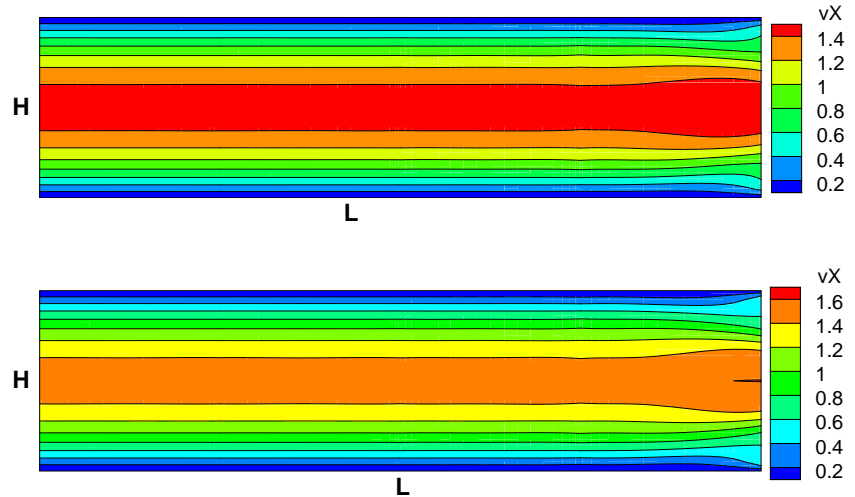


Fig. 4.4: The effect of boundary condition on the velocity field at  $We = 19$  (natural boundary condition) top: classical matrix logarithmic formulation , bottom: classical formulation.

It can be observed in Fig. 4.7a that the maximum relative error with respect to

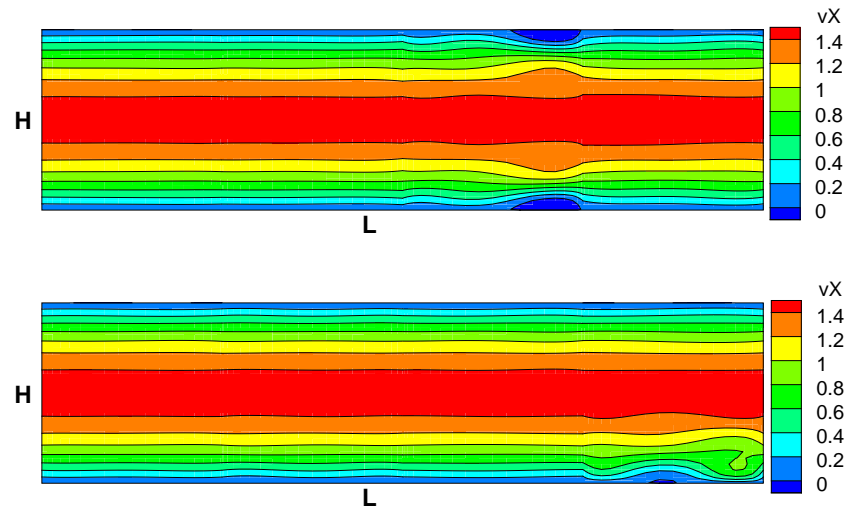


Fig. 4.5: The effect of boundary condition on the velocity field at  $We = 56$  (imposing Dirichlet boundary condition for velocity at outflow) top: classical matrix logarithmic formulation, bottom: classical formulation.

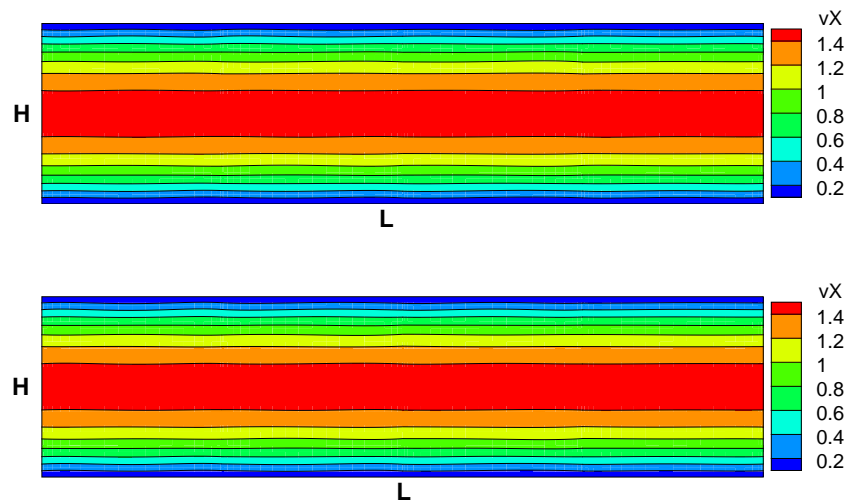


Fig. 4.6: The effect of boundary condition on the velocity field at  $We = 56$  (imposing full Dirichlet boundary condition at outflow) top: classical matrix logarithmic formulation, bottom: classical formulation.

the fully-developed solution increases as the Weissenberg number increases. This plot



is obtained for the log representation and three different boundary conditions, natural boundary condition, Dirichlet boundary condition for velocity and full Dirichlet boundary condition for both velocity and viscoelastic stress, at outflow. It is really difficult to obtain accurate results close to the critical values of  $We$ . Furthermore the residual norm cannot be decreased any further by increasing the number of time steps. The same behavior, increasing magnitude of errors for all variables near the critical Weissenberg number, has been observed for the classical formulation ( Fig. 4.7b). Figure 4.8 shows the relative

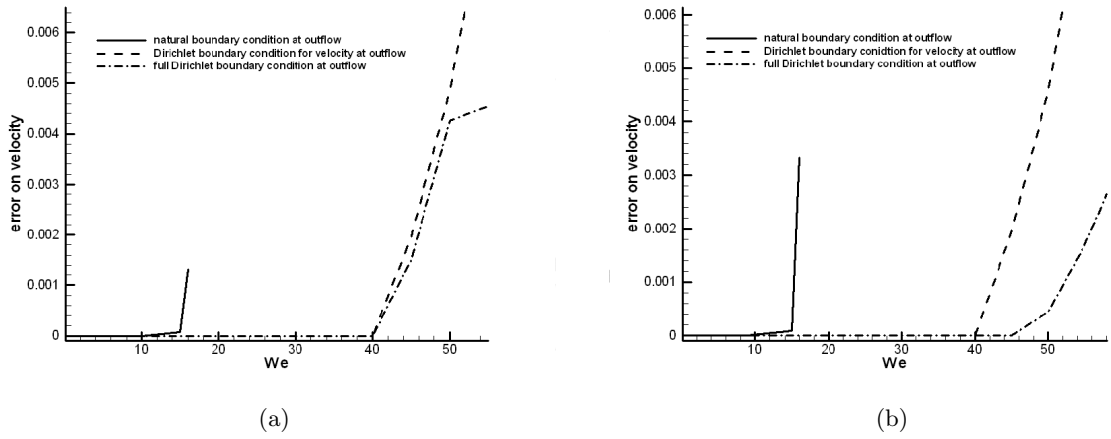


Fig. 4.7: Typical variation of the relative error on the velocity versus the Weissenberg number, a) logarithm conformation b) classical conformation,  $(NE_x, NE_y) = (4, 2)$ ,  $(N_x, N_y) = (4, 5)$ .

errors of the stream-wise velocity versus the number of steps at semi-log plot for both log and classical conformation with outflow natural boundary condition. At low Weissenberg number the relative errors are very low since the standard configuration is a little bit more accurate than the log conformation tensor. Above a given Weissenberg number, these errors increase with the number of steps at an exponential rate which can be easily identified by a straight line. A striking point is that both log and classical conformation tensor break at the same critical Weissenberg number. The effect of different parameters such as channel length,  $L$ , the number of spectral elements in the stream wise,  $NE_x$ , and cross-stream,  $NE_y$ , direction, the polynomial order,  $N_x$  and  $N_y$  has been considered in Table 4.4. It is worth to emphasize that outflow velocity boundary condition has been considered for this test case. The last column corresponds to the relative error of the velocity field based on the Euclidean norm after some arbitrary number of time steps

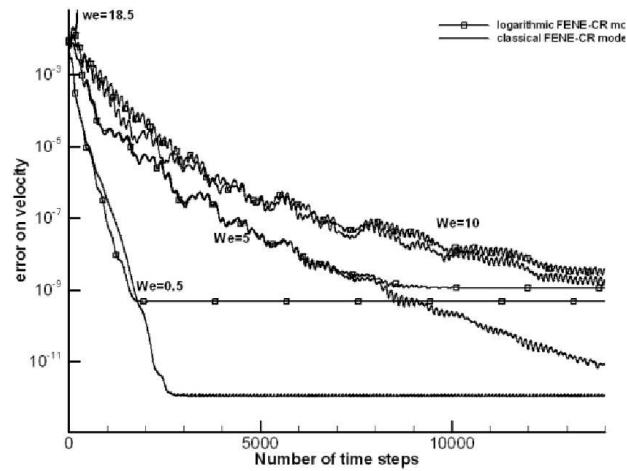


Fig. 4.8: Typical variation of the relative error on the velocity versus the number of time steps with the outflow natural boundary condition

(14000). The infinity symbol indicates that the simulation broke down after some iterates. As it is obvious in this table it is very difficult to decide which mesh is more suitable at high value of  $We$ . The other point is that with a fixed number of elements in both stream wise and cross-stream-wise direction, the instability occurs at low values of  $We$  when the length of channel is reduced. The same observation has been reported by Fiétier [71].

#### 4.6.2 Extended matrix logarithm formulation (EMLF)

According to the previous discussion by directly transforming the classical equation into the matrix logarithm formulation, the HWNP can not be cured satisfactorily in the context of spectral element. This is in agreement with the findings of Russo and Phillips [189] when they tried to apply the CMLF to the Oldroyd-B model with this discretization method. Once again we have to emphasize that the log formulation in the context of finite element for Oldroyd-B and Giesekus [102] and Leonov models [120] works very well at high Weissenberg numbers.

Let us now employ the extended matrix logarithm formulation to the classical consti-

<i>case</i>	$L$	$(NE_x, NE_y)$	$(N_x, N_y)$	$We$	$\frac{\ u - u_{analytical}\ }{\ u_{analytical}\ }$
1	4	(1,1)	(17,11)	24	1.995e-03
2	4	(4,2)	(4,5)	25	$\infty$
3	4	(4,2)	(4,5)	55	5.998e-03
4	4	(4,2)	(4,5)	56	$\infty$
5	4	(2,2)	(4,5)	66	5.600e-03
6	4	(2,2)	(4,5)	67	$\infty$
7	4	(2,2)	(4,7)	44	3.719e-03
8	4	(2,2)	(4,7)	45	$\infty$
9	4	(2,2)	(6,5)	60	4.005e-03
10	4	(2,2)	(6,6)	61	$\infty$
11	8	(2,2)	(4,5)	67	5.178e-03
12	8	(2,2)	(4,5)	68	$\infty$
13	8	(4,2)	(4,5)	65	4.210e-03
14	8	(4,2)	(4,5)	66	$\infty$
15	8	(4,2)	(6,5)	59	4.629e-03
16	8	(4,2)	(6,5)	60	$\infty$
17	16	(2,2)	(4,5)	67	4.738e-03
18	16	(2,2)	(4,5)	68	$\infty$
19	32	(2,2)	(4,5)	67	3.963e-03
20	32	(2,2)	(4,5)	68	$\infty$
21	32	(4,2)	(4,5)	67	4.906e-03
22	32	(4,2)	(4,5)	68	$\infty$

Table 4.4: Weissenberg limitation values when the element decomposition of the domain is fixed and the polynomial orders are varied

tutive equation. The capability of this new algorithm to tackle the high Weissenberg number will be investigated by linear stability analysis as explained in chapter 6.

First, we considered  $4 \times 2$  equally sized elements and  $4 \times 5$  polynomial degrees in the  $x$  and  $y$  directions. We have performed the corresponding time dependent simulation for both classical and extended matrix logarithm formulation. For the classical approaches, one could obtain a critical value of the Weissenberg number equal to 56 while for this

new algorithm one can easily tackle Weissenberg numbers larger than 100. The maximum relative error for the velocity component in stream wise direction with respect to the Weissenberg number is shown in Fig. 4.9 for the EMLF, CMLF and CF. This plot is obtained while imposing only Dirichlet boundary condition for velocity at outflow. At low values of Weissenberg number the order of the error is very low and increases with growing  $We$ . The behavior of matrix logarithm and classical conformation is very similar while for the new extended algorithm the accuracy of the results till  $We = 75$  is very good and decreases at an exponential rate. Nevertheless, the order of accuracy for the new extended algorithm is better with logarithmic and classical one. To show the reliability of

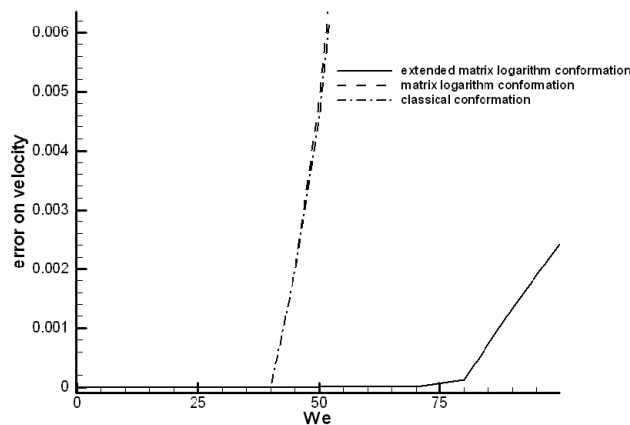


Fig. 4.9: Typical variation of the relative error on the velocity versus the Weissenberg number, VDFVSB,  $(NE_x, NE_y) = (4, 2)$ ,  $(N_x, N_y) = (4, 5)$ .

the solution, we investigated error convergence with respect to mesh refinement in both stream and cross-stream direction at  $We = 1$  and  $We = 10$ , for the new extended matrix logarithm formulation. In Table 4.5 the simulation was performed using  $4 \times 2$  equally sized elements for different polynomial degrees. The maximum relative error of the unknown variables, velocity, pressure and viscoelastic stress is based on the Euclidian norm computed after 14,000 time steps. At  $We = 1$  mesh refinement experiment in cross-stream wise direction improves the convergence and accuracy, while mesh refinement in stream wise direction does not decrease the residual any further. At  $We = 10$ , increasing the polynomial degree in cross-stream wise has a slight effect on decreasing the accuracy. In contrast, increasing the mesh refinement in stream wise direction causes the computation

to break down during the simulation. The significant point is that for the first three rows of Table 4.5 at  $We = 1$  exponential convergence can be observed.

$(N_x, N_y)$	$\frac{\ \tau - \tau_{analytical}\ }{\ \tau_{analytical}\ }$ at $We = 1$	$\frac{\ \tau - \tau_{analytical}\ }{\ \tau_{analytical}\ }$ at $We = 10$
$4 \times 5$	5.433e-4	9.980e-4
$4 \times 7$	2.872e-5	3.166e-3
$4 \times 9$	4.429e-7	8.957e-4
$4 \times 11$	1.507e-7	4.805e-4
$6 \times 5$	1.576e-4	4.316e-2
$6 \times 7$	2.814e-5	6.356e-3
$8 \times 7$	2.960e-5	$\infty$
$10 \times 7$	2.930e-5	$\infty$
$12 \times 7$	2.862e-5	$\infty$

Table 4.5: Error convergence analysis for the new extended matrix logarithm formulation,  $(NE_x, NE_y) = (4, 2)$ .

## 4.7 Conclusion

In this study, we present three different approaches to tackle high Weissenberg number problem. The first one, classical matrix logarithm formulation, is proposed by Fattal and Kupferman [69]; i.e. the second, extended matrix logarithm formulation, is published in [104] and the third one, the tangent hyperbolic, has not yet been implemented. The capability of the first two formulations in the spectral element context has been considered.

First, the ability of time dependent simulation of the classical matrix logarithm without considering the extended algorithm has been tested on a simple unsteady FENE-P Poiseuille flow. One of the possible manifestation of HWNP is the failure of polynomial-based approximation to properly represent the exponential profiles. In this stage, the influence of each differential terms in the constitutive equation for both log and classical representation has been investigated. For classical representation the manifestation of instability is inside the deformation term, while the source of instability for the matrix logarithm formulation is simultaneously inside the nonlinear term including convection

and source terms. The effect of outflow boundary condition reveals that the instability is highly sensitive to boundary condition. According to the concept of hyperbolic equation, imposing a Dirichlet boundary condition for viscoelastic stress at outflow has no physical meaning. However, this type of boundary condition was found slightly better in term of convergence. For the discretization used in this study the reachable Weissenberg number by imposing the velocity Dirichlet boundary condition at outflow is 56. Stable simulations at higher Weissenberg number could be achieved for outflow velocity Dirichlet boundary condition, than for natural boundary condition. In both cases, a numerical instability has been observed near the downstream boundary when the Weissenberg number approached the same critical value.

Another significant point is that the relative errors for the unknown variables, pressure, velocity and viscoelastic stress fields, are very low at low values of Weissenberg number and increase with increasing the Weissenberg number.

With the classical matrix logarithm formulation it has been observed that when the Weissenberg number approached the critical value the simulation stopped because the necessary condition that the square of the corresponding finite extensibility parameter of the polymer should be an upper limit for the trace of the conformation tensor was not satisfied. According to this, we have introduced a new extended matrix logarithm formulation to enforce this condition. Another surprising result is that using the classical matrix logarithm formulation instead of the classical one in the context of spectral elements at least for FENE-P does not help to simulate high Weissenberg number flows. This is clearly different from what has been observed with low-order finite elements, Hulsen et al. [102], and Kwon [120], and finite volumes, Afonso et al. [4].

# Chapter 5

---

## Simulation of abrupt contraction flow

This chapter presents the vortex structure and instability augmentation with increasing the elasticity in inertial flows in planar contraction and contraction-expansion configuration for FENE-P fluid. Moreover the re-entrant corner effect on corner vortices is studied. The calculations are performed using extended matrix logarithm formulation described in the previous chapter. In this study we are interested in the capability of this algorithm for complex geometry. This procedure helps to reach higher values of the Weissenberg number when compared to the classical formulation.

### 5.1 Introduction

The prediction of viscoelastic flows in complex geometries, such as in expansions or contractions, has both scientific interest and industrial relevance. Understanding entry flow of viscoelastic fluids is of importance in fundamental flow-property measurement and in extrusion of polymer melts and solutions. Furthermore, the characteristics of vortices and flow patterns are of particular interest in the design of extrusion dies.

The four to one contraction problem is one of the benchmark problems that numeracists dealing with non-Newtonian fluids are used to face. This problem is such that the fluid enters the inflow section usually with a Poiseuille profile, goes through a contraction where the height of the exit channel is reduced by a factor four with respect to the inlet dimension and exits the computational domain. The non-Newtonian flows are characterized by the presence of corner and lip vortices. Although the geometry looks very simple, solutions for high Weissenberg ( $We$ ) or Deborah ( $De$ ) numbers may not be available. One of the reasons of this failure comes from the fact that the stress components are not square integrable at the corner and are locally singular. One of the main issue for the simulation of contraction flows is the lack of adequate outflow boundary condition. In the past two

decades, considerable efforts have been devoted to the development of numerical simulation of abrupt contraction flows with various methods.

Kim et al. [117] performed high-resolution solutions for viscoelastic 4:1 planar contraction flow problems using a transient finite element method based on the fractional step method (FSM) and stabilization techniques (DEVSS-G/DG) with linear equal-order interpolation function. The fully developed boundary conditions for the velocity and extra stress field are imposed along the inlet. At the outlet, the Neumann boundary condition of velocity is imposed, that is, the gradient-free velocity is considered and the pressure is zero at the outlet. The Oldroyd-B model was used as the constitutive equation. The vortex intensity and the re-attachment length of corner vortex show good agreement with the predictions of the high-resolution finite volume method of Alves et al. [11]. The converged solution could be obtained up to  $We = 2.5$  with the finest mesh used in their study.

Alves et al. [11] performed very accurate numerical results for the vortex size, the vortex intensity and the Couette correction, in planar contraction flows of Oldroyd-B and PTT fluids with both the linear and the exponential stress function, and with a solvent viscosity ratio equal to 1/9. The method is utilised by them does not need a Dirichlet condition for stresses at outlet. In fact, the boundary condition applied is of the Neumann type ( $\partial\tau_{ij}/\partial x$ ) and thus may lead to some localised distortions for the low Reynolds number. The finest mesh employed had over 1 million degrees of freedom. Such degree of mesh fineness is shown to be required for accurate results with the Oldroyd-B fluid, especially at high Deborah numbers, but the shear-thinning PTT fluid in general does not require such accuracy. No upper limit on  $De$  was found for the exponential form of the PTT constitutive model, while an approximate limit of  $De \approx 200$  was found for the linear form

Al Moatssime et al. [10] employed a numerical algorithm for the steady flow of viscoelastic fluid. The conservative law and constitutive equations are solved using the finite volume method (FVM) with a hybrid scheme for the velocities and first-order upwind approximation for the viscoelastic stress. A non-uniform staggered grid system is used. The iterative SIMPLE algorithm is employed to relax the coupled momentum and continuity equations. The non-linear algebraic equations over the flow domain are solved iteratively by the symmetrical coupled Gauss-Seidel (SCGS) method. The full approximation storage multigrid algorithm is used. An Oldroyd-B fluid model was selected for the calculation.



Results are reported for planar 4:1 abrupt contraction at various Weissenberg numbers,  $1.5 \leq We \leq 4.5$ . The fully developed Poiseuille flow is imposed at the inlet and outlet sections. The solutions are found to be stable and smooth. The solutions show that at high Weissenberg number the domain must be long enough. The maximum Weissenberg number which is reported in their paper is  $We = 4.5$ . The convergence of the method has been verified with grid refinement. .

Mompean and Deville [155] performed an Oldroyd-B fluid using the finite volume technique. All inertia terms in the momentum and constitutive equations are taken into account and are discretized in space using a quadratic upwind scheme. Case studies have been conducted in particular for two-dimensional (2D) 4:1 and 3D 4:1:4 planar contractions. In the entry section, far from the upstream of flow disturbance and assuming there was no perturbation in the inflow, all values of the extra-stress components vanish. In this section (entry), a constant value for the pressure is given. In the outlet section the same procedure is used for the pressure, setting it to zero. For the extra-stress components homogeneous Neumann condition (zero gradient) is used, assuming that this boundary is far from flow disturbances. The algorithm was tested up to  $De = 157$ . A steady state solution was found for all cases. The size of the corner vortex for the 4:1 planar contraction, in the 2D case, is in good agreement with previous computations.

Yul Yoo and Na [243] introduced a finite volume technique in an attempt to simulate the planar 4:1 contraction flow of the Oldroyd B fluid on a non-uniform staggered grid system, which incorporates the SIMPLER algorithm in discretizing the momentum equations and the deferred correction method in discretizing the constitutive equations. In the far upstream region of the contraction, the flow can be approximated as a plane Poiseuille flow. The full analytical prescription of the steady flow is imposed at the entry while at the exit the Neumann boundary conditions for the flow variables are imposed. Results are reported at  $0.1 \leq We \leq 20$ . For some combinations of viscoelastic parameters, the size and shape of the corner vortex growth are shown to be in good qualitative agreement with those observed experimentally by others for constant viscosity viscoelastic fluids. In general, however, they seem to be sensitive to the ratio of retardation time to relaxation time.

Aguayo et al. [5] investigated the numerical solution of viscoelastic flows using two con-

trasting high-order finite volume schemes. The numerical techniques employed are time-stepping algorithms: one of hybrid finite element/volume type, the other of pure finite volume form. The momentum-continuity equations are solved by a fractional-staged Taylor-Galerkin pressure-correction procedure and invoke a cell-vertex finite volume scheme for the constitutive law. Fully developed boundary conditions are established at the outflow. A comparison of the two finite volume approaches is presented, concentrating upon the new features posed by the pom-pom class of models in this context of non-smooth flows. Here, the dominant feature of larger shear and extension in the entry zone influences both stress and stretch, so that larger stretch develops around the re-entrant corner zone as Weissenberg number increases, whilst correspondingly stress levels decline.

Lee et al. [128] performed finite element modeling of planar 4:1 contraction flow (isothermal incompressible and creeping) around a sharp entrance corner for favored differential constitutive equations such as the Maxwell, Leonov, Giesekus, FENE-P, Larson, White-Metzner models and the Phan Thien-Tanner model of exponential and linear types. Fully developed flow conditions are applied for the velocity and conformation tensor at the inlet but only for the velocity at the outlet. They have implemented the discrete elastic viscous stress splitting and streamline upwinding algorithms in the basic computational scheme in order to augment stability at high flow rate. For each constitutive model, the upper limit of the Deborah number is obtained under which numerical convergence is guaranteed. The maximum upper limit of Deborah number is reported for Giesekus model with the value of  $De = 200$ . All the computational results are analyzed according to consequences of mathematical analysis for constitutive equations from the viewpoint of stability. It is verified that in general the constitutive equations that was proved globally stable yield convergent numerical solutions for higher Deborah number flows. Therefore one can get solutions for relatively high Deborah number flows when the Leonov, the Phan Thien-Tanner, or the Giesekus constitutive equation is employed as the viscoelastic field equation. The close relationship of numerical convergence with mathematical stability of the model equations is also clearly demonstrated.

Alves and poole [14] investigated the upper-convected Maxwell (UCM) model of viscoelastic flow through smooth planar contractions of various contraction ratios with particular emphasis placed on the divergent flow regime. It is shown that above a critical Deborah number, the flow becomes unsteady and they used an analysis based on the scaling laws

of McKinley et al. [149] for purely elastic instabilities to show that the square of this critical Deborah number varies linearly with contraction ratio in excellent agreement with the numerical results obtained in their study.

Kwon [120] presented an alternative procedure to derive the tensor logarithmic representation of the differential constitutive equation and provided a numerical example with the Leonov model in 4:1 planar contraction flow using SUPG and SU stabilization techniques. Fully developed flow conditions are applied for the velocity and log-conformation tensor at the inlet but only for the velocity at the outlet. Dramatic improvement of the computational algorithm with the stable convergence has been demonstrated. They could achieve  $De = 132$  with a coarse mesh and  $De = 193$  for a refined mesh.

Webster et al.[230] considered transient flows for planar contractions and Oldroyd-B fluids, with increasing flow-rate boundary conditions. Velocity components are imposed at inlet and exit stations, whilst stress is imposed at inlet only. In addition, a pressure level is set at a boundary exit point, hence removing indeterminacy on ambient pressure. They employ a novel hybrid finite volume/element time-dependent algorithm. This scheme is shown to be second-order accurate. The hybrid scheme consists of a Taylor-Galerkin finite element discretisation, and a cell-vertex fluctuation-distribution finite volume approach. These two approaches are coupled at each time-step to solve the parabolic/hyperbolic system of partial differential equations. The finite element section is applied to the mass and momentum conservation equations, whilst the hyperbolic constitutive equation is treated via finite volume discretisation. The application of this time-accurate scheme to complex flows reveals some novel features, in contrast to time-independent (constant flow-rate) driving boundary conditions. In particular, they highlight dynamic flow structure evolution on the field and in stress. Results in this paper are reported at  $0.3 \leq We \leq 2$

Meng et al. [150] developed a new algorithm, which combines the spectral element method with elastic viscous splitting stress (EVSS) method, has been developed for viscoelastic fluid flows in a planar contraction channel. The system of spectral element approximations to the velocity, pressure, extra stress and the rate of deformation variables is solved by a preconditioned conjugate gradient method based on the Uzawa iteration procedure. The numerical approach is implemented on a planar four-to-one contraction channel for a fluid governed by an Oldroyd-B constitutive equation. Fully developed velocity profiles can be

imposed in entry and exit sections. Moreover, the extra-stress tensor based on a fully developed flow is only imposed at the entry section. The behavior of the Oldroyd-B fluids in the contraction channel is investigated for various Weissenberg numbers ( $0.1 \leq We \leq 1.2$ ).

The planar contraction channel flow problems, over the years, have been solved by a variety of numerical techniques and a non exhaustive list of references is given in the bibliography [82, 116, 211, 196, 12, 230, 49, 121, 180, 154, 1, 161, 184, 165, 179, 240, 241, 21, 242, 45, 199]. Most of these numericists encounter the same problem, namely the inadequacy of numerical techniques to describe flow regimes specially close to the entrance of contraction.

The aim of this chapter is to introduce and study the capability of extended matrix logarithm formulation [104] to predict the flow pattern in complex geometry such as 2-D contraction and contraction-expansion geometry which is very popular in the extrusion industry. The influence of Weissenberg number, re-entrant corner shape are examined to investigate corner vortices and augment the instabilities during the simulation.

## 5.2 Test problems

In this study, first we investigate the behavior of 2-D abrupt contraction flow. The main goal of this part is the comparison between the classical and extended matrix logarithm formulation to simulate this singular and complex geometry. In this stage, in particular, attention is given to the differences in vortex development for inertial flows by increasing the values of Weissenberg number.

In the second part of this study, we consider an abrupt contraction-extension geometry in order to predict the flow pattern, The same as before natural boundary condition for both velocity and viscoelastic stress has been imposed for outflow boundary. Considering this geometry is one step forward for our future goal for employing periodic boundary condition. Adopting periodic boundary conditions in stream-wise direction and resorting to spectral element-Fourier discretization will be considered in our future work.

The 2-D time dependent 4:1 contraction flow is shown in Fig. 5.1. time dependent simulation means that we start from a specified initial condition to reach the steady state

of the the flow. Planar contraction consists of two rectangular channels connected by a plate as shown in Fig. 5.1. Here we consider that the contraction occurs only in one transverse direction, say  $y$ . The contraction can be considered as almost two-dimensional except in the vicinity of the side walls if the channel extension in the other transverse direction is large compared to the channel dimension in  $y$ -direction. A particular difficulty associated with simulations of viscoelastic flows through abrupt contraction is the presence of a strong stress singularity at the sharp re-entrant corner. In order to relax the corresponding numerical constraints, a round edge corner with the radius of  $R = 0.009D$  is employed. This value is selected such that the radius of round corner is very small. Center line,  $Y_1 = 0.6125D$ ,  $Y_2 = 0.625D$  and upper wall are those positions which in cross-wise direction which have been used for comparison between different cases. In this study we considered  $D = 1$

Fig. 5.2 shows the schematic diagram of a 2-D 4:1 contraction-expansion flow which is used for the second part of this study. The diameter of round edge is  $d = 0.125D$ . For this test case  $Y_1 = 0.5625D$ ,  $Y_2 = 0.625$  and  $D = 1$ . For both cases the length of each channel is considered long enough to ensure the fully developed condition at the end of the domain. The magnitude of applied pressure gradient is taken to be  $-0.5$  for upstream channel. The magnitude of the applied pressure gradient is selected such that the channel flow rate is very small ( $\approx 0.04$ ). All data plots shown correspond to  $Re = 1$ ,  $R_\mu = 1/9$  and  $b = \sqrt{6}$ . The rest state is used as the initial condition for all variables (velocity, pressure and viscoelastic stress are set to zero). It is worth to say that if we apply exactly zero initial condition for extended  $H$ -conformation tensor the inverse algorithm to transfer  $H$  to  $C$  fails. So far, a small value such as 0.0001 is adjusted for  $H$  conformation tensor as a rest value.

Dirichlet boundary conditions for velocity and viscoelastic stress, imposed at the inflow boundary, are obtained by computing a steady Poiseuille flow. At the outflow boundary, free boundary conditions are applied. Free or natural boundary condition means here that velocity and viscoelastic stress tensor are not imposed on the outflow boundary. Here, the simulations are based on 20000 and 10000 time step with  $\Delta t = 0.0005$  for the first and second geometry respectively. However for some cases because of instability problems, it was impossible to end the simulation successfully. “*EMLF*” and “*CF*” are the abbreviation of extended matrix logarithm formulation and classical formulation which have occasionally

been used in the context.

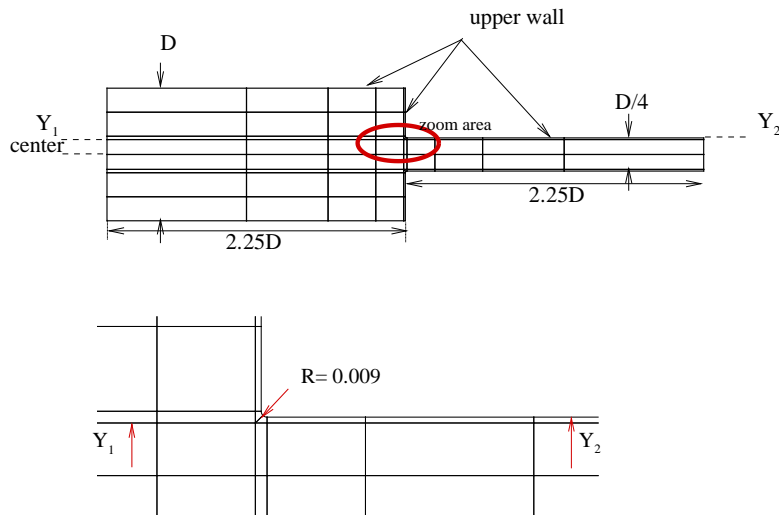


Fig. 5.1: Geometry of 4:1 planar contraction flow with different position of height.

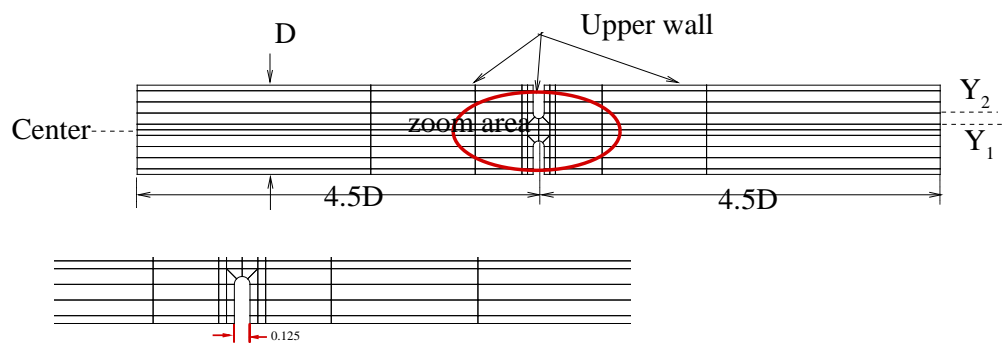


Fig. 5.2: Geometry of 4:1 planar contraction-expansion flow with different position of height.

## 5.3 Results and discussion

### 5.3.1 2-D 4:1 planar contraction flow

Two different mesh characteristics are listed in Table 5.1, in which there are 58 elements for both ones. A uniform polynomial order equal to 7 has been used for Mesh I over the most of the elements except in the vicinity of the re-entrant corner where it has been decreased to 4 in order to improve numerical stability. For the second mesh, Mesh II, the polynomial order increases in each element for both directions. The polynomial order of 10 is employed instead of 7 and 7 instead of 4. We arranged elements in a way that there is interface matching and no mortar element method is used for this study.

First, we investigate the reliability of the solution for Newtonian, EMLF and CF for these two different meshes. To do so, we validate the error convergence analysis with respect to mesh refinement for a Newtonian fluid, EMLF and CF FENE-P model in Table 5.2. The relative error of velocity is based on the Euclidian norm,  $\frac{\|v^{n+1}-v^n\|}{\|v^{n+1}\|}$ , computed after 20000 time steps and reported in Table 5.2. For Newtonian fluid, EMLF and CF at low value of the Weissenberg number ( $We = 0.1$ ) mesh refinement experiment improves the convergence and accuracy. At higher value of Weissenberg ( $We = 8$ ) mesh refinement for EMLF does not improve the accuracy. Whereas for CF, it causes the simulation to break down during the simulation. The same observation has been reported for other unknown variables such as viscoelastic stress.

Degree of freedom	Mesh I	Mesh II
Velocity	5228	10976
Viscoelastic stress	7842	16464
Pressure	1278	3456
number of elements	58	58

Table 5.1: Spectral element mesh characteristic data for contraction geometry

To better understand the convergence rate for both classical and logarithm formulation, Fig. 5.3 and 5.4 represent the relative error of velocity with respect to iteration number at different Weissenberg numbers for Mesh I and Mesh II respectively. For both log and

Mesh	Newtonian fluid	EMLF	EMLF	CF	CF (We=8)
		(We = 0.1)	(We=10)	(We=0.1)	
Mesh I	1.002e-12	5.769e-12	2.100e-5	6.144e-13	1.253e-5
Mesh II	6.387e-15	1.511e-12	7.721e-5	1.538e-15	$\infty$

Table 5.2: Error convergence analysis of the relative error on the velocity,  $\frac{\|u^{n+1}-u^n\|}{\|u^{n+1}\|}$ , for Newtonian, EMLF and CF FENE-P fluids,  $Re = 1$ .

classical formulation we have observed immediate convergence after some iterations at low values of the Weissenberg numbers. At a critical value of the Weissenberg number, suddenly the relative error increases exponentially which prevents the successful numerical approximation. For the classical formulation, with the fine mesh at critical value of Weissenberg number,  $We = 5$ , however the rate of convergence is very good but the simulation stops because Eq. (3.7) is violated.

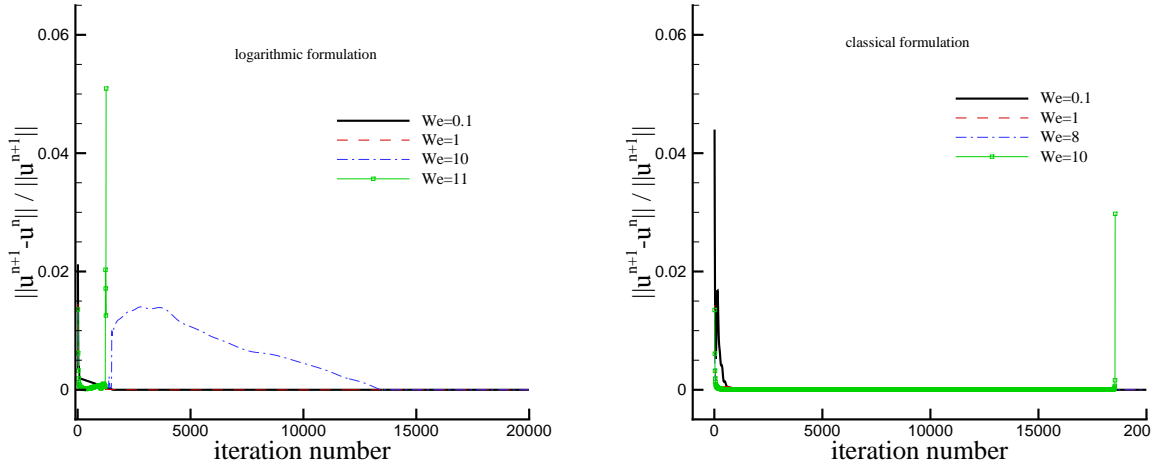


Fig. 5.3: Typical variation of the relative error on the velocity versus the iteration number using Mesh I, left) logarithmic formulation, right) classical formulation.

To check the ability of EMLF algorithm to describe correctly transient flow through contraction geometry, stream-wise velocity,  $u_x$ , and first normal viscoelastic stress,  $\tau_{xx}$ , of both classical and logarithmic conformations are compared at low Weissenberg number,



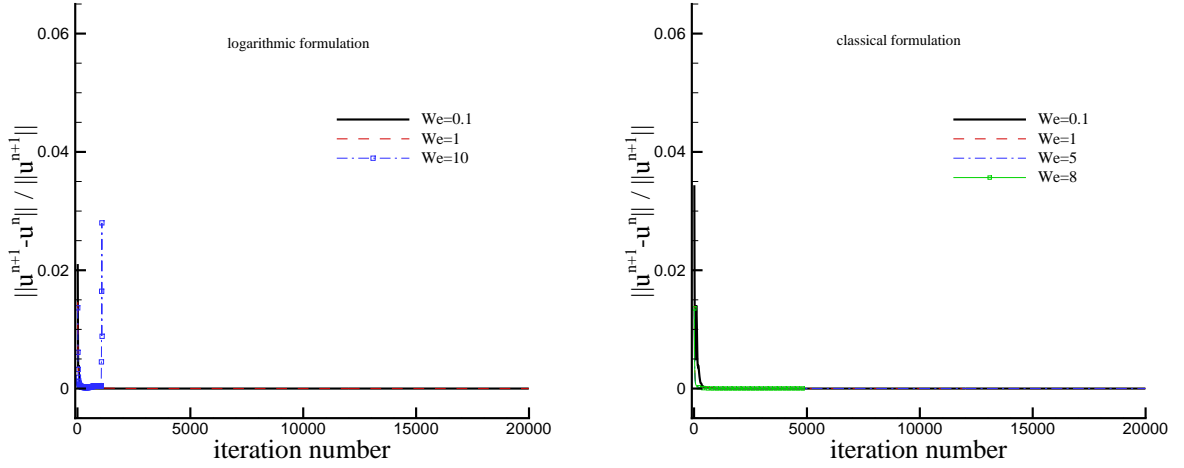


Fig. 5.4: Typical variation of the relative error on the velocity versus the iteration number using Mesh II, left) logarithm formulation, right) classical formulation.

$We = 0.1$ , with Mesh I after 20000 iterations. As shown in Fig. 5.5, the difference between the log and classical conformation is not distinguishable. The validity of the classical algorithm to simulate complex geometry has been shown by Fiétier [71].

In Fig. 5.6 the stream-wise velocity is plotted along the  $x$  axis at different position of  $Y$  for  $We = 0$ ,  $We = 0.1$ ,  $We = 1$ , and  $We = 10$ . The simulations are performed with Mesh I and the extended matrix logarithm formulation. As shown in this figure, the velocity overshoots downstream of the corner increase with increasing values of  $We$ . This figure also shows how the velocity overshoots settles down to its fully developed value along the downstream wall. At  $We = 10$ , which is the maximum attainable Weissenberg for this test case, longer downstream length is required. At low value of Weissenberg number,  $We = 0.1$ , no significant difference is reported between the viscoelastic and Newtonian fluids.

Fig. 5.7 represents the first normal viscoelastic stress,  $\tau_{xx}$ , along the  $x$ -axis. We see the overshoot and undershoot magnitude of  $\tau_{xx}$  in the vicinity of downstream of re-entrant corner. Magnitudes of overshooting increase by increasing the Weissenberg number while the undershoot values increase by decreasing the Weissenberg number. The behavior of

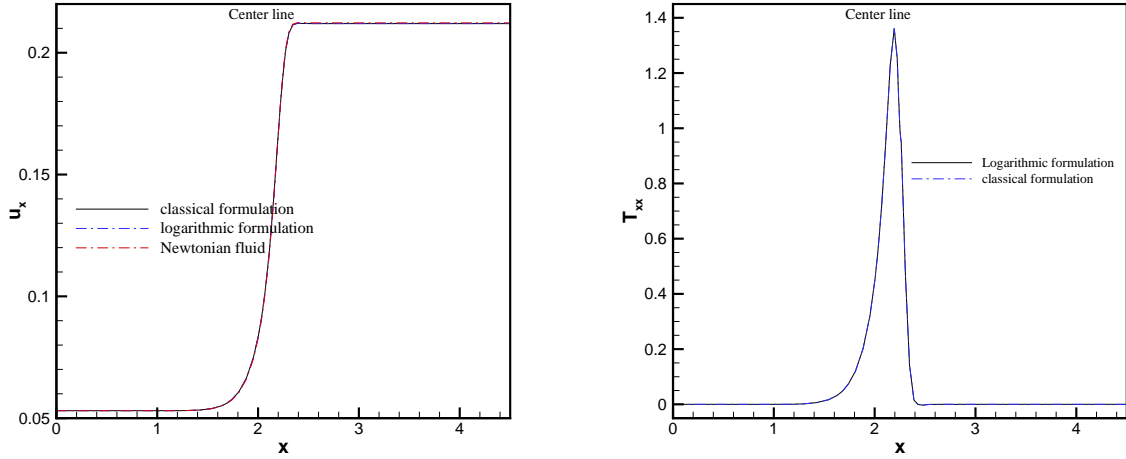


Fig. 5.5: Comparison between log and classical formulation at low Weissenberg number,  $We = 0.1$  using Mesh I.

flow, downstream of the re-entrant corner at  $We = 10$  has more deviation from the fully developed flow and it takes more time to reach the fully developed prescription.

For further investigation, the same type of plots are shown for the shear viscoelastic stress,  $\tau_{xy}$ . The difference between the values of  $\tau_{xy}$  appears after the re-entrant corner. The higher Weissenberg number produces higher values of  $\tau_{xy}$  in the second channel. In contrast, the maximum overshoot or undershoot are obtained for the lower value of the Weissenberg number.

Fig. 5.9-5.11 indicate the effect of the geometry of the re-entrant corner at two different Weissenberg numbers,  $We = 0.1$  and  $We = 10$ . The values of  $u_x$ ,  $\tau_{xx}$  and  $\tau_{xy}$  in center line are chosen for comparison between round corner with radius  $R = .009$  and sharp edge. These test cases have performed with Mesh I after 20000 iterations. These plots show that stable results could be obtained even with a sharp corner. The maximum attainable Weissenberg number for both round and sharp corner with Mesh I and EMLF is  $We = 10$  while for the classical formulation this critical value for the same test case and MeshI is  $We = 8$ .

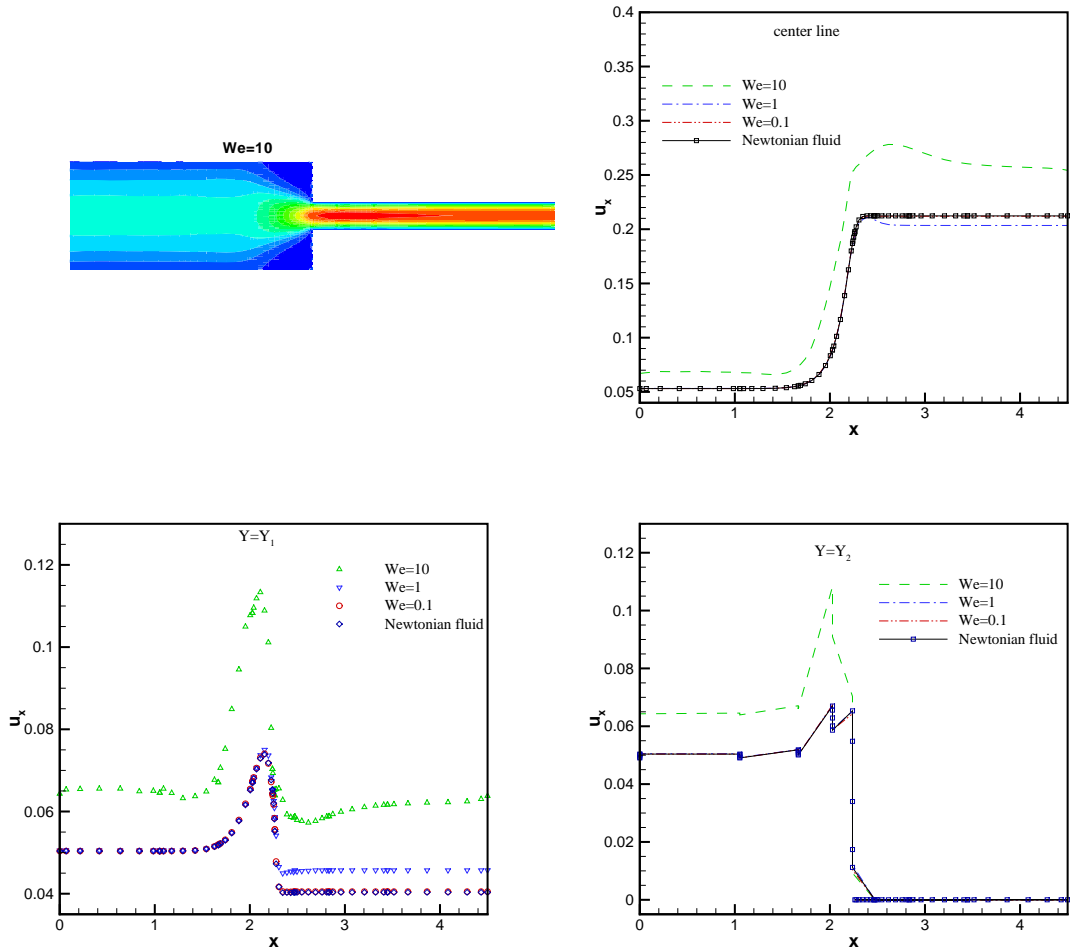


Fig. 5.6: Comparison of the plots of  $u_x$  along the stream-wise direction at different values of  $We$ , EMLF using Mesh I.

The stream function,  $\Psi$ , for  $We = 0$ ,  $We = 1$ ,  $We = 10$  and  $We = 11$  are presented in Fig. 5.12 for round re-entrant corner. The calculation has been performed with Mesh I after 20000 iterations with  $\Delta t = 0.0005$ . For  $We = 11$ , the simulation blows up only after 1268 iterations. At  $We = 10$  negative stream function, dashed line, appears close to the corner while this is not the case for Newtonian and  $We = 1$ . By increasing the Weissenberg number the maximum value of stream function increases. The same plot is shown for sharp corner re-entrant in Fig. 5.13. The maximum value of stream function at  $We = 10$  for sharp corner is higher than that for the round corner. The vortex intensity

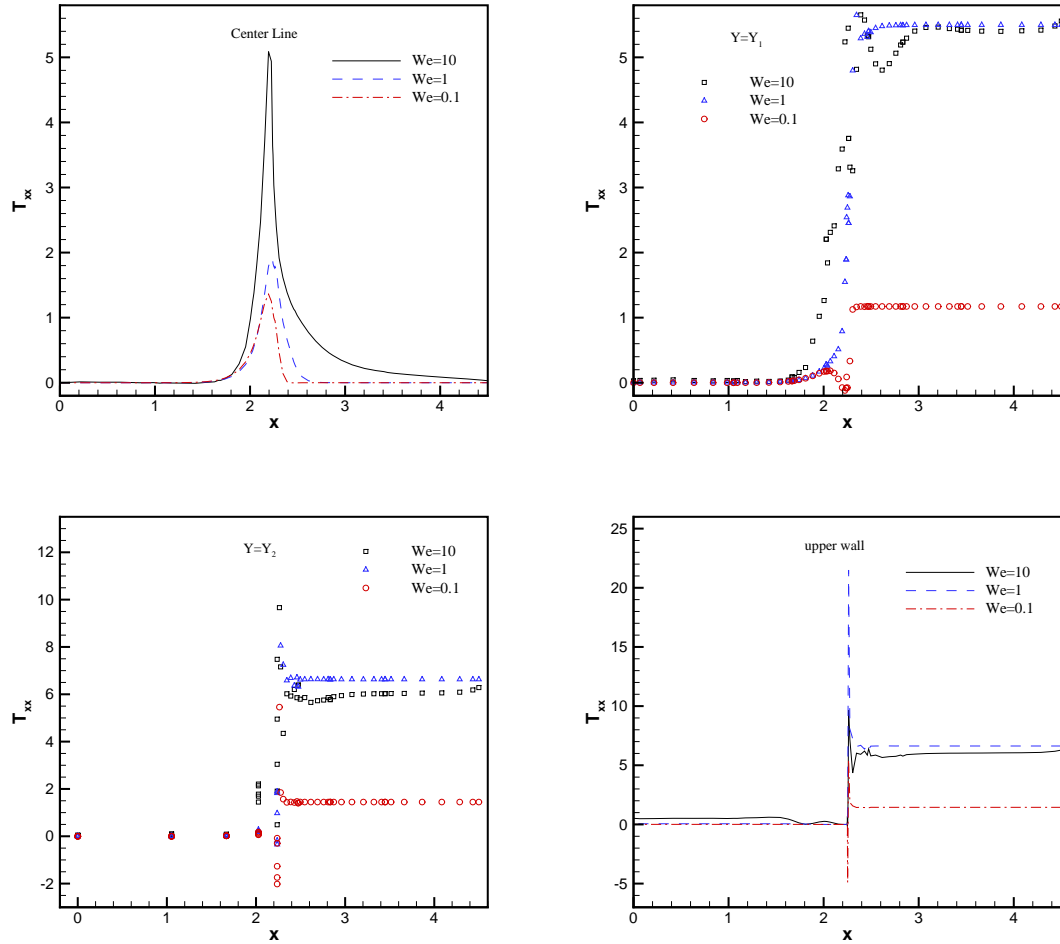


Fig. 5.7: Comparison of the plots of  $\tau_{xx}$  along the stream-wise direction at different values of  $We$ , EMLF using Mesh I.

based on the maximum value of stream function for two meshes, Mesh I and Mesh II, classical and logarithmic conformation are summarized in Table 5.3. At low values of the Weissenberg the vortex intensity is constant while by increasing the Weissenberg number this value increases. The infinity symbol in this table means that the computation breaks down during the simulation and this symbol “NA” means no simulation has been carried out at this Weissenberg number. This table also reveals that critical Weissenberg for classical conformation tensor with Mesh I and II is 8 and 5 respectively, while for logarithm conformation is 10 and 8 respectively.

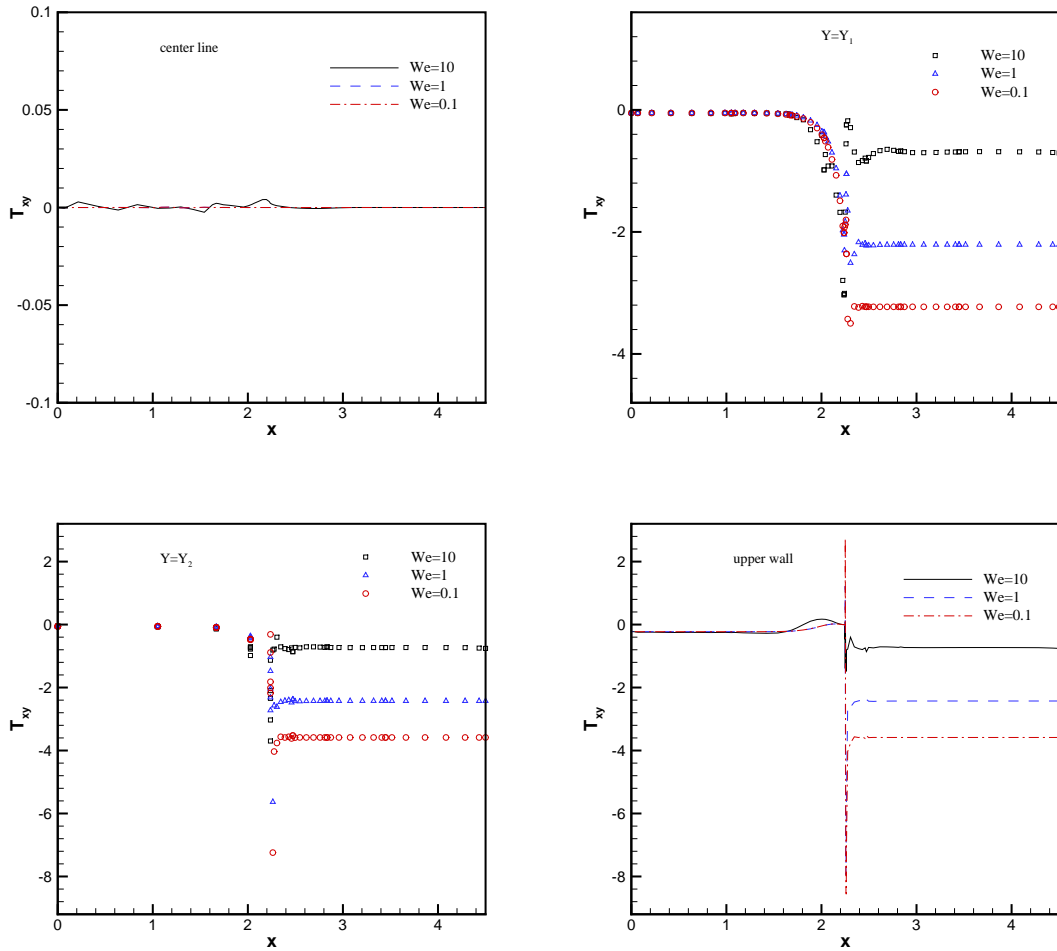


Fig. 5.8: Comparison of the plots of  $\tau_{xy}$  along the stream-wise direction at different values of  $We$ , EMLF using Mesh I.

The results of transient computations obtained by extended matrix logarithm formulation, and Mesh I at  $We = 11$  are presented in Fig. 5.14 in terms of stream function. The results are shown at 6 different times where the last one is the instant when the simulation breaks down. Very quickly after some iterations the unstable stream functions, close to the corner, is excited and instabilities are induced to the upper level of the stream function. The results are represented for round re-entrant corner, meanwhile the same behavior can be observed for the sharp corner.

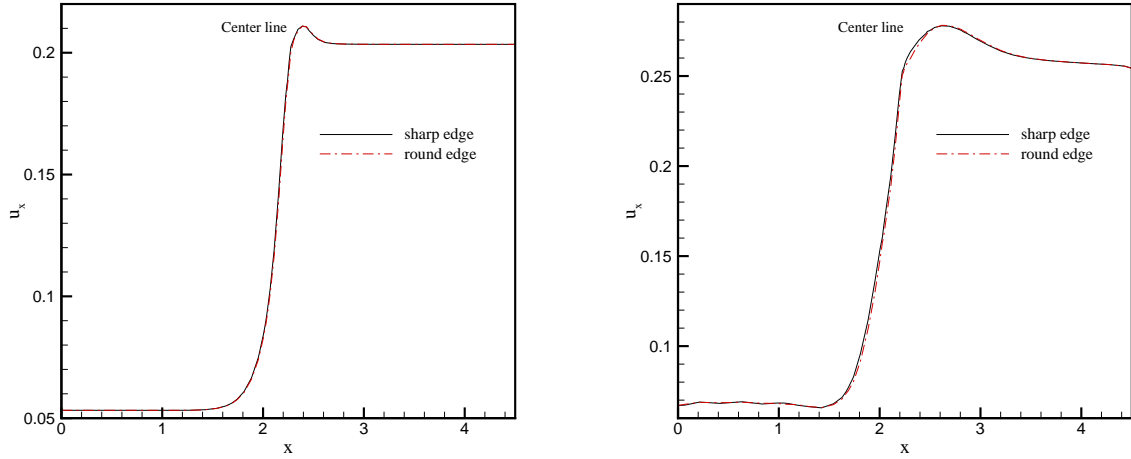


Fig. 5.9: Comparison of  $u_x$  along center line between round and sharp corner using Mesh I and EMLF algorithm, left)  $We = 0.1$ , right)  $We = 10$

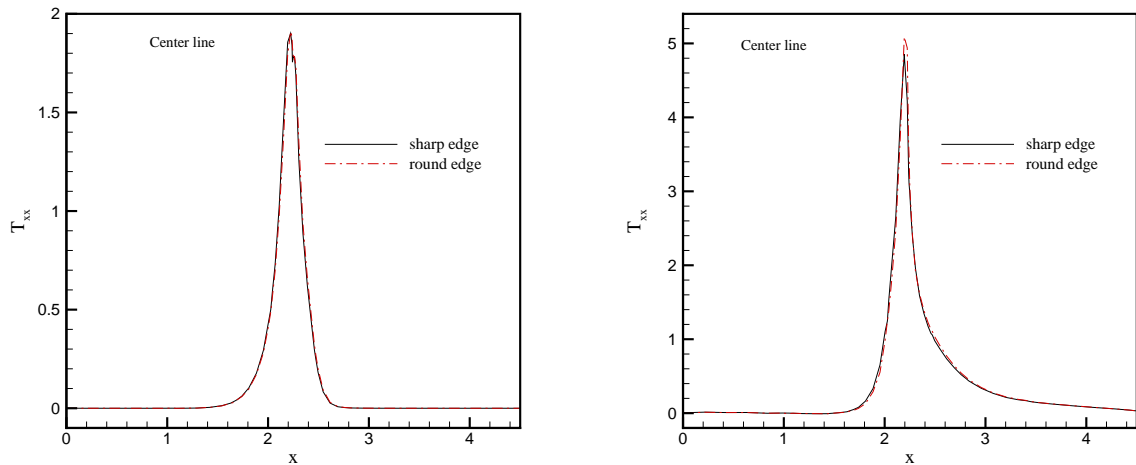


Fig. 5.10: Comparison of  $\tau_{xx}$  along center line between round and sharp corner using Mesh I and EMLF, left)  $We = 0.1$ , right)  $We = 10$ .

It is worth to mention, that no lip vortex onset has been detected with our simulation for the range of investigated contraction ratios (4:1). This is probably due to relatively low values of the corresponding extensional viscosity since this parameter has a strong

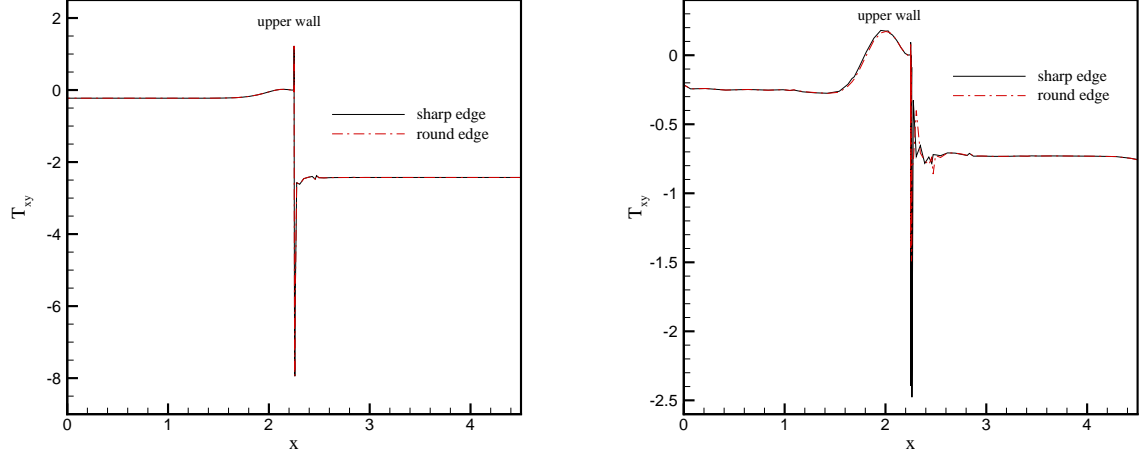


Fig. 5.11: Comparison of  $\tau_{xy}$  along center line between round and sharp corner using Mesh I and EMLF algorithm, left)  $We = 0.1$ , right)  $We = 10$ .

We	Mesh I			Mesh II	
	CF (round edge)	EMLF (round edge)	EMLF (sharp edge)	CF (round edge)	EMLF (round edge)
0	0.041667	0.041667	0.041667	0.041667	0.041667
0.1	0.041667	0.041667	0.041667	0.041667	0.041667
1	0.041667	0.041667	0.041667	0.041732	0.041667
5	NA	NA	0.041873	$\infty$	NA
8	0.042597	NA	NA		0.043376
10	$\infty$	0.043268	0.043384		$\infty$
11		$\infty$	$\infty$		$\infty$

Table 5.3: Vortex intensity as measured by the maximum value of the stream function,  $\Psi_{max}$

influence on the appearance or not of lip vortices as indicated by Boger [28]. In addition, the contraction ratio has very strong influence on the vortex growth mechanism since lip vortices are only present for certain values of this parameter for a given fluid and similar Weissenberg numbers. The reader is referred to Ref. [12] with a view to classifying the structure of flows through contractions. Authors have carried out an extensive simulation program, for various contraction ratios and increasing Deborah numbers, and the resulting steady-state flow patterns in the contraction plane region were classified as corner vortex, lip vortex, or as a combination of lip plus corner vortex structures.

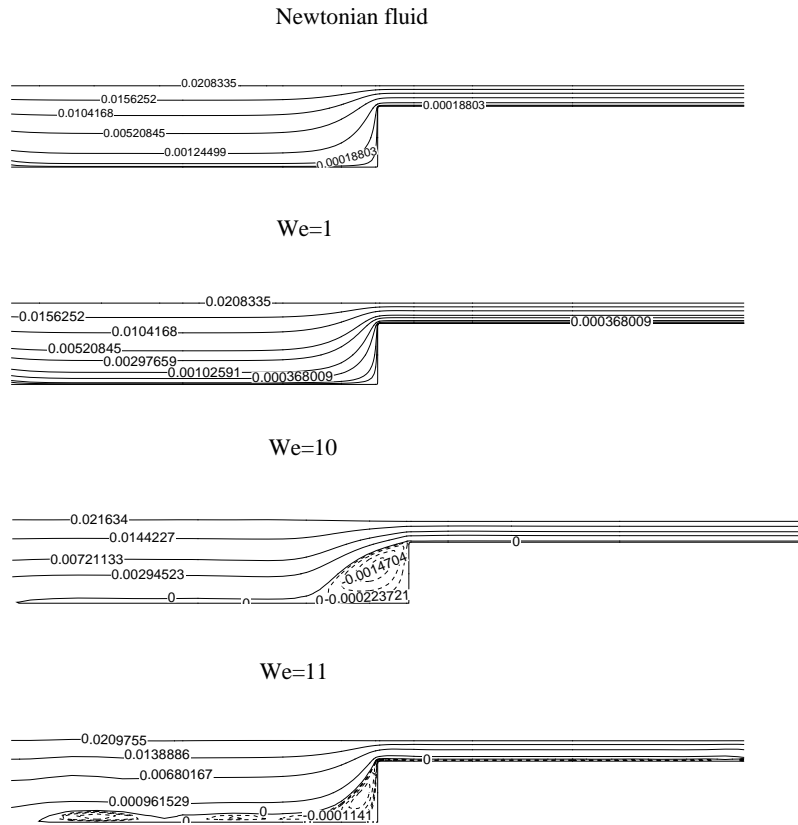


Fig. 5.12: The stream function for EMLF at different Weissenberg number,  $We = 0$ ,  $We = 1$ ,  $We = 10$  and  $We = 11$  using Mesh I and round re-entrant corner.

### 5.3.2 2-D 4:1 planar contraction-expansion flow

The geometry in this case is the 2D 4:1 planar contraction-expansion flow was shown in Fig. 5.2. The mesh characteristics are summarized in Table 5.4 in which there are 104 elements. Here, only EMLF was employed to predict the transient flow of this complex geometry. To validate the accuracy of our algorithm first, we compare the values of stream-wise velocity in center line between Newtonian and FENE-P fluid at  $We = 0.1$ . No distinguishable difference has been detected in this figure (Fig. 5.15). This test case was extremely expensive in terms of CPU time. The results reported in this section performed after 10000 iterations.

It is worth to say that the simulations done in this dissertation have been carried out



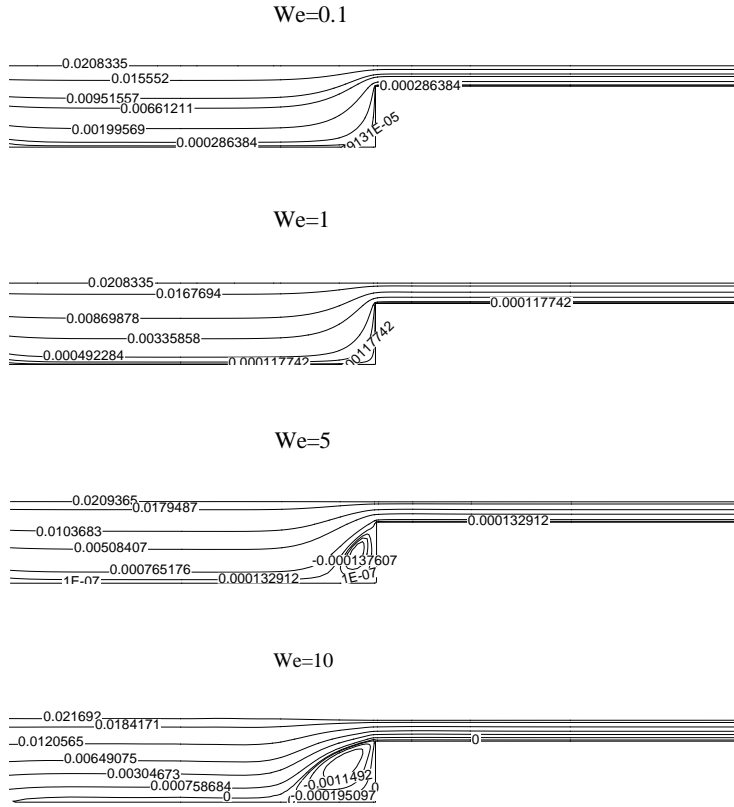


Fig. 5.13: The stream function for EMLF at different Weissenberg number,  $We = 0.1$ ,  $We = 1$ ,  $We = 5$  and  $We = 10$  using Mesh I and sharp re-entrant corner.

on single processor. However, SPECULOOS is written in parallel fashion but there are still some problems in parallelization of viscoelastic part which restricted us to use single processor. The computer architectures used in our case has summarized in Table 5.5. For example, 5s simulation of contraction-expansion geometry takes approximately 3 days running. Fig. 5.16 represents stream function and velocity contour at  $We = 10$  and stream-wise velocity in center line and  $Y_1$  for  $We = 0.1$ ,  $We = 5$  and  $We = 10$ . As for the previous geometry the overshoot velocity occurs downstream of the first entry and increases by increasing the Weissenberg number. At  $We = 10$  after obstacle, very small undershoot appears. The less the fluid elasticity, the fastest the full steady statement. The stream function plot indicates that the vortex zone of the first entry is larger than the second entry. The maximum attainable Weissenberg number is  $10 < We_{critical} < 20$ .

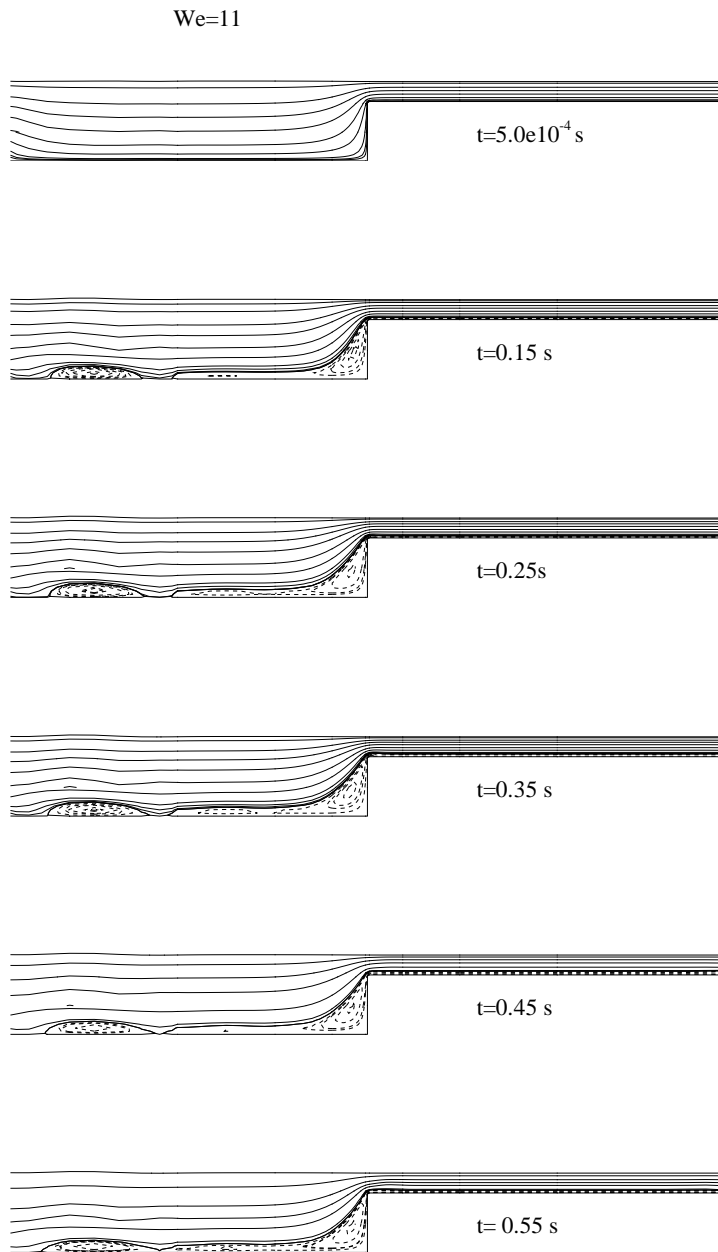


Fig. 5.14: Predicted stream function of instantaneous flow field, 5 different times using EMLF, Mesh I and sharp re-entrant corner.

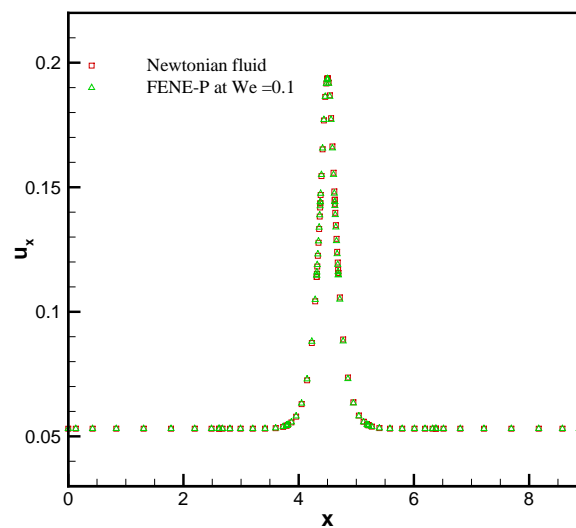
Because of the expense of simulation we did not find the exact value.

Degree of freedom	Mesh III
Velocity	16848
Viscoelastic stress	25272
Pressure	5096
number of element	104

Table 5.4: Spectral element mesh characteristic data for contraction-expansion geometry

pleiades2	
Processor	Xeon(mono proc)
Nprocs	1
$R_\infty$ [GFlops/s]	5.6
Memory addressing	64-bit
Memory size	4 GB

Table 5.5: The computer architectures used

Fig. 5.15: Comparison of stream-wise velocity between Newtonian and FENE-P at  $We = 0.1$ .

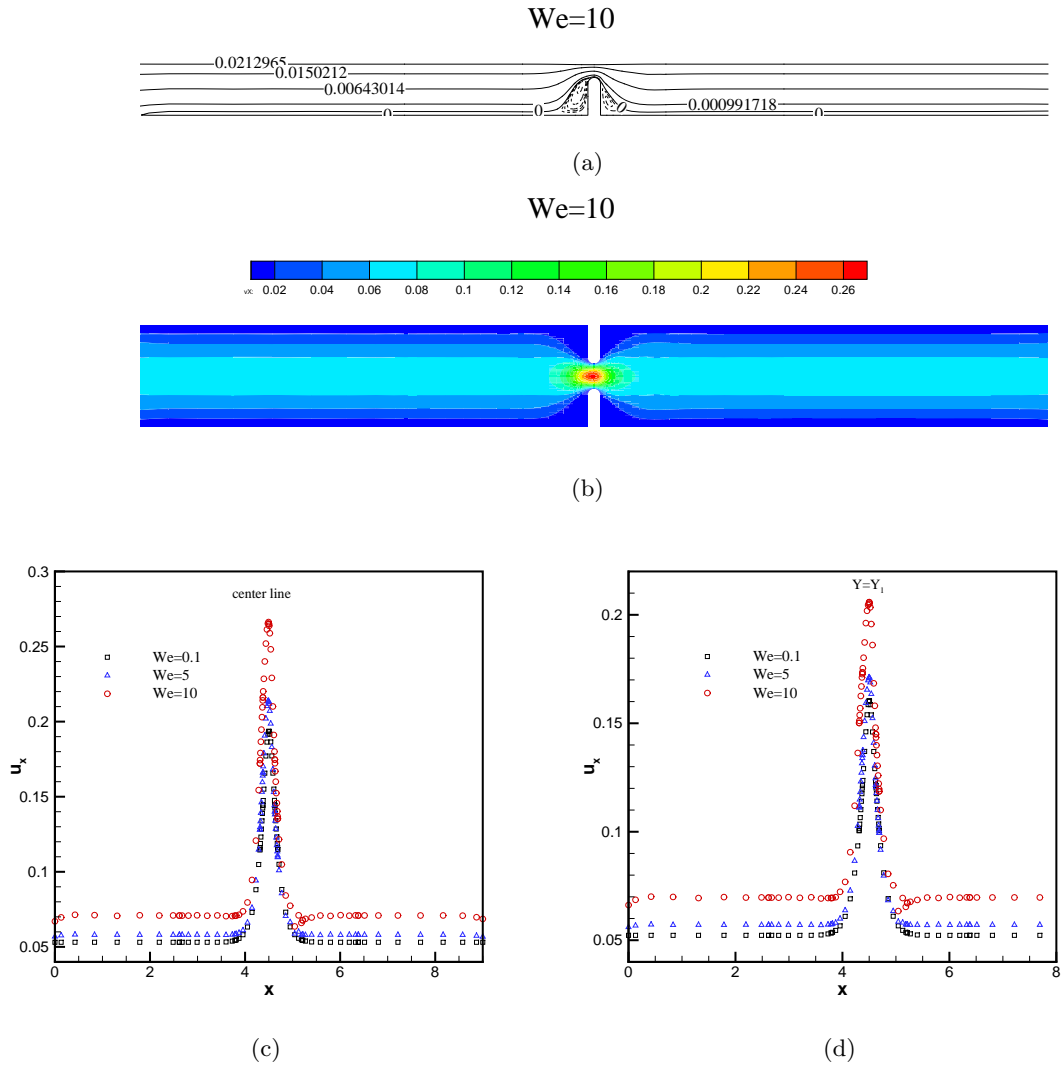


Fig. 5.16: Comparison of stream-wise velocity at different Weissenberg number, a) stream function, b) contour of  $u_x$ , c)  $u_x$  in center line d)  $u_x$  in  $Y_1$ .

The last two figures 5.17-5.18 show the behavior of first normal viscoelastic stress,  $\tau_{xx}$ , and shear viscoelastic stress,  $\tau_{xy}$ , along the center line, at  $Y_1$  and on the upper wall. In Fig. 5.17, in center line the maximum value is due to maximum Weissenberg number while the smallest value corresponds to the minimum Weissenberg number. On the wall the overshoot value is obtained at  $We = 5$  and this result was not expected. The gist point in this geometry is that the fully developed condition is reached very quickly after the second entry even for  $We = 10$  which probably one of the reason why simulation of

this geometry is more stable than the previous one. We observe the same trend for  $\tau_{xy}$  on the upper wall and at  $Y_1$  in Fig. 5.18.

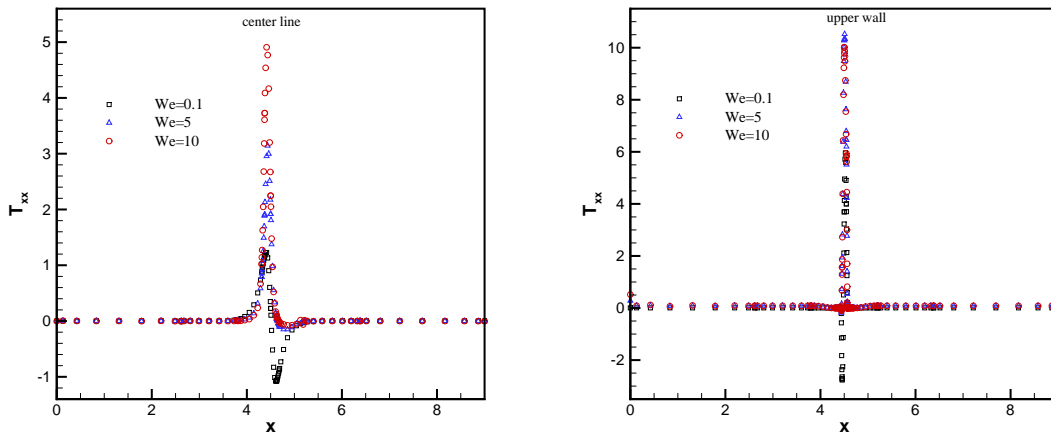


Fig. 5.17: Comparison of plots of  $\tau_{xx}$  along the stream-wise direction, at different Weissenberg number, left) center line, b) upper wall.

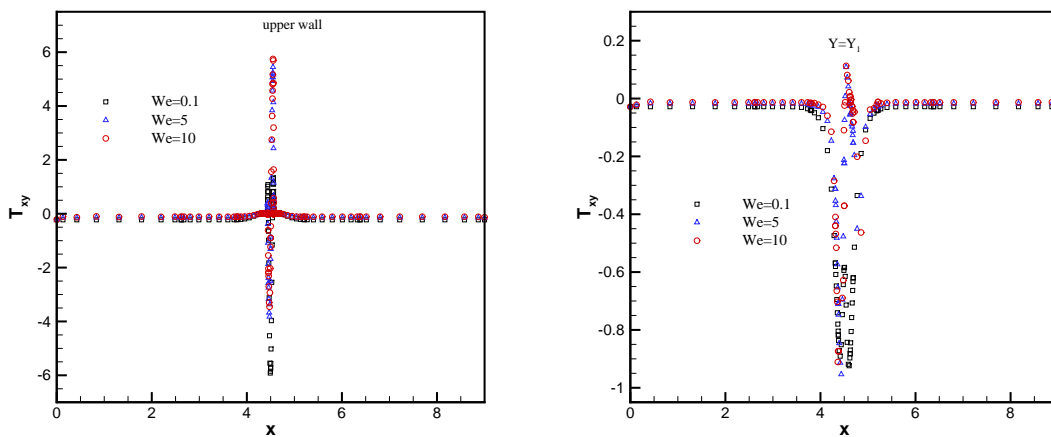


Fig. 5.18: Comparison of plots of  $\tau_{xy}$  along the stream-wise direction, at different Weissenberg number, left) upper wall, b)  $Y_1$ .

## 5.4 Conclusion

In this study, the capability of extended matrix logarithm formulation to predict the flow pattern for complex geometry such as contraction and contraction-expansion was examined. The simulation was carried out for the FENE-P fluid in the context of spectral element method. At low values of the Weissenberg number the convergence rate of the simulation is very fast and the accuracy of numerical simulation is very high. In contrast, increasing the Weissenberg number makes the relative error vary exponentially which prevents the successful numerical simulation. The velocity and viscoelastic-stress overshoot downstream of the entry corner increase with the Weissenberg number. When the level of elasticity in the flow is enhanced, the simulation takes more time step to reach the fully developed condition. Therefore, a longer channel length after entry flow is needed. For the 4:1 contraction geometry, the maximum attainable Weissenberg number by EMLF is 10 while this value for classical formulation is 8. Mesh refinement does not bring any improvement on the accuracy at critical values of the Weissenberg number. Increasing the Weissenberg number also enhances vortex intensity as measured as the maximum value of stream function and also augments the instability close to the re-entrant corner which propagates in the upstream direction. In this study no lip vortex was detected which is due to the considered contraction ratio 4:1. We found that employing round or sharp corner does not have very important improvement to tackle the high Weissenberg number problem. The maximum attainable Weissenberg number for both round and sharp re-entrant corner are the same and equal to  $We = 10$ . The flow patterns in contraction-extension geometry are similar to those obtained by contraction flow. The significant difference is that the corner vortex in the second channel is smaller than the first corner.

One of the key problems in viscoelastic flows is the influence of the outflow boundary conditions, which may induce numerical instabilities if not well suited. According to our previous study about the effect of outflow boundary condition for Poiseuille flow, we found that imposing natural boundary condition introduces instability first in elements which are close to the outflow region and then propagates in the upstream direction. Adopting periodic boundary conditions in stream-wise direction and resorting to spectral element-Fourier discretization might be helpful and this will be considered in our future work.

# Chapter 6

---

## Linear Stability analysis

The understanding of viscoelastic flows in many situations requires not only the steady state solution of the governing equations, but also its sensitivity to small perturbations. Linear stability analysis leads to a generalized eigenvalue problem (GEVP), whose numerical analysis may be challenging, even for Newtonian fluids, because the incompressibility constraint creates singularities that lead to non-physical eigenvalues at infinity. For viscoelastic flows, the difficulties increase due to the presence of continuous spectrum, related to the constitutive equations [215].

To evaluate the capability of the extended matrix logarithm formulation (EMLF) introduced in chapter 4 with the classical conformation tensor, comprehensive studies have been done based on the linear stability analysis to show the influence of this method on the resulting eigenvalue spectra and explain its success to tackle high Weissenberg numbers. With this new method one can treat high Weissenberg number flows at values of practical interest. A neat improvement of the computational algorithm with stable convergence has been demonstrated in this study.

### 6.1 Introduction

As presented before, the basic set of flow equations considered in this thesis consists of a continuity equation stating the incompressibility of the flow, a momentum equation and a constitutive equation in differential form. Carrying out a linear stability analysis of steady flows consists of studying the sensitivity of the base flows to infinitesimal perturbations. The equations are linearized as shown in Section 6.2 by decomposition of the flow variables into their base counterparts and some additional very small perturbations. In the particular cases of two dimensional planar flows (like e.g. Couette and Poiseuille flows) of viscoelastic fluids, most authors resort to the introduction of the stream function

instead of the velocity e.g. [235, 234] (and sometimes also pressure e.g. [91], [113]) in the flow equations. The perturbation is usually introduced in the form of the product of a function of a transverse coordinate  $y$  times a periodic sine or cosine function of the coordinate  $x$  (and possibly  $z$ ) in the other direction(s) and an exponential function of time  $X(y)e^{ik_x x + \nu t}$  (or  $X(y)e^{ik_x x + ik_z z + \nu t}$ ). Symmetric boundary conditions in the streamwise direction are imposed at each inflow and outflow sections. Particular reference cases are obtained for the Couette and Poiseuille flow of UCM and Oldroyd-B fluids for which a generalized equation of the Orr-Sommerfeld type involving solely the stream function can be derived e.g. [90], [186], [113]. The linearized equations may be discretized in the transverse direction  $y$  using a Chebyshev-tau spectral method e.g. [236]. After discretization, a generalized eigenvalue problem of the type:  $\nu \mathbf{B}\mathbf{X} = \mathbf{A}\mathbf{X}$  is obtained, where  $\mathbf{Z}$  is the vector of unknown coefficients of the variable expansions.

Sureshkumar et al. [204] employed an algorithm to compute the extremal eigenvalues of a non-Hermitian matrix, based on Arnoldi-orthogonalization in the linear stability analysis of the viscoelastic Poiseuille flow at high Reynolds numbers. It is shown that this algorithm is both computationally efficient and accurate in reproducing the most unstable modes in the pseudo-spectrally discretized eigenspectrum of the original problem. The Upper Convected Maxwell (UCM), Oldroyd-B and Chilcott-Rallison models are considered for the linear stability analysis of the high Reynolds number viscoelastic Poiseuille flow. Results for the UCM model show a large destabilization of the flow compared to the Newtonian limit, even for low values of flow elasticity,  $\epsilon = We/Re$ , of the order  $10^{-3}$ , realized at high Reynolds numbers for  $We = O(1)$ . Furthermore, it is shown that the number of spectral modes necessary to obtain converged results increases substantially as the flow elasticity is increased. A comparison of the linear stability characteristics of the Oldroyd-B and the UCM models has revealed that the presence of a non-zero solvent viscosity has a pronounced stabilizing effect on the flow. Further stabilization occurs through the introduction of a finite molecular extensibility in the Chilcott-Rallison model.

Anturkar et al. [16] performed a linear stability analysis of n-layer plane Poiseuille flow. Asymptotic solutions are constructed at very small and very large wavenumbers. A numerical analysis is carried out by means of a compound matrix method to identify linearly unstable conditions for wavenumbers of  $O(1)$ . The governing equations and the boundary conditions are conveniently formulated for n-layer flow. The investigated parameters in-



clude the viscosity ratios, the flow rate ratios, the density ratios, the interfacial tensions, and the Stokes and Reynolds numbers.

Grillet et al. [91] investigated the stability of Phan-Thien-Tanner (PTT) model and the Giesekus model in planar shear flows. For the PTT equation, instabilities are predicted for both plane Couette and Poiseuille flows using transient finite-element calculations. A Chebyshev- $\tau$  spectral method is used to confirm that these instabilities are not spurious or an artefact of the finite element formulation. Mechanisms are proposed based on an energy analysis of the most unstable mode for each flow. The stability of plane Couette flow of a Giesekus model is also probed using spectral method and found to be stable for the range of parameters investigated. However, in pressure driven flow, the Giesekus model is unstable over a critical local Weissenberg number based on the shear rate at the channel wall. Grillet et al. [91] presented the complete eigenspectrum for this model in both Couette and Poiseuille flows.

Keiller [112] performed an investigation of artificial, numerical instabilities occurring in time-dependent simulation of planar Couette flow for the upper-convected Maxwell, Oldroyd-B and FENE equations. For creeping flow it is shown that the poor resolution of a continuous spectrum of singular eigenfunctions may lead to an instability criterion  $We_{crit} = O(\Delta x/\Delta y)$  where  $\Delta x$  and  $\Delta y$  are the resolution scales of the computational grid in the streamwise and cross-stream directions respectively. Thus the limiting Weissenberg number is determined not by the absolute refinement of the grid but the relative refinement in the cross-stream to streamwise directions. This instability is less severe for the FENE equation and this is attributed to the lower normal stresses for this equation. In the presence of inertia there is a further artificial numerical instability for the upper-convected Maxwell equation (found also by Renardy and Renardy [186]). It is shown that the presence of an exceedingly small viscous stress component can remove this instability.

An application of eigenfunction analysis of perturbations to study the influence of downstream boundary conditions for entry-flow calculations has been proposed by Keiller [113]. It has been shown that the length scale over which the downstream boundary conditions modify the upstream flow is much smaller than the relaxation length scale of the viscoelastic stress towards its fully developed state for large Weissenberg numbers. Steady entry flows can therefore be computed without extremely long downstream channels since

the flow characteristic features are not significantly altered by the downstream boundary conditions.

Wilson et al. [236] provided a mathematical analysis of the spectrum of the linear stability problem for one and two layer channel flows of the upper-convected Maxwell (UCM) and Oldroyd-B fluids at zero Reynolds number. In their study, they investigated how this structure of the spectrum changes when the flow is changed to include a Poiseuille component, and as the model is changed from the UCM to the more general Oldroyd-B.

Sureshkumar et al. [205] performed the finite element analysis of linear stability of the two-dimensional flow past a linear, periodic array of cylinders in a channel, where the steady-state motion itself is known only from numerical calculations. For a single cylinder or widely separated cylinders, the flow is stable for the range of Deborah number ( $De$ ) accessible in the calculations. The unstable eigenfunction appears as a family of two-dimensional vortices close to the channel wall which travel downstream. This instability is possibly caused by the interaction between a shear mode which approaches neutral stability for  $De \gg 1$  and the periodic modulation caused by the presence of the cylinders.

Fiétier et al. [73] in contrast to the most published work where the equations have only been discretized in the cross-stream direction using a formulation with the stream function, have used the full spatial discretization with spectral elements. They computed the eigenvalue spectra generated by the spatial and temporal discretizations than the ones inherent in the partial differential equations. They investigated the influence of the spatial discretization, the time schemes, the various operators present in the conservation and constitutive equations and boundary conditions on the linear stability of the constitutive models. Fiétier also derives the equations predicting the continuous spectrum of the LPTT and FENE-P fluids [71].

Recently, Atalik and Keunings [19] have carried out a nonlinear analysis of the temporal evolution of finite, two dimensional disturbances for Couette and Poiseuille flows of UCM, Oldroyd-B and Giesekus fluids in both inertial and elastic (i.e. inertialess) regimes. In order to prevent long-time divergence of the numerical solution, a small amount of stress diffusivity in the form of the Laplacian of the viscoelastic stress tensor was added in the constitutive equation. Finite-amplitude quasi-periodic solutions are obtained in the elas-

tic regime for the Poiseuille flow of Oldroyd-B and Giesekus fluids if the viscosity ratio  $R_\mu$  is lower than 0.01. Oscillatory decay of finite perturbations has been observed for all parameter ranges in the corresponding Couette flows.

## 6.2 Linear stability analysis

Linear stability analysis is used to determine the sensitivity of the flow to the infinitesimal perturbations. In order to perform it, the set of governing equations, (3.1), (3.2) and (4.33), is linearized by looking for a solution composed of perturbation ( $\phi_1$ ) added to the known solution of the steady state base flow ( $\phi_0$ ) that satisfies Eqs. (3.1), (3.2), and (4.33):

$$\phi = \phi_0 + \phi_1 \quad (6.1)$$

where  $\phi$  represents the unknown variables such as velocity, pressure and conformation tensor which leads to the following set of relations if only first-order perturbation terms are retained:

$$\nabla \cdot \mathbf{u}_1 = 0 \quad (6.2)$$

$$\frac{\partial \mathbf{u}_1}{\partial t} = -Re[(\mathbf{u}_0 \cdot \nabla)\mathbf{u}_1 + (\mathbf{u}_1 \cdot \nabla)\mathbf{u}_0] + R_\mu \nabla^2 \mathbf{u}_1 - \nabla p_1 + \nabla \cdot \boldsymbol{\tau}_1 \quad (6.3)$$

$$\boldsymbol{\tau}_1 = \frac{1 - R_\mu}{KWe} \mathbf{J}_1 \quad (6.4)$$

$$\begin{aligned} \frac{\partial \mathbf{H}_1}{\partial t} = & -(\mathbf{u}_0 \cdot \nabla)\mathbf{H}_1 - (\mathbf{u}_1 \cdot \nabla)\mathbf{H}_0 + \mathbf{M}_0 \{ \mathbf{J}_0 \cdot \nabla \mathbf{u}_1^T + \mathbf{J}_1 \cdot \nabla \mathbf{u}_0^T + \nabla \mathbf{u}_0 \cdot \mathbf{J}_1 + \nabla \mathbf{u}_1 \cdot \mathbf{J}_0 - \\ & \frac{Kb^2 + tr(\mathbf{J}_0)}{b^2} \frac{\mathbf{J}_1}{KWe} - \frac{tr(\mathbf{J}_1) \mathbf{J}_0 - I}{b^2} \frac{\mathbf{J}_0}{KWe} - \frac{\mathbf{J}_0}{Kb^2} \frac{Kb^2 + tr(\mathbf{J}_0)}{b^2} \frac{tr(\mathbf{J}_1)}{KWe} \\ & \mathbf{J}_0 \frac{tr(\mathbf{J}_0 \cdot \nabla \mathbf{u}_1^T + \mathbf{J}_1 \cdot \nabla \mathbf{u}_0^T + \nabla \mathbf{u}_0 \cdot \mathbf{J}_1 + \nabla \mathbf{u}_1 \cdot \mathbf{J}_0)}{Kb^2} + \mathbf{J}_1 \frac{tr(\mathbf{J}_0 \cdot \nabla \mathbf{u}_0^T + \nabla \mathbf{u}_0 \cdot \mathbf{J}_0)}{Kb^2} \\ & - \frac{\mathbf{J}_0}{Kb^2} \frac{tr(\mathbf{J}_1) tr(\mathbf{J}_0) - tr(I)}{b^2} \frac{KWe}{KWe} - \frac{\mathbf{J}_1}{Kb^2} \frac{Kb^2 + tr(\mathbf{J}_0)}{b^2} \frac{tr(\mathbf{J}_0) - tr(I)}{KWe} \} + \\ & \mathbf{M}_1 \{ \mathbf{J}_0 \cdot \nabla \mathbf{u}_0^T + \nabla \mathbf{u}_0 \cdot \mathbf{J}_0 - \frac{Kb^2 + tr(\mathbf{J}_0)}{b^2} \frac{\mathbf{J}_0 - I}{KWe} + \\ & \mathbf{J}_0 \frac{tr(\mathbf{J}_0 \cdot \nabla \mathbf{u}_0^T + \nabla \mathbf{u}_0 \cdot \mathbf{J}_0)}{Kb^2} - \frac{\mathbf{J}_0}{Kb^2} \frac{Kb^2 + tr(\mathbf{J}_0)}{b^2} \frac{tr(\mathbf{J}_0) - tr(I)}{KWe} \} \end{aligned} \quad (6.5)$$

To linearize the matrix  $\mathbf{M}$  in Eq. (4.33), a first order Taylor development has been applied to each component of this matrix, which leads to Eq. (6.5). At this stage we introduced

a perturbation to the full semi discrete problem (the discretization will solely be applied to space coordinates) of the type:

$$\phi = \Phi e^{\nu t} \quad (6.6)$$

This leads to the following set of equations:

$$\nabla \cdot \mathcal{U}_1 = 0 \quad (6.7)$$

$$\nu \mathcal{U}_1 = C(\mathcal{U}_0, \mathcal{U}_1) + R_\mu \nabla^2 \mathcal{U}_1 - \nabla \mathcal{P}_1 + \nabla \cdot \mathcal{T}_1 \quad (6.8)$$

$$\mathcal{T}_1 = \frac{1 - R_\mu}{KWe} \mathcal{J}_1 \quad (6.9)$$

$$\nu \mathcal{H}_1 = NL_{\mathcal{U}} + NL_{\mathcal{H}} \quad (6.10)$$

where

$$C(\mathcal{U}_0, \mathcal{U}_1) = -Re((\mathcal{U}_0 \cdot \nabla) \mathcal{U}_1 + (\mathcal{U}_1 \cdot \nabla) \mathcal{U}_0) \quad (6.11)$$

$$NL_{\mathcal{U}} = -\mathcal{U}_1 \cdot \nabla \mathcal{H}_0 + \mathcal{M}_0 \left[ \mathcal{J}_0 \cdot \nabla \mathcal{U}_1^T + \nabla \mathcal{U}_1 \cdot \mathcal{J}_0 + \mathcal{J}_0 \frac{tr(\mathcal{J}_0 \cdot \nabla \mathcal{U}_1^T + \nabla \mathcal{U}_1 \cdot \mathcal{J}_0)}{Kb^2} \right] \quad (6.12)$$

$$\begin{aligned} NL_{\mathcal{H}} = & -(\mathcal{U}_0 \cdot \nabla) \mathcal{H}_1 + \mathcal{M}_0 \left\{ \mathcal{J}_1 \cdot \nabla \mathcal{U}_0^T + \nabla \mathcal{U}_0 \cdot \mathcal{J}_1 - \frac{Kb^2 + tr(\mathcal{J}_0)}{b^2} \frac{\mathcal{J}_1}{KWe} - \right. \\ & \frac{tr(\mathcal{J}_1) \mathcal{J}_0 - I}{b^2} \frac{\mathcal{J}_0 - I}{KWe} + \mathcal{J}_0 \frac{tr(\mathcal{J}_1 \cdot \nabla \mathcal{U}_0^T + \nabla \mathcal{U}_0 \cdot \mathcal{J}_1)}{Kb^2} + \\ & \mathcal{J}_1 \frac{tr(\mathcal{J}_0 \cdot \nabla \mathcal{U}_0^T + \nabla \mathcal{U}_0 \cdot \mathcal{J}_0)}{Kb^2} - \frac{\mathcal{J}_0}{Kb^2} \frac{Kb^2 + tr(\mathcal{J}_0)}{b^2} - \\ & \left. \frac{\mathcal{J}_0}{Kb^2} \frac{tr(\mathcal{J}_1) tr(\mathcal{J}_0) - tr(I)}{b^2} - \frac{\mathcal{J}_1}{Kb^2} \frac{Kb^2 + tr(\mathcal{J}_0)}{b^2} \frac{tr(\mathcal{J}_0) - tr(I)}{KWe} \right\} + \\ & \mathcal{M}_1 \left\{ \mathcal{J}_0 \cdot \nabla \mathcal{U}_0^T + \nabla \mathcal{U}_0 \cdot \mathcal{J}_0 - \frac{Kb^2 + tr(\mathcal{J}_0)}{b^2} \frac{\mathcal{J}_0 - I}{KWe} + \right. \\ & \left. \mathcal{J}_0 \frac{tr(\mathcal{J}_0 \cdot \nabla \mathcal{U}_0^T + \nabla \mathcal{U}_0 \cdot \mathcal{J}_0)}{Kb^2} - \frac{\mathcal{J}_0}{Kb^2} \frac{Kb^2 + tr(\mathcal{J}_0)}{b^2} \frac{tr(\mathcal{J}_0) - tr(I)}{KWe} \right\} \end{aligned} \quad (6.13)$$

$\mathcal{U}_0, \mathcal{U}_1, \mathcal{P}_1, \mathcal{H}_0, \mathcal{H}_1, \mathcal{M}_0, \mathcal{M}_1$  represent the variables in linear discretized equations. Adopting the notation of Fiétier and Deville [73], the above equations can be written in operator matrix form:

$$\nu \mathbf{B} \mathbf{x} = \mathbf{A} \mathbf{x} \quad (6.14)$$

where  $\mathbf{x}^T = [\mathcal{P}_1, \mathcal{U}_1, \mathcal{H}_1]$  and

$$\mathbf{B} = \begin{bmatrix} \mathbf{0} & \mathbf{0} & \mathbf{0} \\ \mathbf{0} & \mathbf{I} & \mathbf{0} \\ \mathbf{0} & \mathbf{0} & \mathbf{I} \end{bmatrix} \quad (6.15)$$

and

$$\mathbf{A} = \begin{bmatrix} \mathbf{0} & \nabla \cdot (\mathbf{I}) & \mathbf{0} \\ -\nabla(\mathbf{I}) & C(\mathcal{U}_0, \mathbf{I}) + \mathbf{R}_\mu \nabla^2(\mathbf{I}) & \nabla \cdot (\mathbf{I}) \\ \mathbf{0} & NL_{\mathcal{U}} & NL_{\mathcal{H}} \end{bmatrix} \quad (6.16)$$

Applying this equation leads to a generalized eigenvalue problem whose unknown eigenvalues  $\nu$ , are obtained by using the dgegv routine of the LAPACK library [15].

### 6.3 Problem description

In this chapter, a comprehensive study of the capability of the extended matrix logarithm formulation (EMLF) is performed based on the linear stability analysis. This stability analysis has been used to study the effect of spatial discretization. In this approach we study the effect of mesh refinement on the resulting eigenvalue spectra. However the problem description has been explained in chapter 4, here we mention the main points once again. The 2-D time dependent Poiseuille flow as shown in previous chapter (figure (4.1)) has been considered in this approach. A constant nonzero pressure gradient is imposed on the flow. The magnitude of the applied pressure gradient is selected such that the channel flow rate is equal to one. All data plots shown correspond to  $\Delta t = 0.002$ ,  $Re = 1$ ,  $H = 1$ , (channel height),  $L = 4$ , (channel length),  $R_\mu = 1/9$ ,  $b = \sqrt{6}$ . Natural boundary condition is applied at outflow boundary. No explicit boundary condition is imposed on the pressure since no pressure grid point lies on the boundary of the computational domain. The full analytical prescription of the steady flow has been chosen as the initial condition. The numerical methods are exactly the same as those explained in section 4.6.

### 6.4 Results and discussion

The results of this chapter deal with the extended matrix logarithm formulation algorithm for a time dependent FENE-P fluid. The influence of this method on the resulting eigenvalue spectra can be observed. Here we apply the extended matrix logarithm formulation (EMLF) to the classical constitutive equation.

The numerical eigenspectrum consists of three sets of eigenvalues (a) a continuous spectrum related to the constitutive equation (b) a discrete spectrum that represents the

physical stability characteristics of the flow (c) a spurious eigenspectrum that comes from an artifact of the spatial discretization of the differential eigenvalue problem [215].

The linear stability analysis for viscoelastic fluids flow is really challenging. All the results in the sequel are obtained with natural boundary condition at the outflow section. It is worth to mention that the methodology to obtain the spectra is similar to that used by Fiétier and Deville [73]. In their paper, these authors have shown that a good approximation of whole continuous part of the spectrum for PTT and FENE-P equations has been obtained with this approach.

#### 6.4.1 Influence of Weissenberg number

First, we considered a single element with polynomial order 16 by 10 in stream-wise and cross-wise direction. The selection of these polynomial degrees in stream and cross-wise directions is due to the fact that the simulation was performed using  $4 \times 2$  equally sized elements and  $4 \times 5$  polynomial degrees in the  $x$  and  $y$  directions. In this case the number of degrees of freedom for the linear stability analysis is exactly the same as the number of unknowns for both velocity and viscoelastic stress in the simulation. Figure 6.1 shows the influence of Weissenberg number on the eigenspectrum of this new algorithm at Weissenberg  $10^{-4}$ , 10, 50 and 100. At  $We = 10^{-4}$  all eigenvalues are located in the half negative real eigenspectrum. Overall, the Poiseuille flow of a FENE-P model with one spectral element at  $We = 10^{-4}$  is found unconditionally stable and no dangerous eigenmodes were observed for algorithms. This figure shows that increasing the Weissenberg number expands the eigenvalues along the imaginary axis and also distributes the eigenvalues along the  $x$ -axis. On the other hand, the eigenspectrum obtained by linear stability analysis is sensitive to the Weissenberg number and increasing the Weissenberg number can generate dangerous eigenvalues, which are located in the right-hand half plane.

To investigate the effect of spectral element decomposition on the results we considered  $4 \times 2$  equal space elements with polynomial degrees  $4 \times 5$  in stream and cross-stream direction respectively, at four different Weissenberg numbers equal  $10^{-4}$ , 10, 50, 100, Figure (6.2). In this test case, dangerous eigenvalues can be observed in the right-hand half plane. This plot reveals that element decomposition could be a source of instability for the numerical simulation of viscoelastic fluids. The visible effects of increasing the Weissenberg

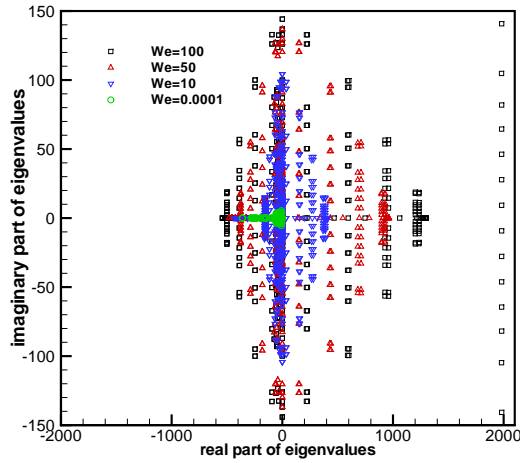


Fig. 6.1: Eigenspectrum of the Poiseuille flow of a FENE-P fluid, single element,  $(N_x, N_y) = (16, 10)$  at  $We = 10^{-4}$ ,  $We = 10$ ,  $We = 50$ , and  $We = 100$ , NBC.

number from  $10^{-4}$  to 100 are the expansion of the eigenspectrum along the imaginary axis and the distribution of dangerous and spurious modes along the positive  $x$ -axis. We would

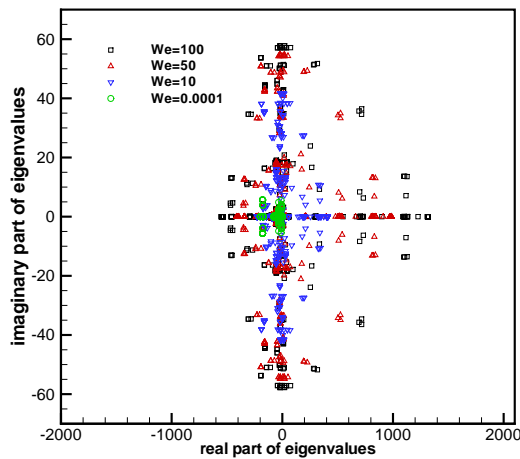


Fig. 6.2: Eigenspectrum of the Poiseuille flow of a FENE-P fluid,  $(NE_x, NE_y) = (4, 2)$ ,  $(N_x, N_y) = (4, 5)$  at  $We = 10^{-4}$ ,  $We = 10$ ,  $We = 50$ , and  $We = 100$ , NBC.

like to emphasize that we have performed the corresponding time dependent simulation

for both classical (CF) and extended matrix logarithm formulation (EMLF) for the conditions mentioned above while imposing Dirichlet boundary condition for velocity at outflow. For the classical approaches, one could obtain a critical value of the Weissenberg number equal to 56 while for this new algorithm one can easily tackle Weissenberg numbers larger than 100.

### 6.4.2 Influence of mesh refinement

Let us now inspect the effect of mesh refinement on the eigenspectrum of the new extended formulation. Figure 6.3 represents the effect of mesh refinement in  $x$ -direction for a single element at  $We = 10$  and three different polynomial degrees,  $(N_x, N_y) = (16, 10)$ ,  $(24, 10)$ , and  $(40, 10)$ . The effect of mesh refinement in the  $x$ -direction on eigenspectrum is more visible in the imaginary axis direction than in the real axis direction. Furthermore refining the mesh in the  $x$ -direction extends the distribution of eigenspectrum in the imaginary axis direction. The larger real parts of dangerous eigenvalues are produced with the coarsest mesh. In contrast, mesh refinement in the cross-stream direction distributes the

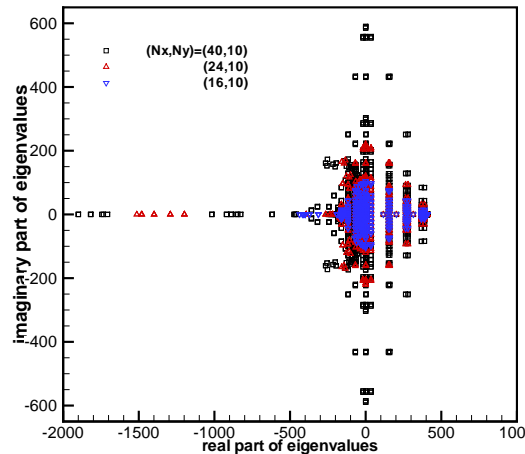


Fig. 6.3: The effect of mesh refinement in the stream wise direction for a Poiseuille flow of a FENE-P fluid at  $We = 10$ , single element, NBC.

eigenspectrum more along the negative real axis direction as it is shown in figure 6.4.

To better understand the effect of mesh refinement in both stream and cross-stream directions the mesh was modified with another procedure, by considering constant polynomial



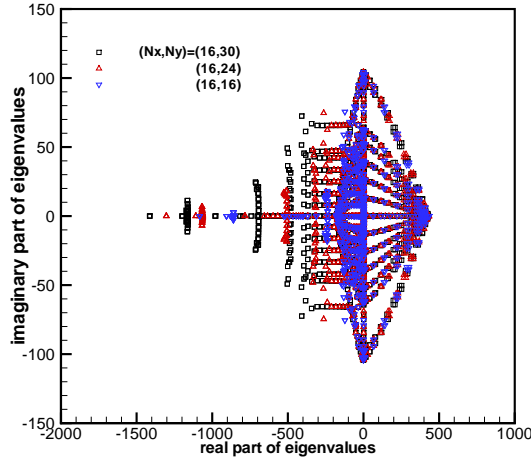


Fig. 6.4: The effect of mesh refinement in the cross-stream direction for the Poiseuille flow of a FENE-P fluid at  $We = 10$ , single element, NBC.

degree and increasing the number of elements in both directions. From the numerical point of view, the elemental decomposition has an important influence on numerical instability observed for simulation of viscoelastic flows with spectral element. Fig. 6.5a and b shows the effect of mesh refinement by increasing the number of elements in stream and cross-wise direction respectively at  $We = 10$  and polynomial degrees  $5 \times 8$  and  $10 \times 4$  for Fig. 6.5a and b respectively. By increasing the number of elements in the stream wise direction, the eigenspectrum is shifted to the right hand side of the real axis. Even, one could achieve positive real eigenvalues by refining the mesh in this direction. On the other hand, increasing the mesh refinement in the stream wise direction increases the number of stream wise wave numbers that can be taken into account but also contributes to expand the eigenvalues spectrum towards the right-hand half plane which may be detrimental to the stability. This means that mesh refinement in x-direction by increasing the number of elements could be one of the source of numerical instability. It is worth mentioning that coarse mesh in spectral element method automatically acts like a filtering to eliminate the spurious modes at the expense of less accurate solutions. The effect of mesh refinement in the cross-stream direction by increasing the number of elements in this direction shifts the whole spectrum to the left hand side. Moreover, when increasing the number of elements in cross-wise direction the spectrum tends to pack along the imaginary axis.

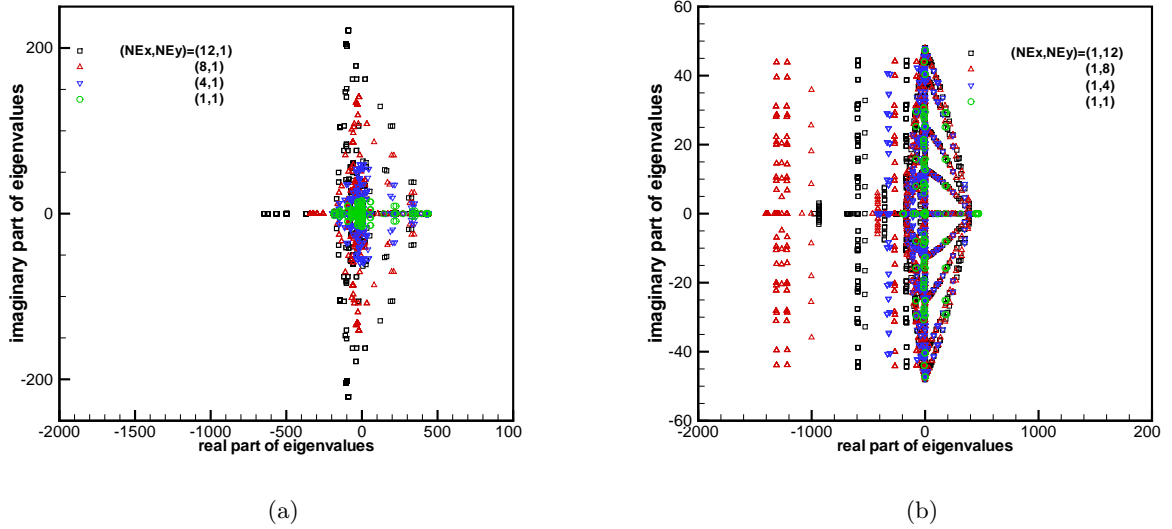


Fig. 6.5: The effect of mesh refinement in the a) stream wise,  $(N_x, N_y) = (5, 8)$  and b) cross-wise direction,  $(N_x, N_y) = (10, 4)$  for a Poiseuille flow of a FENE-P fluid at  $We = 10$ , NBC.

### 6.4.3 Influence of finite extensibility

Figure 6.6 shows the influence of the extensibility parameter,  $b$ , for  $(NE_x, NE_y) = (4, 2)$  and  $(N_x, N_y) = (4, 5)$  at  $We = 1$  in the stream and cross-wise direction respectively. The Oldroyd-B model can be considered as a particular case of the FENE-P model when  $b \rightarrow \infty$ . In this analysis the more dangerous eigenvalues correspond to the smaller extensibility parameter. In contrast to the numerical results obtained for classical FENE-P model by Fiétier and Deville [73] for the similar test case, the extensibility parameter does not have any stabilizing effect on this new algorithm. Therefore the proposed algorithm can also deal well with the Oldroyd-B model.

## 6.5 Influence of outflow boundary condition

The influence of outflow boundary conditions at  $We=100$  can be observed in figures 6.7 and 6.8. Here, only natural (NBC) and periodic (PBC) boundary conditions have been considered. Periodic boundary condition means that the unknown variables at inflow

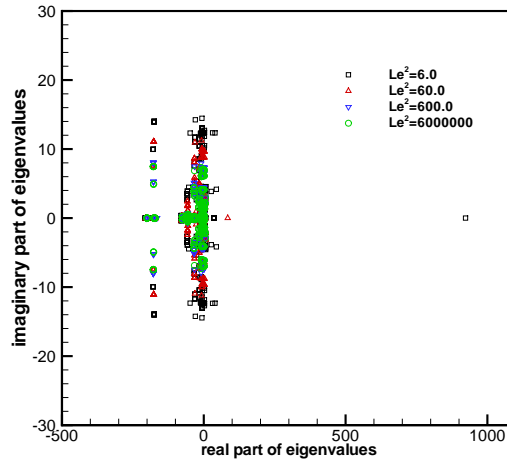


Fig. 6.6: The effect of finite extensibility parameter for the Poiseuille flow of a FENE-P fluid at  $We = 1$ ,  $(NE_x, NE_y) = (4, 2)$ ,  $(N_x, N_y) = (4, 5)$ , NBC.

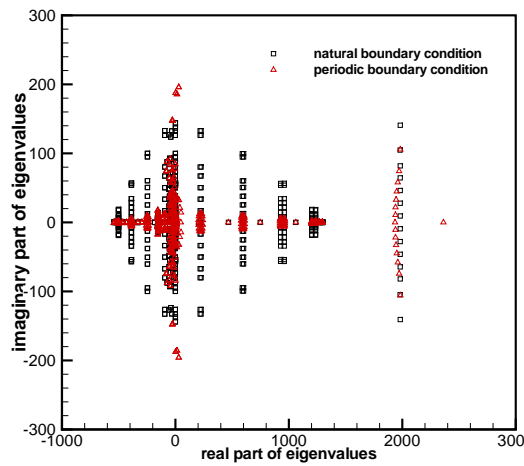


Fig. 6.7: Influence of the boundary conditions on the spectrum, single element,  $(N_x, N_y) = (16, 10)$  at  $We = 100$ .

and outflow grid points are exactly the same. Figure 6.7 corresponds to 1 element and  $16 \times 10$  polynomial degrees in stream wise and cross-wise direction. In figure 6.8, we considered  $(NE_x, NE_y) = (4, 2)$  and  $(N_x, N_y) = (4, 5)$ . For periodic boundary condition more positive eigenmodes are observed in the right-hand half plane. Moreover, using

natural boundary condition expands the eigenspectrum along the imaginary axis while for periodic boundary condition the eigenspectrum is more compressed along the  $y$ -axis. The instability generation might be due to an unsuitable boundary condition at outflow. The same results were observed for  $We = 1, 10$  and  $50$ .

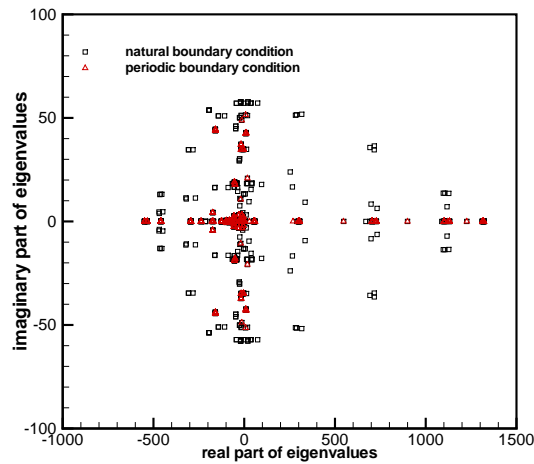


Fig. 6.8: Influence of the boundary conditions on the spectrum,  $(NE_x, NE_y) = (4, 2)$ ,  $(N_x, N_y) = (4, 5)$  at  $We = 100$ .

## 6.6 Conclusion

In this study the capability of the proposed extended matrix logarithm formulation (EMLF) of the conformation tensor in the spectral element context has been considered. With the classical matrix logarithm formulation (CMLF) it has been observed that when the Weissenberg number approached the critical value the simulation stopped because the necessary condition that the square of the corresponding finite extensibility parameter of the polymer should be an upper limit for the trace of the conformation tensor was not satisfied. According to this, we have introduced a new extended matrix logarithm formulation (EMLF) to enforce this condition. We comprehensively studied the improvement of this new algorithm on the eigenspectrum with linear stability analysis. It shows that element decomposition is one of the main source of instability in the spectral element context. On the other hand, the comparison of results obtained with the single element and

---

multi-element configuration shows that the more dangerous eigenmodes are related to the multi-element composition. This means that, the positive real eigenvalues for the single element decomposition have smaller magnitude than for the multi-element decomposition. Moreover, increasing the Weissenberg number distributes the eigenvalues in the right-hand half plane with large magnitude of positive real parts. This can be one of the reason of instability of numerical simulation. In spite of this, the new extended algorithm enables one to obtain stable simulation of viscoelastic flows at Weissenberg number with values of practical interest i.e. larger than 100 for this specific mesh. There are still some associated problems that must be considered and investigated in the future as the accuracy of the results when approaching the critical values is very low and refining the mesh proved to be not very helpful. In particular, it is compulsory to understand more deeply the mechanism of instability generation. A comprehensive study about the growth of spurious modes with time evolution, mesh refinement and boundary condition or any other affected parameters is necessary. This would help in defining an appropriate filtering technique to stabilize simulations. This investigation will be presented in Chapter 7.



# Chapter 7

---

## Filter-based stabilization technique

The challenge for computational rheologists is to develop efficient and stable numerical schemes in order to obtain accurate numerical solutions for the governing equations at values of practical interest of the Weissenberg number,  $We$ , i.e. within the range [0-150]. One of the associated problems for numerical simulation of viscoelastic fluids is that the accuracy of the results when approaching critical values at which numerical instabilities occur is very low and refining the mesh proved to be not very helpful. In this study, to understand more deeply the mechanism of instability generation a comprehensive study about the growth of spurious modes with time evolution, mesh refinement, boundary conditions and Weissenberg number or any other affected parameters has been performed. Then to get rid of these spurious modes the filter based stabilization of spectral element methods proposed by Boyd [32] in modal basis and Fischer and Mullen in nodal basis [75] was applied. This filter technique is very useful to eliminate spurious modes for one element decomposition, while in the case of multi-element configuration, the performance of this technique is not ideal. Since the performance of filter-based stabilization of spectral element acts very well for one element decomposition, one possible remedy to solve the associated problem of multi-element decomposition is mesh-transfer technique which means: first mapping the multi-element configuration to one element configuration, applying filter-based stabilization technique to this new topology and hereafter transferring the filtered variables to the original configuration. This way of implementing filtering is very useful for the Oldroyd-B fluids when a moderate number of grid points is used.

### 7.1 Introduction

One of the worst obstacle for numerical simulation of viscoelastic fluids is the presence of spurious modes during the simulation. At high Weissenberg number, many schemes suffer from instabilities and numerical convergence may not be attainable. This is often

attributed to the presence of solution singularities due to the geometry, the dominant non-linear terms in the constitutive equations, or the change of type of the underlying mixed-form differential system [109, 107]. In the past two decades, considerable efforts have been devoted to the development of robust and stable numerical methods for simulating non-trivial flows of complex fluids. Without any exception, the standard viscoelastic models like Oldroyd-B, Maxwell, Phan-Thien-Tanner, FENE-P, etc. have failed in the simulation of high Weissenberg number flows in any available numerical techniques such as: finite difference, finite volume, finite elements, spectral elements, etc. [173].

In the framework of the spectral element method [60] for simulation of fluid flows, severe stability problems have also been encountered, especially when facing problems having weak physical diffusion. Actually, spectral approximations are much less numerically diffusive than low-order ones and according to this drawback, even minor errors can make the simulation unstable. To remove nascent instabilities induced by numerical techniques or infirmity of constitutive equation, applying stabilization methods or filtering is compulsory.

Upwind techniques are introduced to ensure stability and prevent unphysical upstream propagation of disturbances. An example is provided by Marchal and Crochet [144]. They applied the so-called streamline upwind (SU) method to the constitutive equation, which consists of adding an artificial, first-order, stream-wise diffusion term to the classical weak form of the constitutive equation. In the context of finite element methods, it was shown by Rosenberg and Keuning [188] that global upwinding techniques may produce inaccurate results in regions of steep velocity gradients. The streamline integration scheme, which in essence is a method of characteristics applied to the purely hyperbolic constitutive model, leads to stable and accurate stress predictions even close to singularities. The key advantage in using streamline integration is that it does not produce cross-stream diffusion, which can distort in a non-negligible way, the stress field near boundary layer regions.

The SUPG formulation [33] induces numerical damping in the constitutive equation which has the well-known effect of stabilizing the solution. This formulation has been used successfully by Chauvière and Owens for the benchmark problems relative to the steady flows of a sphere falling in a tube and past a cylinder in a channel, using spectral elements [43, 42]. In these papers, additional stabilization has been obtained by using an element by element (EE) solver technique. This technique benefits from the hyperbolic character



of the constitutive equation. First, the elements, are ordered according to their location along the streamline, then the constitutive equation is solved on each element, which makes possible the use of a direct solver. The inflow boundary conditions are obtained from the upstream elements determined by following the streamlines or the problem inflow boundary conditions.

Another alternative classical upwind method for finite element is the discontinuous Galerkin or Lesaint-Raviart method, which has been applied to viscoelastic flows by Fortin et al. [77]. The viscoelastic stress is approximated discontinuously from one element to the next. The continuous Galerkin approach has been shown to present stability and convergence properties similar to those of the SU method [105].

Gerritsma and Phillips [85, 84] have recommended the use of discontinuous approximation of the extra-stress between spectral elements for non-smooth problems i.e. problems with singularities or stress boundary layers. They have claimed that a continuous extra-stress approximation can not reproduce jumps in the velocity gradient approximation without generation of spurious oscillations in the whole computational domain. They have also suggested that the extra-stress approximation be at least the same as that of the velocity approximation within one spectral element on a non-staggered grid, so that a well-posed problem is obtained. Although they brought proofs of their statements only for Stokes flows, it is likely that such a formulation can be also applied to the viscoelastic stress tensor.

Another stabilization method is called the elastic-viscous stress-splitting (EVSS) method [222, 183, 185] which is based on adding an elliptic contribution in the weak form of the momentum equation. There are two principal features associated with this method, stress-splitting and recovery of velocity gradients. For smooth viscoelastic flows, Khomami et al. [115] have demonstrated that for steady state problems, the EVSS formulation coupled with upwinding for the constitutive equation (and likewise hp schemes), provides a more stable discretisation than a standard formulation (either Galerkin or EVSS/Galerkin) without upwinding. Marginal stability improvements are noted for EVSS above conventional stress equation treatments. In the same context, Rajagopalan et al. [185] have shown, for a wide range of solvent viscosities, that the EVSS scheme is more accurate and stable than two alternative choices, namely the viscous and explicit elliptic momentum equation (EEME) schemes. Another modification so called DEVSS (D stands for

discrete) of the initial EVSS method has been proposed by Gu enette and Fortin [93]. The formulation is based on the introduction of the rate of deformation tensor as an additional unknown. Contrary to the popular EVSS method, no change of variable is performed into the constitutive equation. The main advantage of this method relies on the fact that it extends to more complicated rheological models where it is difficult or impossible to perform a change of variable into the constitutive equation. Moreover, this method is easier to implement since the constitutive equation remains unaltered. Recently, Fan, et al. [68] have proposed an alternative to the EVSS-based formulations related to the concept of Galerkin/least square perturbations proposed by Franca et al. [78]. The Galerkin/least-square method consists of adding to the usual Galerkin method terms that are functions of the residual of the Euler-Lagrange equations evaluated element wise. The added perturbation terms are designed to enhance stability of the original Galerkin method; since the Euler-Lagrange equations are satisfied by the exact solutions consistency is preserved in this method.

Other stabilization methods have been recently proposed in the spectral element context like the so-called bubble stabilization technique by Canuto et al. [36] or collocation techniques with modified grid by Funaro [81]. According to our knowledge, until recently their use has been applied only to Newtonian flows.

Boyd [32] proposed a simple filter which satisfies the same boundary condition. The key idea is to rewrite variables in term of new basis functions, modal basis, which individually satisfy homogeneous boundary conditions and then apply the filter to modify the coefficient of these basis functions without disturbing the boundary conditions. The filter sum can then be converted back into the original Chebyshev or Legendre basis.

Mullen and Fischer [75] have proposed the same filter as Boyd but in nodal basis for spectral element methods to remove instabilities induced by the nonlinear convection term in the momentum equation. The filter is applied after each time step on an element by element basis to both velocity and stress fields.

Fischer et al. [76] employ the filter-based stabilization technique for development and implementation of an efficient spectral element code for simulating transitional flows in complex three-dimensional domains. Critical to this effort is the use of geometrically non-

conforming elements that allow localized refinement in regions of interest, coupled with a stabilized high-order time-split formulation of the semi-discrete Navier Stokes equations. Till now this filtering has been applied to Newtonian flow.

The aim of this chapter is to apply the filter-based stabilization technique for the simulation of viscoelastic flows. To understand more deeply the mechanism of instability generation, a comprehensive study about the growth of spurious modes with time evolution, boundary condition, mesh refinement, finite extensibility parameter and Weissenberg number has been done. Then to get rid of these nascent instabilities, the filter-based stabilization technique is applied. At the end of our discussion we more focus on the mathematical property of the constitutive equation and we investigate the effect of different parameters. The C++ toolbox SPECULOOS [66] has been used and adapted to handle this simulation and analysis.

## 7.2 Filter-based stabilization technique

Despite the success of the spectral element methods (SEM) in the applications of among many examples, incompressible flows, severe stability problems have also been encountered, especially when facing problems having weak physical diffusion. These problems result from the fact that spectral approximations are much less numerically diffusive than low-order ones, even minor errors and under resolution can make the calculation unstable [239]. For a long time, numerous filtering techniques have been proposed to overcome the stability problem. In the frame of spectral element approximations it is however, essential to preserve the inter-element continuity, as discussed in [32]. One of the most recent and successful filtering technique in the framework of spectral element method for Newtonian fluid specifically for large eddy simulation is that one has been proposed by Boyd [32] in modal basis. It is based on interpolations in physical space: Given the variable  $v$  on a Gauss-Lobatto-Legendre (GLL) mesh with  $(N + 1)^d$  nodes per element (where  $d$  is the space dimension and  $N$  is the degree of the polynomial approximation in each direction), in each element one uses the polynomial interpolate to compute  $v$  at the  $N^d$  nodes-GLL mesh, so that one obtains a new polynomial approximation, the degree of which in each direction is then  $N - 1$ . Using this polynomial one interpolates back on the initial grid. This filter of the highest frequencies is applied at each time step. An important advantage

of the technique is that inter element continuity and boundary conditions are preserved.

In this study to get rid of instabilities of viscoelastic fluids which are induced by either numerical origin or mathematical modeling of constitutive equation or coupling of both sources, we apply the filter-based stabilization technique at the end of each time step of mass-momentum and constitutive equations. The filtering operation is performed by applying a given transfer function to a modal basis.

### 7.2.1 Description of the filter

In this section we adopt the notation of section 5.4 of Roland Bouffanais's thesis [30]. The modal basis introduced in the p-version of finite elements and first used by Boyd [32] as filtering technique is presented in its one-dimensional version, the extension to two and three dimensions being straightforward by the use of tensor products. It is built up on the reference parent element  $\hat{\Omega} = [-1; 1]$  of the spectral element method as:

$$\begin{aligned} \phi_0 &= \frac{1 - \xi}{2} & \phi_1 &= \frac{1 + \xi}{2} \\ \phi_j &= L_j(\xi) - L_{j-2}(\xi) & 2 \leq j \leq N & \quad \xi \in \hat{\Omega} = [-1, 1] \end{aligned} \quad (7.1)$$

where  $L_j$  is the Legendre polynomial of degree  $j$ . Unlike the Lagrange-Legendre nodal basis used in our spectral element calculations, this modal basis forms a hierarchical set of polynomials allowing to define in an explicit and straightforward manner a low-pass filtering procedure. Any variable  $v$  can be expressed in this basis by the relation:

$$v(\xi) = \sum_{j=0}^N \check{v}_j \phi_j(\xi) \quad (7.2)$$

where  $\check{v}$  is unknown variable in modal bases. In matrix notation one reads:

$$\mathbf{v} = \mathbf{\Phi} \check{\mathbf{v}} \quad (7.3)$$

where

$$\Phi_{ij} = \phi_j(\xi_i) \quad (7.4)$$

The filtering operation is performed in the spectral modal space through a diagonal matrix  $\mathbf{K}$  whose components are chosen in order to fulfill the required properties of the filter. The filtering process for a one-dimensional problem is expressed by:

$$\bar{\mathbf{v}} = \mathbf{\Phi} \mathbf{K} \mathbf{\Phi}^{-1} \mathbf{v} = \mathbf{G} \mathbf{v} \quad (7.5)$$

### 7.2.2 Transfer function

$C^0$ -continuity, conservation of constants, invertibility and low-pass filtering are obtained by properly choosing the transfer function represented by the diagonal transfer matrix  $\mathbf{K}$ . As the filter acts in another basis than the one used for our spectral element calculations,  $C^0$ -continuity is preserved if the boundaries of the elements are not affected by the filtering procedure. One can notice that the only shape functions having non-zero values at the element boundaries are  $\phi_0$  and  $\phi_1$ , while  $\phi_j$ ,  $j \geq 2$  are bubble functions. The functions  $\phi_0$  and  $\phi_1$  that are linear Lagrange interpolants are responsible for imposing the non-zero values on element edges, i.e.  $C^0$ -continuity. Therefore, the transfer function coefficients must satisfy the relationship:

$$K_{ij} = \delta_{ij} \quad i, j \leq 1 \quad (7.6)$$

with  $\delta_{ij}$  the Kronecker operator. If  $K_{ij}$  verifies Eq. (7.6), the constants are conserved after filtering because they are expressed as a linear combination of  $\phi_0$  and  $\phi_1$ . The modal filter is not projective if all diagonal coefficients  $K_{ii}$  are non-zeros. The last required property is to perform low-pass filtering in frequency. As this modal basis forms a hierarchical set of polynomials, low-pass filtering is done by damping the high-degree polynomial contributions. The transfer matrix is expressed by:

$$K_{ij} = \delta_{ij} \kappa(i) \quad (7.7)$$

with the continuous transfer function

$$\kappa(k) = \frac{1}{1 + (\eta \frac{\max(0, k-n)}{N})^2} \quad \eta \geq 0 \quad (7.8)$$

where  $\eta$  is a filtering rate and  $n$  is an integer constant depending on the constitutive equation. Here  $\kappa(k) = 1$  for  $k \leq n$ .

The effect of filtering rate,  $\eta$ , on 1-D unity spectrum for Oldroyd-B and FENE-P has been shown in Fig. 7.1. As it is obvious in this figure, the largest value of  $\eta$  means the sharpest shape of filtering for eliminating the modes. This is the reason why we chose  $\eta = 10$  for this study.

To satisfy the condition of Eq. (7.6), it is necessary to impose  $n \geq 1$ . To perform an appropriate low-pass filtering for viscoelastic fluids, first we computed the analytical spectrum of the constitutive equation in modal basis with  $N_x = 9$  and  $N_y = 9$ . We observed

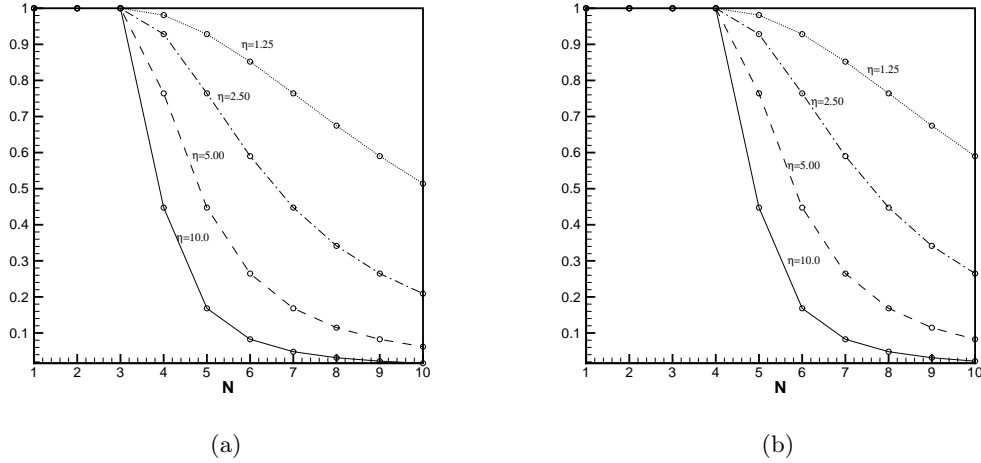


Fig. 7.1: Filtering 1-D unit spectrum for different values of the filtering rate,  $\eta = 1.25$ ,  $\eta = 2.5$ ,  $\eta = 5$ ,  $\eta = 10$ , a) Oldroyd-B, b) FENE-P

that for Poiseuille Oldroyd-B and FENE-P flows one has to preserve the first three and four physical modes, respectively. According to this observation,  $n = 2$  for Oldroyd-B and  $n = 3$  for FENE-P model could be suitable values. To more clarify, in Fig. 7.2, one element unity spectrum is filtered with three different shape functions at filtering rate,  $\eta = 10$ . In this study we have used the two last ones (c) and (d) for Oldroyd-B and FENE-P models respectively. This shape of transfer function is similar to that one classically used in Refs. [30].

### 7.2.3 Problem description

In this study, to understand more deeply the mechanism of instability generation, a study about the growth of spurious modes with time evolution, has been done. The effect of different parameters such as mesh refinement, boundary conditions, Weissenberg number, and finite extensibility has been investigated. To do so, first we compute the difference between the spectrum obtained by simulation and that one obtained by analytical one with time evolution for each variable in modal basis. The analytical spectrum of the modal basis has been derived from the full prescription of the steady flow. For fluids of the FENE family in spite of the fact that no simple expression for  $H$  conformation tensor can be derived analytically, the constitutive equation becomes a set of nonlinear algebraic

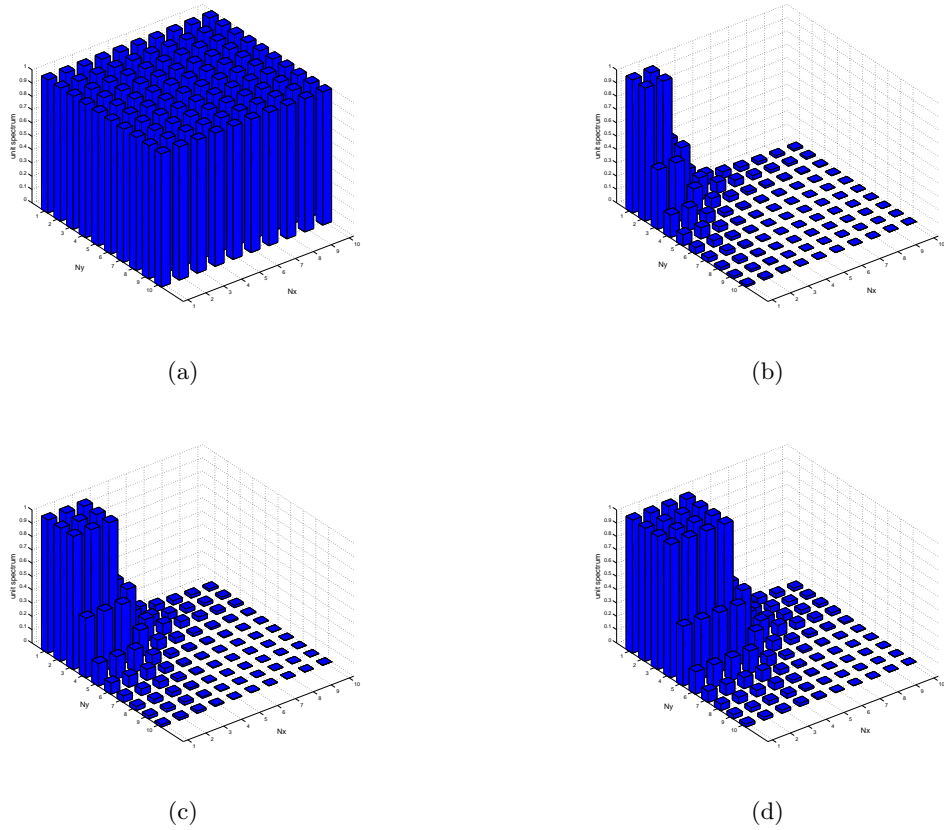


Fig. 7.2: Filtering one element unit spectrum,  $\eta = 10$ , a) unit spectrum, b) Newtonian fluids  $n=1$ , c) Oldroyd-B  $n=2$ , d) FENE-P  $n=3$

equations, where for the fully developed Poiseuille flow the transverse component of the velocity is equal to zero and all quantities except the pressure are dependent on  $y$  only [104, 74]. Analytical solutions are available for an Oldroyd-B fluid as reported in [74, 229]. Moreover, to investigate the influence of element decomposition we consider both multi-element and single element decompositions.

In a second stage, to get rid of these spurious modes, filter-based stabilization of spectral element methods proposed by Boyd is applied to both FENE-P and Oldroyd-B fluids. To verify the influence of element decomposition on this filter, we consider both single and multi-element decomposition. This filter acts better for the single element comparing the multi-element decomposition. According to this fact, a new technique to apply this

filter, the so called mesh-transfer technique, is proposed. The details of this method are explained in [30, 31]. Let us summarize the main principles of mesh-transfer technique by following the notation of Bouffanais et al. To provide a new mesh topology, it is mandatory to transfer some information from the previous mesh to the new one. The main requirement imposed to this so-called mesh-transfer operation is to conserve the spectral accuracy of the SEM. As it has been explained in previous chapter the velocities and viscoelastic stress are expanded over a GLL grid and the pressure over a GL one. Therefore the mesh-transfer technique must be capable of transferring fields defined over GL and GLL grids.

Let us consider two meshes  $\mathcal{M}_1$  and  $\mathcal{M}_2$  corresponding to different mesh topology of the same computational domain and the mesh-transfer operation from  $\mathcal{M}_1$  to  $\mathcal{M}_2$ . In the sequel, the following decompositions in terms of spectral elements is assumed:

$$\Omega_i \cup \partial\Omega_i = \bigcup_{e=1}^{E_i} \Omega_i^e \quad \text{for } i = 1, 2. \quad (7.9)$$

As the computational domain remains unchanged, for each spectral element  $\Omega_2^e$ , of  $\mathcal{M}_2$  we have:

$$\Omega_2^e \subset (\Omega_1 \cup \partial\Omega_1) \quad \forall e = 1, \dots, E_2 \quad (7.10)$$

Due to Eq. 7.10 the mesh-transfer technique only requires an interpolation procedure. Let us note the physical location of the set of GLL grid points of a spectral element  $\Omega_2^{e_2}$ , ( $e_2 = 1, \dots, E_2$ ) by  $\mathbf{x}_{ij,2}^{e_2}$  with ( $i = 1, \dots, N_{x,2} + 1; j = 1, \dots, N_{y,2} + 1$ ),  $N_{x,2}$  (resp.  $N_{y,2}$ ) being the order of the polynomial interpolation in the x-direction (resp. y-direction) for the mesh  $\mathcal{M}_2$  (with the same notations,  $N_{x,2}$  and  $N_{y,2}$  can be different from  $N_{x,1}$  and  $N_{y,1}$  respectively). The proposed algorithm can be summarized in three steps:

- Find the spectral element  $\Omega_1^{e_1}$  of  $\mathcal{M}_1$  containing  $\mathbf{x}_{ij,2}^{e_2}$ ;
- Determine the position  $\mathbf{r}_1^{e_1}$  of  $\mathbf{x}_{ij,2}^{e_2}$  within the parent element  $\hat{\Omega}_1^{e_1}$  of  $\Omega_1^{e_1}$ ;
- Compute the value of the field at the point  $\mathbf{x}_{ij,2}^{e_2}$  given  $\mathbf{r}_1^{e_1}$ , the GLL Lagrangian interpolation basis and the values of the field at the GLL grid points of  $\Omega_1^{e_1}$ .

$\mathbf{x}_{ij}$  and  $\mathbf{r}_1$  are the physical and parent coordinates respectively.



In the third stage, we focus on the mathematical property of the constitutive equation for the FENE-P family. We examine the effect of Weissenberg number, mesh refinement and time step. The 2-D time dependent Poiseuille flow shown in Fig. 7.3 has been considered in this approach. Here, time dependent simulation means that we start from a specified initial condition based on the full prescription of the fully-developed steady flow for all variables by analytical (Oldroyd-B) or numerical (FENE-P) to reach the steady state of the the flow. The computational domain consists of two parallel fixed walls. A constant nonzero pressure gradient is imposed on the flow. Magnitude of the applied pressure gradient is selected such that the channel flow rate is equal to one. All data plots shown correspond to  $Re = 1$ ,  $H = 1$ , (channel height),  $L = 4$ , (channel length),  $R_\mu = 1/9$ ,  $b = \sqrt{6}$  unless other values are specified. Dirichlet boundary conditions for velocity and viscoelastic stress, imposed at the inflow boundary, are obtained by computing a steady Poiseuille flow. At the outflow boundary, free boundary conditions are applied. Free or natural boundary condition means here that velocity and viscoelastic stress tensor are not imposed on the outflow boundary. To compare the effect of outflow boundary on the results, Dirichlet condition for velocity is also considered. No explicit boundary condition is imposed on the pressure since no pressure grid point lies on the boundary of the computational domain. The full analytical prescription of the steady flow has been chosen as the initial condition. The set of equations (3.1), (3.2) and (3.6) are discretized in space and time with numerical techniques have been explained in section 4.6 and with more details in Chapter 3.

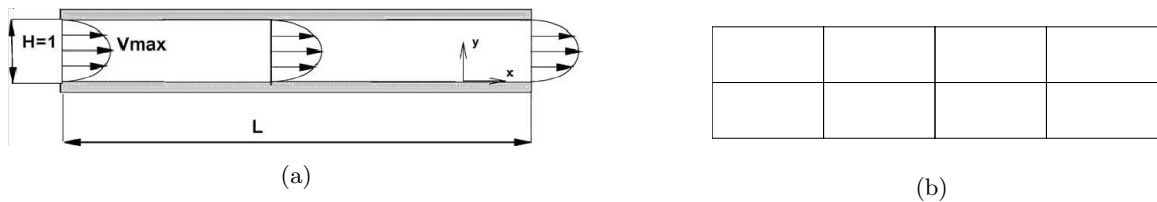


Fig. 7.3: a) Poiseuille flow in a planar channel, b) typical mesh decomposition.

### 7.3 Results and discussion

The first part of results is devoted to obtain the modal spectrum of stream-wise velocity, first normal stress and shear stress with respect to the time evolution for the FENE-P

model. The three variables are non-zero quantities in 2-D fully developed Poiseuille flow and the spectra in the appearance not the magnitude would be roughly the same. An investigation of the influence of various mesh and physical parameters has been carried out. Here, the numerical results of simulation are based on 3000, 4000 and 5000 time steps as a maximum number of iterations with  $\Delta t = 0.002$ . However for many cases because of instability problems, the numerical simulation blows up sooner than the chosen time step. It was impossible to finish the computation successfully. The first figure of each set represents the spectrum of the fully analytical prescription of the steady flow. Depending on the number of time steps which simulation successfully passes before blow up, we represent maximum norm of unknown variable,  $|v_{analytical}^* - v_{simulation}^*|$ , at five different times. First and last time steps are considered for every cases, but for intermediate simulations, we pay more attention to the instant when modes are excited. The variables in the label of the figures and tables are named with superscript  $'*$ ' which means the spectrum of that variable on the modal basis are considered.

Then in the second part of the simulation, we apply the filter-based stabilization method for the FENE-P and Oldroyd-B models. In contrast with the previous works, which employed the filter based stabilization method element by element, we propose a new way of filter implementation. The capability of this technique will be discussed with more details in the following section. In the last part of this study we focus on the appearance of numerical instabilities for the FENE-P constitutive equation during the computation. This simulation is based on  $\Delta t = 0.002$  and  $\Delta t = 0.0002$ . Because of instability problems, the numerical simulation blows up before reaching the end of the time integration. Also, we investigate the effect of different parameters such as Weissenberg number and mesh refinement on the computational results.

## 7.4 Results without filtering

### 7.4.1 Influence of Weissenberg number

Table 7.1 and Fig. 7.4-7.5 represent the effect of Weissenberg number at  $We = 100$ ,  $We = 10$ , and  $We = 1$  respectively. These time dependent simulations have been done for  $(4 \times 2)$  elements and  $(6 \times 6)$  polynomial degree in stream-wise and cross-wise direction

respectively with outflow natural boundary condition. The reason for selection  $(6 \times 6)$  polynomial order is that this is the maximum polynomial degree enabling completion of time dependent simulation at  $We = 1$  with natural boundary condition. These simulations are based on 5000 time steps with  $\Delta t = 0.002$ . However, for  $We = 100$  and  $We = 10$ , because of instability problems, the numerical simulation blows up sooner than the chosen time step. The first figure in each set represents the spectrum of the full analytical prescription of the steady flow of first normal viscoelastic stress component. Table 7.1 represents the maximum variation of the modal spectrum of the first normal stress with respect to the analytical one at time step 1, 5, 7, 11 and 13. The results show how fast the spurious modes are generated and excited during the simulation at  $We = 100$ . We observed that the first excited modes are induced at two last elements near the outflow region and immediately penetrate upstream and cover the whole domain. At  $We = 10$ , Fig. 7.4, around time steps 101, spurious modes make observable deviation from the analytical one and till time step 3180 where significant difference between simulation and analytical values occurs, the numerical simulation continues. At  $We = 1$ , Fig. 7.5 the simulation is done successfully and the magnitude of unphysical modes at the end of the simulation is of the order of  $10^{-3}$ .

The effect of Weissenberg number for single element at  $(7 \times 7)$  polynomial degree

Time step	1	5	7	11	13
$ \tau_{xx}^{*analytical} - \tau_{xx}^* $	$10^{-3}$	11	12	14	25

Table 7.1: Maximum variation of modal spectrum of  $\tau_{xx}$  with time evolution at  $b^2 = 6$ ,  $We = 100$ ,  $(NE_x, NE_y) = (4, 2)$ ,  $(N_x, N_y) = (6, 6)$  and Natural outflow boundary condition.

are shown in Fig. 7.6 and Table 7.2. According to the fact that this is the maximum polynomial degree enabling completion of time dependent simulation at  $We = 1$  with natural boundary condition, we chose this polynomial degree to investigate the influence of Weissenberg number on the modal spectrum. Magnitude of spurious modes at  $We = 100$ , Table 7.2, and  $We = 10$ , Fig. 7.6 for single element are less severe than those obtained by the multi-element decomposition. The presence of these spurious modes causes the loss of accuracy of the variables at the end of the simulation.

$We$	Time step	1	101	1001	4001	5000
100	$ \tau_{xx}^{*analytical} - \tau_{xx}^* $	0.03	1.50	1.00	3.00	2.50
10	$ \tau_{xx}^{*analytical} - \tau_{xx}^* $	0.08	0.90	0.35	0.38	0.40

Table 7.2: Maximum variation of modal spectrum of  $\tau_{xx}$  with time evolution at  $b^2 = 6$ ,  $(NE_x, NE_y) = (1, 1)$ ,  $(N_x, N_y) = (7, 7)$  and Natural outflow boundary condition.

### 7.4.2 Influence of mesh refining

Fig. 7.7 and Table 7.3 show the effect of mesh refining at  $We = 1$  with outflow natural boundary condition for  $(4 \times 2)$  element in stream and cross-wise direction respectively. Three different polynomial degrees  $(7 \times 7)$ ,  $(8 \times 8)$ , and  $(10 \times 10)$  are chosen for this test case with 5000 time steps and  $\Delta t = 0.002$ . For each of polynomial degree, the simulation was never successful. As it is obvious in this figure the most excited modes are concentrated in two last elements close to the outflow region. These unphysical modes grow very fast and after 100 iterations the simulation blows up. As mentioned before for polynomial degree,  $(6 \times 6)$  one can carry out the simulation accurately as shown in Fig. 7.5. In fact, increasing the polynomial degree by only one order, from 6 to 7, causes this instability problem so it is worth enough to discuss more mathematically the effect of increasing of polynomial degrees on results to understand the effect on the simulation. Discussion about this fact is postponed till Section (7.5.3).

$(N_x, N_y)$	Time step	1	2	15	25	34	35	45	56
$(8, 8)$	$ \tau_{xy}^{*analytical} - \tau_{xy}^* $	0.01	0.25	-	3.50	-	-	4.50	$3.50 \times 10^9$
$(10, 10)$	$ \tau_{xy}^{*analytical} - \tau_{xy}^* $	0.01	0.70	3.00	-	200.00	$5 \times 10^5$		

Table 7.3: Maximum variation of modal spectrum of  $\tau_{xy}$  with time evolution at  $b^2 = 6$ ,  $We = 1$ ,  $(NE_x, NE_y) = (4, 2)$  and Natural outflow boundary condition.

Let us consider, the effect of mesh refining by increasing the polynomial degree is considered for single element at  $We = 1$ , and outflow natural boundary condition for  $(10 \times 10)$  and  $(15 \times 15)$  polynomial degrees. The maximum number of time step is chosen 3000 with time interval equals to  $\Delta t = 0.002$ . On the corresponding Figures (7.8-7.9), it may be observed again that the unphysical modes are induced and excited during the simulation.

Magnitude of these nasty modes are  $O(10^{-1})$  and  $O(10^{+10})$  for these two polynomial degrees respectively. By increasing the polynomial degree the growth of spurious modes is enhanced and this is the reason why for  $(15 \times 15)$  polynomial degree after 51 time steps the simulation breaks down, while for  $(10 \times 10)$  polynomial degree the simulation can be carried out till 3000 time steps.

### 7.4.3 Influence of finite extensibility parameter

Let us now inspect the effect of the extensibility parameter,  $b$ , on the modal spectrum of stream-wise velocity. Fig. 7.10 and Table 7.4 represent the effect of finite extensibility parameter for  $(4 \times 2)$  elements and  $(6 \times 6)$  polynomial degree at  $We = 1$  in stream and cross-wise direction respectively. The Oldroyd-B model can be considered as a particular case of the FENE-P model when  $b \rightarrow \infty$ . For all these three finite extensibility parameters  $b^2 = 60$ ,  $b^2 = 6 \times 10^3$ , and  $b^2 = 6 \times 10^6$ , numerical simulation blows up after some iteration. We have to emphasize that one can do time dependent simulation successfully while using finite extensibility equals to  $b^2 = 6$  with the same conditions, Fig. 7.5.

$b^2$	Time step	1	11	21	41	51	81	101	121
60	$ V_{x \text{ analytical}}^* - V_x^* $	0.10	0.12	0.35	-	0.70	80.00		
$6 \times 10^3$	$ V_{x \text{ analytical}}^* - V_x^* $	0.12	0.14	-	1.00	-	-	2.50	14.00

Table 7.4: Maximum variation of modal spectrum of  $V_x$  with time evolution at  $We = 1$ ,  $(NE_x, NE_y) = (4, 2)$ ,  $(N_x, N_y) = (6, 6)$  and Natural outflow boundary condition.

The influence of the finite extensibility parameter,  $b$ , on single element at  $We = 1$  can be observed in Figures 7.11-7.12 and Table 7.5. Outflow natural boundary condition is imposed with  $(12 \times 12)$  polynomial degree. The reason for selecting this polynomial degree for this test case is that  $(12 \times 12)$  is the maximum polynomial degree enabling completion of simulation at  $We = 1$  and  $b^2 = 6$  with natural boundary condition. So by increasing the finite extensibility parameter we can investigate its effect on the modal spectrum. These test cases correspond to 5000 time steps as a maximum number of iterations with  $\Delta t = 0.002$ . At  $b^2 = 6$ , however some spurious modes grow during the simulation but the maximum difference of numerical spectrum and analytical one is  $O(10^{-4})$ , which is a very satisfactory result. Increasing the finite extensibility boosts magnitude of spurious modes

and causes unsuccessful simulation.

$b^2$	Time step	1	25	30	50	100	114	200	280	310
60	$ V_x^* \text{ analytical} - V_x^* $	0.16	0.50	-	0.80	1.50	350.00			
$6 \times 10^3$	$ V_x^* \text{ analytical} - V_x^* $	0.23	-	0.85	-	-	-	3.00	3.30	$2 \times 10^{13}$

Table 7.5: Typical variation of modal spectrum of stream-wise velocity with time evolution at  $We = 1$ ,  $(NE_x, NE_y) = (1, 1)$ ,  $(N_x, N_y) = (12, 12)$  and Natural outflow boundary condition.

#### 7.4.4 Influence of outflow boundary condition

The influence of outflow boundary condition at  $We = 1$  can be observed in Figures 7.13 and 7.14. Here, only Dirichlet boundary condition for velocity (nothing imposed for the viscoelastic stress tensor) at outflow is considered. Fig. 7.13 corresponds to  $(4 \times 2)$  elements and  $(7 \times 7)$  polynomial degree in stream-wise and cross-wise direction. The main reason for selection this polynomial degree is that it is impossible to do simulation at this order with natural boundary condition at  $We = 1$ , so we are interested in investigating the effect of other outflow boundary condition on stabilizing results. In Fig. 7.14, we consider single element and  $(15 \times 15)$  polynomial degree at  $We=1$ , which is an unstable case with natural boundary condition. This analysis has been done with 3000 time steps as a maximum number of iteration at  $\Delta t = 0.002$ . Comparison of Fig. 7.13 and 7.7 reveals that the numerical simulation is sensitive to the outflow boundary condition. Actually by imposing Dirichlet velocity boundary condition at outflow one can finish the time dependent simulation successfully and get an accurate enough result. The order of error of spurious modes at the end of simulation is  $O(10^{-3})$  for shear stress, which is in contrast with those obtained by natural outflow boundary condition. The same behavior is observed for single element by comparison between Fig. 7.14 and 7.9.

Now it is clear that the outflow boundary condition has very important effects on the manifestation of instabilities. Imposing natural boundary condition at outflow governs the system not only by the state in the interior of the region, but also by the information brought by incoming characteristics which enter the region. Furthermore, imposing natural boundary condition introduces instability first in elements which are close to the

outflow region and afterwards these spurious modes penetrate upstream very fast. So imposing Dirichlet velocity boundary at outflow was found better in term of convergence and stabilization. We would like to emphasize that imposing periodic boundary condition for both velocity and viscoelastic stress at inflow and outflow boundary condition, induces the same behavior in the growth of instabilities alike imposing only velocity boundary condition at outflow.

## 7.5 Results with filtering

### 7.5.1 Influence of filter-based stabilization of spectral element method

After reporting a comprehensive study about the mechanisms of instability and investigating the effect of different parameters on the growth of instabilities, let us inspect the effect of filter-based stabilization techniques proposed by Boyd. However, the idea behind the filter based stabilization of Boyd in modal basis and Fischer in nodal basis is the same, in this study, we only considered the Boyd's stabilization technique. The results reported in this section are obtained by multi-element configurations and those obtained by single element are skipped. To enable one to compare the results, for different cases, only the modal spectrum of shear stress is shown, however non-zero spectra, stream-wise velocity and first normal stress in 2-D poiseuille flow, have the same behavior in the growth of instabilities. For more details about the parameters of filtering and shape function refer to section 7.2.1.

Regarding the previous analysis, concerning the effect of mesh refinement at  $We = 1$  for  $(4 \times 2)$  elements in the stream and cross-wise directions, the maximum polynomial degrees in both direction enabling completion of time dependent simulation with time interval  $\Delta t = 0.002$  and natural outflow boundary condition successfully is  $(6 \times 6)$ , if no filtering is used. To check the capability of this filter based technique we start with polynomial degree  $(7 \times 7)$ . Fig. 7.15 represents the effect of applying the considered filter at each time step during the simulation. Even though this filter is useful to eliminate spurious modes, there are still some unphysical modes that remain till the end of the simulation leading to an error of the order of  $O(10^{-2})$  and decrease the accuracy of results. Comparing this result with Fig. 7.7 clarifies the difference between filtered and non-filtered cases for the same conditions. As it is obvious in Fig. 7.7, simulation without employing

filtering for  $(7 \times 7)$  polynomial degree stops after 103 time steps because of the presence of the unstable modes,  $O(10^3)$ .

Table 7.6 also indicates the effect of imposing of filter based stabilization technique for  $(10 \times 10)$  and  $(15 \times 15)$  polynomial degrees and  $(4 \times 2)$  element in the stream and cross-wise directions. Applying this filter for polynomial order  $(10 \times 10)$  also cures the significant unphysical modes, but for polynomial degree  $(15 \times 15)$  employing filter based technique only postpones the fast growth of nasty modes and after 2541 iteration simulation stops.

$(N_x, N_y)$	Time step	1	11	131	301	401	1001	1501	2541	3001
$(10, 10)$	$ \tau_{xy}^*_{analytical} - \tau_{xy}^* $	0.01	0.14	0.50	-	-	0.01			0.01
$(15, 15)$	$ \tau_{xy}^*_{analytical} - \tau_{xy}^* $	0.01	-	-	0.01	1.40	-	14.00	35.00	

Table 7.6: Maximum variation of modal spectrum of  $\tau_{xy}$  with time evolution after applying filtering at  $b^2 = 6$ ,  $We = 1$ ,  $(NE_x, NE_y) = (4, 2)$  and natural outflow boundary condition

The effect of filter based stabilization technique for Oldroyd-B fluids is shown in Fig. 7.17. Oldroyd-B is considered as a particular case of the FENE-P model when  $b \rightarrow \infty$ . This test case corresponds to  $(4 \times 2)$  elements and  $(6 \times 6)$  polynomial degree in stream and cross-wise direction at  $We = 1$  and natural boundary condition. After 3000 iterations with  $\Delta t = 0.002$ , because of appearance of spurious modes of order  $O(10)$ , the simulation ends with an unphysical numerical solution. However, without employing the filter-based technique simulation stops very soon, after 121 iterations (Fig. 7.10), but applying filtering only postpones the time of excitation of nasty modes and their growth.

### 7.5.2 Influence of mesh-transfer technique

What we observed in the previous section was that applying the filter-based stabilization technique as such on the elements for the FENE-P model could be useful to damp and eliminate spurious modes, but at the end of the simulation some spurious modes still remain and increasing the polynomial degree proved to be not very helpful. Applying this filter for Oldroyd-B model only postpones the time when the instability sets in and the numerical simulation and the performance of this technique is not ideal for Oldroyd-B. According to our observation, we found that the performance of this technique while using



a one element decomposition is better than for a multi-element decomposition. Probably, decomposition of elements in the x-direction is an obstacle for this technique due to the presence of interfaces between elements. One possible remedy to solve the associated problem of multi-element decomposition is to employ a mesh-transfer technique. As we explained in section 7.2.3, at each time step, one has to map the multi-element to a single element configuration, where one employs the filter-based stabilization technique and then transfers back to the filtered variable to the first topology. To do so, we choose three different test cases. Fig. 7.18 represents the results for FENE-P model for  $(15 \times 15)$  polynomial degree, while Fig. 7.19 and Table 7.7 correspond to the same test cases for Oldroyd-B with  $(6 \times 6)$  and  $(15 \times 15)$  polynomial degrees respectively. These test cases have been carried out for  $(4 \times 2)$  element in the stream and cross-wise directions and with natural outflow boundary condition at  $We = 1$  and  $\Delta t = 0.002$ .

In Fig. 7.18, at each time step first we map a  $(4 \times 2)$  and  $(15 \times 15)$  element and polynomial degree topology to single element with  $(61 \times 61)$  polynomial order, then we apply filter-based stabilization for this simple topology and afterwards transfer back each filtered variable to the original configuration. To preserve the spectral accuracy we map the multi-element configuration to a single one with a polynomial order at least equals to the maximum number of nodes for multi-element configuration in each direction. In the above configuration the number of nodes in stream and cross-wise direction are 61 and 31 respectively. So as a maximum number of nodes we chose the single element topology with  $(61 \times 61)$  polynomial degree. Inspection of Figures 7.18 and Table 7.6 reveals that applying mesh-transfer technique enhances the performance of filter-based stabilization and also decreases the penetration of nasty waves. After 4000 time steps the order of error for mesh-transfer technique, Figure(7.18), is  $O(1)$  while without employing the mesh-transfer technique, the order of error after 2541 iterations in Table 7.6 is  $O(10)$ .

In Fig. 7.19, first we map  $(4 \times 2)$  and  $(6 \times 6)$  element and polynomial degree configuration to a new topology with one element and  $(25 \times 25)$  polynomial degree (this polynomial degree is chosen with the same reason as explained above), apply the filtering and transfer back to the original mesh. Results clearly reveal that employing mesh-transfer technique for Oldroyd-B is very efficient. The order of error of modal spectrum of shear viscoelastic stress after 4000 iterations is  $O(10^{-5})$ , which is impossible to obtain the same accuracy while using filter-based stabilization technique, element by element, Fig. 7.17.

The same behavior is also observed in Table 7.7. Again we transfer our configuration,  $(4 \times 2)$  elements with  $(15 \times 15)$ , to a single element by  $(61 \times 61)$  polynomial degree. This time dependent simulation has been done for 4000 time steps with  $\Delta t = 0.002$ . The maximum relative error at the end of the simulation is ordered of  $O(10^{-3})$ , which is less accurate than the previous test case. So far, we can conclude that way of implementing filtering is very useful for Oldroyd-B when a moderate number of points is used for one element intermediate grid.

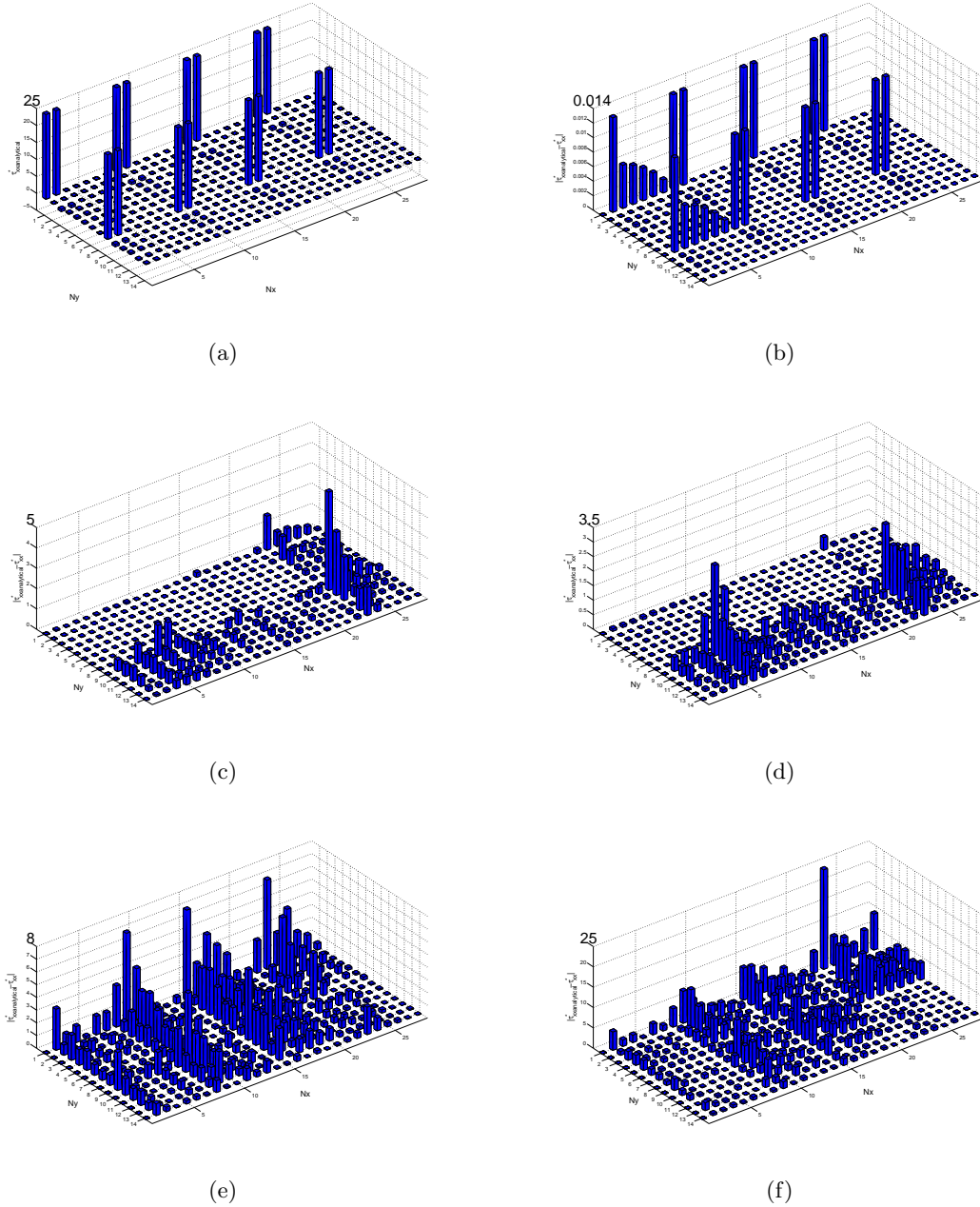


Fig. 7.4: Typical variation of modal spectrum of  $\tau_{xx}$  with time evolution at  $b^2 = 6$ ,  $We = 10$ ,  $(NE_x, NE_y) = (4, 2)$ ,  $(N_x, N_y) = (6, 6)$  and Natural outflow boundary condition, a)full analytical prescription of the steady flow, b) time step=1, c)time step=101, d)time step=1001, e)time step=3001, f)time step=3180

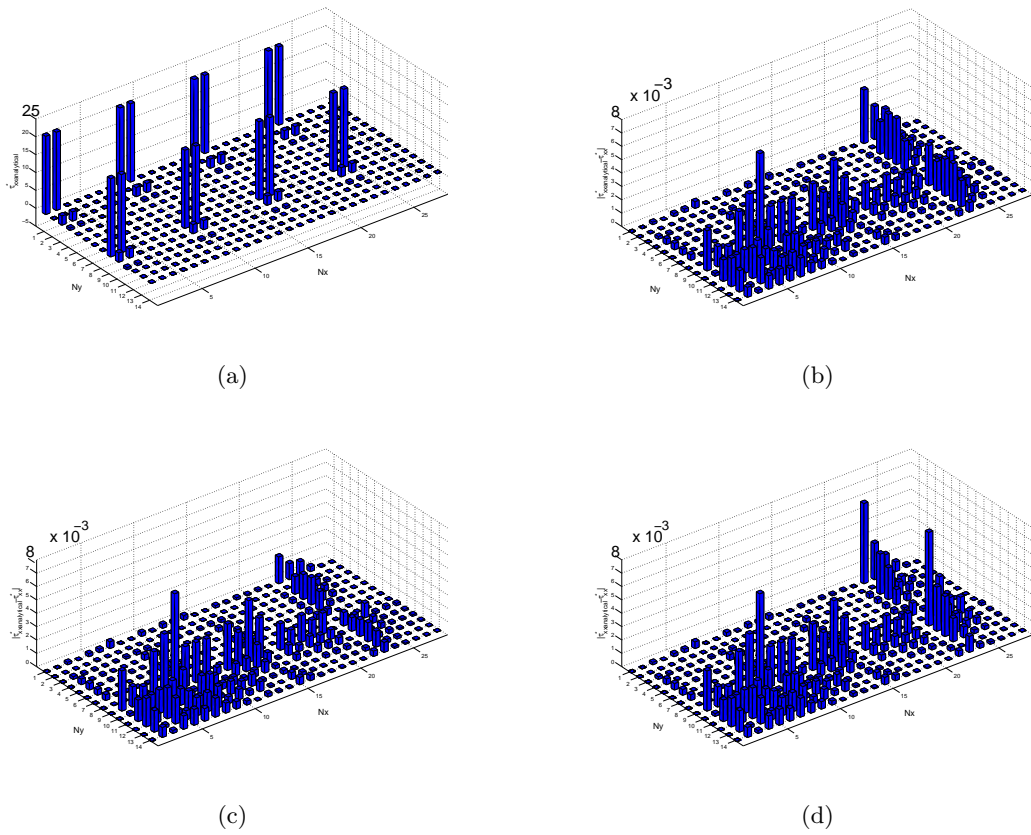
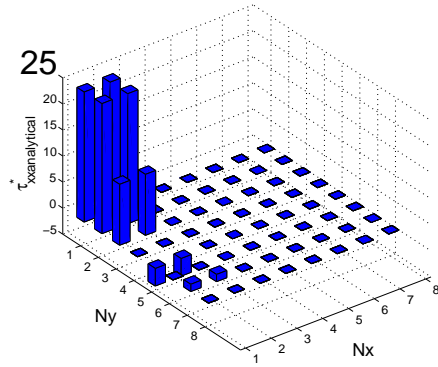
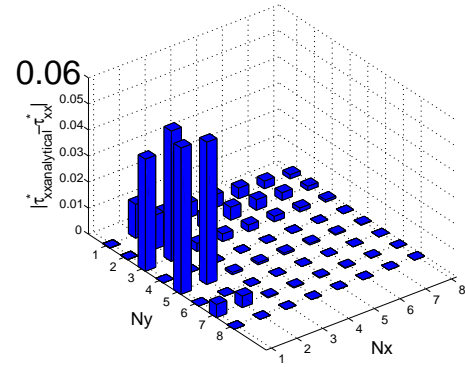


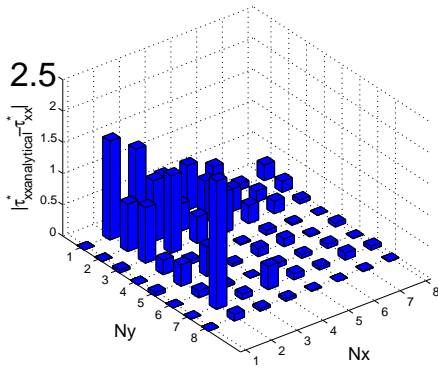
Fig. 7.5: Typical variation of modal spectrum of  $\tau_{xx}$  with time evolution at  $b^2 = 6$ ,  $We = 1$ ,  $(NE_x, NE_y) = (4, 2)$ ,  $(N_x, N_y) = (6, 6)$  and Natural outflow boundary condition, a) full analytical prescription of the steady flow, b) time step=4501, c)time step=4801, d)time step=5000



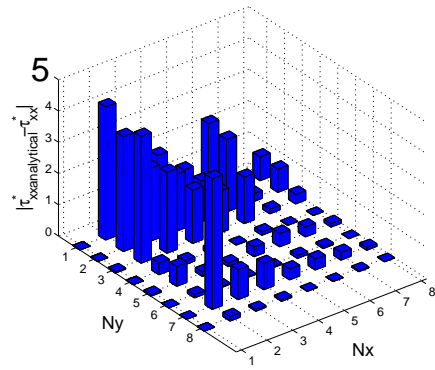
(a)



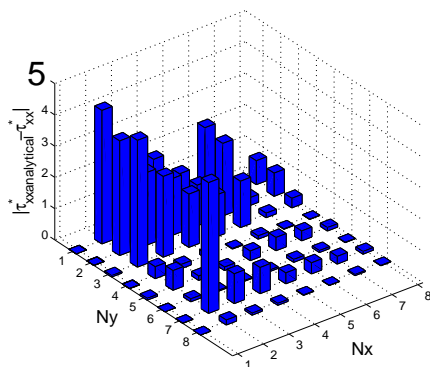
(b)



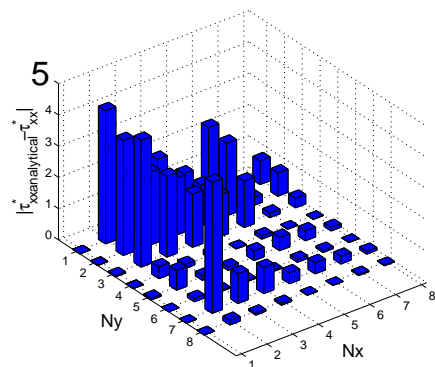
(c)



(d)



(e)



(f)

Fig. 7.6: Typical variation of modal spectrum of  $\tau_{xx}$  with time evolution at  $b^2 = 6$ ,  $We = 10$ ,  $(NE_x, NE_y) = (1, 1)$ ,  $(N_x, N_y) = (7, 7)$  and Natural outflow boundary condition, a)full analytical prescription of the steady flow, b) time step=1, c)time step=101, d)time step=4001, e)time step=4501, f)time step=5000

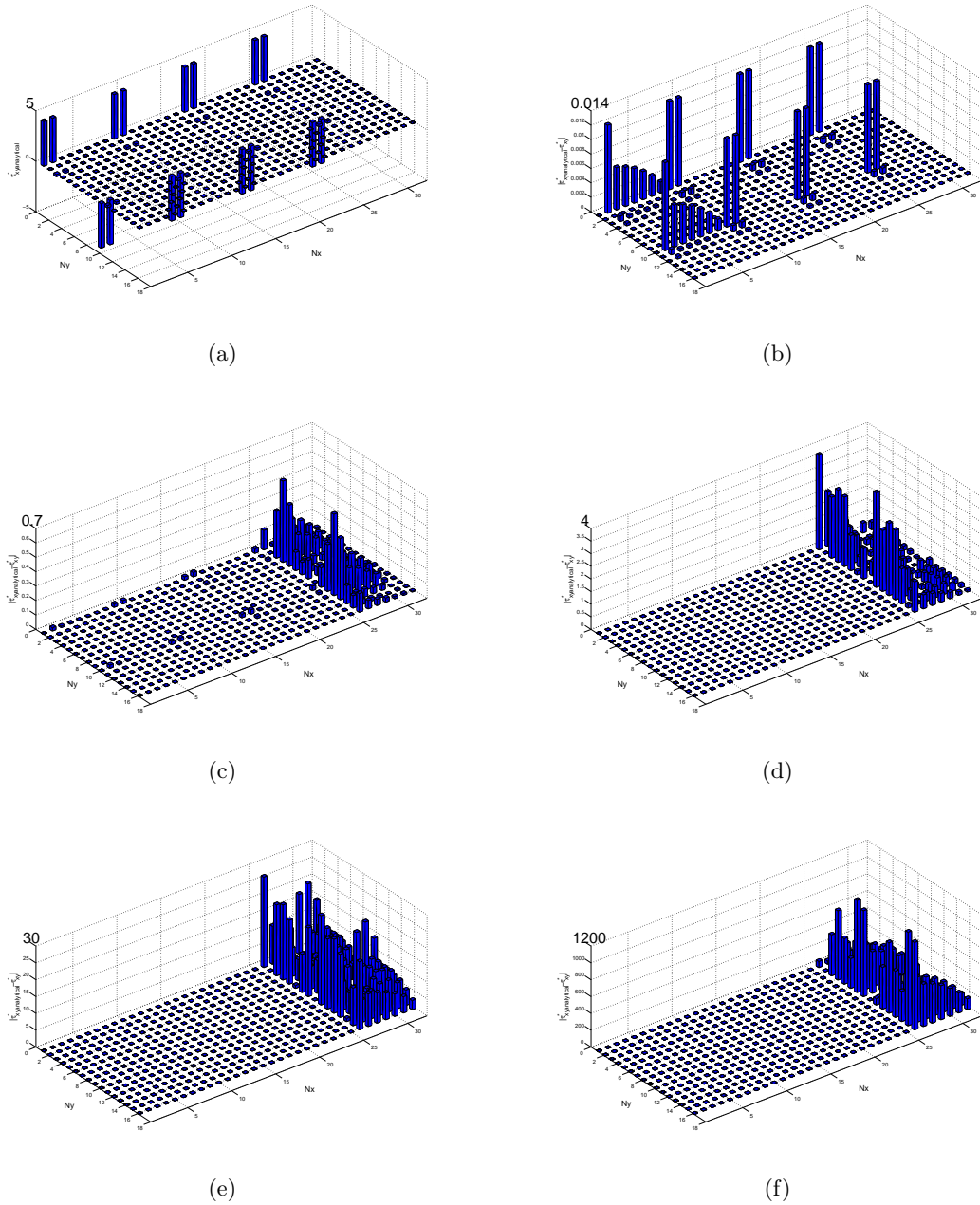


Fig. 7.7: Typical variation of modal spectrum of  $\tau_{xy}$  with time evolution at  $b^2 = 6$ ,  $We = 1$ ,  $(NE_x, NE_y) = (4, 2)$ ,  $(N_x, N_y) = (7, 7)$  and Natural outflow boundary condition, a)full analytical prescription of the steady flow, b) time step=1, c)time step=10, d)time step=50, e)time step=100, f)time step=103

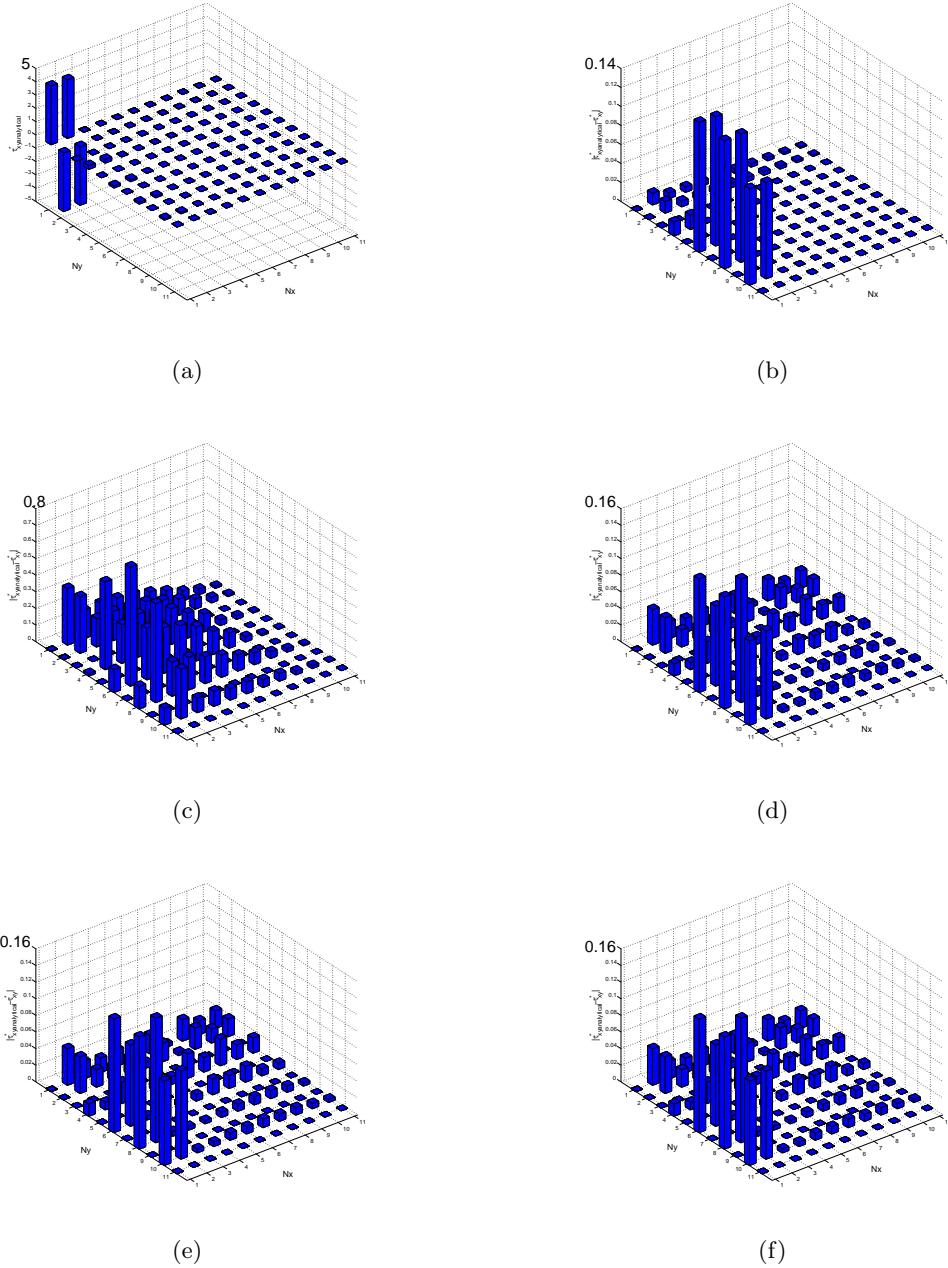


Fig. 7.8: Typical variation of modal spectrum of  $\tau_{xy}$  with time evolution at  $b^2 = 6$ ,  $We = 1$ ,  $(NE_x, NE_y) = (1, 1)$ ,  $(N_x, N_y) = (10, 10)$  and Natural outflow boundary condition, a)full analytical prescription of the steady flow, b) time step=1, c)time step=101, d)time step=1001, e)time step=2001, f)time step=3000

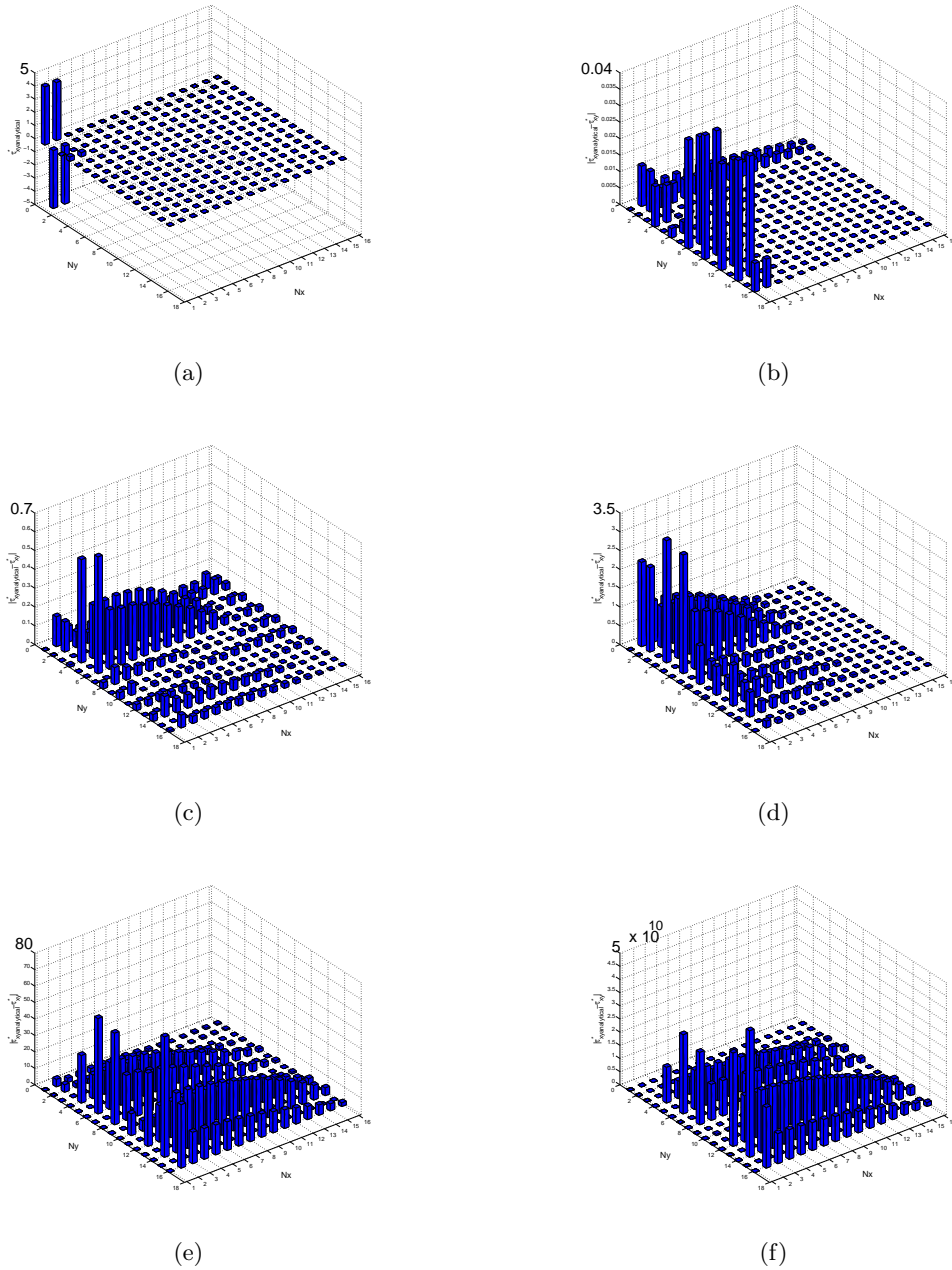


Fig. 7.9: Typical variation of modal spectrum of  $\tau_{xy}$  with time evolution at  $b^2 = 6$ ,  $We = 1$ ,  $(NE_x, NE_y) = (1, 1)$ ,  $(N_x, N_y) = (15, 15)$  and Natural outflow boundary condition, a) full analytical prescription of the steady flow, b) time step=1, c) time step=5, d) time step=20, e) time step=50, f) time step=51



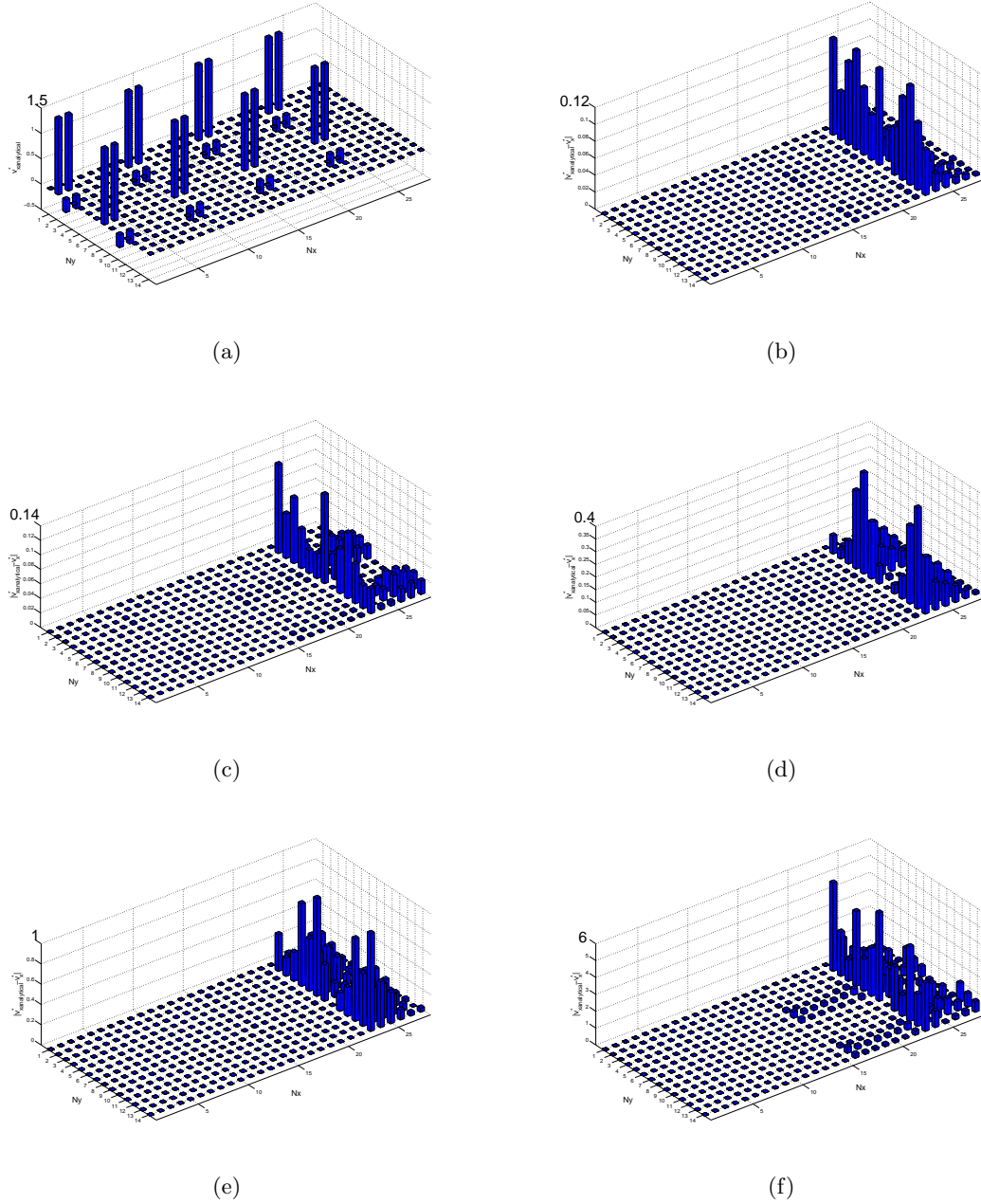


Fig. 7.10: Typical variation of modal spectrum of  $V_x$  with time evolution at  $b^2 = 6 \times 10^6$ ,  $We = 1$ ,  $(NE_x, NE_y) = (4, 2)$ ,  $(N_x, N_y) = (6, 6)$  and Natural outflow boundary condition, a) full analytical prescription of the steady flow, b) time step=1, c)time step=11, d)time step=21, e)time step=61, f)time step=121

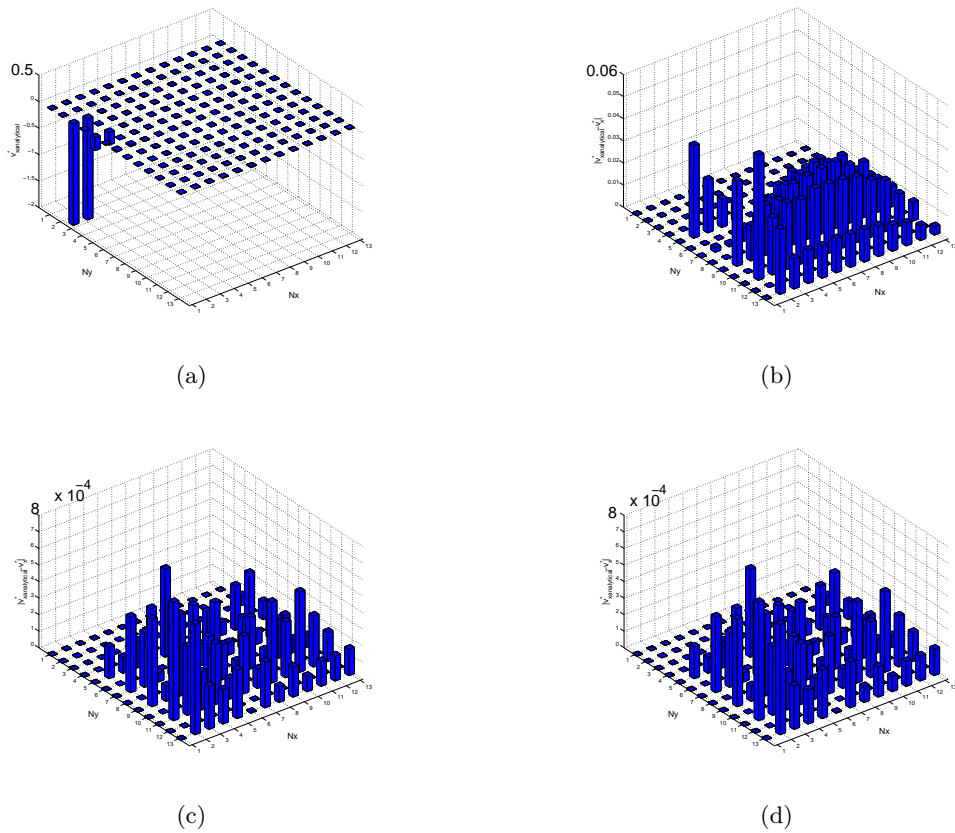


Fig. 7.11: Typical variation of modal spectrum of  $V_x$  with time evolution at  $b^2 = 6$ ,  $We = 1$ ,  $(NE_x, NE_y) = (1, 1)$ ,  $(N_x, N_y) = (12, 12)$  and Natural outflow boundary condition, a) full analytical prescription of the steady flow, b) time step=1, c) time step=4001; d) time step=5000

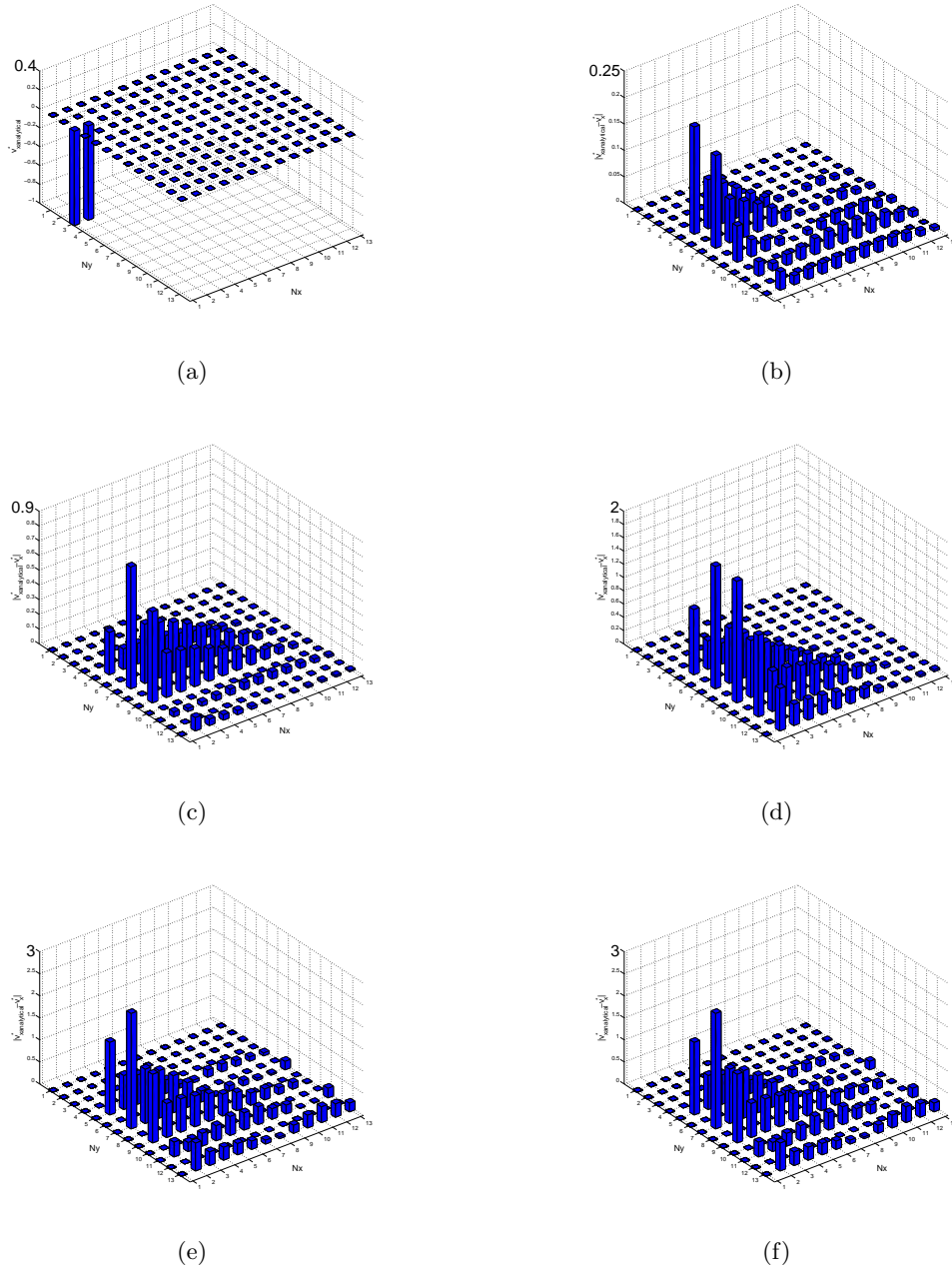


Fig. 7.12: Typical variation of modal spectrum of  $V_x$  with time evolution at  $b^2 = 6 \times 10^6$ ,  $We = 1$ ,  $(NE_x, NE_y) = (1, 1)$ ,  $(N_x, N_y) = (12, 12)$  and Natural outflow boundary condition, a)full analytical prescription of the steady flow, b) time step=1, c)time step=30, d)time step=100, e)time step=200, f)time step=219

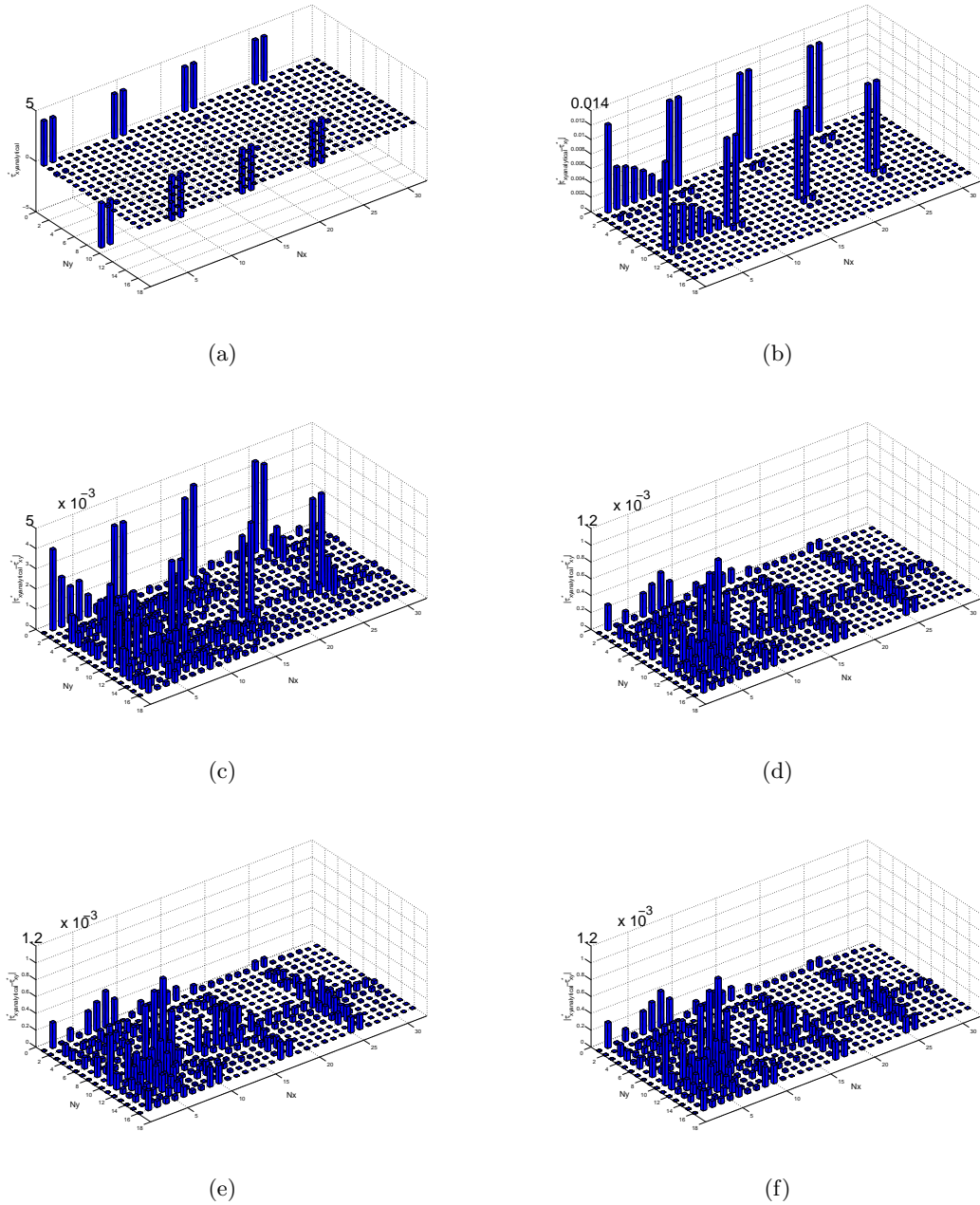


Fig. 7.13: Typical variation of modal spectrum of  $\tau_{xy}$  with time evolution at  $b^2 = 6$ ,  $We = 1$ ,  $(NE_x, NE_y) = (4, 2)$ ,  $(N_x, N_y) = (7, 7)$  and Dirichlet velocity outflow boundary condition, a)full analytical prescription of the steady flow, b) time step=1, c)time step=101, d)time step=1001, e)time step=2001, f)time step=3000

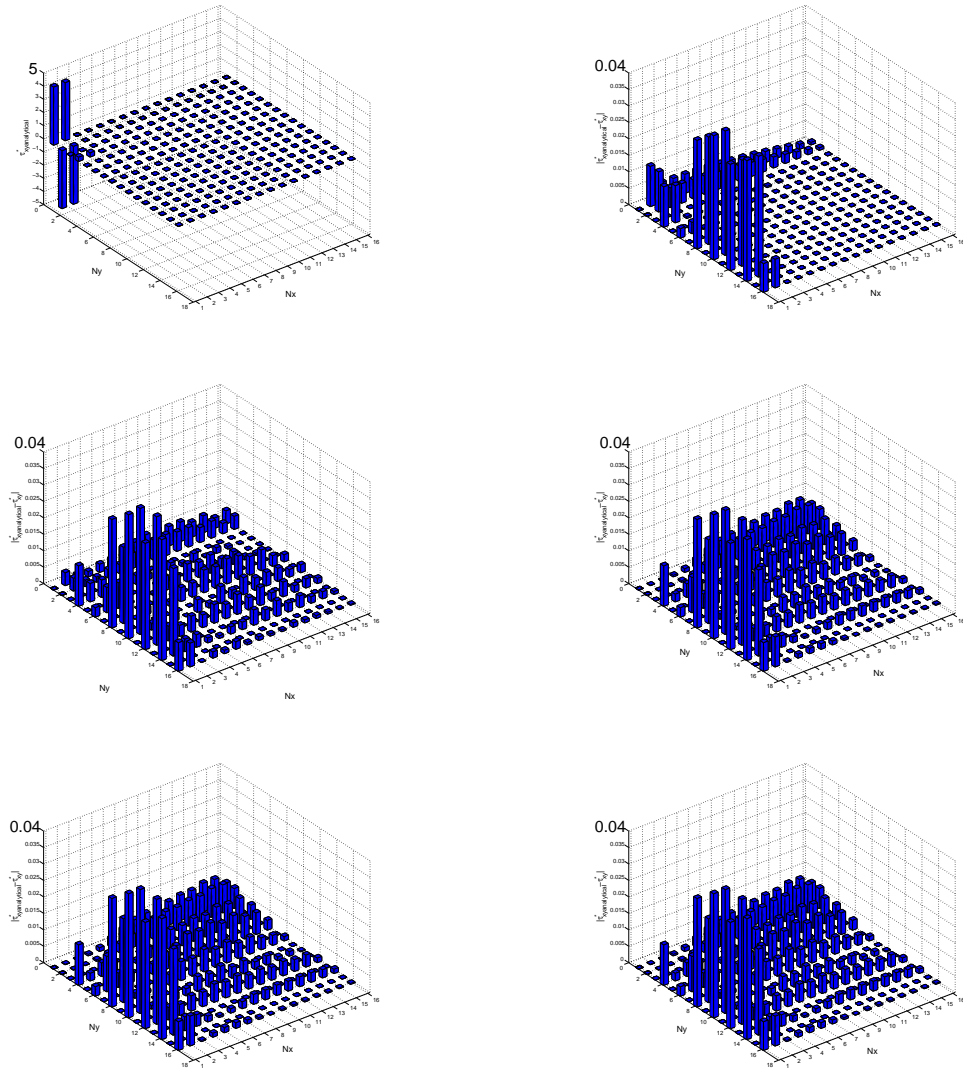


Fig. 7.14: Typical variation of modal spectrum of  $\tau_{xy}$  with time evolution at  $b^2 = 6$ ,  $We = 1$ ,  $(NE_x, NE_y) = (1, 1)$ ,  $(N_x, N_y) = (15, 15)$  and Dirichlet velocity outflow boundary condition, a) full analytical prescription of the steady flow, b) time step=1, c) time step=101, d) time step=1001, e) time step=2001, f) time step=3000

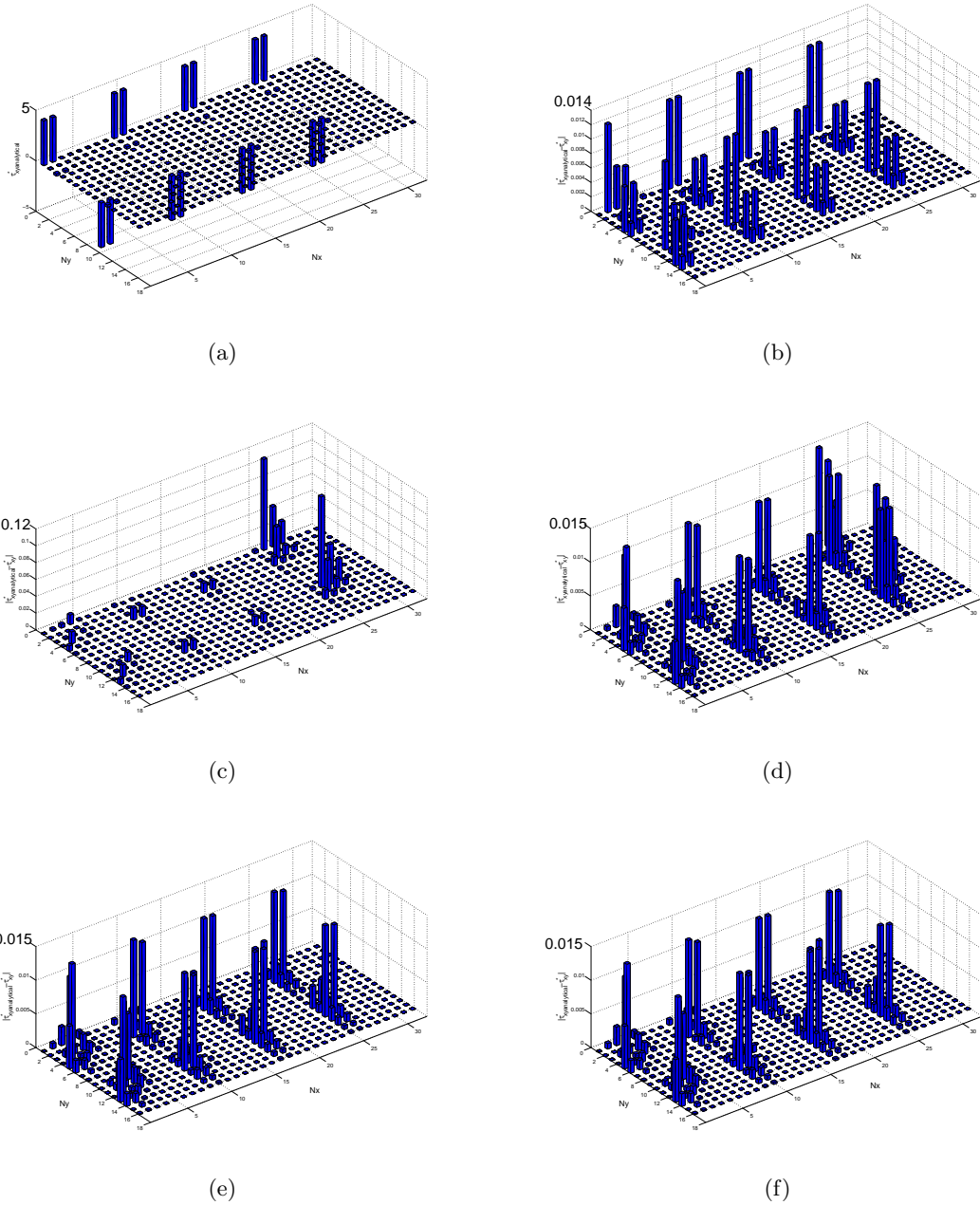


Fig. 7.15: Typical variation of modal spectrum of  $\tau_{xy}$  with time evolution after applying filtering at  $b^2 = 6$ ,  $We = 1$ ,  $(NE_x, NE_y) = (4, 2)$ ,  $(N_x, N_y) = (7, 7)$  and natural outflow boundary condition, a) full analytical prescription of the steady flow, b) time step=1, c) time step=181, d) time step=301, e) time step=1001, f) time step=3000

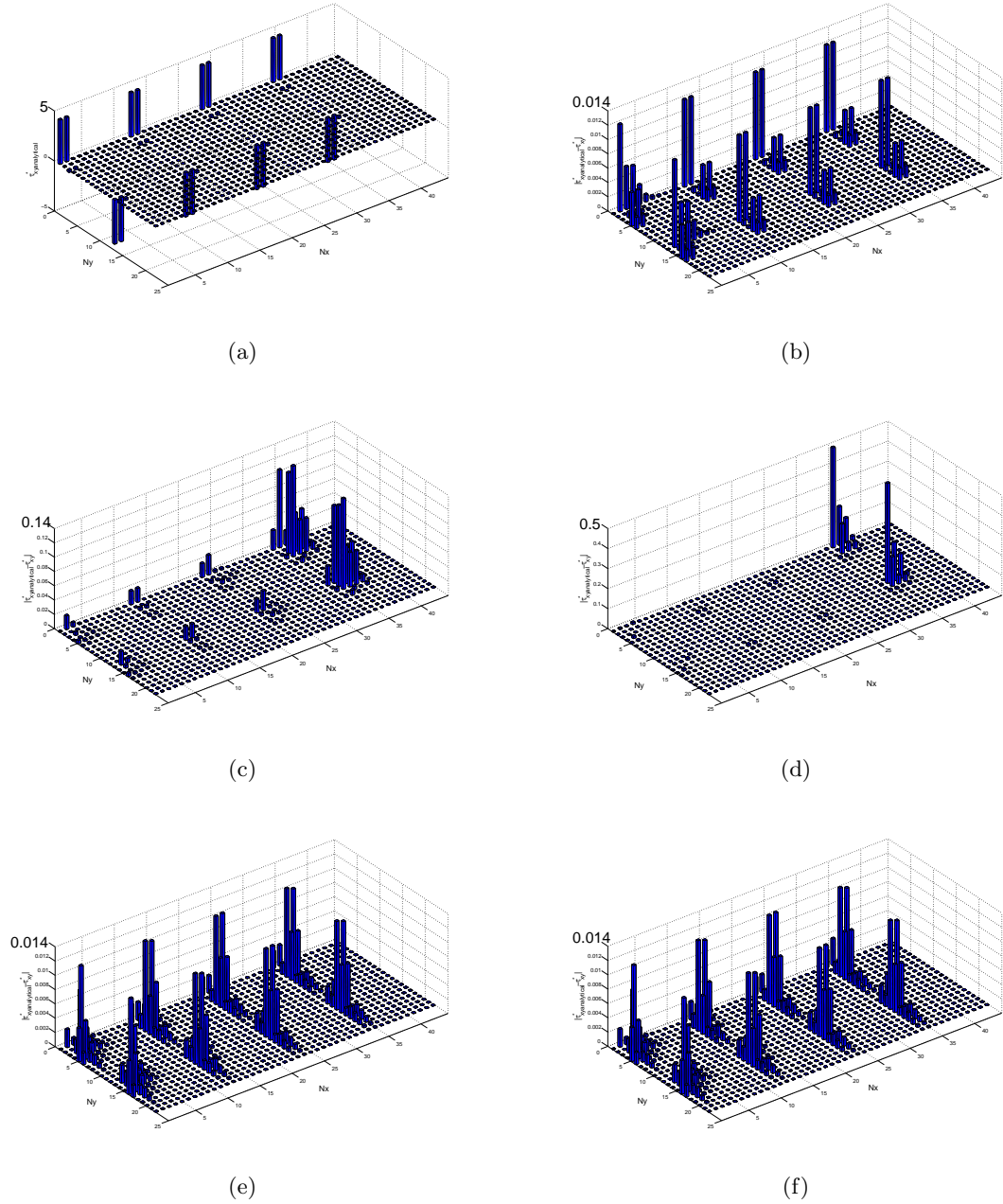


Fig. 7.16: Typical variation of modal spectrum of  $\tau_{xy}$  with time evolution after applying filtering at  $b^2 = 6$ ,  $We = 1$ ,  $(NE_x, NE_y) = (4, 2)$ ,  $(N_x, N_y) = (10, 10)$  and natural outflow boundary condition, a)full analytical prescription of the steady flow, b) time step=1, c)time step=11, d)time step=131, e)time step=1001, f)time step=3000



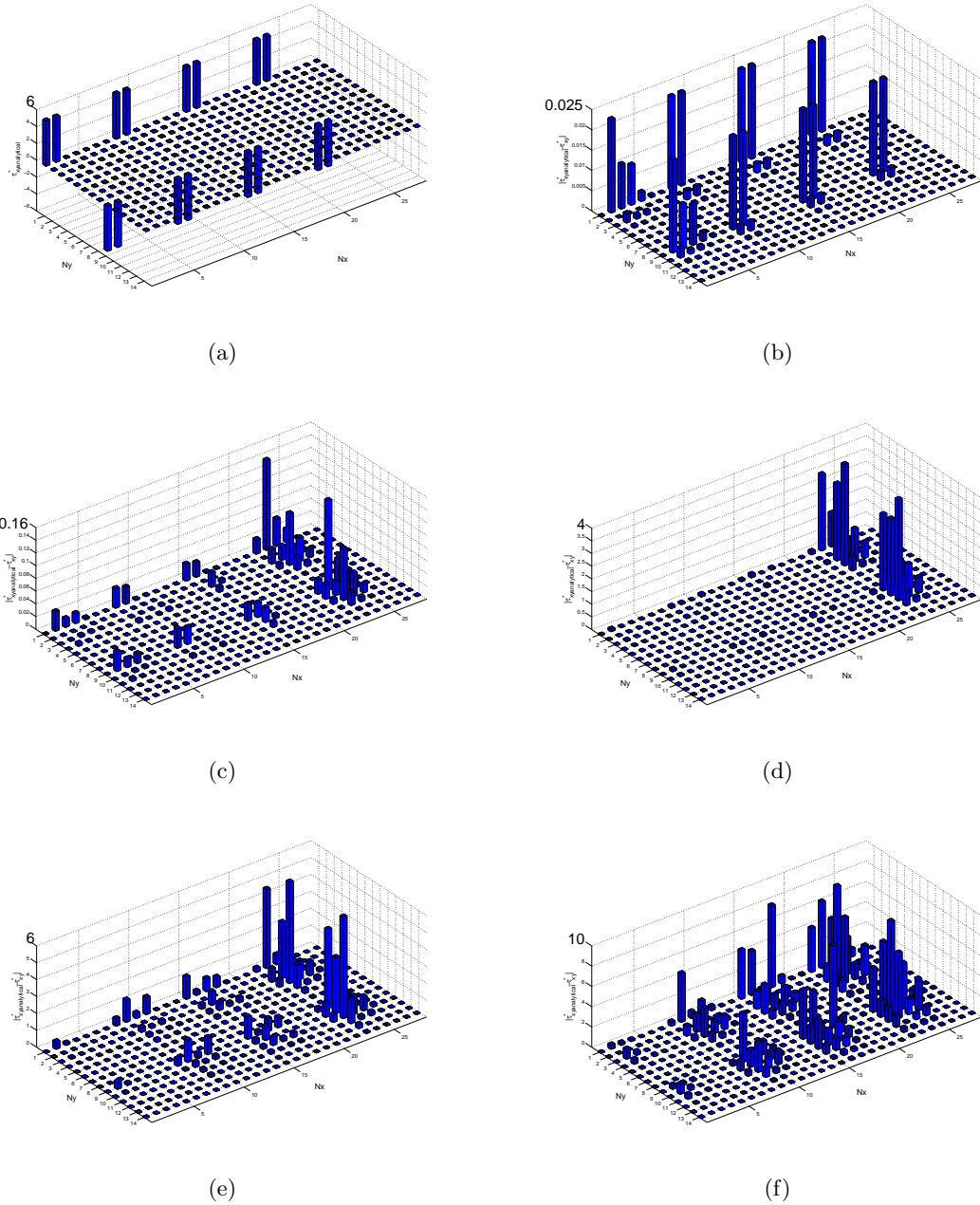


Fig. 7.17: Typical variation of modal spectrum of  $\tau_{xy}$  with time evolution after applying filtering at  $b^2 = 6 \times 10^6$ ,  $We = 1$ ,  $(NE_x, NE_y) = (4, 2)$ ,  $(N_x, N_y) = (6, 6)$  and natural out-flow boundary condition, a)full analytical prescription of the steady flow, b) time step=1, c)time step=101, d)time step=1001, e)time step=2001, f)time step=3000



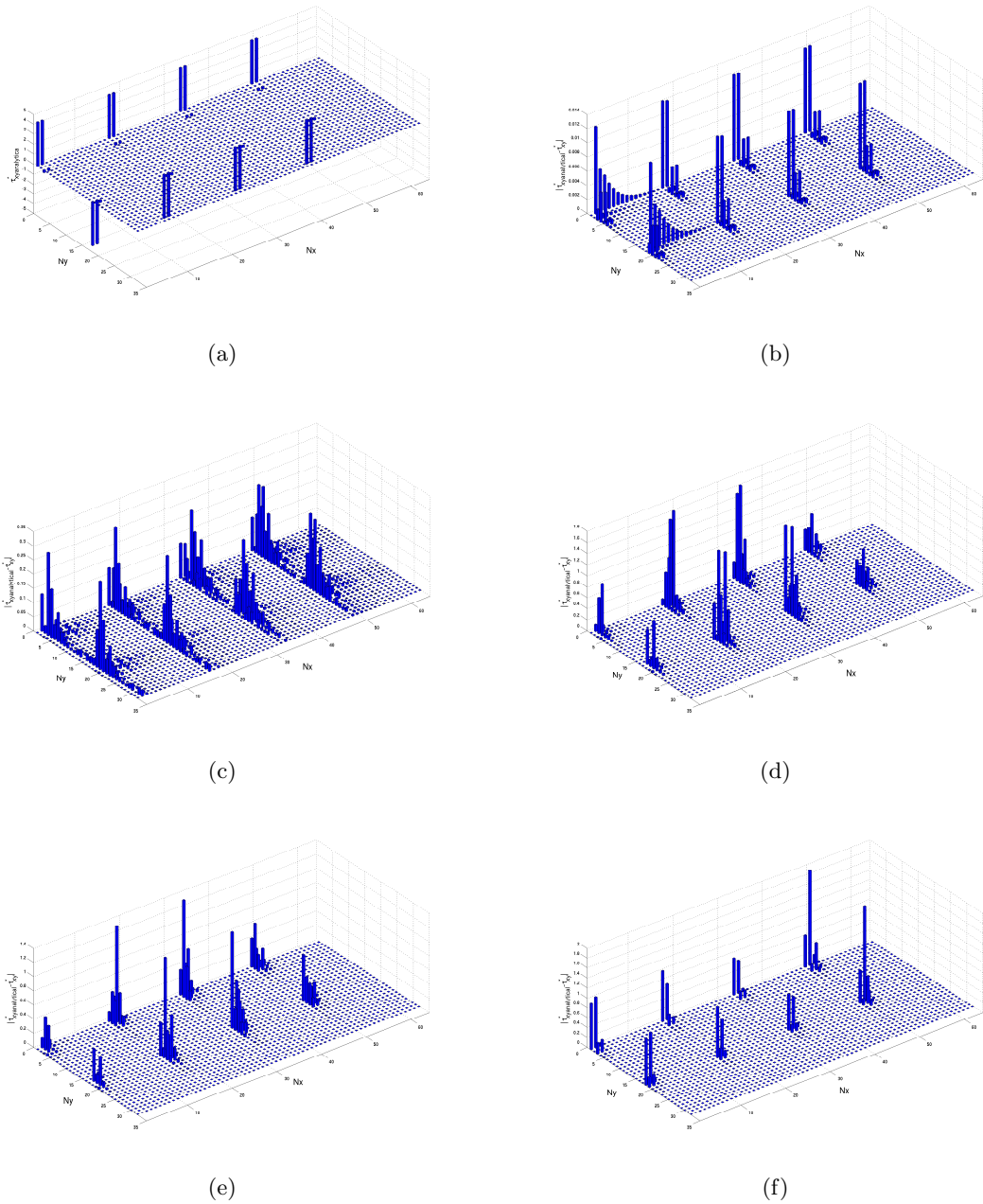


Fig. 7.18: Typical variation of modal spectrum of  $\tau_{xy}$  with time evolution and mesh-transfer technique, FENE-P,  $We = 1$ ,  $(NE_x, NE_y) = (4, 2)$ ,  $(N_x, N_y) = (15, 15)$  and natural outflow boundary condition, a) full analytical prescription of the steady flow, b) time step=1, c) time step=1001, d) time step=2001, e) time step=3001, f) time step=4000

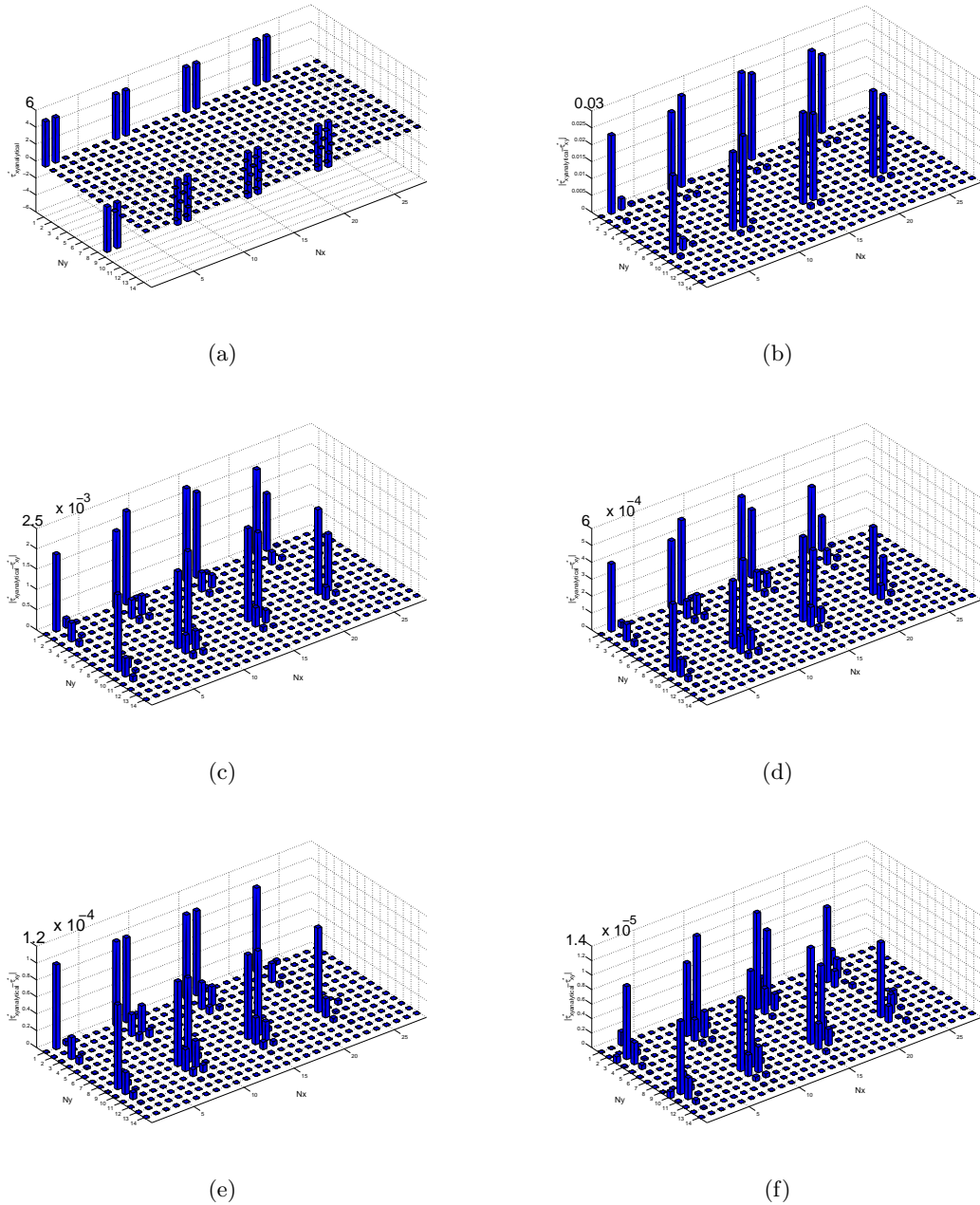


Fig. 7.19: Typical variation of modal spectrum of  $\tau_{xy}$  with time evolution and mesh-transfer technique, Oldroyd-B,  $We = 1$ ,  $(NE_x, NE_y) = (4, 2)$ ,  $(N_x, N_y) = (6, 6)$  and natural outflow boundary condition, a)full analytical prescription of the steady flow, b) time step=1, c)time step=1001, d)time step=2001, e)time step=3001, f)time step=4000

Time step	1	1001	2001	3001	4000
$ \tau_{xy}^*_{analytical} - \tau_{xy}^* $	0.03	0.01	$4 \times 10^{-3}$	$1.10 \times 10^{-3}$	$10^{-3}$

Table 7.7: Maximum variation of modal spectrum of  $\tau_{xy}$  with time evolution and mesh-transfer technique, Oldroyd-B,  $We = 1$ ,  $(NE_x, NE_y) = (4, 2)$ ,  $(N_x, N_y) = (15, 15)$  and natural outflow boundary condition

### 7.5.3 Influence of time step

In a previous study [104], we provide a modification of the matrix logarithm formulation of Fattal and Kupferman [70, 69], in order to preserve the positive eigenvalues of the conformation tensor at each time step and also bound the trace of the conformation tensor above by the square of the finite extensibility parameter. However, this new formulation which conserves symmetric positive definiteness of the conformation tensor and also bounds the maximum value of the trace of the conformation tensor, can be helpful but there are still problems of instabilities. Regarding the mathematical model for the FENE-P family Eq. (3.6), in the denominator of the formulation,  $1 - tr(C)/b^2$  appears. Whenever the computational value of  $tr(C)$  is very close to  $b^2$ , the denominator of the equation tends to zero. On the other hand, the viscoelastic stress tends to infinity, which does not have any physical meaning. In this study we do not try to improve the formulation and restrict ourselves to investigating the effect of Weissenberg number and mesh refinement on the computational value of maximum of trace of the conformation tensor. In the following we will show that one of the reason for instabilities in FENE-P fluids is when the trace of the conformation tensor is very close to  $b^2$ . We would emphasize that figures shown in this section are obtained with natural boundary condition, while the same behavior is observed for velocity Dirichlet boundary at outflow. Results reported in this section are obtained with two different time steps,  $\Delta t = 0.002$  and  $\Delta t = 0.0002$ . Because of explicit time marching scheme for the nonlinear terms in momentum and constitutive equations, the Courant-Friedrichs-Lewy (CFL) stability condition should be satisfied during the simulation

$$\max_k |\lambda_k \Delta t| = S \cdot CFL \quad (7.11)$$

where

$$CFL = \max_{c, \Delta x} \frac{c \Delta t}{\Delta x} \quad (7.12)$$

$\lambda_k$  is the eigenvalue of the problem,  $c$  is the propagation speed, and  $S$  is an order-unity coefficient that depends on the discretization. For the spectral element method  $S$  is a nonlinear function of  $N$  [60] (see Fig. 3.5.2 of this reference). We would emphasize that the CFL condition in this study is always met and the presence of instability reported in this section is observed for time steps satisfying the CFL number.

Fig. 7.20 represents the effect of Weissenberg numbers on the maximum of the trace of the conformation tensor for time intervals,  $\Delta t = 0.002$ . This test case has been done for  $(4 \times 2)$  elements and  $(4 \times 5)$  polynomial degree in stream and cross-wise direction. As we suppose before, the attained maximum of  $tr(C)$  increases by increasing the Weissenberg number. At  $We = 100$ , the maximum of which is close to  $b^2 = 6$ , which makes the simulation extremely difficult for this value of Weissenberg number. Indeed, by the smallest oscillation of the trace of the conformation tensor, the value of viscoelastic stress grows unbounded which is the worst condition of the simulation of viscoelastic fluids. Since the difference between this time interval and smaller one,  $\Delta t = 0.0002$  is indistinguishable, only the result of  $\Delta t = 0.002$  is shown.

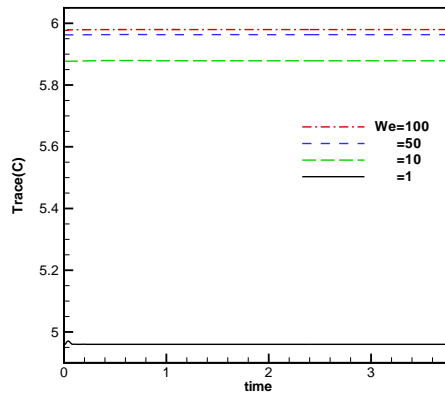


Fig. 7.20: Influence of the Weissenberg number on the maximum of  $tr(c)$ ,  $(NE_x, NE_y) = (4, 2)$ ,  $(N_x, N_y) = (4, 5)$ , natural outflow boundary condition,  $\Delta t = 0.002$

The next two test cases indicate the effect of mesh refinement by increasing the polynomial degree at  $\Delta t = 0.002$  and  $\Delta t = 0.0002$ . Fig. 7.21 shows the effect of mesh refinement in stream-wise direction at  $We = 100$  and  $(4 \times 2)$  elements in stream and cross-wise

direction. As it is clear in this figure, increasing the polynomial degree in stream-wise direction, enhances the value of trace of the conformation tensor sharply. At polynomial degree  $(10 \times 5)$  and  $(8 \times 5)$  the maximal values of the trace of the conformation tensor are still less than the selected bounded value of the conformation tensor,  $b^2 = 6$ , but they are close enough to the bounded value according to the precision of computer. In this region, unphysical values of viscoelastic stress are achieved which enforces the computation to blow up. The significant difference between these two time intervals is that at  $\Delta t = 0.002$ , the appearance of instability occurs at low times  $t$ , while for the smaller time interval the start point of instability is postponed till  $t = 2$ .

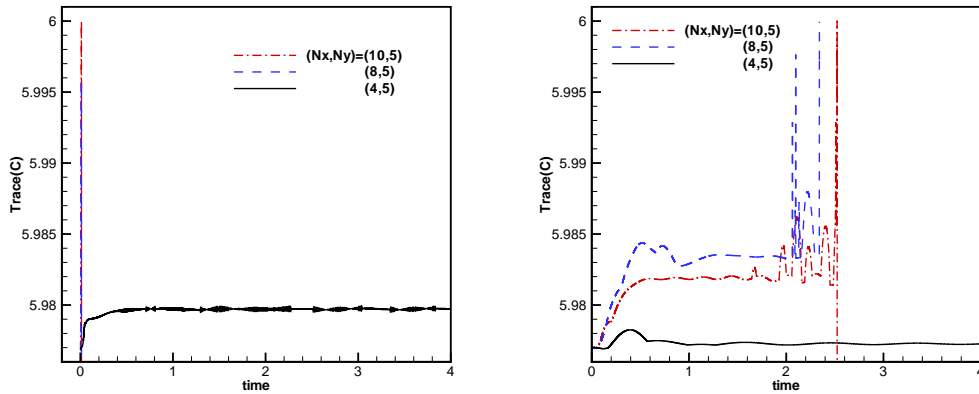


Fig. 7.21: Influence of mesh refinement on the maximum of  $tr(C)$ ,  $(NE_x, NE_y) = (4, 2)$ ,  $We = 100$ , natural outflow boundary condition, Left)  $\Delta t = 0.002$ , right)  $\Delta t = 0.0002$

Figure 7.22 shows the effect of mesh refinement by increasing the polynomial degree in cross-wise direction at  $We = 100$  and  $(4 \times 2)$  element in stream and cross-wise direction respectively. Increasing the polynomial degree in cross-wise direction produces large oscillations during the computation at  $\Delta t = 0.002$  while at  $\Delta t = 0.0002$  increasing the polynomial degree does not have any significant effect.

The last two test cases are devoted to the examination of mesh refinement by increasing the the number of elements in stream and cross-wise direction at  $We = 100$ . Fig. 7.23 represents the effect of mesh refinement on trace of conformation tensor by increasing the number of element in stream-wise direction with  $(4 \times 10)$  polynomial degree respectively

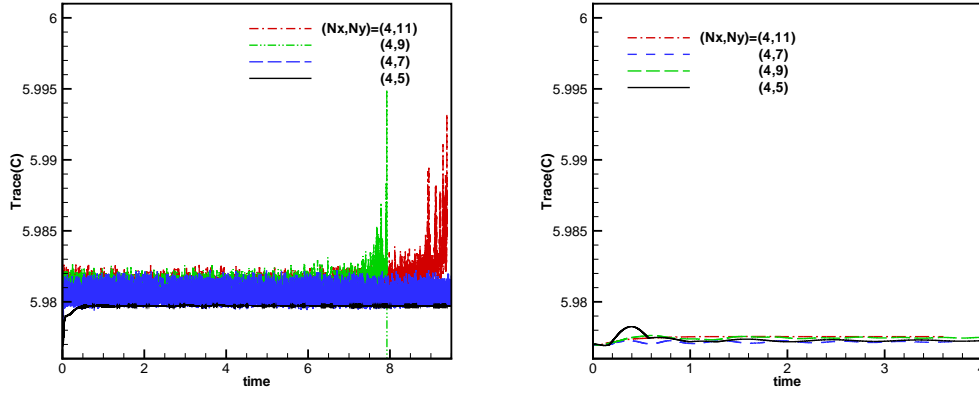


Fig. 7.22: Influence of mesh refinement on the maximum of  $tr(C)$ ,  $(NE_x, NE_y) = (4, 2)$ ,  $We = 100$ , natural outflow boundary condition, Left)  $\Delta t = 0.002$ , right)  $\Delta t = 0.0002$

in the stream and cross-wise directions. In the cross-wise direction, we chose a large value of polynomial degree to ensure acceptable refined mesh in this direction. In this test case, as before increasing the number of element increases the maximum value of the trace of the conformation tensor as well as magnitude of the oscillation during the simulation. At small values of time interval, the instability appears later. Fig. 7.24 shows the effect of

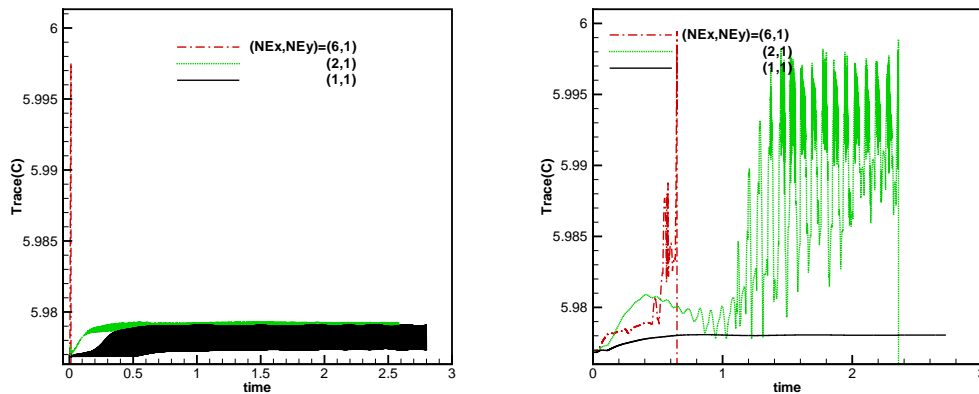


Fig. 7.23: Influence of mesh refinement on the maximum of  $tr(C)$ ,  $(N_x, N_y) = (4, 10)$ ,  $We = 100$ , natural outflow boundary condition, Left)  $\Delta t = 0.002$ , right)  $\Delta t = 0.0002$

mesh refinement by increasing the number of elements in cross-wise direction by  $(10 \times 5)$

polynomial degree in stream and cross-wise direction. A polynomial degree equal to 10 in the stream-wise direction is selected in order to obtain an enough refined mesh in this direction. The great difference between this figure and the previous ones is that increasing the number of element in cross-wise direction, stabilizes the simulation and decreases the oscillation of maximum trace of conformation tensor during time evolution. Moreover, smaller time interval improves the behavior of the results with time evolution.

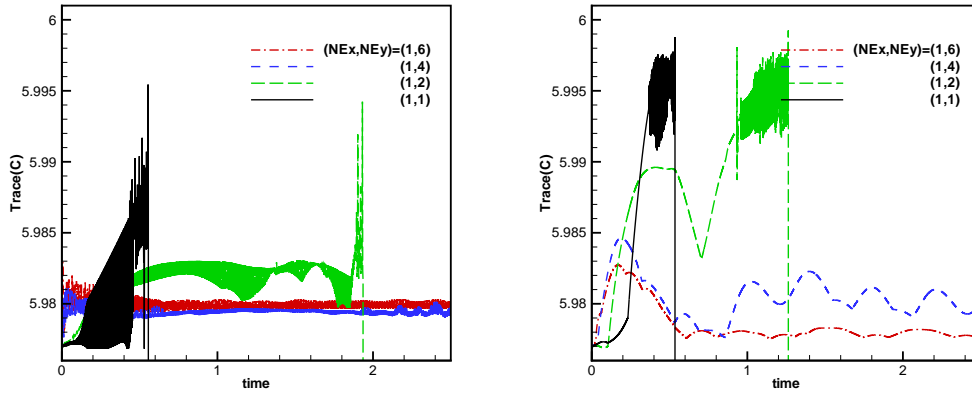


Fig. 7.24: Influence of mesh refinement on the maximum of  $tr(C)$ ,  $(N_x, N_y) = (10, 5)$ ,  $We = 100$ , natural outflow boundary condition, Left)  $\Delta t = 0.002$ , right)  $\Delta t = 0.0002$

## 7.6 Conclusion

In this study to understand more deeply the mechanism of numerical instability generation in the simulation of flows of FENE-P family, a comprehensive study about the growth of spurious modes with time evolution, Weissenberg number, mesh refinement, finite extensibility parameter and outflow boundary condition was undertaken using a modal basis representation. Increasing the Weissenberg number usually leads to the manifestation of numerical instabilities in simulation of viscoelastic fluid flows. For multi-element decomposition, the instability first appears in elements in outflow region and propagates very fast upstream. Mesh refinement enhances the growth of spurious modes in the domain. This is the reason why refining the mesh proved to be not helpful for computing viscoelastic flows. Increasing the finite extensibility parameter enhances magnitude of dangerous

modes and causes simulation crashes. The effect of outflow boundary condition reveals that the instability is highly sensitive to its type. Applying velocity Dirichlet boundary at outflow as opposed to natural boundary condition was found better in terms of convergence and stabilization. Imposing condition of the latter type at outflow governs the system not only by the state in the interior of the region, but also by the information brought by incoming characteristics which enter the region. Probably this is the reason why applying outflow natural boundary induces first the generation of instability in the outflow region.

The capability of filter-based-stabilization technique proposed by Boyd [32] has been examined. However, this filter is capable to suppress the high frequency modes but there are still some nascent instabilities which grow by mesh refinement, therefore applying a filter-based technique can not treat the instability problem completely. We also observed that the performance of filter-based stabilization technique is very useful to eliminate spurious modes for one element decomposition, while in the case of multi-element configuration the performance of this technique is not ideal. Regarding this fact, a new way of implementation, using the so called mesh-transfer technique is used. This way of implementing filtering is very useful for Oldroyd-B when a moderate number of grid points is used.

In the last part of this study, we showed that however preserving the symmetric positive definiteness of the conformation tensor and bounding the trace of the conformation tensor less than the finite extensibility parameter, helps to obtain stable computation but another problem that can easily appear is that the attained value of trace of conformation tensor tends to the corresponding bounded value related to the finite extensibility. Due to the presence of the term  $1 - tr(C)/b^2$  in the denominator of the viscoelastic stress formulation of FENE-P, tends to zero, this causes unbounded growth of the viscoelastic stress, which does not have any physical meaning. Indeed, by the smallest oscillation of the trace of the conformation tensor, the value of viscoelastic stress grows unbounded which is the worst condition of the simulation of viscoelastic fluids. Mesh refinement in stream-wise direction by increasing both polynomial degree or number of element, increases the maximum value of the trace of the conformation tensor which makes the simulation to reach the dangerous zone and finally unbounded instability is generated. Mesh refinement in cross-wise direction by increasing the polynomial degree has the same effect, while mesh refinement in cross-wise direction by increasing the number of element has the opposite behavior. The



---

great difference is that increasing the number of elements in cross-wise direction, stabilizes the simulation and decreases the oscillation of the maximum trace of conformation tensor with time evolution. Moreover, smaller time interval improves the behavior of the results with time evolution. Regarding the transformation suggested by Fattal et al. [70, 221], symmetric positive definiteness (SPD) is preserved during the simulation but overflow and underflow numerical errors happen when the classical conformation tensor is reconstructed from exponential formulation with either infinite positive eigenvalue or infinite negative eigenvalue using the logarithm formulation. So development of mathematical models to preserve both SPD of the conformation tensor and bound magnitude of eigenvalues when reconstructing the classical formulation is mandatory. Such an investigation is underway.

Employing this mesh transfer filtering technique for complex geometry such as 2-D contraction flow is our interest for future works. Moreover, according to this fact that the main reason of instabilities in simulation of time dependent Poiseuille flow is the reflection of outgoing wave from outflow region, the 2-D spatial discretization using spectral element in cross-wise direction coupled with Fourier expansion in periodic stream-wise direction, seems to be a viable way of handling the test case.



# Chapter 8

---

## Summary and conclusion

The description of the outcomes and summary of this work follow the structure of the dissertation. The details below are gathered from the multiple conclusions presented at the end of each chapter.

### 8.1 General summary

From numerical point of view for calculation of complex fluids, differential constitutive equations for the stress tensor are generally preferred over those of the integral type. Among differential constitutive models FENE-P due to its features is chosen for this study. Oldroyd-B is also considered as a limit case of the FENE-P model when the finite extensibility tends to infinity.

A spectral element method with a high-order time discretization scheme has been selected since time-dependent accurate solutions are expected. In addition, non-dissipative and non-dispersive properties are required if one expects to observe transient or periodic phenomena like physical instabilities.

The key issue of the simulation of the viscoelastic fluids is that the eigenvalues of the conformation tensor should remain positive at all steps of the simulation. Negative eigenvalues cause the unbounded growth of instabilities in the flow. Fattal and Kupferman [69] proposed to reformulate the classical constitutive equation using a new variable namely the logarithmic formulation. This transformation enforces the eigenvalues of the conformation tensor to remain positive for all steps of the simulation. However, satisfying the symmetric positive definiteness (SPD) of the conformation tensor during the simulation is the necessary condition for stability, but definitely, it is not the sufficient condition to reach meaningful results. Another distinct constraint for the FENE-P equation is that

the square of the corresponding finite extensibility parameter of the polymer must be an upper limit for the trace of the conformation tensor. To mathematically satisfy these two conditions, we introduce a new method based on the transformation of the classical constitutive equation. In the first stage, we transform the classical constitutive equation based on the conformation tensor,  $\mathbf{C}$ , to a new one based on the tensor  $\mathbf{J}$ , which bounds the maximum value of the trace of the conformation tensor. In the second stage, we transform the tensor  $\mathbf{J}$  to a so called matrix logarithm conformation tensor  $\mathbf{H}$ , based on the idea proposed by Fattal and Kupferman in order to obtain positive eigenvalues for the  $\mathbf{J}$  and  $\mathbf{C}$  conformation tensors.

First, the ability of time dependent simulation of the classical matrix logarithm without considering the extended algorithm has been tested on a simple unsteady FENE-P Poiseuille flow. One of the possible manifestation of HWNP is the failure of polynomial-based approximation to properly represent the exponential profiles. In this stage, the influence of each differential terms in the constitutive equation for both log and classical representation has been investigated. For classical representation the manifestation of instability is inside the deformation term, while the source of instability for the matrix logarithm formulation is simultaneously inside the nonlinear term including convection and source terms. The effect of outflow boundary condition reveals that the instability is highly sensitive to the boundary condition. According to the concept of hyperbolic equation, imposing a Dirichlet boundary condition for viscoelastic stress at outflow has no physical meaning. However, this type of boundary condition was found slightly better in term of convergence. For the discretization used in this study the reachable Weissenberg number by imposing the velocity Dirichlet boundary condition at outflow is 56. Stable simulations at higher Weissenberg number could be achieved for outflow velocity Dirichlet boundary condition, than for natural boundary condition. In both cases, a numerical instability has been observed near the downstream boundary when the Weissenberg number approached same critical value. Another surprising result is that using the classical matrix logarithm formulation instead of the classical one in the context of spectral elements at least for FENE-P does not help to simulate high Weissenberg number flows. This is clearly different from what has been observed with low-order finite elements, Hulsen et al. [102], and Kwon [120], and finite volumes, Afonso et al. [4].

The capability of extended matrix logarithm formulation to predict the flow pattern for

complex geometries such as contraction and contraction-expansion was examined. At low values of the Weissenberg number, the convergence rate of the simulation is very fast and the accuracy of the numerical simulation is very high. In contrast increasing the Weissenberg number increases the relative error exponentially which prevents the successful numerical simulation. The velocity and viscoelastic-stress overshoot downstream of the entry corner increase with increasing the Weissenberg number. The highest elasticity takes more time to reach to the fully developed condition after over or under shooting. So it necessitates a longer channel length after entry flow. The maximum attainable Weissenberg number by EMLF is 10 while this value for classical formulation is 8. Mesh refinement experience at critical values of the Weissenberg number does not improve nor increase the accuracy. Increasing the Weissenberg number also increases vortex intensity as measured based on the maximum value of stream function and also augments the instability close to the re-entrant corner which propagates to the upstream direction. In this study no lip vortex was detected which is due to the considered contraction ratio 4:1. We found that employing round or sharp corner does not have very important improvement to tackle the high Weissenberg number problem. The maximum attainable Weissenberg number for both round and sharp re-entrant corner are the same and equal to  $We = 10$ . The flow patterns in contraction-extension geometry are similar to those obtained by contraction flow. The significant difference is that the corner vortex in the second entry is smaller than the first corner.

We comprehensively studied the improvement of this new algorithm on the eigenspectrum with linear stability analysis. It shows that element decomposition is one of the main source of instability in the spectral element context. On the other hand, the comparison of results obtained with the single element and multi-element configuration shows that the more dangerous eigenmodes are related to the multi-element composition. This means that, the positive real eigenvalues for the single element decomposition have smaller magnitude than for the multi-element decomposition. Moreover, increasing the Weissenberg number distributes the eigenvalues in the right-hand half plane with large magnitude of positive real parts. This can be one of the reason of instability of numerical simulation. In spite of this, the new extended algorithm enables one to obtain stable simulation of viscoelastic flows at Weissenberg number with values of practical interest i.e. larger than 100 for this specific mesh.

To understand more deeply the mechanisms of numerical instability generation in the simulation of flows of FENE-P family, a comprehensive study about the growth of spurious modes with time evolution, Weissenberg number, mesh refinement, finite extensibility parameter and outflow boundary condition was undertaken using a modal basis representation. Increasing the Weissenberg number usually leads to the manifestation of numerical instabilities in simulation of viscoelastic fluid flows. For multi-element decomposition, the instability first appears in elements near the outflow region and propagates very fast upstream. Mesh refinement enhances the growth of spurious modes in the domain. This is the reason why refining the mesh proved to be not helpful for computing viscoelastic flows. Increasing the finite extensibility parameter enhances magnitude of dangerous modes and causes simulation crashes. The effect of outflow boundary condition reveals that the instability is highly sensitive to its type. Applying velocity Dirichlet boundary at outflow as opposed to natural boundary condition was found better in terms of convergence and stabilization. Imposing condition of the latter type at outflow governs the system not only by the state in the interior of the region, but also by the information brought by incoming characteristics which enter the region. Probably this is the reason why applying outflow natural boundary induces first the generation of instability in the outflow region.

The capability of filter-based-stabilization technique proposed by Boyd has been examined. However, this filter is capable to suppress the high frequency modes but there are still some nascent instabilities which grow by mesh refinement. Therefore applying a filter-based technique can not treat the instability problem completely. We also observed that the performance of filter-based stabilization technique is very useful to eliminate spurious modes for one element decomposition, while in the case of multi-element configuration the performance of this technique is not ideal. Regarding this fact, a new way of implementation, using the so called mesh-transfer technique is used. This way of implementing filtering is very useful for Oldroyd-B when a moderate number of grid points is used.

In the last part of this study, we showed that however preserving the symmetric positive definiteness of the conformation tensor and bounding the trace of the conformation tensor less than the finite extensibility parameter, helps to obtain stable computation. However, another problem that can easily appear is that the attained value of trace of conformation tensor tends to the bounded value of finite extensibility parameters. Due to the presence of the term  $1 - \text{tr}(C)/b^2$  in the denominator of the viscoelastic stress formu-

lation of FENE-P, goes to zero, this causes unbounded growth of the viscoelastic stress, which does not have any physical meaning. Indeed, by the smallest oscillation of the trace of the conformation, the value of viscoelastic stress grows unbounded which is the worst condition of the simulation of viscoelastic fluids. Mesh refinement in stream-wise direction by increasing both polynomial degree or number of element, increases the maximum value of the trace of the conformation tensor which makes the simulation to reach the dangerous zone and finally unbounded instability is generated. Mesh refinement in cross-wise direction by increasing the polynomial degree has the same effect, while mesh refinement in cross-wise direction by increasing the number of element has the opposite behavior. The great difference is that increasing the number of elements in cross-wise direction, stabilizes the simulation and decreases the oscillation of the maximum trace of conformation tensor with time evolution.

## 8.2 Outlook and perspectives

The most straight forward extensions to this work would be as the following domains:

One of the key problems in viscoelastic flows is the influence of the boundary conditions, which may induce numerical instabilities if not well suited. Adopting periodic boundary conditions in stream-wise direction and resort to spectral elements-Fourier discretization seems to be helpful. With periodic boundary condition in stream-wise direction, virtually, there is no boundary at inlet and outlet section. So one does not need to worry about the inlet and outlet interaction. It will help understanding the mechanisms of intrinsic instability of the some viscoelastic models like the Oldroyd-B, FENE-P. The key idea, therefore, is to employ spectral element discretization in cross-wise direction and Fourier expansion along stream-wise direction. Spectral element-Fourier discretisations are well suited to direct numerical simulation of flows where the geometry exhibits arbitrary complexity in a sectional plane but is infinite or periodic in an orthogonal direction.

According to our knowledge and the know-how acquired during this thesis, the instability problems of viscoelastic fluids are more relevant to dissatisfaction of mathematical characteristic of viscoelastic fluids. We heavily propose a comprehensive study of mathematical meaning of constitutive equations and employing methods which preserve the

mathematical concepts of constitutive equations.

Another important issue is to extend the method for the closure of the approximation to a general 3-dimensional basis which would enable a better modelling of the logarithm formulation.

Along the work having done by Habisreutinger [96], employing the grid filter model for simulation of viscoelastic fluids is our interest for future works.



# Appendix A

---

## Appendix A

Any symmetric positive definite matrix can be diagonalized as:

$$\mathbf{C} = \mathbf{Q} \begin{pmatrix} e^{h_1} & 0 & 0 \\ 0 & e^{h_2} & 0 \\ 0 & 0 & e^{h_3} \end{pmatrix} \mathbf{Q}^T \quad (\text{A-1})$$

where  $\mathbf{Q}$  is the orthogonal matrix containing the eigenvector  $n_i$  as its column vectors. In the 2D configuration  $\mathbf{C}$  is defined as:

$$\mathbf{C} = \begin{pmatrix} C_{11} & C_{12} \\ C_{12} & C_{22} \end{pmatrix} = \begin{pmatrix} n_1^2 e^{h_1} + n_2^2 e^{h_2} & n_1 n_2 (e^{h_1} - e^{h_2}) \\ n_1 n_2 (e^{h_1} - e^{h_2}) & n_2^2 e^{h_1} + n_1^2 e^{h_2} \end{pmatrix} \quad (\text{A-2})$$

If one inserts Eq. (A-2) into Eq. (3.5) the following equation for  $\dot{\mathbf{C}}$  can be easily obtained in the framework of the FENE-P model.

$$\begin{aligned} \dot{\mathbf{C}} = & \begin{pmatrix} 2C_{11} \frac{\partial u_1}{\partial x_1} + 2C_{12} \frac{\partial u_1}{\partial x_2} & C_{11} \frac{\partial u_2}{\partial x_1} + C_{22} \frac{\partial u_1}{\partial x_2} \\ C_{11} \frac{\partial u_2}{\partial x_1} + C_{22} \frac{\partial u_1}{\partial x_2} & 2C_{22} \frac{\partial u_2}{\partial x_2} + 2C_{12} \frac{\partial u_2}{\partial x_1} \end{pmatrix} \\ & - \frac{1}{We} \frac{1}{1 - \frac{C_{11} + C_{22}}{Le^2}} \begin{pmatrix} C_{11} - \frac{1 - \frac{C_{11} + C_{22}}{Le^2}}{K} & C_{12} \\ C_{12} & C_{22} - \frac{1 - \frac{C_{11} + C_{22}}{Le^2}}{K} \end{pmatrix} \end{aligned} \quad (\text{A-3})$$



# Bibliography

---

- [1] ABOUBACAR, M., MATALLAH, H., AND WEBSTER, M. Highly elastic solutions for Oldroyd-B and Phan-Thien/Tanner fluids with a finite volume/element method: Planar contraction flows. *J. Non-Newtonian Fluid Mech.* 103, 1 (2002), 65–103.
- [2] ABOUBACAR, M., PHILLIPS, T., TAMADDON-JAHROMI, H.R., S., AND B.A., WEBSTER, M. High-order finite volume methods for viscoelastic flow problems. *J. Comput. Phys.* 199, 1 (2004), 16–40.
- [3] ABOUBACAR, M., AND WEBSTER, M. A cell-vertex finite volume/element method on triangles for abrupt contraction viscoelastic flows. *J. Non-Newtonian Fluid Mech.* 98, 2-3 (2001), 83–106.
- [4] AFONSO, A., OLIVEIRA, P. J., PINHO, F. T., AND ALVES, M. A. The log-conformation tensor approach in the finite-volume method framework. *J. Non-Newtonian Fluid Mech.* 157 (2009), 55–65.
- [5] AGUAYO, J., PHILLIPS, P., PHILLIPS, T., TAMADDON-JAHROMI, H., SNIGEREV, B., AND WEBSTER, M. The numerical prediction of planar viscoelastic contraction flows using the pom-pom model and higher-order finite volume schemes. *J. Comput. Phys.* 220, 2 (2007), 586–611.
- [6] AKSEL, N. A brief note from the editor on the "second-order fluid". *Acta Mech.* 157, 1-4 (2002), 235–236.
- [7] AL-BAALI, M., AND FLETCHER, R. Variational method for non-linear least square. *J. Opt. Res. Soc.* 36 (1985), 405–421.
- [8] AL MOATASSIME, H., AND ESSELAOUI, D. A finite volume approach for unsteady viscoelastic fluid flows. *Int. J. Numer. Meth. Fluids* 39, 10 (2002), 939–959.
- [9] AL MOATSSIME, H., ESSELAOUI, D., HAKIM, A., AND RAGHAY, S. Finite volume multigrid method of the planar contraction flow of a viscoelastic fluid. *Int. J. Numer. Meth. Fluids* 36, 8 (2001), 885–902.

- 
- [10] AL MOATSSIME, H., ESSELAOUI, D., HAKIM, A., AND RAGHAY, S. Finite volume multigrid method of the planar contraction flow of a viscoelastic fluid. *International Journal for Numerical Methods in Fluids* 36, 8 (2001), 885–902.
- [11] ALVES, M., OLIVEIRA, P., AND PINHO, F. Benchmark solutions for the flow of Oldroyd-B and PTT fluids in planar contractions. *J. Non-Newt. Fluid Mech.* 110, 1 (2003), 45–75.
- [12] ALVES, M., OLIVEIRA, P., AND PINHO, F. On the effect of contraction ratio in viscoelastic flow through abrupt contractions. *J. Non-Newt. Fluid Mech.* 122, 1-3 (2004), 117–130.
- [13] ALVES, M., PINHO, F., AND OLIVEIRA, P. Effect of a high-resolution differencing scheme on finite-volume predictions of viscoelastic flows. *J. Non-Newt. Fluid Mech.* 93, 2-3 (2000), 287–314.
- [14] ALVES, M., AND POOLE, R. Divergent flow in contractions. *J. Non-Newt. Fluid Mech.* 144, 2-3 (2007), 140–148.
- [15] ANDERSON, E., BAI, Z., BISCHOF, C., BLACKFORD, S., DEMMEL, J., DONGARRA, J., CROZ, J. D., GREENBAUM, A., HAMMARLING, S., MCKENNEY, A., AND SORENSEN, D. *LAPACK User's guide*. SIAM Philadelphia, 1999.
- [16] ANTURKAR, N., PAPANASTASIOU, T., AND WILKES, J. Linear stability analysis of multilayer plane Poiseuille flow. *Phys. Fluids A* 2, 4 (1990), 530–541.
- [17] ARIEL, P. A new finite-difference algorithm for computing the boundary layer flow of viscoelastic fluids in hydromagnetics. *Comput. Method. Appl. M.* 124, 1-2 (1995), 1–13.
- [18] ASVADUROV, S., KNIZHNERMAN, L., AND PABON, J. Finite-difference modeling of viscoelastic materials with quality factors of arbitrary magnitude. *Geophys.* 69, 3 (2004), 817–824.
- [19] ATALIK, K., AND KEUNINGS, R. Non-linear temporal stability analysis of viscoelastic plane channel flows using a fully-spectral method. *J. Non-Newt. Fluid Mech.* 102, 2 (2002), 299–319.

- 
- [20] AVGOUSTI, M., LIU, B., AND BERIS, A. N. Spectral methods for the viscoelastic time-dependent flow equations with applications to Taylor-Couette flow. *Int. J. Numer. Meth. Fluids* 17, 1 (1993), 49–74.
- [21] AZAIEZ, J., GUÉNETTE, R., AND AÏT-KADI, A. Numerical simulation of viscoelastic flows through a planar contraction. *J. Non-Newton. Fluid Mech.* 62, 2-3 (1996), 253–277.
- [22] BAAIJENS, F. Mixed finite element methods for viscoelastic flow analysis: A review. *J. Non-Newton. Fluid Mech.* 79, 2-3 (1998), 361–385.
- [23] BERIS, A., AVGOUSTI, M., AND SOUVALIOTIS, A. Spectral calculations of viscoelastic flows: evaluation of the Giesekus constitutive equation in model flow problems. *J. Non-Newton. Fluid Mech.* 44, C (1992), 197–228.
- [24] BERNSTEIN, B., KEARSLEY, E. A., AND ZAPAS, L. J. An equation of state for non-Newtonian fluids. *Trans. Soc. Rheol.* 7 (1963), 391–410.
- [25] BIRD, R., AND WIEST, J. Constitutive equations for polymeric liquids. *Annu. Rev. Fluid Mech.* 27, 1 (1995), 169–193.
- [26] BIRD, R. B., ARMSTRONG, R. C., AND HASSAGER, O. *Dynamics of polymeric liquids*, vol. 1. Wiley, New York, 1987.
- [27] BODARD, N. *Interaction fluide-structure par la méthode des éléments spectraux*. PhD thesis, École Polytechnique Fédérale de Lausanne, 2006. no. 3503.
- [28] BOGER, D. Viscoelastic flows through contractions. *Ann. Review Fluid Mech.* 19 (1987), 157–182.
- [29] BOGER, D., AND WALTERS, K. *Rheological phenomena in focus*. Elsevier, Amsterdam, 1993.
- [30] BOUFFANAIS, R. *Simulation of shear-driven flows : transition with a free surface and confined turbulence*. PhD thesis, Ecole Polytechnique Fédérale de Lausanne, no. 3837, 2007.
- [31] BOUFFANAIS, R., AND DEVILLE, M. O. Mesh update techniques for free-surface flow solvers using spectral element method. *Journal of Scientific Computing* 27, 1-3 (2006), 137–149.

- 
- [32] BOYD, J. P. Two comments on filtering (artificial viscosity) for Chebyshev and Legendre spectral and spectral element methods: preserving boundary conditions and interpretation of the filter as a diffusion. *J. Comput. Phys.* *143*, 1 (1998), 283–288.
- [33] BROOKS, A. N., AND HUGHES, T. J. R. Streamline upwind Petrov-Galerkin formulations for convection dominated flows with particular emphasis on the incompressible Navier-Stokes equations. *Comput. Meth. Appl. Mech. Engrg.* *32* (1982), 199–259.
- [34] BUGGISCH, H., AND AKSEL, N. An exact solutions of a viscoelastic Ekman layer with suction. *J. Non-Newt. Fluid Mech.* *36*, C (1990), 351–359.
- [35] CANUTO, C., HUSSAINI, M. Y., QUARTERONI, A., AND ZANG, T. A. *J. Spectral Methods in Fluid Dynamics*. Springer-Verlag, Berlin, 1988.
- [36] CANUTO, C., RUSSO, A., AND VAN KEMENADE, V. Stabilized spectral methods for the Navier-Stokes equations: residual-free bubbles and preconditioning. *Comput. Meth. Appl. Mech. Engrg.* *166* (1998), 65–83.
- [37] CARNEIRO DE ARAUJO, J., GOMES, P., AND RUAS, V. Study of a finite element method for the time-dependent generalized Stokes system associated with viscoelastic flow. *J. Comput. Appl. Math.* (2010).
- [38] CHANDIO, M., SUJATHA, K., AND WEBSTER, M. Consistent hybrid finite volume/element formulations: Model and complex viscoelastic flows. *Int. J. Numer. Meth. Fluids* *45*, 9 (2004), 945–971.
- [39] CHAUVIÈRE, C., AND OWENS, R. A new spectral element method for the reliable computation of viscoelastic flow. *Comput. Methods Appl. Mech.* *190*, 31 (2001), 3999–4018.
- [40] CHAUVIÈRE, C., AND OWENS, R. A robust spectral element method for simulations of time-dependent viscoelastic flows, derived from the Brownian configuration field method. *J. Sci. Comput.* *17*, 1-4 (2002), 191–199.
- [41] CHAUVIÈRE, C., AND OWENS, R. G. How accurate is your solution? error indicators for viscoelastic flow calculations. *J. Non-Newt. Fluid Mech.* *95* (2000), 1–33.

- [42] CHAUVIÈRE, C., AND OWENS, R. G. Wiggle-free spectral element methods for non-Newtonian flows. In *Proceedings of the 16th IMACS World Congress* (Lausanne, Switzerland, 2000), M. Deville and R. G. Owens eds.
- [43] CHAUVIÈRE, C., AND OWENS, R. G. A new spectral element method for the reliable computation of viscoelastic flow. *Comput. Meth. Appl. Mech. Engrg.* 190 (2001), 3999–4018.
- [44] CHEN, T., COX, C., LEE, H., AND TUNG, K. Least-squares finite element methods for generalized Newtonian and viscoelastic flows. *Appl. Numer. Math.* (2010).
- [45] CHEON CHOI, H., HO SONG, J., AND YUL YOO, J. Numerical simulation of the planar contraction flow of a Giesekus fluid. *J. Non-Newt. Fluid Mech.* 29, C (1988), 347–379.
- [46] CHILCOTT, M. D., AND RALLISON, J. Creeping flow of dilute polymer solutions past cylinders and spheres. *J. Non-Newt. Fluid Mech.* 29, 1-3 (1988), 381–432.
- [47] CHOI, Y., HULSEN, M., AND MEIJER, H. An extended finite element method for the simulation of particulate viscoelastic flows. *J. Non-Newt. Fluid Mech.* 165, 11-12 (2010), 607–624.
- [48] CHOW, S.-S., AND CAREY, G. Numerical approximation of generalized Newtonian fluids using Powell-Sabin-Heindl elements: I. theoretical estimates. *Int. J. Numer. Meth. Fl.* 41, 10 (2003), 1085–1118.
- [49] CLEMEUR, N., RUTGERS, R., AND DEBBAUT, B. Numerical simulation of abrupt contraction flows using the Double Convected Pom-Pom model. *J. Non-Newt. Fluid Mech.* 117, 2-3 (2004), 193–209.
- [50] COLEMAN, B., AND NOLL, W. An approximation theorem for functionals, with applications in continuum mechanics. *Arch. Ration. Mech.An.* 6, 1 (1960), 355–370.
- [51] CORONADO, O. M., ARORA, D., BEHR, M., AND PASQUALI, M. A simple method for simulating general viscoelastic fluid flow with an alternate log conformation formulation. *J. Non-Newt. Fluid Mech.* 147 (2007), 189–199.
- [52] COUZY, W. *Spectral element discretization of the unsteady Navier-Stokes equations and its iterative solution on parallel computers*. PhD thesis, École Polytechnique Fédérale de Lausanne, 1995. no. 1380.

- 
- [53] COUZY, W., AND DEVILLE, M. Spectral-element preconditioners for the Uzawa pressure operator applied to incompressible flows. *J. Sci. Comput.* 9, 2 (1994), 107–122.
- [54] CRIMINALE, W. O., ERICKSEN, J. L., AND FILBEY, G. L. Steady shear flow of non-Newtonian fluids. *Arch. Ration. Mech.An.* 1 (1958), 410–417.
- [55] CROCHET, M. J., DAVIES, A., AND WALTERS, K. *Numerical simulation of non-Newtonian flow*. Elsevier, Amsterdam, 1984.
- [56] CROSS, M. M. Rheology of non-Newtonian fluids: A new flow equation for pseudo-plastic systems. *J. Colloid Sci.* 20 (1965), 417–437.
- [57] CURRIE, P. Calculation on the Doi-Edwards model for concentrated polymer systems. *Plas. in Med. Surg.* 1 (1980), 357–362.
- [58] DEALY, J. M., AND LARSON, R. G. *Structure and Rheology of Molten Polymers*. Clarendon Press, Oxford, 1986.
- [59] DEMIR, H. Numerical modelling of viscoelastic cavity driven flow using finite difference simulations. *Appl. Math. Comput.* 166, 1 (2005), 64–83.
- [60] DEVILLE, M., FISCHER, P., AND MUND, E. *High-order methods for incompressible fluid flow*. Cambridge University Press, Cambridge, 2002.
- [61] DOI, M., AND EDWARDS, S. Dynamics of concentrated polymer systems. part 1. Brownian motion in equilibrium state. *J. Chem. Soc. Faraday Trans.* 74 (1978), 1789–1801.
- [62] DOI, M., AND EDWARDS, S. Dynamics of concentrated polymer systems. part 2. molecular-motion under flow. *J. Chem. Soc. Faraday Trans.* 74 (1978), 1802–1817.
- [63] DOI, M., AND EDWARDS, S. Dynamics of concentrated polymer systems. part 3. constitutive equation. *J. Chem. Soc. Faraday Trans.* 74 (1978), 1818–1832.
- [64] DOI, M., AND EDWARDS, S. Dynamics of concentrated polymer systems. part 4. rheological properties. *J. Chem. Soc. Faraday Trans.* 75 (1979), 38–54.
- [65] DOI, M., AND EDWARDS, S. *The theory of polymer dynamics*. Clarendon Press, Oxford, 1986.



- [66] DUBOIS-PELERIN, Y., VAN KEMENADE, V., AND DEVILLE, M. O. An object-oriented toolbox for spectral element analysis. *J. Sci. Comput.* 14 (1999), 1–29. <http://sourceforge.net/projects/openspeculoos/develop>.
- [67] EDUSSURIYA, S., WILLIAMS, A., AND BAILEY, C. A cell-centred finite volume method for modelling viscoelastic flow. *J. Non-Newt Fluid Mech.* 117, 1 (2004), 47–61.
- [68] FAN, Y., TANNER, R. I., AND PHAN-THIEN, N. Galerkin/least-square finite-element methods for steady viscoelastic flows. *J. Non-Newt. Fluid Mech* 84, 2-3 (1999), 233–256.
- [69] FATTAL, R., AND KUPFERMAN, R. Constitutive laws for the matrix-logarithm of the conformation tensor. *J. Non-Newt. Fluid Mech.* 123 (2004), 281–285.
- [70] FATTAL, R., AND KUPFERMAN, R. Time-dependent simulation of viscoelastic flow at high Weissenberg number using the log-conformation representation. *J. Non-Newt. Fluid Mech.* 126 (2005), 23–37.
- [71] FIÉTIER, N. *Numerical simulation of viscoelastic fluid flows by spectral element methods and time dependent algorithms*. PhD thesis, École Polytechnique Fédérale de Lausanne, 2002. no. 2631.
- [72] FIÉTIER, N., AND DEVILLE, M. Simulations of time-dependent flows of viscoelastic fluids with spectral element methods. *J. Sci. Comput.* 17, 1-4 (2002), 649–657.
- [73] FIÉTIER, N., AND DEVILLE, M. O. Linear stability analysis of time-dependent algorithms with spectral element methods for the simulation of viscoelastic fluids. *J. Non-Newt. Fluid Mech.* 115 (2003), 157–190.
- [74] FIÉTIER, N., AND DEVILLE, M. O. Time dependent algorithms for simulation of viscoelastic flows with spectral element methods: applications and stability. *J. Comput. Phys.* 186 (2003), 93–121.
- [75] FISCHER, P., AND MULLEN, J. Filter-based stabilization of spectral element methods. *C. R. Acad. Sci. Paris* 332 (2001), 265–270.
- [76] FISCHER, P. F., KRUSE, G. W., AND LOTH, F. Spectral element methods for transitional flows in complex geometries. *J. Sci. Comput.* 17, 1 (2002), 81–98.

- [77] FORTIN, M., AND FORTIN, A. A new approach for the fem simulation of viscoelastic flows. *J. Non-Newt. Fluid Mech* 32, 295-310 (1989).
- [78] FRANCA, L. P., AND STENBERG, R. Error analysis of some Galerkin least squares methods for the elasticity equations. *SIAM J. Numer. Anal.* 28, 6 (1991), 1680–1697.
- [79] FRANK, X., AND LI, H. Negative wake behind a sphere rising in viscoelastic fluids: A lattice Boltzmann investigation. *Phys. Rev. E: Stat., Nonlinear, Soft Matter Phys.* 74, 5 (2006).
- [80] FU, C.-Q., JIANG, H.-M., YIN, H.-J., SU, Y.-C., AND ZENG, Y.-M. Finite volume method for simulation of viscoelastic flow through a expansion channel. *J. Hydrodyn.* 21, 3 (2009), 360–365.
- [81] FUNARO, D. A new scheme for the approximation of advection-diffusion equations by collocation. *SIAM Journal on Numerical Analysis* 30, 6 (1993), 1664–1676.
- [82] GANVIR, V., LELE, A., THAOKAR, R., AND GAUTHAM, B. Simulation of viscoelastic flows of polymer solutions in abrupt contractions using an arbitrary Lagrangian Eulerian (ALE) based finite element method. *J. Non-Newt Fluid Mech.* 143, 2-3 (2007), 157–169.
- [83] GERRITSMAN, M. Direct minimization of the discontinuous least-squares spectral element method for viscoelastic fluids. *J. Sci. Comput.* 27, 1-3 (2006), 245–256.
- [84] GERRITSMAN, M., AND PHILLIPS, T. Discontinuous spectral element approximations for the velocity-pressure-stress formulation of the Stokes problem. *Int. J. Numer. Meth. Eng.* 43, 8 (1998), 1401–1419.
- [85] GERRITSMAN, M., AND PHILLIPS, T. Compatible approximation spaces for the velocity-pressure-stress formulation for creeping flows. *Appl. Numer. Math.* 33, 1 (2000), 225–231.
- [86] GIESEKUS, H. A simple constitutive equation for polymer fluids based on the concept of deformation-dependent tensorial mobility. *J. Non-Newt. Fluid Mech.* 11, 1-2 (1982), 69–109.
- [87] GIESEKUS, H. Constitutive equations for polymer fluids based on the concept of configuration-dependent molecular mobility: a generalized mean-configuration model. *J. Non-Newt. Fluid Mech.* 17, 3 (1985), 349–372.

- [88] GIESEKUS, H. Several comments of the paper "some remarks on useful theorems for the second order fluid" by P.N. Kaloni. *J. Non-Newt. Fluid Mech.* 33, 3 (1989), 343–348.
- [89] GIRAUD, L., D'HUMIÈRES, D., AND LALLEMAND, P. A lattice Boltzmann model for Jeffreys viscoelastic fluid. *Europhys. Lett.* 42, 6 (1998), 625–630.
- [90] GORODTSOV, V. A., AND LEONOV, A. I. On a linear instability of a plane parallel Couette flow of viscoelastic fluid. *J. Appl. Math. Mech.* 31 (1967), 310–319.
- [91] GRILLET, A., BOGAERDS, A., PETERS, G., AND BAAIJENS, F. Stability analysis of constitutive equations for polymer melts in viscometric flows. *J. Non-Newt. Fluid Mech.* 103, 2-3 (2002), 221–250.
- [92] GUDUNOV, S. K. Finite difference method for numerical computation of discontinuous solution of the equations of fluid dynamics. *Math sb.* 47 (1959), 271. Translated from Russian by I. Bohachevsky.
- [93] GUÉNETTE, R., AND FORTIN, M. A new mixed finite element method for computing viscoelastic flows. *J. Non-Newt. Fluid Mech.* 60, 1 (1995), 27–52.
- [94] GWYNLLYW, D., AND PHILLIPS, T. The influence of Oldroyd-B and PTT lubricants on moving journal bearing systems. *J. Non-Newt. Fluid Mech.* 150, 2-3 (2008), 196–210.
- [95] HABETLER, G., AND SCHIFFMAN, R. A finite difference method for analyzing the compression of poro-viscoelastic media. *Comput.* 6, 3-4 (1970), 342–348.
- [96] HABISREUTINGER, M. A. *Grid Filter Models for the Large eddy simulation of fluid flows*. PhD thesis, École Polytechnique Fédérale de Lausanne, 2010.
- [97] HACKLEY, V. A., AND FERRARIS, C. F. *Guide to Rheological Nomenclature: Measurements in Ceramic Particulate Systems*. U.S. Dept. of Commerce, Technology Administration, National Institute of Standards and Technology, Gaithersburg, 2001.
- [98] HAO, J., AND PAN, T.-W. Simulation for high Weissenberg number. Viscoelastic flow by a finite element method. *Appl. Math. Lett.* 20, 9 (2007), 988–993.

- [99] HIRSCH, C. *Numerical Computation of Internal and External Flows*, vol. 2. Wiley Series in Numerical Methods, 1990.
- [100] HOUSIADAS, K. D., AND BERIS, A. An efficient fully implicit spectral scheme for DNS of turbulent viscoelastic channel flow. *J. Non-Newt. Fluid Mech.* 122, 1-3 (2004), 243–262.
- [101] HUILGOL, R. R., AND PHAN-THIEN. *Fluids mechanics of viscoelasticity*. Rheology series 6, Elsevier science B. V., Amsterdam, Netherlands, 1997.
- [102] HULSEN, M., R.FATTAL, AND R.KUPFERMAN. Flow of viscoelastic fluid past a cylinder at high Weissenberg number: stabilized simulation using matrix logarithms. *J. Comput. Phys.* 127 (2005), 27–39.
- [103] ISPOLATOV, I., AND GRANT, M. Lattice Boltzmann method for viscoelastic fluids. *Phys. Rev. E: Stat., Nonlinear, Soft Matter Phys.* 65, 5 (2002), 056704/1–056704/4.
- [104] JAFARI, A., FIÉTIER, N., AND DEVILLE, M. A new extended matrix logarithm formulation for the simulation of viscoelastic fluids by spectral elements. *Comput. Fluids* 39, 9 (2010), 1425–1438.
- [105] JOHNSON, C., NÄVERT, U., AND PITKÄRANTA, J. Finite element methods for linear hyperbolic problems. *Comput. Meth. Appl. Mech. Engrg.* 45, 285-312 (1984).
- [106] JOHNSON, J. M., AND SEGALMAN, D. A model for viscoelastic fluid behavior which allows non-affine deformation. *J. Non-Newt. Fluid Mech.* 2, 3 (1977), 255–270.
- [107] JOSEPH, D., AND SAUT, J. Change of type and loss of evolution in the flow of viscoelastic fluids. *J. Non-Newt. Fluid Mech* 20 (1986), 117–141.
- [108] JOSEPH, D. D. *Fluid dynamics of viscoelastic liquids*. Springer, New York, 1990.
- [109] JOSEPH, D. D., RENARDY, M., AND SAUT, J. C. Hyperbolicity and change of type in the flow of viscoelastic fluids. *Arch. Ration. Mech. Anal* 87 (1985), 213.
- [110] KARNIADAKIS, G., ISRAELI, M., AND ORSZAG, S. High-order splitting methods for the incompressible Navier-Stokes equations. *J. Comput. Phys.* 97, 2 (1991), 414–443.
- [111] KAYE, A. An equation of state for non-Newtonian fluids. *Br. J. Appl. Phys.* 17, 6 (1966), 803–806.

- [112] KEILLER, R. Numerical instability of time-dependent flows. *J. Non-Newt. Fluid Mech.* 43, 2-3 (1992), 229–246.
- [113] KEILLER, R. Spatial decay of steady perturbations of plane Poiseuille flow for the Oldroyd-B equation. *J. Non-Newt. Fluid Mech.* 46, 2-3 (1993), 129–142.
- [114] KHAN, S., AND LARSON, R. Comparison of simple constitutive equations for polymer melts in shear and biaxial and uniaxial extensions. *J. Rheol.* 31, 3 (1987), 207–234.
- [115] KHOMAMI, B., TALWAR, K. K., AND GANPULE, H. K. A comparative study of higher- and lower-order finite element techniques for computation of viscoelastic flows. *J. Rheol.* 38, 2 (1994), 255–289.
- [116] KIM, J., CHUNG, C., AHN, K., AND LEE, S. Time-Weissenberg number superposition in 4:1 planar contraction flow of a viscoelastic fluid. *Nihon Reoroji Gakkaishi* 33, 4 (2005), 191–197.
- [117] KIM, J., KIM, C., KIM, J., CHUNG, C., AHN, K., AND LEE, S. High-resolution finite element simulation of 4:1 planar contraction flow of viscoelastic fluid. *J. Non-Newt. Fluid Mech.* 129, 1 (2005), 23–37.
- [118] KRISTEK, J., AND MOCZO, P. Seismic-wave propagation in viscoelastic media with material discontinuities: A 3D fourth-order staggered-grid finite-difference modeling. *Bull. Seismol. Soc. Am.* 93, 5 (2003), 2273–2280.
- [119] KRÖGER., M. Dumbbell model for dilute and semi-dilute solutions. *Lect. Notes. Phys.* 675, 1 (2005), 13–23.
- [120] KWON, Y. Finite element analysis of planar 4:1 contraction flow with the tensor-logarithmic formulation of differential constitutive equations. *Korea-Australia Rheology J.* 4 (2004), 183–191.
- [121] KWON, Y., KIM, S., AND KIM, S. Finite element modeling of high Deborah number planar contraction flows with rational function interpolation of the Leonov model. *Korea Australia Rheology J.* 15, 3 (2003), 131–150.
- [122] KWON, Y., AND LEONOV, A. Stability constraints in the formulation of viscoelastic constitutive equations. *J. Non-Newt. Fluid Mech.* 58, 1 (1995), 25–46.

- [123] LALLEMAND, P., D'HUMIÈRES, D., LUO, L.-S., AND RUBINSTEIN, R. Theory of the lattice boltzmann method: Three-dimensional model for linear viscoelastic fluids. *Phys. Rev. E: Stat., Nonlinear, Soft Matter Phys.* 67, 2 1 (2003), 212031–2120319.
- [124] LARSON, R. Instabilities in viscoelastic flows. *Rheol. Acta* 31, 3 (1992), 213–263.
- [125] LARSON, R. G. *Constitutive equations for polymer melts and solutions*. Butterworth's Series in Chemical Engineering, Stoneham, 1988.
- [126] LASO, M., AND ÖTTINGER, H. Calculation of viscoelastic flow using molecular models: the CONNFFESSIT approach. *J. Non-Newton. Fluid Mech.* 47, C (1993), 1–20.
- [127] LEE, A., SHAQFEH, E., AND KHOMAMI, B. A study of viscoelastic free surface flows by the finite element method: Hele-Shaw and slot coating flows. *J. Non-Newton. Fluid Mech.* 108, 1-3 (2002), 327–362.
- [128] LEE, J., YOON, S., KWON, Y., AND KIM, S. Practical comparison of differential viscoelastic constitutive equations in finite element analysis of planar 4:1 contraction flow. *Rheol. Acta* 44, 2 (2004), 188–197.
- [129] LEONOV, A. Analysis of simple constitutive equation for viscoelastic fluids. *J. Non-Newton. Fluid Mech.* 42 (1992), 323–350.
- [130] LEONOV, A. I. Viscoelastic constitutive equations and Rheology for high-speed polymer processing. *J. Polym. Int.* 36 (1995), 187–193.
- [131] LEVENBERG, K. A method for the solution of certain problems in least square. *J. Appl. Math* 2 (1944), 164–168.
- [132] LI, H.-B., AND FANG, H.-P. Lattice Boltzmann simulation of transverse wave travelling in Maxwell viscoelastic fluid. *Chin. Phys.* 13, 12 (2004), 2087–2090.
- [133] LI, X., HAN, X., AND WANG, X. Numerical modeling of viscoelastic flows using equal low-order finite elements. *Comput. Method. Appl. M.* 199, 9-12 (2010), 570–581.
- [134] LOZINSKI, A., OWENS, R., AND QUARTERONI, A. On the simulation of unsteady flow of an Oldroyd-B fluid by spectral methods. *J Sci Comput* 17, 1-4 (2002), 375–383.

- 
- [135] LU, Z., WANG, L., AND FAN, Y. p-version of finite element methods for steady viscoelastic flows between eccentric rotating cylinders. *J. Hydrody.* 11, 3 (1999), 19–25.
- [136] MA, X., SYMEONIDIS, V., AND KARNIADAKIS, G. A spectral vanishing viscosity method for stabilizing viscoelastic flows. *J. Non-Newt. Fluid Mech.* 115, 2-3 (2003), 125–155.
- [137] MACHMOUM, A., AND ESSELAOUI, D. Finite element approximation of viscoelastic fluid flow using characteristics method. *Comput. Meth. Appl. Mech. Eng.* 190, 42 (2001), 5603–5618.
- [138] MADAY, Y., PATERA, A., AND RONQUIST, E. An operator-integration-factor splitting method for time-dependent problems: Application to incompressible fluid flow. *J. Sci Comput.* 5, 4 (1990), 263–292.
- [139] MADAY, Y., AND PATERA, A. T. Spectral element methods for the incompressible Navier-Stokes equations. *State-of-the-Art Surveys Comput. Mech.* (1989), 71–143.
- [140] MALASPINAS, O., COURBEBAISSE, G., AND DEVILLE, M. Simulation of generalized Newtonian fluids with the lattice Boltzmann method. *Int. J. Mod. Phys. C* 18, 12 (2007), 1939–1949.
- [141] MALASPINAS, O. P. *Lattice Boltzmann method for the simulation of viscoelastic fluid flows*. PhD thesis, École Polytechnique Fédérale de Lausanne, 2009.
- [142] MALEVANETS, A., AND YEOMANS, J. Lattice Boltzmann simulations of complex fluids: Viscoelastic effects under oscillatory shear. *Faraday Disc.* 112 (1999), 237–248.
- [143] MALKIN, A. The state of the art in the rheology of polymers: Achievements and challenges. *Polymer Science - Series A* 51, 1 (2009), 80–102.
- [144] MARCHAL, J., AND CROCHET, M. A new mixed finite element for calculating viscoelastic flow. *J. Non-Newt. Fluid Mech.* 26, 1 (1987), 77–114.
- [145] MARQUARDT, D. An algorithm for least square estimation on nonlinear parameters. *J. Appl. Math.* 11 (1963), 431–441.

- [146] MARRUCCI, G. Dynamics of entanglements: A nonlinear model consistent with the Cox-Merz rule. *J. Non-Newt. Fluid Mech.* 62, 2-3 (1996), 279–289.
- [147] MARRUCCI, G., GRECO, F., AND IANNIRUBERTO, G. Integral and differential constitutive equations for entangled polymers with simple versions of CCR and force balance on entanglements. *Rheol. Acta* 40, 2 (2001), 98–103.
- [148] MCKINLEY, G., ARMSTRONG, R., AND BROWN, R. The wake instability in viscoelastic flow past confined circular cylinders. *Philos Trans. Roy. Soc. A* 344, 1671 (1993), 265–304.
- [149] MCKINLEY, G., PAKDEL, P., AND OZTEKIN, A. Rheological and geometric scaling of purely elastic flow instabilities. *J. Non-Newt. Fluid Mech.* 67, 1-3 (1996), 19–47.
- [150] MENG, S., LI, X., AND EVANS, G. Spectral element method for viscoelastic flows in a planar contraction channel. *Int. J. Numer. Meth. Fluids* 42, 3 (2003), 323–348.
- [151] MEYERS, M. *Dynamic behavior of materials*. Wiley, New York, 1994.
- [152] MEYERS, M., GRAY III, G., AND THADHANI, N. The dynamic behavior of materials: An introduction. *J. Met.(JOM)* 62, 1 (2010), 14–15.
- [153] MISSAGHI, K., AND PETRIE, C. Stretching the Phan-Thien-Tanner model: stress growth and creep. *J. Non-Newt. Fluid Mech.* 11, 3-4 (1982), 283–294.
- [154] MOMPEAN, G. On predicting abrupt contraction flows with differential and algebraic viscoelastic models. *Comput. and Fluids* 31, 8 (2002), 935–956.
- [155] MOMPEAN, G., AND DEVILLE, M. Unsteady finite volume simulation of Oldroyd-B fluid through a three-dimensional planar contraction. *J. Non-Newt. Fluid Mech.* 72, 2-3 (1997), 253–279.
- [156] MOMPEAN, G., AND THAIS, L. Finite volume numerical simulation of viscoelastic flows in general orthogonal coordinates. *Math. Comput. Simulat.* 80 (2010), 2185–2199.
- [157] MU, Y., ZHAO, G., ZHANG, C., CHEN, A., AND LI, H. Three-dimensional simulation of planar contraction viscoelastic flow by penalty finite element method. *Int. J. Numer. Meth. Fluid.* 63, 7 (2010), 811–827.



- [158] MUNIZ, A., SECCHI, A., AND CARDOZO, N. High-order finite volume method for solving viscoelastic fluid flows. *Braz. J. Chem Eng.* 25, 1 (2008), 153–166.
- [159] NADAU, L., AND SEQUEIRA, A. Numerical simulations of shear dependent viscoelastic flows with a combined finite element-finite volume method. *Comput. Math. Appl.* 53, 3-4 (2007), 547–568.
- [160] NG, R.-Y., AND LEAL, L. A study of the interacting FENE dumbbell model for semi-dilute polymer solutions in extensional flows. *Rheol. Acta* 32, 1 (1993), 25–35.
- [161] NIGEN, S., AND WALTERS, K. Viscoelastic contraction flows: Comparison of axisymmetric and planar configurations. *J. Non-Newton. Fluid Mech.* 102, 2 (2002), 343–359.
- [162] OLDROYD, J. An approach to non-Newtonian fluid mechanics. *J. Non-Newton. Fluid Mech.* 14 (1984), 9–46.
- [163] OLDROYD, J. G. On the formulation of rheological equations of state. *Proc. Roy. Soc. Lond. A* 200 (1950), 523–541.
- [164] OLIVEIRA, P. Method for time-dependent simulations of viscoelastic flows: Vortex shedding behind cylinder. *J. Non-Newton. Fluid Mech.* 101, 1-3 (2001), 113–137.
- [165] OLIVEIRA, P., AND PINHO, F. Plane contraction flows of upper convected Maxwell and Phan-Thien-Tanner fluids as predicted by a finite-volume method. *J. Non-Newton. Fluid Mech.* 88, 1-2 (1999), 63–88.
- [166] OLSSON, F. A solver for time-dependent viscoelastic fluid flows. *J. non-Newton. Fluid Mech.* 51, 3 (1994), 309–340.
- [167] OLSSON, F. *A numerical method for modeling time-dependent viscoelastic fluid flow.* PhD thesis, Kungl Tekniska Hö gskolan, Stockholm, Sweden, 1995.
- [168] OLSSON, F., AND YSTRÖM, J. Some properties of the upper convected Maxwell model for viscoelastic fluid flow. *J. Non-Newton. Fluid Mech.* 48, 1-2 (1993), 125–145.
- [169] ONISHI, J., CHEN, Y., AND OHASHI, H. Dynamic simulation of multi-component viscoelastic fluids using the lattice Boltzmann method. *Phys. A: Stat. Mech. Appl.* 362, 1 (2006), 84–92.

- [170] OWENS, R., CHAUVIÈRE, C., AND PHILIPS, T. A locally-upwinded spectral technique (lust) for viscoelastic flows. *J. Non-Newt. Fluid Mech.* 108, 1-3 (2002), 49–71.
- [171] OWENS, R., CHAUVIÈRE, C., AND PHILIPS, T. A locally-upwinded spectral technique (lust) for viscoelastic flows. *J. Non-Newt. Fluid Mech.* 108, 1-3 (2002), 49–71.
- [172] OWENS, R., AND PHILLIPS, T. Steady viscoelastic flow past a sphere using spectral elements. *Int. J. Numer. Meth. Eng.* 39, 9 (1996), 1517–1534.
- [173] OWENS, R., AND PHILLIPS, T. *Computational Rheology*. Imperial College Press, London, 2002.
- [174] PATANKAR, S. *Numerical heat transfer and fluid flow*. McGraw-Hill, New York, 1980.
- [175] PATERA, A. A spectral element method for fluid dynamics: Laminar flow in a channel expansion. *J. Comput. Phys.* 54, 3 (1984), 468–488.
- [176] PEROT, J. B. An analysis of the fractional step method. *J. Comput. Phys.* 108, 1 (1993), 51–58.
- [177] PETERLIN, A. Excluded volume effect on light scattering of the coiled linear macromolecule. *J. Chem. Phys.* 23, 12 (1955), 2464–2465.
- [178] PHAN-THIEN, N., AND TANNER, R. A new constitutive equation derived from network theory. *J. Non-Newt. Fluid Mech.* 2, 4 (1977), 353–365.
- [179] PHILLIPS, T., AND WILLIAMS, A. Viscoelastic flow through a planar contraction using a semi-Lagrangian finite volume method. *J. Non-Newt. Fluid Mech.* 87, 2-3 (1999), 215–246.
- [180] PHILLIPS, T., AND WILLIAMS, A. Comparison of creeping and inertial flow of an Oldroyd B fluid through planar and axisymmetric contractions. *J. Non-Newt. Fluid Mech.* 108, 1-3 (2002), 25–47.
- [181] PILITSIS, S., AND BERIS, A. Calculations of steady-state viscoelastic flow in an undulating tube. *J. Non-Newt. Fluid Mech.* 31, 3 (1989), 231–287.
- [182] PILITSIS, S., AND BERIS, A. Pseudospectral calculations of viscoelastic flow in a periodically constricted tube. *Comput. Meth. Appl. Mech. Engin.* 98, 3 (1992), 307–328.

- [183] P.W. CHANG, T.W. PATTEN, B. F. Collocation and Galerkin finite element methods for viscoelastic fluid flow-i. : Description of method and problems with fixed geometry. *Comput. Fluids* 7 (1979), 267–283.
- [184] RAGHAY, S., AND HAKIM, A. Numerical simulation of White-Metzner fluid in a 4:1 contraction. *Int. J. Numer. Meth. Fluids* 35, 5 (2001), 559–573.
- [185] RAJAGOPALAN, D., ARMSTRONG, R., AND BROWN, R. Finite element methods for calculation of steady, viscoelastic flow using constitutive equations with a Newtonian viscosity. *J. Non-Newton. Fluid Mech* 36 (1990), 159–192.
- [186] RENARDY, M., AND RENARDY, Y. Linear stability of plane Couette flow of an upper convected Maxwell fluid. *J. Non-Newton. Fluid Mech.* 22, 1 (1986), 23–33.
- [187] RIVLIN, R. S., AND ERICKSEN, J. L. Stress-deformation relations for isotropic models. *Arch. Ration. Mech.An.* 4 (1955), 323–425.
- [188] ROSENBERG, J., AND KEUNINGS, R. Numerical integration of differential viscoelastic models. *J. Non-Newton. Fluid Mech* 39 (1991), 269–290.
- [189] RUSSO, G., AND PHILLIPS, T. private communication.
- [190] SADANANDAN, B., AND SURESHKUMAR, R. Numerical eigenspectrum of non - viscometric viscoelastic flows: Results for the periodic channel flow. *J. Non-Newton. Fluid Mech.* 108, 1-3 (2002), 143–161.
- [191] SAENGER, E., AND BOHLEN, T. Finite-difference modeling of viscoelastic and anisotropic wave propagation using the rotated staggered grid. *Geophys.* 69, 2 (2004), 583–591.
- [192] SAHIN, M., AND WILSON, H. A semi-staggered dilation-free finite volume method for the numerical solution of viscoelastic fluid flows on all-hexahedral elements. *J. Non-Newton. Fluid Mech* 147, 1-2 (2007), 79–91.
- [193] SAHIN, M., AND WILSON, H. A parallel adaptive unstructured finite volume method for linear stability (normal mode) analysis of viscoelastic fluid flows. *J. Non-Newton. Fluid Mech.* 155, 1-2 (2008), 1–14.

- [194] SANDRI, D. Numerical study of a new finite element method for the approximation of viscoelastic fluid flow problems. *J. Non-Newt. Fluid Mech.* 118, 2-3 (2004), 103–120.
- [195] SHAQFEH, E. Purely elastic instabilities in viscometric flows. *Annu. Rev. Fluid Mech.* 28 (1996), 129–185.
- [196] SIRAKOV, I., AINSER, A., HAUCHE, M., AND GUILLET, J. Three-dimensional numerical simulation of viscoelastic contraction flows using the Pom-Pom differential constitutive model. *J. Non-Newt. Fluid Mech.* 126, 2-3 (2005), 163–173.
- [197] SMITH, G. D. *Numerical Solution of Partial Differential Equations: Finite Difference Methods, Third edition.* Oxford Applied Mathematics and Computing Science Series, Oxford, 1984.
- [198] SMITH, M., ARMSTRONG, R., BROWN, R., AND SURESHKUMAR, R. Finite element analysis of stability of two-dimensional viscoelastic flows to three-dimensional perturbations. *J. Non-Newt. Fluid Mech.* 93, 2-3 (2000), 203–244.
- [199] SONG, J., AND YOO, J. Numerical simulation of viscoelastic flow through a sudden contraction using a type dependent difference method. *J. Non-Newt. Fluid Mech.* 24, 2 (1987), 221–243.
- [200] SUCCI, S. *The Lattice Boltzmann equation for fluid dynamics and beyond.* Oxford university press, Oxford, 2001.
- [201] SUN, C., XIAO, Y., YIN, X., AND PENG, H. Stability condition of finite difference solution for viscoelastic wave equations. *Earthq. Sci.* 22, 5 (2009), 479–485.
- [202] SUN, J., SMITH, M., ARMSTRONG, R., AND BROWN, R. Finite element method for viscoelastic flows based on the discrete adaptive viscoelastic stress splitting and the discontinuous Galerkin method: DAVSS-G/DG. *Journal of Non-Newtonian Fluid Mechanics* 86, 3 (1999), 281–307.
- [203] SURESHKUMAR, R., AND BERIS, A. Effect of artificial stress diffusivity on the stability of numerical calculations and the flow dynamics of time-dependent viscoelastic flows. *J. Non-Newt Fluid Mech.* 60, 1 (1995), 53–80.

- [204] SURESHKUMAR, R., AND BERIS, A. N. Linear stability analysis of viscoelastic Poiseuille flow using an Arnoldi-based orthogonalization algorithm. *J. Non-Newton. Fluid Mech.* 56, 2 (1995), 151–182.
- [205] SURESHKUMAR, R., SMITH, M., ARMSTRONG, R., AND BROWN, R. Linear stability and dynamics of viscoelastic flows using time-dependent numerical simulations. *J. Non-Newton. Fluid Mech.* 82, 1 (1999), 57–104.
- [206] TANNER, R. *Engineering Rheology*. Oxford University press, Oxford, 1966.
- [207] TANNER, R. Engineering Rheology. *Chem. Eng. Aust. (CEA) ChE* 7, 4 (1982), 18–19, 22.
- [208] THOMPSON, K. W. Time dependent boundary conditions for hyperbolic systems. *J. Comput. Phys.* 68 (1987), 1–24.
- [209] TIMMERMANS, L., MINEV, P., AND VAN DE VOSSE, F. An approximate projection scheme for incompressible flow using spectral elements. *Int. J. Numer. Meth. Fluids* 22, 7 (1996), 673–688.
- [210] TOMÉ, M., MANGIAVACCHI, N., CUMINATO, J., CASTELO, A., AND MCKEE, S. A finite difference technique for simulating unsteady viscoelastic free surface flows. *J. Non-Newton. Fluid Mech.* 106, 2-3 (2002), 61–106.
- [211] TREBOTICH, D., COLELLA, P., AND MILLER, G. A stable and convergent scheme for viscoelastic flow in contraction channels. *J. Comput. Phys.* 205, 1 (2005), 315–342.
- [212] TURNER, M. J., CLOUGH, R. W., MARTIN, H. C., AND TOPP, L. P. Stiffness and deflection analysis of complex structures. *J. Aeronaut. Soc.* 23 (1956), 805.
- [213] VAITHIANATHAN, T., AND COLLINS, L. R. Numerical approach to simulating turbulent flow of a viscoelastic polymer solution. *J. Comput. Phys.* 187 (2003), 1–21.
- [214] VAITHIANATHAN, T., ROBERT, A., BRASSEUR, J., AND COLLINS, L. An improved algorithm for simulating three-dimensional, viscoelastic turbulence. *J. Non-Newton. Fluid Mech.* 140, 1-3 (2006), 3–22.
- [215] VALÉRIO, J., CARVALHO, M., AND TOMEI, C. Efficient computation of the spectrum of viscoelastic flows. *J. Comput. Phys.* 228, 4 (2009), 1172–1187.

- [216] VAN KEMENADE, V., AND DEVILLE, M. Application of spectral elements to viscoelastic creeping flows. *J. Non-Newt. Fluid Mech.* 51, 3 (1994), 277–308.
- [217] VAN KEMENADE, V., AND DEVILLE, M. Spectral elements for viscoelastic flows with change of type. *J. Rheol.* 38, 2 (1994), 291–307.
- [218] VAN OS, R., AND GERRITSMAN, M. A variable order spectral element scheme applied to the velocity-pressure-total-stress formulation of the upper convected Maxwell model. *J. Non-Newt. Fluid Mech.* 108, 1-3 (2002), 73–97.
- [219] VAN OS, R., AND PHILLIPS, T. The prediction of complex flows of polymer melts using spectral elements. *J. Non-Newt. Fluid Mech.* 122, 1-3 (2004), 287–301.
- [220] VAN OS, R., AND PHILLIPS, T. Efficient and stable spectral element methods for predicting the flow of an XPP fluid past a cylinder. *J. Non-Newt. Fluid Mech.* 129, 3 (2005), 143–162.
- [221] VAN OS, R. G. M., AND PHILLIPS, T. N. Spectral element methods for transient viscoelastic flow problem. *J. Comput. Phys.* 201 (2004), 286–314.
- [222] VAN SCHAFTINGEN, J. J., AND CROCHET, M. J. A comparison of mixed methods for solving the flow of a Maxwell fluid. *Int. J. Numer. Methods Fluids* 4 (1984), 1065–1081.
- [223] VERSTEEG, H., AND MALALASEKRA, W. *An Introduction to Computational Fluid Dynamics: The Finite Volume Method Approach*. Adison-Wesley, Reading, 1995.
- [224] WACHS, A., AND CLERMONT, J.-R. Non-isothermal viscoelastic flow computations in an axisymmetric contraction at high Weissenberg numbers by a finite volume method. *J. Non-Newt. Fluid Mech.* 95, 2-3 (2000), 147–184.
- [225] WACHS, A., CLERMONT, J.-R., AND KHALIFEH, A. Computations of non-isothermal viscous and viscoelastic flows in abrupt contractions using a finite volume method. *Eng. Computation. (Swansea, Wales)* 19, 7-8 (2002), 874–901.
- [226] WARICHET, V., AND LEGAT, V. Adaptive hp-finite element viscoelastic flow calculations. *Comput. Method. Appl. M.* 136, 1-2 (1996), 93–110.

- [227] WARICHET, V., AND LEGAT, V. Adaptive high-order prediction of the drag correction factor for the upper-convected Maxwell fluid. *J. Non-Newt. Fluid Mech.* 73, 1-2 (1997), 95–114.
- [228] WARNER JR., H. Kinetic theory and Rheology of dilute suspensions of finitely extendible dumbbells. *Ind. Eng. Chem. Fundam.* 11, 3 (1972), 379–387.
- [229] WATERS, N. D., AND KING, M. J. The unsteady flow of an elastico-viscous liquid in a straight pipe of circular cross section. *J. Non-Newt. Fluid Mech.* 4 (1971), 204–211.
- [230] WEBSTER, M., TAMADDON-JAHROMI, H., AND ABOUBACAR, M. Transient viscoelastic flows in planar contractions. *J. Non-Newt Fluid Mech.* 118, 2-3 (2004), 83–101.
- [231] WEBSTER, M., TAMADDON-JAHROMI, H., AND ABOUBACAR, M. Time-dependent algorithms for viscoelastic flow: Finite element/volume schemes. *Numer. Methods Partial Differential Equations* 21, 2 (2005), 272–296.
- [232] WEBSTER, M. F. *The numerical solution of rheological flow problems*. PhD thesis, University of Wales, Aberystwyth, U.K., 1979.
- [233] WIEST, J. A differential constitutive equation for polymer melts. *Rheol. Acta* 28, 1 (1989), 4–12.
- [234] WILSON, H., AND RALLISON, J. Instability of channel flow of a shear-thinning White-Metzner fluid. *J. Non-Newt. Fluid Mech.* 87, 1 (1999), 75–96.
- [235] WILSON, H., AND RALLISON, J. Instability of channel flows of elastic liquids having continuously stratified properties. *J Non-Newt. Fluid Mech.* 85, 2-3 (1999), 273–298.
- [236] WILSON, H., RENARDY, M., AND RENARDY, Y. Structure of the spectrum in zero Reynolds number shear flow of the UCM and Oldroyd-B liquids. *J. Non-Newt. Fluid Mech.* 80, 2-3 (1999), 251–268.
- [237] WOLF-GRADROW, D. A. *Lattice-Gas Cellular Automata and Lattice Boltzmann models: An introduction*. Springer, Verlag, 2000.
- [238] WOODS, L. C. A note on the numerical solution of fourth order differential equations. *Aero. Qu.* 5 (1954), 176.

- 
- [239] XU, C. Stabilization methods for spectral element computations of incompressible flows. *J. Sci. Comput.* 27 (2006), 495–505.
- [240] XUE, S., PHAN THIEN, N., AND TANNER, R. Numerical investigations of Lagrangian unsteady extensional flows of viscoelastic fluids in 3-D rectangular ducts with sudden contractions. *Rheol. Acta* 37, 2 (1998), 158–169.
- [241] XUE, S.-C., PHAN-THIEN, N., AND TANNER, R. Three dimensional numerical simulations of viscoelastic flows through planar contractions. *J. Non-Newt. Fluid Mech.* 74, 1-3 (1998), 195–245.
- [242] YUAN, X., BALL, R., AND EDWARDS, S. Dynamical modelling of viscoelastic extrusion flows. *J. Non-Newt. Fluid Mech.* 54, C (1994), 423–435.
- [243] YUL YOO, J., AND NA, Y. A numerical study of the planar contraction flow of a viscoelastic fluid using the SIMPLER algorithm. *J. Non-Newt. Fluid Mech.* 39, 1 (1991), 89–106.
- [244] ZHANG, Y., WANG, H., AND TANG, T. Simulating two-phase viscoelastic flows using moving finite element methods. *Commun. Comput. Phys.* 7, 2 (2010), 333–349.
- [245] ZHAO, W.-J., CHEN, L.-Q., AND ZU, J. Finite difference method for simulating transverse vibrations of an axially moving viscoelastic string. *Appl. Math. Mech-Engl.* 27, 1 (2006), 23–28.
- [246] ZIENKIEWICZ, O. C., TAYLOR, R. L., AND NITHIARASU, P. *The Finite Element Method for Fluid Dynamics, Sixth Edition*. Butterworth-Heinemann, Oxford, 2005.



# Curriculum vitae

---

Teaching-Assistant and Ph.D. student	Iranian
Laboratory of Computational Engineering	Born on August 3, 1981
Department of Mechanical Engineering	Email: azadehjafari1@gmail.com
Swiss Federal Institute of Technology- Lausanne	
1015 Lausanne, Switzerland	

## Education

- Ph.D. in Mechanical Engineering
  - Swiss Federal Institute of Technology-Lausanne (EPFL), Lausanne, Switzerland, December 2010
  - *Dissertation*: Simulation of time-dependent viscoelastic fluid flows by spectral elements
  - *Thesis Advisor*: Professor Michel O. Deville
- M.S. in Mechanical Engineering
  - Tehran University, Tehran, Iran, April 2006
  - *Dissertation*: Numerical study of Unsteady Turbulent Flow around a Square Cylinder Confined in a Channel Using Low Reynolds Number Eddy-Viscosity Models
  - *Thesis Advisor*: Professor Mehrdad Raisee Dehkordi
- B.S. in Mechanical Engineering
  - Yazd University, Tehran, Iran, September 2003
  - *Dissertation*: Simulation of the collector of solar water heater
  - *Thesis Advisor*: Professor Shahram Talebi

## Journal Publication

1. Azadeh Jafari, Nicolas Fiétier, Michel Deville. Simulation of viscoelastic fluids in 2-D abrupt contraction by spectral element method, submitted to *J. Non-Newt. Fluid Mech.*, November 2010.
2. Azadeh Jafari, Nicolas Fiétier, Michel Deville. Simulation of flows of viscoelastic fluids at high Weissenberg number using a filter-based stabilization of the spectral element method, submitted to *Comput. Fluids*, August 2010.
3. Azadeh Jafari, Nicolas Fiétier, Michel Deville. A New Extended Matrix Logarithm Formulation for Simulation of Viscoelastic Fluids with Spectral Elements. *Comput. Fluids*, 39(9), 1425-1438, 2010.
4. M. Raisee, A. Jafari, H. Babaei, H. Iacovides, Two-Dimensional Prediction of Time-Dependent, Turbulent Flow around a Square Cylinder Confined in a Channel, *Int. J. Numer. Meth. Fluids*, 62, 1232-1263, 2010.

## Conference Presentations and Proceeding Publications

1. Azadeh Jafari, Nicolas Fiétier, Michel O. Deville. Time Dependent of 2D 4:1 Contraction Flow of Viscoelastic Fluids Using the Logarithm Conformation Tensor. 82<sup>nd</sup> Annual Meeting of the Society of Rheology, Santa Fe, New Mexico, USA, 24-28 October 2010,
2. Azadeh Jafari, Nicolas Fiétier, Michel O. Deville. Filter Based Stabilization of Spectral Element Method for Stabilizing viscoelastic flows. 6<sup>th</sup> Annual European Rheology Conference, CD of Scientific Program and Abstracts, Supported by Anton Paar, Goteborg - Sweden, 7-9 April 2010.
3. Azadeh Jafari, Nicolas Fiétier, Michel O. Deville. Simulation of Viscoelastic Fluids at high Weissenberg Number Using the Extended Matrix Logarithm Formulation. Proceeding of the 5<sup>th</sup> International Symposium on Food Rheology and Structure pages 598-599, Laboratory of Food Process Engineering, Institute of Food Science and Nutrition ETH University, Editors: Peter Fischer, Michael Polard, Erich J. Windhab, Zurich, Switzerland, 15-18 June 2009.

4. Azadeh Jafari, Nicolas Fiétier, Michel O. Deville. A New Extended Algorithm of the Matrix Logarithm Formulation for Transient Viscoelastic Flows. 5<sup>th</sup> Annual European Rheology Conference, CD of Scientific Program and Abstracts, Supported by Anton Paar, Cardiff-United Kingdom, 15-17 April 2009.
5. Azadeh Jafari, Michel O. Deville, Nicolas Fiétier. Spectral Elements Analysis for Viscoelastic Fluids at High Weissenberg Number Using Logarithmic Conformation Tensor Model. 6<sup>th</sup>. International Conference of Numerical Analysis and Applied Mathematics (ICNAAM), AIP Conference Proceedings 278-281, volume 1048, Editors: Theodore E. Simos, George Psihoyios, Ch. Tsitouras, Kos, Greece, 16-20 September 2008.
6. M. Raisee, A. Jafari, H. Iacovides. Two-Dimensional Prediction of Unsteady Turbulent Flow around a Square Cylinder Confined in a Channel, IUTAM Symposium on Unsteady Separated Flows and their Control. Greece, June 2007.
7. A. Jafari, M. Raisee. Numerical Study of Turbulent Flow around a Square Cylinder Using Two Low-Re Number Models. European Conference on Computational Fluid Dynamics, Netherlands, conference proceeding, 417, 2006.
8. M. Raisee, Z. Niroobakhsh, A. Jafari. Hydrodynamic and Thermal Characteristics of Non-Newtonian Fluids in Uniformly Heated Two Dimensional and Axi-Symmetric passage. European Conference on Computational Fluid Dynamics, Netherlands, conference proceeding, 418, 2006.
9. M. Raisee, A. Jafari. Investigation of Low-Reynolds Number Eddy-Viscosity Models for prediction of Characteristic of Flow around a Square Cylinder in both Steady and Unsteady Turbulent Flow. 10th Fluid Dynamic conference, Iran, Yazd, 2006.

## Honors, Awards, & Fellowships

- Awarded by Erna Hamburger grant, 2010-2011
- SOR (Society of Rheology) Travel Grant Recipient, 2010
- BSR (British Society of Rheology) Travel Grant Recipient, 2010
- Swiss National Science Foundation, 2007-2010

- First class honors in thermo fluid among 4 years at Yazd University, 1999-2003
- Ranked 2<sup>nd</sup>/25000 in chemical competition among high school students, Iran 1997.
- Silver medal in sport competition among guidance school students, 1992

### Teaching-Assistant Experience

- Continuum media mechanics, Bachelor of Science in mechanical engineering, Spring 2009.
- fluid Mechanics, Bachelor of Science in mechanical engineering, 2002-2003.
- Power Plant, Bachelor of Science in mechanical engineering, 2002-2003

### Related Experience

- Working on the project of hydroelectric power plant of Karun III (The largest hydroelectric power plant in Iran), 2003-2004
- Working in Qushm cement company, 2004-2005.
- Working in Niroo research institute on the project of “Investigation the technical, economical and environmental comparison of compressing and absorption ”, 2005

### IT Skills

- Languages and Scripts: C++, C, FORTRAN, MPI, bash
- Operating System: Unix/Linux/Windows
- Software: Tecplot, Matlab, AutoCAD,EES, Paraview